Optimised thermosyphon solar hot water heater — simulation, design and experimental analysis

Sebastian Brandmayr

PhD

2012

Optimised thermosyphon solar hot water heater — simulation, design and experimental analysis

Sebastian Brandmayr

A thesis submitted in partial fulfilment
of the requirements of De Montfort University
for the degree of Doctor of Philosophy (PhD)

April 2012

Institute of Energy and Sustainable Development
De Montfort University Leicester

CENTRE OF EXCELLENCE FOR RENEWABLE ENERGY RESEARCH
Ingolstadt University of Applied Sciences

Declaration

I declare that the content of this submission is my own work. The contents of the work have not been submitted for any other academic or professional award. I acknowledge that this thesis is submitted according to the conditions laid down in the regulations. Furthermore, I declare that the work was carried out as part of the course for which I was registered at De Montfort University, United Kingdom from January 2008 until April 2012. I draw attention to any relevant considerations of rights of third parties.

Abstract

Thermosyphon systems represent 70–80 % of the solar-thermal capacity installed worldwide. Outside of China — the world's largest thermosyphon system market — thermosyphon systems using flat-plate collectors are the dominant configuration. In Southern Europe conventionally-designed thermosyphon systems with a collector area of about 2.0 m² and a storage tank of 180 l are able to deliver about 70 % of the annually needed hot water of a four person household.

However, research into the performance of thermosyphon systems has stagnated in recent years, hence the primary objective of this research was to evaluate in detail the physical factors affecting the performance of flat plate thermosyphon systems hence pointing the way towards improved performance. The investigation consisted of the implementation of a detailed dynamic system simulation, which included the development of new component models, the validation of the new component models via laboratory testing, the use of the system model in a sensitivity analysis of the significance of individual component performance and finally the testing of an improved prototype thermosyphon system.

Eighteen different geometrical and physical parameters were investigated in the sensitivity analysis to find the most significant design factors. The sensitivity analysis incorporated three different European locations, but the dependency of the optimal thermosyphon system configuration on the location was found to be rather weak.

The research concluded that a performance improvement from 70 % to 85 % of the hot water demand of a four-person household could be achieved with an improved system configuration.

The improved system prototype addressed cost reduction by the material selection for the storage tank and its built-in components as well as the selection of aluminium for the solar absorber and the use of prefabricated parts for the system support. Reverse thermosyphoning was prevented by adjusting the tank and collector inlet/outlet co-locations, while the availability of hot water was enhanced by improved hydraulic design of the storage tank.

Suggestions for further work included the development of more detailed component models and long-term testing of improved system configurations.

Acknowledgements

This research project was carried out at the *Institute of Energy and Sustainable Development* at *De Montfort University Leicester* in cooperation with the *CENTRE OF EXCELLENCE FOR RENEWABLE ENERGY RESEARCH* at *Ingolstadt University of Applied Sciences*.

I would like to thank my supervising team namely Prof. Vic Hanby, Prof. Wilfried Zörner and Dr. Simon Rees for the initiation of this research work, for their excellent support and guidance as well as for the revision of this thesis.

Furthermore, I would like to give special thanks to my industrial project partner *CitrinSolar*, in particular to Franz-Dominik Treikauskas and Hanns Koller. They were always willing to give support when needed and provided me with parts and prototypes.

Moreover, I am very grateful to the students and colleagues who accompanied me during the years at the *CENTRE OF EXCELLENCE FOR RENEWABLE ENERGY RESEARCH*, especially to Holger Müller, Hermann Riess, Matthias Sonnleitner and Christoph Trinkl. They gave me support whenever needed and made the university much more than just a place to work.

Finally, I would like to thank my parents Hans and Gertrud, my girlfriend Conny as well as my siblings Julia and Felix for their support and their encouragement throughout the work.

Table of Contents

List of Figures

List of Tables

Abbreviations

AM	Air Mass
CARNOT	Conventional and Renewable Energy Systems Optimization Toolbox
cf.	compare (Latin: confer)
CFD	Computational Fluid Dynamics
CVD	Chemical Vapour Deposition
DIN	Deutsches Institut für Normung
EU	European Union
ESTIF	European Solar-Thermal Industry Federation
e.g.	for example
eqn.	Equation
eq.	Equivalent
ISO	International Organization for Standardisation
kW_{th}	Kilowatt thermal
MW_{th}	Megawatt thermal
PC	Polycarbonate
PET	Polyethylene Terephtalate
PMMA	Polymethylmethacrylate
PP	Polypropylene
PVC	Polyvinylchloride
PVD	Physical Vapour Deposition
UP	Unsaturated Polyester
UV	Ultra Violet Light
UP	Unsaturated Polyester
THV	Thermo Hydraulic Vector
TRNSYS	Transient System Simulation Program

Symbols

a, s	Coefficients	[-]
b	Element Number	[-]
A	Area	[m²]
c	Heat Capacity	[J kg^{-1} K^{-1}]
C_b	Bond Conductance	[W m^{-1} K^{-1}]
d	Diameter	[m]
dT	Temperature Gradient	[K]
dt	Time Step	[s]
e	Surface Roughness	[m]
f	Friction Factor	[-]
f_{sol}	Solar Fraction	[-]
F	Fin Efficiency	[-]
F'	Collector Efficiency Factor	[-]
F_R	Heat Removal Factor	[-]
g	Gravity	[m s^{-2}]
G	Solar Irradiation	[W m^{-2}]
h	Convective Heat Transfer Coefficient	[W m^{-2} K^{-1}]
H	Daily Solar Radiation	[MJ m^{-2}]
k	Heat Conductivity	[W m^{-1} K^{-1}]
ki	Incidence Angle Modifier	[-]
l	Length	[m]
m	Mass	[kg]
$\dot{m}$	Mass Flow Rate	[kg s^{-1}]
M	Daily Mass Flow	[kg]
(MC)	Thermal Capacity	[J K^{-1}]
n	Number / Refractive Index	[-]
Nu	Nusselt Number (Dimensionless Heat Transfer Coefficient)	[-]
o	Arc Length	[m]
Δp	Pressure Difference	[Pa]
p	Pressure	[Pa]
Pr	Prandtl Number (Fluid Specific)	[-]

Q	Energy	[MJ]
$\dot{q}, \dot{Q}$	Energy Flux	[W]
R	Heat Resistance	[K W^{-1}]
Re	Reynolds Number	[-]
s	Chord Length	[m]
t	Time	[s]
T	Temperature	[°C]
(UA)	Heat Loss Coefficient	[W K^{-1}]
U_L	Overall Collector Heat Loss Coefficient	[W $m^{-2}K^{-1}$]
u	Heat Loss	[W m^{-2} K^{-1}]
v	Velocity	[m s^{-1}]
V	Volume	[m^3]
$\dot{V}$	Volume Flow Rate	[m^3 h^{-1}]
w	Collector Width	[m]
W	Distance between Riser Tubes	[m]
x	Function	[-]
z	Height / Thickness	[m]

Subscripts

absorber, abs	Absorber
add	Additional
air	Air
amb	Ambient
as	Asymmetric
aux	Auxiliary
av	Average
axial	Axial
b	Bottom
branch	Branch
buo	Buoyancy
circum	Circumference
col	Collector
cover	Cover Plate
down	Downwards
dyn	Dynamic
e	Edge
eff	Effective
eq	Equivalent
exch	Heat Exchanger
fictive	Fictive
fin	Fin
fluid	Fluid
glass	Glass
h	Convective
header	Collector Header Tube
hor	Horizontal
in	Inlet, Inner
ini	Initial Condition
inner	Inner

insulation	Insulation
j	Matrix Index
k	Node Index, Conductive
L	Left
La	Langhaar Formula
load	Load
loss	Losses
lin	Linear
mantle	Mantle
mean	Mean
n	Number
node	Node
outer, out	Outer
pipe	Pipe
qua	Quadratic
r	Radiative
red	Reduced
R	Right
Re	Reynolds Number
riser	Collector Riser Tube
sky	Sky
sol	Solar
source	Source
spacing	Spacing
sum	Summarised
stag	Stagnation
store	Storage Tank
sys	System
t	Top
th	Thermal
tilt	Tilt (Angle)
up	Upwards

use	Usable
wall	Pipe Wall
water	Water
wind	Wind

Greek Symbols

α	Absorption Coefficient	[-]
β	Chord Angle	[°]
ε	Emission Coefficient	[-]
γ	Collector Tilt Angle	[°]
λ	Wave Length	[m]
Δ	Difference	[-]
ζ	Friction Coefficient	[-]
η	Collector Efficiency	[-]
η_0	Zero Loss Efficiency	[-]
κ	Thermal Conductivity	[W m^{-1} K^{-1}]
μ	Dynamic Viscosity	[kg m^{-1} s^{-1}]
ρ	Density	[kg m^{-3}]
ρ_{glass}	Reflexion Coefficient Glazing	[-]
τ	Transmission Coefficient	[-]
$(\tau\alpha)$	Transmission/Absorption Product (optical characteristics of the transparent cover)	[-]
γ	Collector Tilt Angle	[°]
θ	Beam Angle	[°]

1 Introduction

In 2009, thermosyphon systems represented 70–80 % of the solar thermal capacity installed worldwide. The overall market share of thermosyphon systems in the newly installed capacity worldwide was at 85 % (2009). In China — the world's leading solar heating market — 95 % of the newly installed systems are thermosyphon systems (Mauthner and Weiss, 2011). The typical Chinese system is composed of a 180 l hot water storage and a 4 m² evacuated tube collector (Fawer and Magyar, 2009).

In Europe, the world's second important market, the market share of thermosyphon systems was fairly static at 30 %. The typical European thermosyphon system uses flat-plate collectors instead of evacuated tube collectors.

In the recent years, thermosyphon systems have not been a serious focus for the research and development activities of most European manufacturers. This is quite surprising considering their enormous market potential. In standard solar-thermal literature, thermosyphon systems are generally treated in a cursory manner.

In spite of this lack of industrially-driven research, thermosyphon systems are currently becoming of increasing interest to Central European manufacturers of solar-thermal components and systems. These manufacturers are confronted with increasingly saturated local markets and, therefore, look for possibilities in export, mainly concerning regions around the Mediterranean Sea. In these regions, thermosyphon systems respond to the customers' demands in an ideal manner. The production of daily hot water is adequate and there is little or no need for space heating. Thermosyphon systems replace the commonly used electrical water heaters.

By reducing the share of electricity used for hot water preparation, thermosyphon systems offer great potential for the displacement of fossil fuels. In 2007, 56 % of the electricity consumed in Europe was produced by combusting fossil fuels (Verband Deutscher Maschinen- und Anlagenbau, 2010). This power generation causes an increasing concentration of air pollutants such as carbon dioxide and nitrogen oxides, which come along with local and global environmental problems.

The utilisation of solar energy and other renewable energy sources such as wind or water does not generate carbon dioxide or other air pollutants (during operation). The solar energy annually available worldwide is about 10,000 times higher than the world's primary

energy demand (Quaschning, 2009). The availability of (technically usable) solar energy depends on the geographic location. The localised annual amount of available solar energy is nearly constant and varies only slightly interannually. Solar energy offers one major advantage as it is not subject to political pressures from other states or military attacks, as is the case with oil, and, therefore, a secure and reliable energy source with high potential of minimising environmental damage.

In general, thermosyphon solar hot water heaters do not need electricity to be operated. Thermosyphon systems directly convert solar energy into heat, which is stored in a hot water storage tank until it is needed. To ensure a certain hot water temperature in times of adverse weather, either an electrical heating element, which keeps the storage tank at a certain temperature, or a continuous flow heater, attached in between the storage tank and the consumer, can be applied. The heating element will lower, depending on the installed electrical power (Wenxian and Enrong, 1995), the amount of solar supplied hot water. The continuous flow heater has the advantage of a higher amount of solar supplied hot water, as the storage tank temperature is not influenced by this measure (Michaelides and Wilson, 1996).

This thesis focuses on the reduction of supplementary energy for the preparation of hot water. This can be achieved by optimising the additional heating device or by optimising the amount of heat produced by the solar-thermal system. The thesis focuses on the latter. This research is necessary as commercially-available systems are generally of suboptimal design and hence have a lowered potential for reducing greenhouse gas emissions. The manufacturers of these systems are ‘locked in’ to that suboptimal design and not able to optimise such systems, as the necessary knowledge concerning the geometrical and physical dependencies has not been enhanced for many years. A closed development cycle described in this thesis is intended to address this problem. This approach is unique in the solar-thermal sector.

Within the research project, a collaboration between Ingolstadt University of Applied Sciences and the company CitrinSolar Energie- und Umwelttechnik GmbH (CitrinSolar) was established. CitrinSolar is a solar collector and storage tank manufacturer and is interested in thermosyphon systems for the European and Northern African market. During the research project information was continuously exchanged. CitrinSolar provided the thermosyphon system prototype for the system tests.

1.1 Thermosyphon Solar Water Heaters

Thermosyphon solar domestic hot water systems in general consist of three major parts: the solar-thermal collector, the storage tank and the interconnecting piping between collector and storage. This kind of solar-thermal application works on circulation of the collector fluid through natural convection. The key to operation of thermosyphon systems is the location of the storage tank above the collector panels. By connecting the upper outlet of the collector to the top of the storage and the lower part of the storage to the collector inlet, a closed-loop system is created as shown in Figure 1.1.

During hours of sunshine, the collector converts the solar radiation into heat and warms up the heat carrier within the collector. The fluid becomes less dense than the fluid in the storage tank. The fluid, in the system as shown in Figure 1.1 actually tap water, flows into the storage tank through the collector risers and the connecting pipes, while colder water from the storage tank sinks down to the collector inlet. So, a continuous system circulation, at a low flow rate as compared to pumped solar-thermal systems, is created.

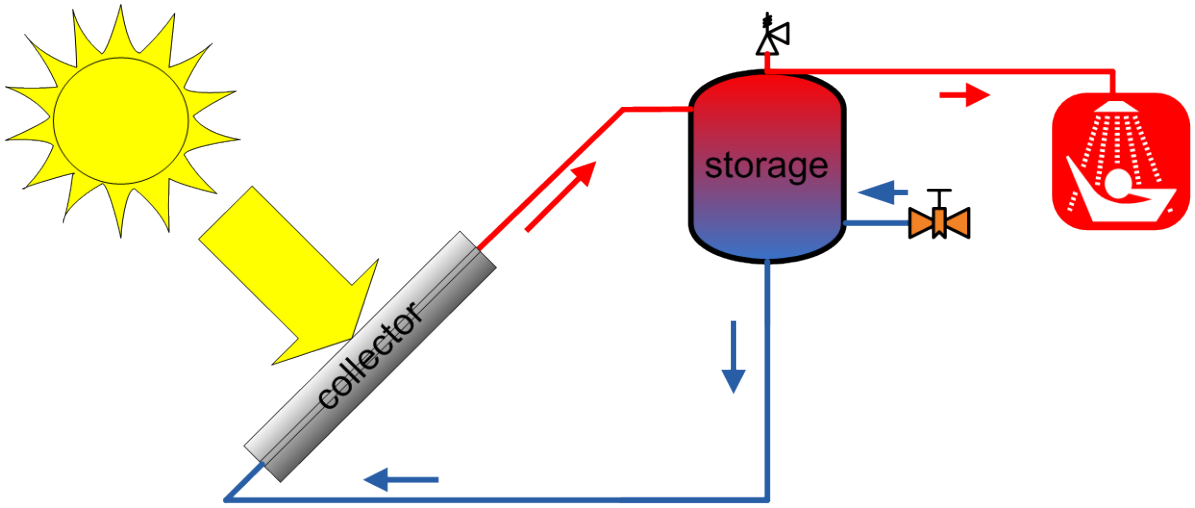

Figure 1.1: Functional Principle of a Thermosyphon System

The flow rate in such a natural circulation thermosyphon system depends on many variables and varies throughout day and year, depending on the absorbed radiation, fluid temperatures, system geometry and many other factors. According to Duffie and Beckman (2006), thermosyphon systems may be described as self-adjusting, with increasing solar gain leading to increasing flow rates through the collector.

There are two main sizes as far as thermosyphon systems are concerned (Brandmayr and Zörner, 2007). On the one hand, there are systems with a collector area of about 2 m² and approximately 180 l of hot water storage for two to four person households. On the other hand, there are systems available with about 300 l of storage volume and a collector area of about 4 m² which meet the requirements of households with about four to six persons. A similar result can be derived from a worldwide manufacturer survey published in 2010, in which 17 out of 47[1] manufacturers had systems with 1.8-2.4 m² collector area combined with a 150-200 l storage tank volume and 9 of them systems with 4.0-4.5 m² collector area and 300 l storage tank volume in their portfolio (Meyer, 2010).

1.2 Technical Weaknesses of State-of-the-Art Thermosyphon Systems

State-of-the-art thermosyphon systems nowadays show a number of unsolved technical problems, which the thesis aims to address:

- Reverse thermosyphoning occurs in times with a hot storage tank and low irradiation, e.g. during night. In case of reverse thermosyphoning, hot water from the storage flows back into the collector. The collector is then working as a heat exchanger to the colder surrounding. Hence, the system additionally cools down during night.
- The hydraulic design of the storage tank in most available systems is rather poor. While taking water from the storage, the stratification within the tank is destroyed by the cold tap water. This has a negative effect on the daily system performance.
- Many systems suffer from overheating problems as high-efficiency collectors designed for pumped systems are simply combined with storage tanks without regard to the collector storage tank ratio. During summer times, these systems are able to reach storage temperatures of above 100 °C, even under typical operation conditions, hence become a danger to users.
- A weakness of many thermosyphon systems is the hydraulic design of the solar circuit and especially of the connecting pipes. In some systems, the return pipe is welded on the absorber sheet. Therefore, the fluid is already preheated before it enters the actual absorber. This slows down the density dependent natural convection

[1] 6 manufacturers did not mention either their collector area or their storage tank volume

of the whole system depending on the fluid temperature in the range of 6–9 % (cf. calculation scheme in Appendix A). Other manufacturers use corrugated pipes that cause a high pressure drop. This type of piping has a negative impact on the developing flow rate.

1.3 Target of the Research Programme

The research described in this thesis aims at the development of a thermosyphon system with a single solar collector and a storage tank volume of about 180 l that outperforms state-of-the-art systems in terms of maximised annual hot water output at reduced production costs based on a closed development cycle approach specified and applied in this thesis.

The objective of testing and simulating a market available reference thermosyphon system is to provide the ability to quantify the optimisation measures developed in this thesis.

The development of a broad simulation-based sensitivity analysis to identify and analyse the design driving factors is a further target of this thesis. The simulation aims at linking geometrical correlations and material properties directly with the annual energy output of the thermosyphon system.

The simulation environment chosen, MATLAB/SIMULINK (The Mathworks, 2011) and an extension called CARNOT (Hafner et al., 1999) offers the framework for the simulation of all kinds of renewable energy systems, but it lacks a double mantle heat exchanger storage tank model. Thus, a storage tank model was developed and verified by data from the monitoring of a reference thermosyphon system.

A further issue addressed is the dependency of the system configuration on different European climatic conditions, namely Ingolstadt, Rome and Malaga. Various publications on thermosyphon system performance and optimisation, like Karaghouli and Alnaser (2001), Sharia et al. (1994) and Budihardjo et al. (2003) refer to a certain location but do not give a hint on the transferability to other locations.

By comparing different materials and their properties the thesis aims at a material selection for the thermosyphon system coming along with a noticeable cost reduction potential at the same durability and efficiency as the reference system. Furthermore, the technical weaknesses described in Chapter 1.2 are addressed.

The design and construction of a thermosyphon system prototype based on the simulation results, the cost reduction analysis and a literature review is a subsequent target of the thesis.

The purpose of the prototype system is to verify the optimisation measures developed and applied by test data gained with system parts and the whole thermosyphon system.

A further issue addressed within this thesis is aimed at the reducing of greenhouse gas emissions for daily hot water preparation by optimising the amount of heat produced by the solar-thermal system.

1.4 Work Packages of the Programme

Most former investigations in the field of thermosyphon solar hot water heaters were conducted either theoretically, by simulating the system behaviour under steady state conditions, or experimentally by performing in- or outdoor tests. Hence, there is limited validation of system models. This research includes the analysis of thermosyphon systems in theory, transferring mathematical models into simulation, validation of the simulation, the design of a prototype based on simulation results and eventually the testing of the prototype. The validated thermosyphon system model is intended to provide researchers in the field of solar-thermal applications as well as manufacturers with the possibility of adapting their thermosyphon systems to differing climatic conditions and customers´ demands.

The programme of research undertaken consists of five main parts:

I. Comprehensive literature review of research on thermosyphon systems including a market analysis,
II. Functional analysis of thermosyphon systems and formulation of mathematical descriptions,
III. Identification and analysis of design driving component and system parameters using simulation models,
IV. Development, construction and testing of a thermosyphon system following from simulation, including a cost analysis,
V. Validation of the simulation model using measurement data.

2 Comprehensive Market and Literature Review

The market and literature review focuses on possible target markets and their commercial background, gathers trends and gives a résumé on relevant developments in the area of thermosyphon systems.

2.1 Market and Competition Analysis

The aim of the market and competition analysis is to give an overview of the current energy policy and the financial possibilities of the target regions and the market potential for solar-thermal applications. This work is necessary to fix the customers' demands regarding the system development.

2.1.1 Europe

It was the European Union's (EU) aim to increase the solar-thermal collector area currently installed in its member countries to 100 million m² by 2010 (European Commission, 1997). This corresponds to a total capacity of 70,000 MW_{th} calculated using 0.7 kW_{th} m^{-2}, a factor introduced by the European Solar Industry Federation (2005). This scenario estimated an annual growth rate of 20 % starting at an installed collector area of 6.5 million m² in 1995.

Towards the end of 2006, the total capacity of all European solar-thermal systems was about 13,454 MW_{th}, which equals an installed collector area of about 19.22 million m² or an average annual European market growth of 7.5 % since 1995 (European Solar Industry Federation, 2007a). As the goals set for 2010 in the EU white book (European Commission, 1997) were not achievable, at the end of 2007 a new target for the year 2020 was declared. The target was defined within the programme 'Key issues for renewable heat in Europe' (K4RES-H) under the title 'Setting verifiable targets for Solar-Thermal' (European Solar Industry Federation, 2007b). Within this programme two scenarios were identified. The minimum target or "Austria scenario" deals with an installed solar-thermal capacity of 199 kW_{th}/1,000 capita. The second, the ambitious target set by European Solar Industry Federation (ESTIF) (Table 2.1) is the '1 m² per capita scenario'. ESTIF pointed out that this ambitious target has to be adjusted to country specific conditions, as not every country is able to reach this goal in 2020.

Table 2.1: Scenarios for the Development of the European Solar-Thermal Market until 2020

	Capacity in operation 2005 [GW_{th}]	Capacity in operation 2020 [GW_{th}]	Average market growth rate 2006 – 2020 [% p.a.]	Capacity in operation per capita 2020 [kW_{th}/1,000 capita]
"Austria scenario" (minimum target)	10.9	91.2	16 %	200 (eq. 0.285 m²)
"1 m² per capita scenario" (ambitious target)		320.4	31 %	700 (eq. 1 m²)

Source: European Solar Industry Federation, 2007b

The 2010 market data on the European solar-thermal market indicate that with an installed capacity of 24.1 GW_{th} Europe is on its way to reach the "Austria scenario" by 2020 (European Solar Industry Federation, 2011).

Nevertheless, major changes on the European solar-thermal market are ongoing. In 2005, Europe's three main solar-thermal markets were Germany (47 % market share), Austria (12 %) and Greece (11 %). Together they represented about 70 % of the entire European market (European Solar Industry Federation, 2006).

In 2007, Spain (10 %), France (9 %) and Italy (9 %) showed a significant and continuing market growth (European Solar Industry Federation, 2008) and got ahead of Austria (7 %) and Greece (6 %) in 2008 (European Solar Industry Federation, 2009).

In 2010, Italy (13 %) became the second largest European solar-thermal market just behind Germany (31 %) (European Solar Industry Federation, 2011).

As far as the use of thermosyphon systems is concerned, Italy, Spain and France are very promising for the manufacturers from Germany and Austria seeking export possibilities. Greece, a very large thermosyphon system market, is not relevant for export efforts due to its low prices and high density of local manufacturers.

The Italian market, still only 2/3 of the European annual average of 47.6 kW_{th}/1,000 capita newly installed capacity, showed a strong growth over the last years. A tax rebate for investments in solar-thermal installations led to this development. The tax break programme is continued until the end of 2011 and, therefore, a good market development can be expected (European Solar Industry Federation, 2011). Besides that, Italy has the ambitious target of being Europe's largest solar-thermal market by 2020.

The Spanish solar-thermal market profited from a law that came into force in September 2006 which makes it necessary for almost all newly built houses to produce 30–70 % of

the needed hot water by solar energy (European Solar Industry Federation, 2006). With this legal obligation, Spain served as a pioneer within Europe. This law led to a noticeable market growth up to 2008. Spain even became Europe's second largest market for solar-thermal systems. In 2009, the world financial crisis and the declining construction market lead to a market decrease of 10 % (European Solar Industry Federation, 2010). This trend continued in 2010, therefore, the Spanish solar-thermal market is now close to the 2007 level (European Solar Industry Federation, 2011).

France was able to increase its national market by a factor of 90 in just 10 years. The reason for this development is the so called 'plan soleil' ('sun plan'). Since 2006, 50 % of the costs for a solar-thermal installation are rebated from the incoming tax (European Solar Industry Federation, 2006, 2009). After a peak in 2008, in 2009 and 2010 a market reduction to the level of 2007 took place (European Solar Industry Federation, 2011). While the market penetration with systems for multifamily housing is still increasing, especially the individual applications such as single family housing are declining. This decline is linked to the market opportunities of thermosyphon systems.

In 2009, the market share of newly installed thermosyphon systems in Europe was 30 % (Mauthner and Weiss, 2011), which equalled a newly installed collector area of 1,283,400 m² (European Solar Industry Federation, 2010).

2.1.2 North Africa and Middle East

Moving away from the European solar-thermal market and focusing on the North African market, only limited financial possibilities can be found on the inhabitants' side by comparing the countries' Gross Domestic Product (GDP) with Germany. But especially these economically weak countries have a high annual amount of sunshine ideal for the use of solar-thermal applications.

In Tunisia for example, the estimated GDP was only about 7,900 US-$ in 2008 (Germany: 34,800 US-$) (Central Intelligence Agency, 2009). By contrast, Tunisia has an annual amount of sunshine hours of about 2,800–3,200 (Germany: 1,300–2,000) at an ambient temperature of about 20 °C (Germany: 8.2 °C).

These prevailing conditions make all Northern African countries like Tunisia, Algeria, Libya, Morocco and Egypt ideal markets for the most simple solar-thermal water heaters of all, the thermosyphon systems.

In Tunisia, various efforts have been made by the German–Tunisian chamber of commerce and industry, which has noticed the demand for presenting German solar-thermal and photovoltaic technologies in order to create joint ventures and enable German manufacturers to reach new markets (German–Tunisian Chamber of Commerce and Industry, 2005). In 2005, a programme called PROSOL was established by the Tunisian government. This forced an increase of the annual sale of solar-thermal capacity from 4.9 MW_{th} in 2004 to 58.8 MW_{th} in 2010 (Baccouche, 2011).

In the Middle East, especially, Israel attracts attention due to its high density of thermosyphon solar water heaters. One reason for this has been the legal restraint, introduced in 1980, to install solar-thermal water heaters on newly built houses. Meanwhile solar-thermal applications are accepted and are considered to be a cost-efficient investment. Nowadays four times more solar-thermal systems are voluntarily renewed than are included into new buildings (Pilgard, 2005). The market share of thermosyphon systems newly installed in Israel in 2009 lay at 65 % (Mauthner and Weiss, 2011).

2.1.3 Competition Analysis

In a worldwide competition analysis, the data of more than 50 thermosyphon system manufacturers were collected and evaluated by Brandmayr and Zörner (2007). This analysis was updated and replenished in 2008.

2.1.3.1 Solar Collectors

Thermosyphon systems outside of China commonly use flat-plate collectors (Figure 2.1). Only a few manufacturers have, in most cases, non-pressurized systems with evacuated tube collectors in their product range.

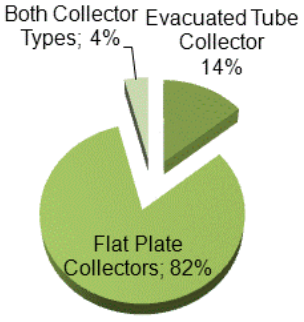

Figure 2.1: Collector Types used in Thermosyphon Systems

In contrast to the rest of the world, solely thermosyphon systems with evacuated tubes are sold in China. There are two main reasons for this:

- Evacuated tubes are produced at very low cost within China. However, these tubes barely reach the quality and durability of those produced in Europe. Therefore, the export share of Chinese solar-thermal products is still low. In 2009 the export share was only at 5 % (Fawer and Magyar, 2009).
- In China, most of the thermosyphon systems sold are non-pressurised systems with only a single hydraulic circuit. In these systems, collector and storage make up one unit as the evacuated tubes are plugged into the storage tank especially perforated for this purpose which, in turn, is easy and low-cost to produce.

Regarding flat-plate collector thermosyphon systems, many manufacturers have several different absorber coatings, according to the climatic and the customers' demands in their programme. In most cases, the same system is available with a solar black painted absorber or a selective coated absorber. According to Meyer (2009), selective coated absorbers are dominating also in thermosyphon systems, whereas non-selective coated absorbers are only used for low standard systems. Nowadays, most manufacturers of thermosyphon systems use ultrasonic welded absorbers for their high standard products. Together with laser welded absorbers these absorbers represent more than 75 % of the used production technology.

2.1.3.2 Storage Tank

Regardless of the collector type used, horizontally installed storage tanks are dominant (94 % market share), vertically oriented storage tanks are an exception (Figure 2.2). The aesthetic advantage of using a horizontal storage tank is that such systems can be built visually compact (Figure 2.3). The installation of horizontally orientated tanks on a system mounting or on an inclined roof is easier. An essential advantage of a vertical storage tank, however, is the achievement of good temperature stratification. Thus, a higher hot water standard for the users can be achieved.

Meyer (2009) shows a trend towards enamelled steel storage tanks. The market share of stainless steel storage tanks fell from 40 % in 2008 to 30 % in 2009.

Figure 2.2: Pressure-Less Thermosyphon System with Vertical Hot Water Storage and Horizontal Supply Tank in Turkey

Figure 2.3: Pressurized System with Horizontal Storage Tank in Greece

2.1.3.3 Hydraulic Circuits

The survey clearly shows the customers' demand for systems that operate under tap pressure. In most cases, non-pressurised systems come along with direct flow evacuated tube collectors (Figure 2.4).

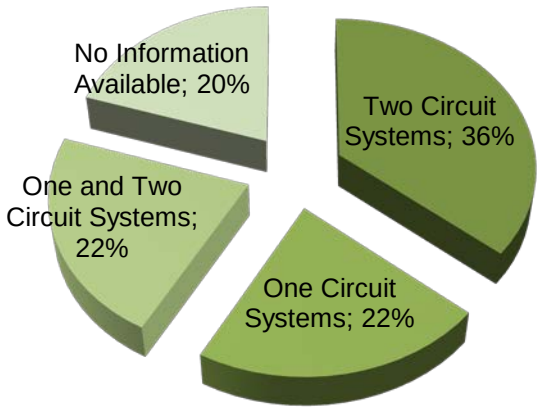

Figure 2.4: Number of Hydraulic Circuits

Distinguishing between one or two circuit systems reveals a trend towards systems with two hydraulic circuits. These systems are the most expensive ones to manufacture. Due to their collector circuit filled with antifreeze, however, they offer one major advantage — they can be used in areas with frost, too. The maintenance of two circuit systems has an

advantage, as possible contaminations, with e.g. lime and particulate material, in tap water, can only be found in the storage tank. During the periodical change of the sacrificial anode the storage tank can be cleaned. In one circuit systems, these contaminations narrow the pipe cross-section and reduce the system performance (Morrison et al., 1998).

2.1.4 Trends

Summarising the market and competition analysis, on the global thermosyphon market two contradictory trends are observed from the central European point of view.

On the one hand, it is necessary to reduce costs, because e.g. German manufacturers have to leave their local, technically well-engineered and expensive markets and are now confronted with competitors from Australia, Greece, Israel, Spain, Turkey and China.

On the other hand, the target markets are affected by a permanently growing standard of living coming along with an increasing demand for comfort resulting in higher requirements on the system performance. Additionally, design and aesthetics are equally becoming more and more important (Figure 2.5).

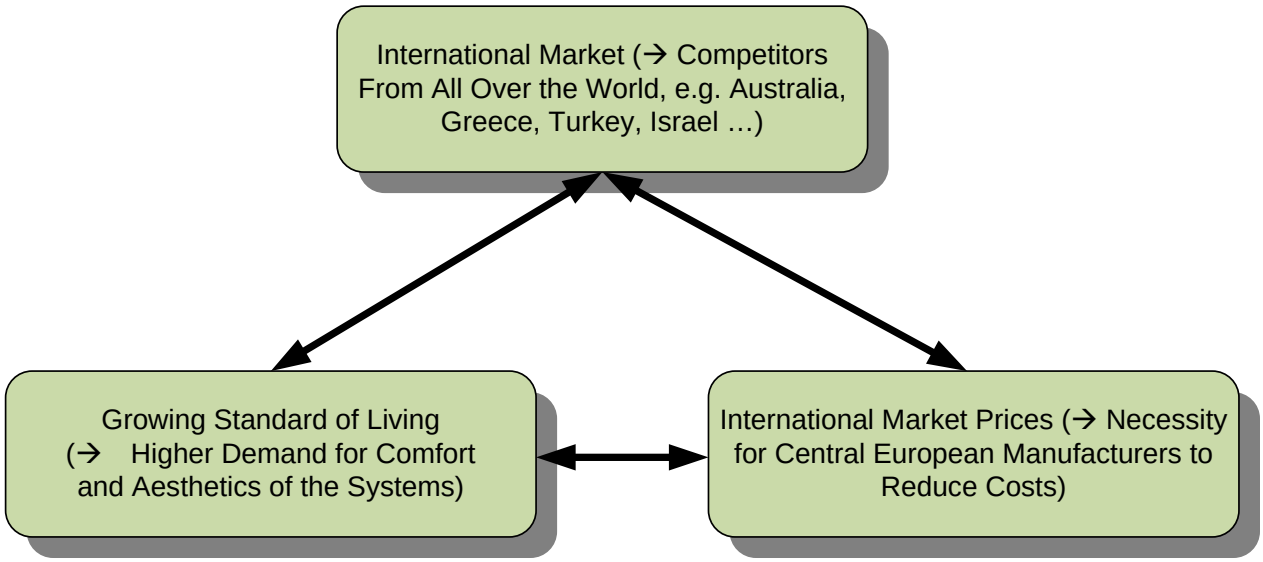

Figure 2.5: Contradictory Trends on the Thermosyphon Market

2.2 Comprehensive Literature Review

A simple approach to illustrate possible thermosyphon system configurations is shown in Table 2.2. By multiplying the number of solutions in each row, there are theoretically

about 8,750 possibilities to generate more or less efficiently working thermosyphon systems. In fact, this is only a theoretical figure, as some combinations are mutually exclusive, like a system with no additional heat exchanger, water/glycol as heat transfer medium and one circuit.

Table 2.2: Theoretical system configurations

	Solar Collector(s)		
Collector Type	flat-plate collector	polymeric tube or foil collector	evacuated-tube collector
Glazing	unglazed	glazed	multi-glazed
Coating	black paint	solar paint	selective coating
	Storage Tank		
Arrangement	horizontal tank	vertical tank	
Heat Exchanger Configuration	no additional heat exchanger needed	double mantle heat exchanger	pipe heat exchanger
	Heat Transfer Medium		
Type	water	water/glycol mixture	phase-change fluid
	Hydraulics		
Number of Hydraulic Circuits	1	2	
System Pressure	non-pressurised	pressurised	partly pressurised
	System Layout		
Storage / Collector Position	storage above collector	collector outlet at the same height as storage top edge	storage below collector top edge

The state-of-the-art systems use either evacuated-tube collectors or flat-plate collectors as energy source, which halves the number of possibilities already.

In the last decade, scientific work on direct flow evacuated tube system testing, development, simulation and optimisation was published exemplarily by Budihardjo et al. (2002, 2003, 2007), Morrison et al. (2004, 2005) and Budihardjo and Morrison (2009). The major disadvantage of direct flow evacuated tube systems is their limited pressure resistance as the evacuated absorber tube is directly plugged into the storage tank (Figure 2.6).

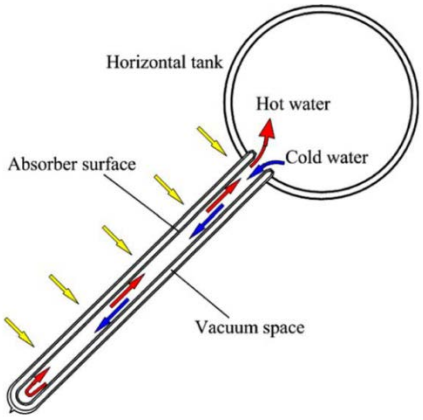

Figure 2.6: Scheme of a Close-Coupled Direct Flow Evacuated Tube System (Morrison et al., 2004)

Redpath et al. (2009, 2010) and Redpath (2012) focused on thermosyphon evacuated tube heat-pipe systems with special regard to northern maritime climate. The collectors used for the experimental investigation of the proposed system layout were standard heat pipe solar collectors, combined with an experimental storage tank setup (Figure 2.7). The annual performance was found to be dependent on the position of the condenser. The system with the condenser located inside the fluid manifold outperformed the system using condensers clamped to the manifold. The diurnal performance of heat pipe thermosyphon system also depends on the inclination of the manifold to the horizontal.

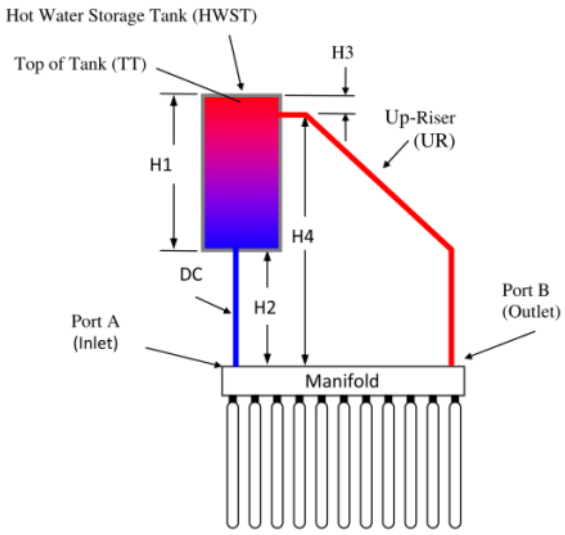

Figure 2.7: Schematic View of the Heat Pipe Thermosyphon System Investigated by Redpath (2010)

The pressure resistance of such a heat pipe thermosyphon system however depends on the design of the manifold. As tap water is directly circulating through the collector manifold, a good water quality is needed to avoid lime and particulate material at the conden-

ser.

Chow et al. (2011) experimentally and numerically compared a direct flow with a similar heat pipe evacuated tube system under climatic conditions of Hong Kong (CN). The heat pipe system slightly outperformed the direct flow system. By performing an additional cost analysis and calculating the payback time based on a TRNSYS simulation, the authors found a flat-plate collector thermosyphon system (not tested during the experiments) to be more suitable for Hong Kong, than evacuated tube collector systems. A second comparative study by Huang et al. (2010) favoured flat-plate collectors for the use in the Chinese province Kunming. Their experiments used a direct flow evacuated tube system, a direct flow flat-plate collector system and a two circuit flat-plate collector system filled with anti-freeze in the collector circuit. Under the given test conditions the direct flow flat-plate collector system performed best, but was not recommended due to its low freeze protection. The direct flow evacuated tube collector system offered a better freeze protection but performed 5 % below the flat-plate collector system. The double mantle heat exchanger storage flat-plate collector system performed in between the two systems mentioned. This system was found by the authors to be recommended for the use in China.

The main focus of this investigation is on southern European and Northern African customer demands. Therefore, literature on thermosyphon systems with emphasis on systems using flat-plate collectors is reviewed in detail. Flat-plate collector systems with phase-changing heat transfer medium have been exemplarily investigated by Yilmaz (1991), Hussein (2003), Nada et al. (2004), Esen and Esen (2005), Chen et al. (2009), Chien et al. (2011) and Ordaz-Flores et al. (2011). Those thermosyphon systems are reported to work at daily system efficiency comparable or even slightly better to fluid driven thermosyphon systems. The problem coming along with phase change heat transfer mediums like R134a and R407C is the big global warming potential when getting into air. Thermosyphon systems working by evaporating ethanol have to be evacuated to lower the boiling point of ethanol from 78.2 °C at ambient pressure p_{abs} = 1013 mbar to p_{abs} = 150 mbar and 34 °C, a pressure measured in a thermosyphon system tested at the University's testing rig. Those systems however have to be completely preassembled at the manufacturer to control the filling and sealing processes and to ensure proper system functionality.

This thesis focuses on fluid driven flat-plate collector thermosyphon systems with double

mantle heat exchangers, as those systems are found to offer a durable, freeze resistant and good performing solution for the daily hot water preparation.
Besides literature on thermosyphon systems, interesting and transferable developments in other fields of (solar-)thermal engineering are also taken into consideration in this thesis.

For annual analyses of solar thermal systems the solar fraction f_{sol} is considered. According to ISO 9488 (1999) the solar fraction is defined as “energy supplied by the solar part of a system divided by the total system load.”

$$f_{sol} = \frac{Q_{sol}}{Q_{load}} \tag{2.1}$$

with

f_{sol}	Solar Fraction	[-]
Q_{sol}	Solar Energy Supply	[kWh]
Q_{load}	Total System Load	[kWh]

Equation (2.1) is valid for solar only and solar preheat systems and also applied in test standard DIN EN 12976-2 (2006). If a backup heating device is included into the solar storage tank the solar fraction is commonly defined according to Duffie and Beckmann (2006) (equation (2.2)). This definition is used for the calculations throughout this thesis.

$$f_{sol} = \frac{Q_{load} - Q_{aux}}{Q_{load}} \tag{2.2}$$

with

f_{sol}	Solar Fraction	[-]
Q_{aux}	Auxiliary Energy Supply	[kWh]
Q_{load}	Total System Load	[kWh]

According to this definition of f_{sol} all storage tank heat losses are included in the solar fraction. But a certain portion of the occurring heat losses only exist when the storage

tank is kept at a certain temperature by the conventional heating system. Scheller (1985) discussed this problem more in detail.

2.2.1 System Level

Gupta and Garg (1968) observed that the temperature increase between inlet and outlet of a collector in a thermosyphon system is nearly constant during times of sunshine. Nowadays, a selective coated collector in a pumped system is assumed to reach a temperature rise between in- and outlet of about 10 °C, while modern thermosyphon systems work in the range of 10–30 °C depending on the system configuration.

An interesting detail of Gupta and Garg's investigation is a height variation between collector header and the bottom of the storage tank in the range of -0.3 – +0.6 m. For their experimental trials they used a one-circuit thermosyphon system filled with water. Under clear sky conditions there is nearly no measurable height dependency of the storage tank temperature. But the height differences show a significant influence on the collector flow rates. The higher the storage is located above the collector the higher the flow rate becomes.

Norton and Probert (1983) reported on a thermosyphon system developed by Matushita Electric Works Ltd. (Iwata et al., 1980) that uses two collectors; one flat tilted summer collector and one steeply inclined collector to achieve maximized system efficiency during winter times (Figure 2.8). A special interest of the development was to prevent the system from reverse thermosyphoning during night. The summer collector is fed by the bottom of the storage tank. The hot summer collector outlet re-enters the storage tank also at its bottom and is piped internally to the top of the storage. The winter collector is fed by a limb at the same height as the collector outlet on the right hand side. In order to cool down the limb, as a hot limb reduces the temperature depending thermosyphonic flow rate, the cold water from mains enters the storage tank through the limb.

Späte (1982) compared the daily energy output of two different one-circuit thermosyphon systems, one with a 1.5 m² meander type absorber and a 110 l storage tank volume and the other with two header-riser absorbers (1.75 m² in total) and 200 l storage tank volume. The header-riser type shows with 72.6 l m^{-2} h^{-1} high flow rates through its absorber at a given Irradiation of G = 800 W m^{-2} at a low temperature rise of about 5.8 K compared

to 26.0 K temperature rise at a flow rate of 12.7 l m^{-2} h^{-1} within the meander type absorber. Späte concluded that the performance of the meander type absorber system, which was always below the performance of the header-riser type absorber, can be improved by changing the collector type.

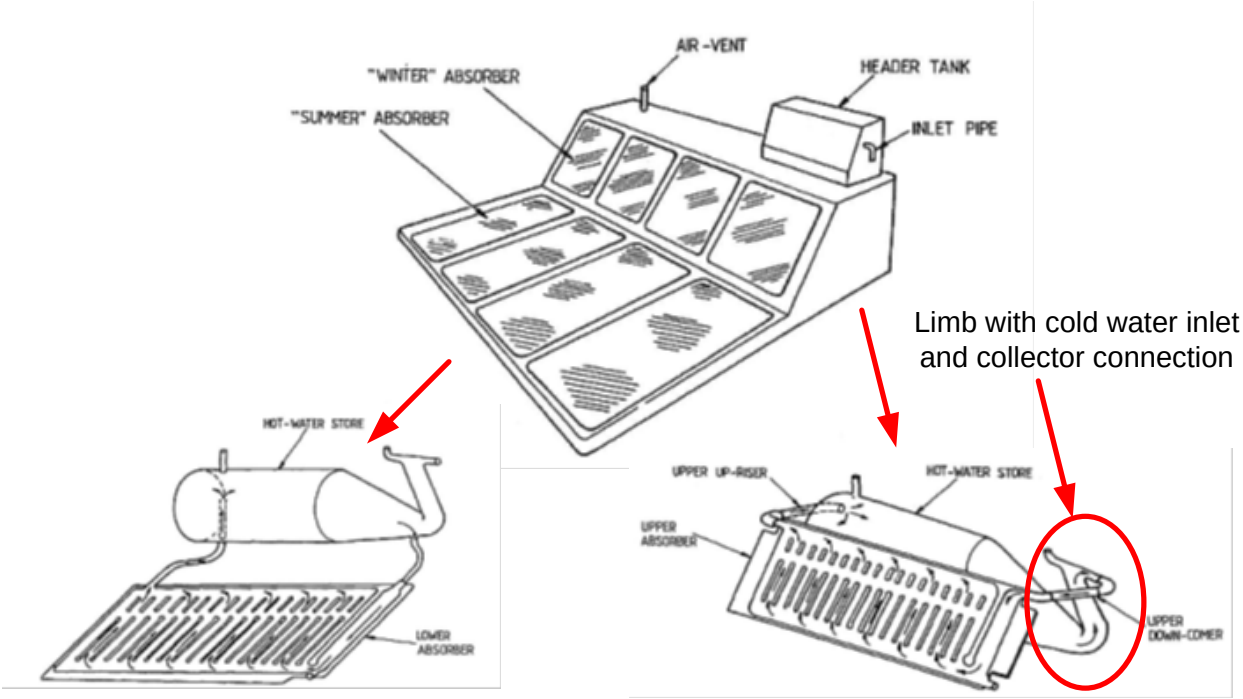

Figure 2.8: Matushita Thermosyphon System with Winter and Summer Collector (Norton and Probert, 1983)

Scheller (1985) compared thermosyphon and pumped solar-thermal systems under the climatic conditions of Central Europe. He came to the result that there is nearly no difference in the annual solar fraction of thermosyphon systems and pumped systems in case of a one family household use. The influence of the storage tank volume on the annual solar fraction is not distinctive. Hence, it is not necessary to adjust the storage tank volume to the collector area (up to 5 m²). From the economic point of view storage volumes of 100-200 l shall be chosen.

Scheller also investigated the influence of the piping within the collector and concluded that a diameter of 10 mm shall be preferred for an optimum system performance. Bigger diameters have neither a positive nor a negative influence. As far as the heat exchanger inside the storage tank, in this case a pipe heat exchanger, is concerned, a surface area of 2 m² shall be implemented into the storage. A heat exchanger surface of only 1 m²

leads to a reduced solar fraction in the range of 7–10 %. Scheller´s work includes also a design approach to avoid reverse thermosyphoning during night. By piping the collector outlet through the bottom of the storage and the collector inlet through the collector casing, thermal losses of inlet and outlet piping are equal, hence reverse thermosyphoning does not occur as shown in Figure 2.9 case (B).

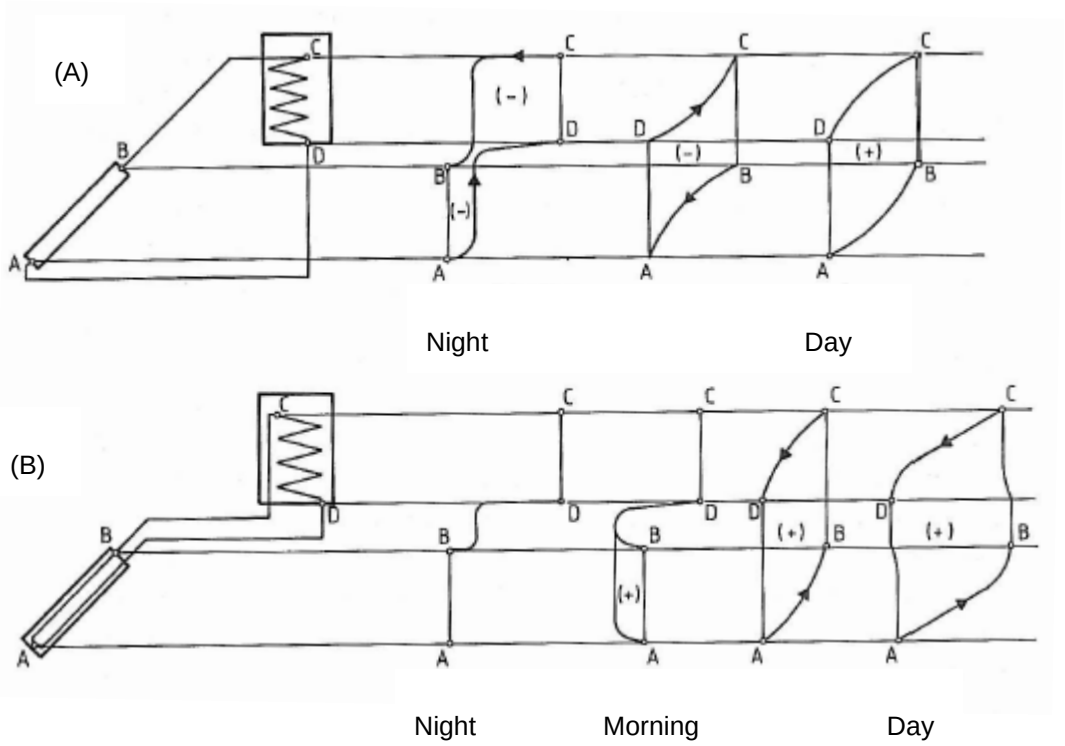

Figure 2.9: Approach to Avoid Reverse Thermosyphoning (Scheller, 1985)

Gmür (2002) developed a non-return valve with a silicon foil membrane in order to avoid reverse thermosyphoning mechanically (Figure 2.10). This solution, however, introduces an additional flow resistance to the system that can have a negative effect on the thermosyphonic flow rate.

Figure 2.10: Foil Membrane Non-Return Valve (Gmür, 2002)

Morrison and Braun (1985) developed a mathematical thermosyphon model for flat-plate absorber systems which is up to now a standard subroutine in TRNSYS (Transient System Simulation Program; Klein et al., 1997), a commonly used simulation tool in solar engineering. The model is validated with measurement data of two different one-loop thermosyphon systems. Using the model, the performance of a pumped and a thermosyphon system is compared. Operated at a daily load volume (M_{load}) to daily collector flow rate (M_{col}) of $M_{col}/M_{load} = 1$ (Figure 2.9), both system types show a very similar performance.

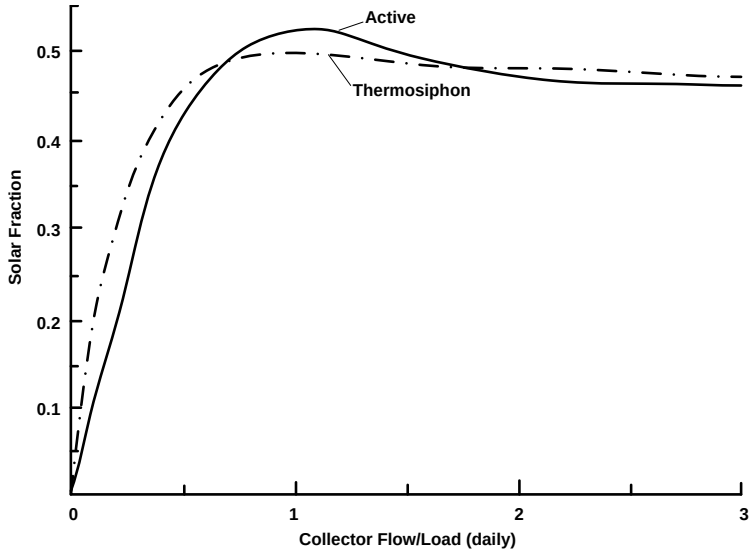

Figure 2.11: Comparison of Pumped and Thermosyphon System Performance (cf. Morrison and Braun, 1985)

Comparing a pumped system at high flow rate to a thermosyphon system at the optimum ratio of $M_{col}/M_{load} = 1$, the thermosyphon system outperforms the pumped system due to a better thermal stratification inside the storage tank. Comparing a thermosyphon system

with a vertical tank to one with a horizontal tank, the vertical storage tank system performs at $M_{col}/M_{load} = 1$ by about 6 % better than the horizontal system. Both thermosyphon systems had an auxiliary heater in order to keep the upper part of the storage tank at a desired temperature of 63 °C.

Shariah et al. (1994) carried out a computer simulation in order to achieve optimised design parameters for thermosyphon systems with vertical storage tanks under the climatic conditions of Los Angeles. Concerning collector parameters, heights of in- and outlet and also tank volume, a sensitivity analysis using solar fraction and system efficiency as target values was carried out.

In order to improve existing systems tested according to the method given in Standard ISO 9459-2 (ISO, 1995), Belessiotis and Mathioulakis (2001) developed a simple approach to link the main design parameters of a solar only thermosyphon system, which means there is no additional backup heating facility, to the measurement results represented by equation (2.3):

$$Q_{sys} = a_1 H + a_2 (T_{ini} - T_{amb,mean}) + a_3 \qquad (2.3)$$

with

a_1	Coefficient 1 from Linear Regression	[m²]
a_2	Coefficient 2 from Linear Regression	[MJ K^{-1}]
a_3	Coefficient 3 from Linear Regression	[MJ]
H	Daily Solar Radiation	[MJ m^{-2}]
Q_{sys}	System Energy Output under Test Conditions	[MJ]
$T_{amb,mean}$	Mean Ambient Temperature	[°C]
T_{ini}	Tank Temperature Before and After the Test	[°C]

First, the instantaneous energy balance of the system including collector and storage tank are drawn setting heat losses in the piping to zero. Afterwards, the equation is integrated over the testing period. The result of this integration is equation (2.4), which is quite similar to equation (2.3):

$$Q_{sys} = s_1 H + s_2 (T_{ini} - T_{amb,mean}) \tag{2.4}$$

$$s_1 = \frac{ki_{mean} A_{col} \eta_0}{1 + \frac{(MC)_{col}}{(MC)_{store}} + \frac{(UA)_{col}}{(UA)_{exch}} + \frac{\Delta t (UA)_{col}}{2(MC)_{store} + \Delta t (UA)_{store}}} \tag{2.5}$$

$$s_2 = \frac{-2\Delta t (UA)_{col}}{\left(2 + \frac{\Delta t (UA)_{store}}{(MC)_{store}}\right)\left(1 + \frac{(MC)_{col}}{(MC)_{store}} + \frac{(UA)_{col}}{(UA)_{exch}}\right) + \frac{\Delta t (UA)_{col}}{(MC)_{store}}} \tag{2.6}$$

with

A_{col}	Collector Aperture Area	[m²]
H	Daily Solar Radiation	[MJ m^{-2}]
ki_{mean}	Mean Incidence Angle Modifier	[-]
$(MC)_{col}$	Thermal Collector Capacity	[J K^{-1}]
$(MC)_{store}$	Thermal Storage Tank Capacity	[J K^{-1}]
Q_{sys}	System Energy Output	[MJ]
s_1	Calculated Coefficient 1	[m²]
s_2	Calculated Coefficient 2	[MJ K^{-1}]
T_{ini}	Tank Temperature Before and After the Test	[°C]
$T_{amb,mean}$	Mean Ambient Temperature	[°C]
$(UA)_{col}$	Collector Heat Loss Coefficient	[W K^{-1}]
$(UA)_{exch}$	Overall Heat Transfer Coefficient of the Heat Exchanger	[W K^{-1}]
$(UA)_{store}$	Tank Heat Loss Coefficient	[W K^{-1}]
Δt	Sunlit Period	[s]
η_0	Zero Loss Efficiency	[-]

If there is measurement data available, the system behaviour can be parametrically optimised by varying the main physical values of the thermosyphon system. Figure 2.12 exemplarily shows the influence of the heat transfer coefficient on the daily energy output of

the whole system. In the design phase, this approach can also be used to identify technical problems.

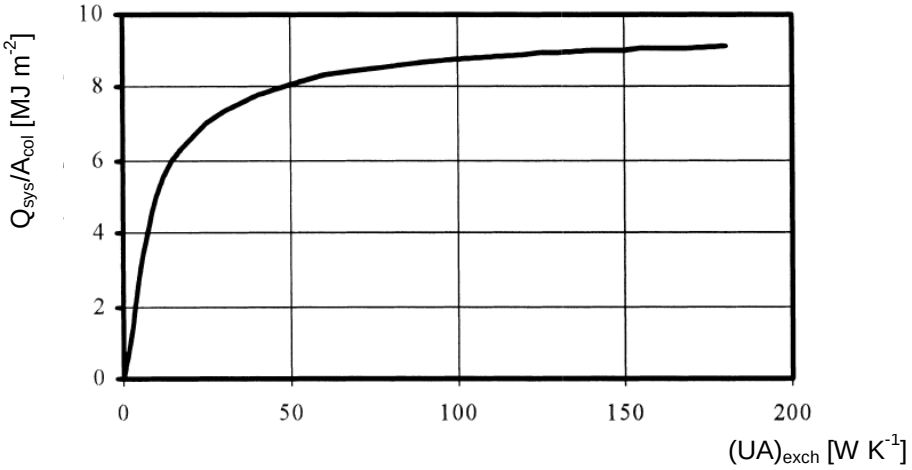

Figure 2.12: Variation of Energy Output as a Function of the Heat Transfer Coefficient of the Heat Exchanger (Belessiotis and Mathioulakis, 2001)

In 2006, Wilhelms and Schabbach (2006) carried out a study within the project 'NEGST' (New Generation of Solar-Thermal Systems) comparing drain back pumped solar systems with thermosyphon systems for the Southern European market and came to the conclusion that thermosyphon systems outperform drain back systems in terms of energetic amortisation and that both system types are quite similar concerning the annual gained energy.

The various publications on system level are of great value concerning the development of the optimised thermosyphon solar hot water heater. One of the goals is to design a system setup with a daily collector flow to a load volume ratio of more than 1. This can be achieved in several ways, as e.g. the collector flow rate is a function of collector and storage height and the collector layout. However, it is necessary to investigate whether the results of the analysis of one-circuit systems are transferable to a two-circuit thermosyphon water heater or if there are additional effects which have to be taken into consideration. The discussed analytical system optimisation approach can also be used for the sensitivity analysis within the simulation work package. Reverse thermosyphoning apparently can be avoided either by special valves or by a suitable overall system design. Further literature on thermosyphon systems can be found in the bibliography section in Appendix F.

2.2.2 Solar Collector

In general, solar-thermal collectors can be divided into stationary and sun tracking concentrating collectors. According to Kalogirou (2004), there are three types of stationary collectors, compound parabolic collectors, evacuated-tube collectors and flat-plate collectors. Especially flat-plate collectors are part of this survey.

A flat-plate collector consists out of four main components, the glazing, the absorber, the insulation and the casing (Figure 2.13).

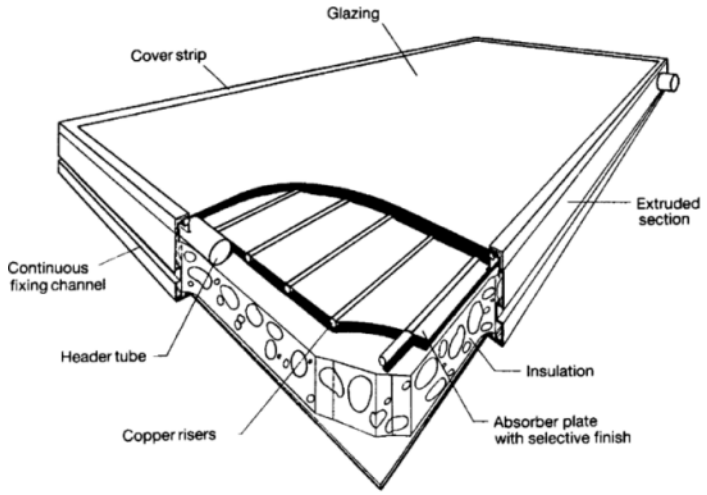

Figure 2.13: Layout of a Flat-Plate Collector (Kalogirou, 2004)

The glazing has a major influence on the collector efficiency. Frei (1998) published typical transmission factors for glazing materials, as shown in Table 2.3. Ruesch and Brunold (2009) published a work dealing with the long-term stability of different glazing materials. The testing period covered 20 years and two different climates. In particular the tested polymers polyvinylchloride (PVC), polycarbonate (PC), unsaturated polyester (UP) and polyethylene terephthalate (PET) heavily degraded and are, therefore, not applicable to collector glazing.

Table 2.3: Comparison of Solar Collector Glazing Materials (Frei, 1998)

Cover Material	Thickness [mm]	Weight [kg m^{-2}]	Transmission [-]
Heat strengthened glass	4	10	0.84
Heat strengthened low iron glass	4	10	0.91
PC	4	4.9	0.80
PMMA	4	4.8	0.84
PMMA (double wall sheet)	16	5.0	0.77

After 20 years of exposure, glass (standard ferrous and low iron glass) and polymethylmethacrylate (PMMA) showed only a small deterioration of their transmission characteristics and can be used for solar collectors. PMMA, however, has some disadvantages making this material not suitable for all glazing applications. It is brittle and has a limited temperature range of use. In the area of PC, currently research is being done with UV filters. One promising attempt is to bond a PMMA layer as UV filter onto a PC glazing (Jorgensen et al., 2005).

According to Frei (1998), heat strengthened low iron glass typically has a transmission coefficient of $\tau = 0.91$. This value even can be improved by using anti-reflective layers on the glass. Anti-reflective layers have a refractive index below $n = 1.3$ which lowers the reflection of sunlight passing the glass (Figure 2.14). Calculation schemes for multiple reflections can be found in Duffie and Beckmann (2006), Eicker (2001) and Khartchenko (2004).

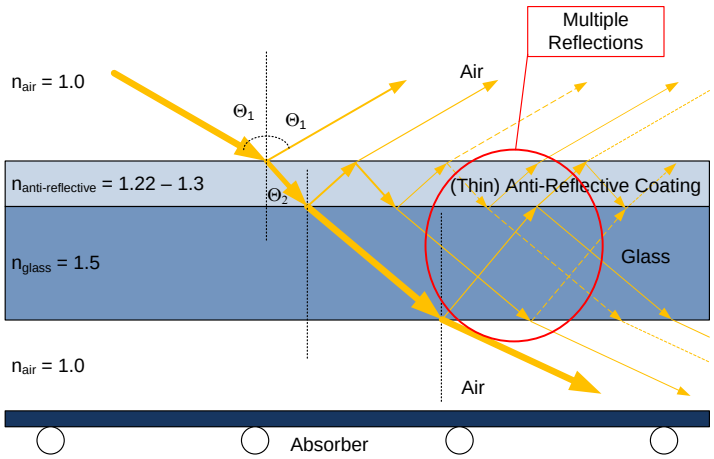

Figure 2.14: Simplified Working Principle of Anti-Reflective Coating Applied on Glass

Gombert et al. (1997) summarised the anti-reflective coating techniques to porous surfaces produced by etching the substrate material, porous sol-gel coatings and sub wavelength surface-relief gratings. Due to its mechanical stability and environmentally friendly production process porous sol-gel coatings are very promising. Porous sol-gel coatings enhance the transmission of light through the glazing by up to 3 % per glass surface, which was proved theoretically and experimentally. The results of this study are in analogy to measurements conducted by Flückinger (2007) resulting in a transmission coefficient of $\tau = 0.96$ for anti-reflective coated solar glass. Furbo and Shah (2003) conducted

a simulation study concerning the influence of anti-reflective collector glazing on the annual system output of a solar domestic hot water system, a solar combi system and a solar thermal heating plant under Danish weather conditions. For the solar domestic hot water systems the annual solar fraction can be enhanced by 10 % starting at a solar fraction of 25 % or 4 % starting at a solar fraction of 60 %. The application of anti-reflective coatings results in a higher transmission of sunlight and a higher energy flux inside the collector. It results in higher stagnation temperatures — this might be a problem when optimising a system already designed for a high annual solar fraction.
In the collector design the material choice for sealants and insulation has to be adapted to these temperatures. The usage of anti-reflective coated glass is coming along with additional costs of approximately 4–6 € per m² (Frei, 2012; Furbo and Shah, 2003[2]).

The solar absorber is the most intensely investigated part of a flat-plate collector. There are three different absorber types more or less suitable for the use in thermosyphon systems, harp, meander and volumetric absorbers (Figure 2.15).

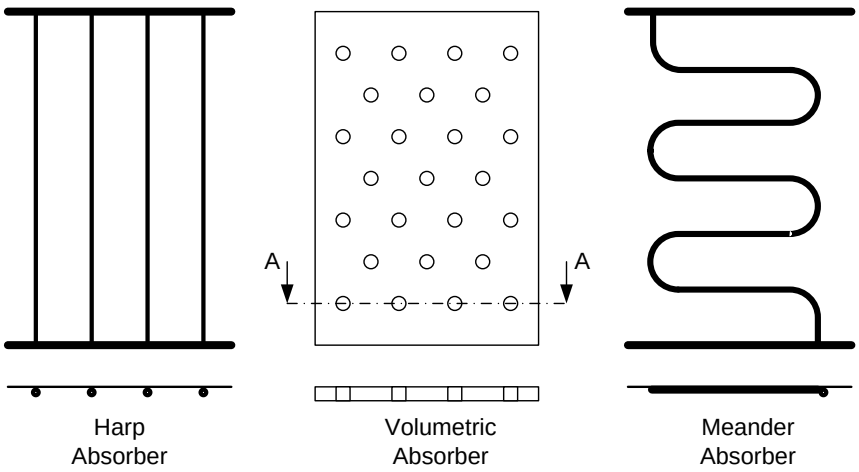

Figure 2.15: Common Flat-Plate Collector Absorber Types

Harp absorbers come along with a low pressure drop, a medium collector efficiency factor F' (cf. equation (2.23)) and in forced circulated systems an inhomogeneous flow distribution in the riser tubes (Weibrecht et al., 2002).

[2]2003: 6 USD per m² approx. 5.30 €

The collector efficiency factor of meander type absorbers is comparable to harp absorbers. Uniform flow distribution is achieved as there is only one riser tube, which, however, causes a high pressure drop.

Volumetric absorbers have a very high efficiency factor at a medium or low pressure drop. Depending on the baffle design, a homogenous flow distribution can be realised. One limitation of most of the volumetric absorbers is the reduced pressure resistance. During times of stagnation, modern (pumped) solar-thermal systems reach up to 5 bar (Viessmann-Werke, 2008).

Figure 2.16 shows the occurring pressure drop for different absorber designs measured at Ingolstadt University and published by a test laboratory. The tests were carried out using water at 20 °C. In thermosyphon systems the flow is driven by buoyancy and so the pressure drop of the solar collector has an influence on the developing flow rate that is not to neglect. A further discussion on the flow rate and flow distribution in different solar thermal systems can be found in Chapter 5.1.

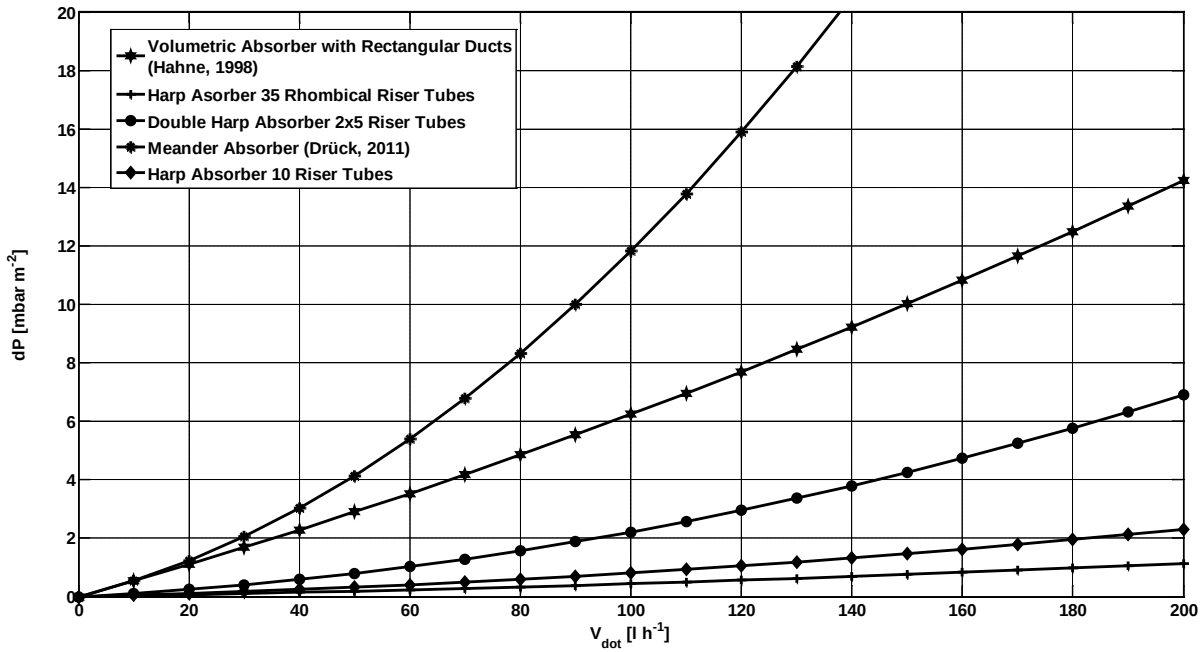

Figure 2.16: Pressure Drop per Square Metre of Different Absorber Types

Treikauskas (2009) investigated the materials used for solar thermal-absorbers in the last 30 years (Table 2.4). Especially in the 1980s many different materials, such as polymers, steel, engineering fibres, aluminium and copper were used.

Table 2.4: Overview of Absorber Materials (excerpt; Treikauskas, 2009)

Material	Advantages	Disadvantages
Aluminium	+ high thermal conductivity + low density → low weight + easy to process + inexpensive	- low corrosion resistance - high energy input for primary Al production
Steel	+ easy to process + inexpensive + low energy input for steel production	- low thermal conductivity - high density → high weight - low corrosion resistance
Copper	+ high thermal conductivity + corrosion resistant + high durability + easy to process	- high density → high weight - expensive
Polymers	+ low density → low weight + corrosion resistant + low energy input for polymer production	- very low thermal conductivity - low temperature durability

Hermann (2005) mentioned roll bond aluminium solar absorbers produced and sold in the 1970s. Those systems disappeared from the market as corrosion problems appeared. The main reason according to Hermann was atmospheric oxygen inside the fluid channels.

Peuser et al. (2001) reviewed collector designs of the past and mentioned the occurring corrosion problems with aluminium collectors being dependent on the materials used in the solar thermal system, the presence of corrosion inhibitors in the solar fluid and the storing of the collectors beforehand to the installation. While storing the collectors without caps on in- and outlet, moisture and particulate material got into the absorber where the oxidation process started.

Aluminium absorbers were coated with nickel pigmented anodized aluminiun known as Sunstrip or Evidal-S coating. Those coatings suffered especially from degradation (oxidation) due to moisture (Figure 2.17, Köhl et al., 1989 and Peuser et al. 2001).

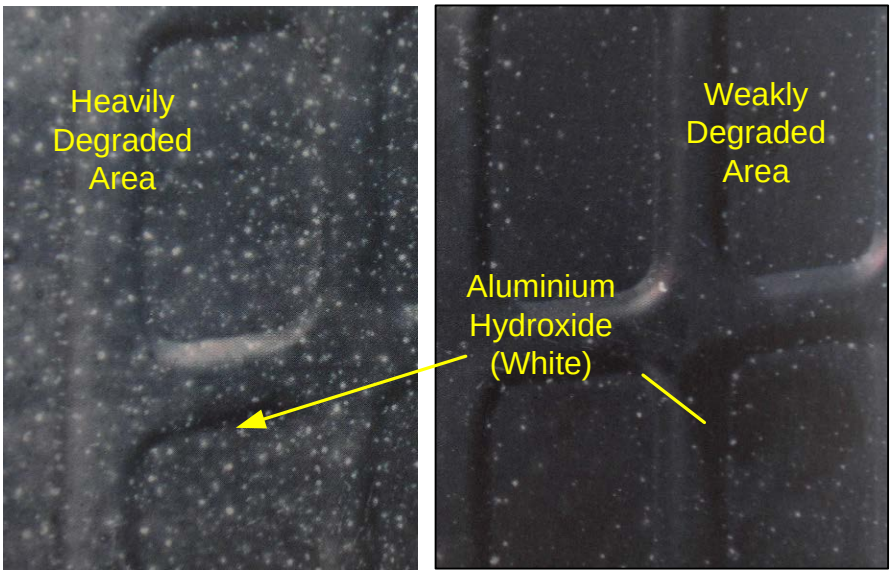

Figure 2.17: Degraded Nickel Pigmented Anodised Roll Bond Absorber (Peuser et al., 2001)

Modern PVD and CVD selective coatings on aluminium, as mentioned later in this Chapter do not show the corrosion problems.

However, well-designed and maintained aluminium collector systems can show a good durability. Hahne (2000) reported about a seasonal storage system with 211 m² collector area for the use in a low temperature heat pump assisted heating system which has been in operation for 15 years. Three different kinds of unglazed aluminium solar collectors (Figure 2.18) were installed. The unglazed non-selective aluminium absorbers have not caused any trouble during operation.

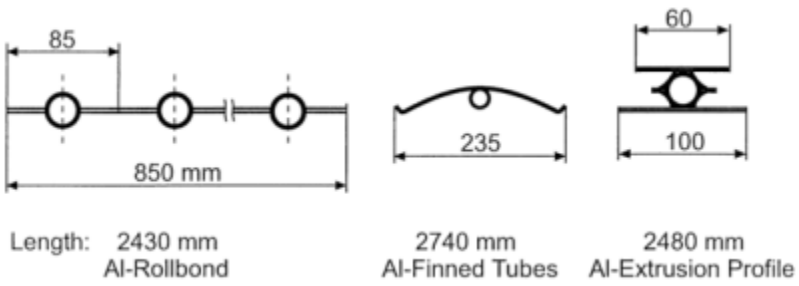

Figure 2.18: Unglazed Aluminium Absorbers for a Seasonal Storage System (Hahne, 2000)

During the 1990s up to the early 2000s absorbers fully made out of copper were predominant, as the copper price was low and copper offered a good corrosion resistance.

To connect absorber and piping, several technologies, such as bonding, clamping, soldering and welding are employed. Nowadays, laser and ultrasonic welding are dominating the market (Treikauskas, 2009).

In 2008 63 % of the solar absorbers produced for the German market used copper sheets. In 2010 already 63 % of the absorber sheets were of aluminium with a predicted increase of further 4 % for 2011 (Meyer, 2011). The reasons for this trend are the corrosion resistance and long-term stability of copper, the reduced material cost for aluminium (Holle, 2011) and the improved manufacturing technology. Epp (2012) showed the price development for copper +154 % and for aluminium +49% in the years from 1995 to 2011 with very volatile copper prices. The trends from the German market can be applied to the rest of Europe.

The corrosion resistant copper pipes are welded to the aluminium absorber sheets. Welding of copper and aluminium comes along with two problems. The first problem are the different temperature expansion coefficients of the metals — $23.8*10^{-6}\,K^{-1}$ for aluminium and $16.8*10^{-6}\ K^{-1}$ for copper (Beitz and Grote, 1997 and Walcher, 1989) — and the material tensions coming along at absorber temperatures different to the manufacturing temperature. The other problem is the galvanic oxidation between aluminium absorber and copper pipes in combination with moisture inside the collector casing. This can be overcome by realising an adequate dry microclimate inside the collector, which is mainly driven by the water adsorption potential of the collector insulation material, cf. Holck et al. (2003) or Köhl et al. (2007).

Ostermann (1998) investigated the contact corrosion of aluminium and copper in general and recommended not to use this material combination in industrial environment, maritime climate and at the presence of any kind of water or moisture.

Kammer (2009) mentioned aluminium absorber designs using extrusion moulding, brazing or clamping of piping and absorber based on a literature review of the 1970s. The aluminium alloys used are pure aluminium out of the [1xxx] family and alloys out of the [3xxx] family. An interesting aspect of the solar collector designs is an aluminium foil applied on the insulation material working as a diffusion barrier for water and thus moisture inside the solar collector.

Nowadays, manufacturers of aluminium alloys deliver pipes for the use in solar thermal systems belonging to the [3xxx] forgeable alloys. The main alloying element used is manganese (Mn). Those one-phase alloys are not thermosetting (Askeland, 1996) and can be welded and brazed. The chemical composition of a market available solar aluminium alloy is shown in Table 2.5.

Table 2.5: Aluminium Alloy for the Use as Absorber Piping (Standard-Metallwerke, 2012)

	Si	Fe	Cu	Mn	Mg	Cr	Zn	Ti	Others		Al
									Single	Total	
S-LIFE SOLAR ®	0.5	0.7	0.1	0.7-1.4	0.3	0.1	0.2	0.1-0.4	0.05	0.15	Remainder

For the brazing of aluminium tubes zinc free fillers are needed, as zinc causes corrosion at high temperatures. The fillers for the brazing process have to be based on aluminium silicium AlSi. According to De Cardernas (2012) drilling of the manifolds and not punching should be preferred to optimise the joint quality.

Holle (2011) recommends avoiding cutting and drilling of copper and aluminium pipes on the same machine at the same time as copper chips and burr residues might remain in the aluminium pipe.

For a proper corrosion protection the heat transfer fluid has to contain corrosion inhibitors. Heat transfer fluids fulfilling this requirement are available on the market. The use of aluminium absorbers in direct solar thermal (thermosyphon) or freshwater circulating systems is not reasonable as freshwater contains atmospheric oxygen which starts oxidation.

Zinc should not be contained in the whole solar thermal system. Brass and copper fittings should be avoided. At brass fittings dezincification takes place at high temperatures (Beitz and Grote, 1997). Hydro (N.N., 2010) recommends stainless-steel, aluminium or non-metallic fittings and pipes. Salt spray corrosion tests have been successfully performed with solar aluminium alloys (Standard-Metallwerke, 2012 and Hydro, 2012).

Two circuit thermosyphon solar hot water systems offer prevailing conditions for full aluminium absorbers. Those systems are delivered as full packages, so the plumber will not use own material, like fittings and pipes.

As the heat conductivity of [3xxx] aluminium is with 180–280 W m^{-1} K^{-1} (Sandner et al., 2006 and Askeland, 1996) lower than the conductivity for copper 385–402 W m^{-1} K^{-1} (Sandner et al., 2006 and Askeland, 1996) the material thickness has to be increased from 0.2-0.25 mm to 0.35-0.45 mm to reach the same collector efficiency. Despite the doubling of the material thickness, the density of aluminium — 2,700 kg m^{-3} — is factor 3 lower than that of copper — 8,930 kg m^{-3} (Beitz and Grote, 1997) — and still results in a weight reduction.

Sharia et al. (1999) varied the thermal conductivity for a given solar collector in a thermosyphon system in the range of 10–400 W m^{-1} K^{-1} using a TRNSYS simulation and incorporating a heating rod in the storage tank. The annual solar fraction increased only by 3 % when switching from aluminium (220 W m^{-1} K^{-1}) to a copper absorber (385 W m^{-1} K^{-1}) keeping the absorber thickness constant (Figure 2.19). The characteristic collector factors — fin efficiency factor F (equation (2.24)), collector efficiency factor F' (equation (2.23)) and heat removal factor F_R (equation (2.16)) were strongly dependent on the materials' heat conductivity.

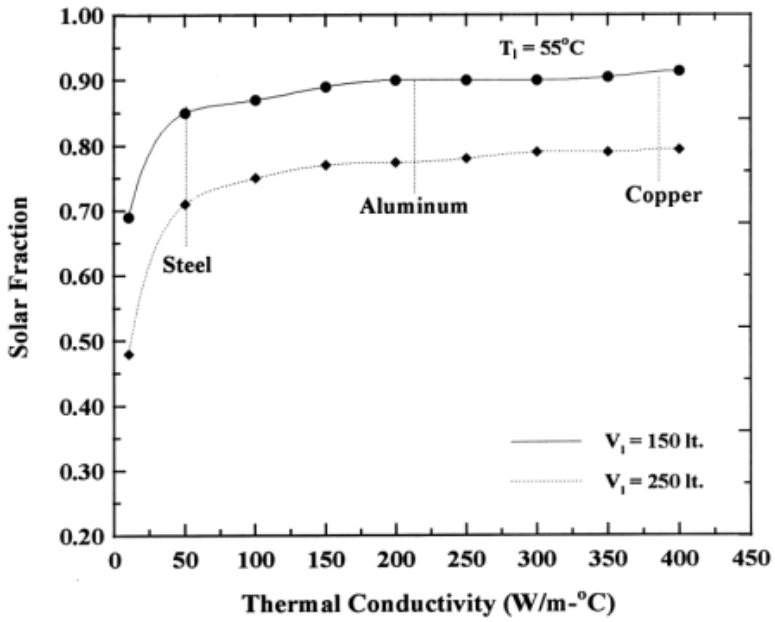

Figure 2.19: Solar Fraction of a Thermosyphon System in Dependence of the Absorber Conductivity at Load Temperature T_l = 55 °C (Sharia et al., 1999)

De Cardenas (2012) compared the costs for manufacturing a 2 m² harp made fully out of copper or aluminium. The raw material and brazing costs for the aluminium only harp were 67 % below the costs for the copper solution.

As the positive facts of full aluminium absorbers are predominant this construction principle is recommended for the thermosyphon system prototype.

In order to improve the energy efficiency of solar-thermal collectors selective coatings were developed. Selective surfaces have a high absorption coefficient α for solar radiation combined with a low emittance ε of long-wave thermal radiation. This combination of absorption and emission values is necessary as 98 % of the incoming radiation is at a wavelength below λ = 3 µm, while 99 % of the radiation emitted by gray or black bodies below 100 °C is above λ = 3 µm (Goswami et al., 2000).

Figure 2.20 shows the solar spectrum outside the earth atmosphere at air mass = 0 (AM0) and after passing the atmosphere at air mass = 2 (AM2). Besides the solar spectrum, the temperature depended blackbody radiation or thermal emission is shown. According to this diagram, an ideal selective coating has unity absorptance beginning at λ = 0.2 µm. The wave length of the shift to unity reflectance depends on the application. For collectors working at an absorber temperature below T_{abs} = 100 °C, the switching point shall be in the range of 3 µm < λ < 5 µm (Buhrmann, 1983 andGoswami et al., 2000). The transition for high temperature applications, meaning T_{abs} > 200 °C, has to be in the range of 2 µm < λ < 3 µm (Buhrmann, 1983) as highlighted in Figure 2.20.

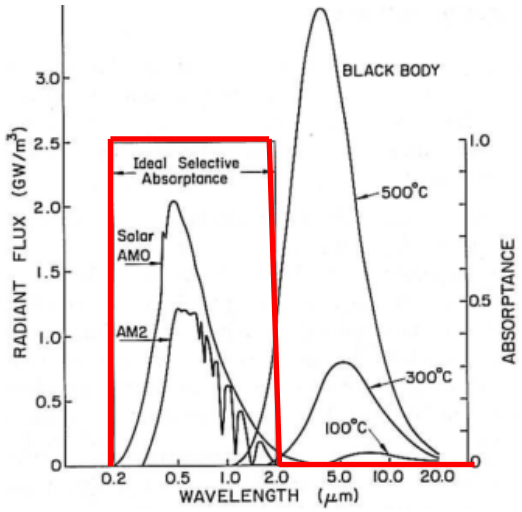

Figure 2.20: Solar Radiation Before and After Passing the Atmosphere and Blackbody Radiation (Buhrmann, 1983)

Up to the 1970s, non-selective black paint was used to coat the absorber coming along with the negative effects of blackbody radiation. Thereafter, medium selective coatings

like black chrome coatings were developed. Nowadays, black chrome is still used in solar-thermal applications. Figure 2.21 shows the selective characteristics of 3 different black chrome coatings. Beginning at λ = 2 μm, black chrome starts switching from good absorptance to high reflectance.

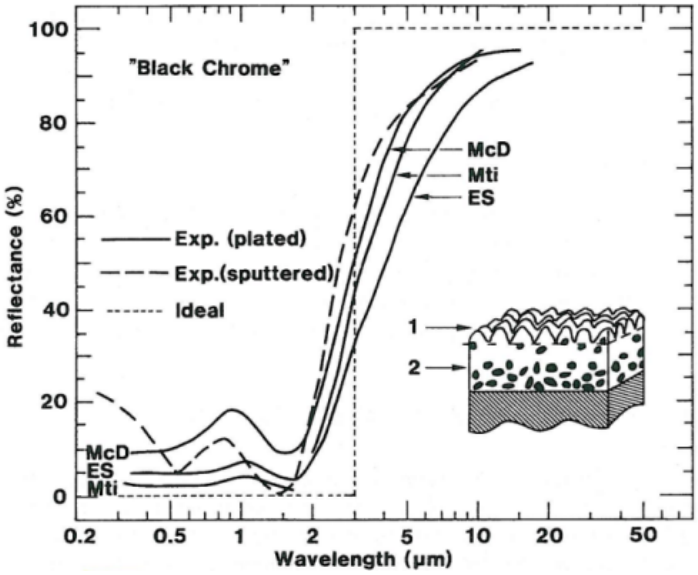

Figure 2.21: Selective Characteristics of Different Black Chrome Coatings (Niklasson and Granqvist, 1991)

Corresponding to Drück (2009) black chrome coatings suffer above all from oxidation caused by moisture, oxygen, sulphur dioxide, nitrogen oxide and salt, causing an increasing emission coefficient and a decreasing absorption potential. In order to improve the long-term stability and to further reduce the emissions, new absorber coatings have been developed in the past.

State-of-the-art are highly selective surfaces. Such surfaces are applied using different deposition methods, like Physical Vapour Deposition (PVD) or Chemical Vapour Deposition (CVD) and consist for example of Titan-Nitride-Oxide (TiNOX) or cermets. Drück (2009) compared the efficiency and stagnation temperature of different coatings at G = 1,000 W m^{-2}, $T_{absorber}$ = 50 °C and T_{sky} = 20 °C (Table 2.6).

Table 2.6: Optical and Thermal Characteristics of Different Coatings (excerpt; Drück, 2009)

Material	**Non Selective Black Paint**	**Black Chrome**	**TiNOX**
α [–]	0.98	0.96	0.95
ε [–]	0.98	0.14	0.05
T_{stag} [°C]	125	325	492

In order to minimise the heat losses from the back of flat-plate solar collectors (U_b), insulation in the range of 30–60 mm thickness is integrated into the collector casing. Solar collectors used in Central or Northern Europe are additionally insulated at the casing side in the range of 10–25 mm. The insulation materials used are either mineral wool or a combination of mineral wool and polyurethane foam (Table 2.7). This combination is necessary as the long-term stability of polyurethane is limited to 90 °C. But then, polyurethane is a better insulation material compared to mineral wool. In order to reflect the emitted blackbody radiation from the absorbers backside an aluminium foil can be laminated onto the insulation material.

Table 2.7: Temperature Range, Heat Conductivity and Cost of Various Insulation Materials (Reyer et al., 2002; Roesch, 1999)

Material	**Maximum Temperature [°C]**	**Heat Conductivity [W m^{-1} K^{-1}]**	**Cost [€ m^{-3}]**
Foam Glass	600	0.045–0.110	275-400
Mineral Wool	550-900	0.040–0.080	50-200
Polyurethane	90	0.025–0.060	125-245
Coconut Fibre	270	0.040–0.080	50-200

Andoh et al. (2010) compared two nearly identical thermosyphon systems under the conditions of Ivory Coast, Africa. At one collector 50 mm coconut fibre insulation was applied, while the other collector was insulated using a 50 mm glass wool layer. The system using the glass wool insulation performed at an overall efficiency of 58 %, 6 % better than the coconut fibre insulated collector. However, the material costs for coconut fibre under the market conditions of Ivory Coast are 25 % less than those for the glass wool collector. To compare both insulation materials seriously, not only the material costs have to be considered. The energetic difference in combination with the local price per kWh heat has to be calculated over the estimated life cycle of such a water heater. This life cycle analysis shall be relevant for the material choice.

The overall heat loss U_L in a flat-plate collector is the sum of top losses from the transparent glazing U_t, edge losses from the perimeter of the collector casing U_e and losses through the insulated collector bottom U_b (equation (2.7)).

$$U_L = U_t + U_e + U_b \tag{2.7}$$

with

U_L	Overall Heat Loss	[W m^{-2} K^{-1}]
U_t	Top Heat Loss	[W m^{-2} K^{-1}]
U_e	Edge Heat Loss	[W m^{-2} K^{-1}]
U_b	Bottom Heat Loss	[W m^{-2} K^{-1}]

At the collector outer surface both convective and radiative heat losses occur. The convective heat losses h_h are mainly driven by the wind speed, while the radiative losses h_r occur due to temperature differences between the collector and the ambient. Equation (2.12) represents the basic calculation of the backside and edge losses. According to Eicker (2001) the losses $1/h_h + 1/h_r$ can be set to a constant value of 0.04 m² K W^{-1}.

$$U_{b,e} = \left(\frac{z}{k} + \frac{1}{h_h} + \frac{1}{h_r} \right)^{-1} \tag{2.8}$$

with

$U_{b,e}$	Edge/Bottom Heat Loss	[W m^{-2} K^{-1}]
z	Insulation Thickness	[m]
k	Heat Conductivity Insulation	[W m^{-1} K^{-1}]
h_h	Convective Heat Loss	[W m^{-2} K^{-1}]
h_r	Radiative Heat Loss	[W m^{-2} K^{-1}]

The edge losses are referenced to the collector area, as an accurate calculation is complicated (Duffie, Beckmann, 2006). This is possible as the influence of the edge losses in a well-designed system is rather small (equation (2.9)).

$$U_e = \frac{(UA)_e}{A_{col}} \tag{2.9}$$

with

U_e	Edge Heat Loss	[W m^{-2} K^{-1}]
$(UA)_e$	Edge Loss Coefficient - Area Product	[W K^{-1}]
A_{col}	Collector Area	[m²]

The top losses can be described as the result of convection and radiation between parallel plates (Duffie, Beckmann, 2006). Under stationary conditions Khartchenko (2004) summarises the heat flux through the glazing being equal to the thermal losses of the absorber in glazing direction. This allows the following equation (2.10).

$$U_t = \left(\frac{1}{h_h} + \frac{1}{h_r} \right)^{-1} \tag{2.10}$$

with

U_t	Top Heat Loss	[W m^{-2} K^{-1}]
h_h	Convective Heat Loss	[W m^{-2} K^{-1}]
h_r	Radiative Heat Loss	[W m^{-2} K^{-1}]

Figure 2.22 shows a sectional drawing of a typical flat-plate collector with the occurring heat losses. The distance $z_{spacing}$ between absorber and glazing directly influences the top losses and the edge losses of the solar collector, while the insulation thickness $z_{insulation}$ only influences the bottom losses.

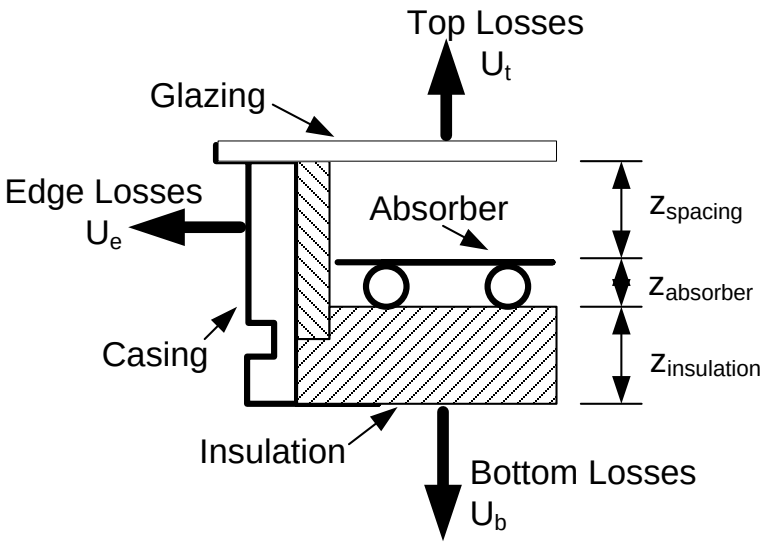

Figure 2.22: Sectional Drawing of a Typical Flat-Plate Collector

Vestlund et al. (2009) analysed the thermal performance of gas-filled flat-plate collectors. According to their simulation, the overall heat loss U_L of a sealed inert gas filled solar-thermal collector can be improved by 20 % compared to an air filled collector. They found two optimum distances for the height of $z_{spacing}$ independent of the gas used. The first is in the range of $z_{spacing}$ = 3–9 mm followed by a local maximum of heat losses. The other minimum can be found in the range of $z_{spacing}$ = 30–45 mm. As the optimum distance between absorber and glass directly depends on the collector slope γ and the (design point) fluid temperature, the distance $z_{spacing}$ has to be calculated for the specific case of operation. The short distance minimum of an air filled solar collector is found to vary from $z_{spacing}$ = 7.5 mm at γ = 15 ° and T_{fluid} = 100 °C to $z_{spacing}$ = 9.2 mm at γ = 60 ° and T_{fluid} = 25 °C.

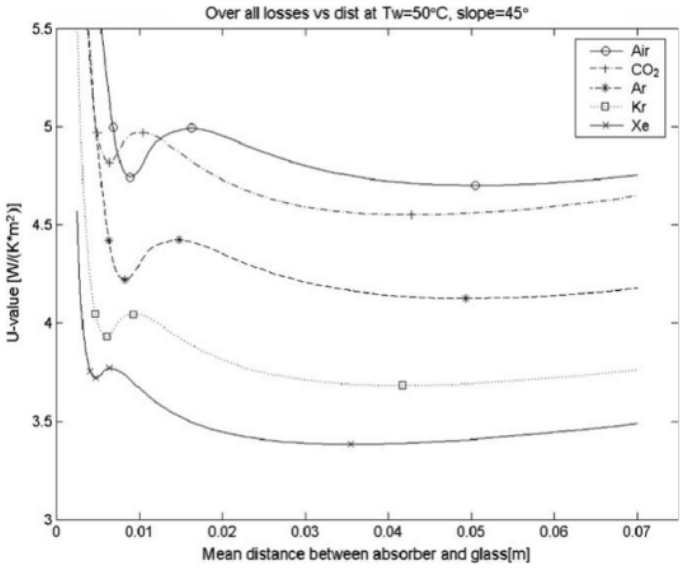

Figure 2.23: Influence of the Spacing and Gas Filling between Absorber and Glazing on the Overall Collector Heat Loss (Vestlund et al., 2009)

The efficiency of a (glazed) flat-plate collector can be described as the ratio of available solar energy at the collector glazing and the usable outgoing heat flux (equation (2.11)).

$$\eta = \frac{\dot{Q}_{use}}{A_{abs} G} = \frac{\dot{m} c (T_{out} - T_{in})}{A_{abs} G} \tag{2.11}$$

with

A_{abs}	Absorber Area	[m²]
c	Heat Capacity Fluid	[J kg^{-1} K^{-1}]
G	Solar Irradiation	[W m^{-2}]
$\dot{m}$	Mass Flow Rate	[kg s^{-1}]
T_{in}, T_{out}	Collector In- and Outlet Temperature	[°C]
$\dot{Q}_{use}$	Usable Energy	[W]
η	Collector Efficiency	[-]

The usable heat flux is given by the energy available after passing the glazing and the absorbers (selective) surface minus the occurring overall collector heat losses U_L caused by temperature differences (equation (2.12) and (2.13)).

$$\dot{Q}_{use} = (\tau\alpha)_{eff} A_{abs} G - U_L (T_{abs} - T_{amb}) A_{abs} \quad (2.12)$$

$$\eta = \underbrace{(\tau\alpha)_{eff}}_{\eta_0} - \frac{U_L (T_{abs} - T_{amb})}{G} \quad (2.13)$$

with

A_{abs}	Absorber Area	[m²]
G	Solar Irradiation	[W m^{-2}]
T_{abs}	Absorber Temperature	[°C]
T_{amb}	Ambient Temperature	[°C]
U_L	Overall Collector Heat Losses	[W m^{-2} K^{-1}]
η_0	Zero Loss Efficiency	[-]
η	Collector Efficiency	[-]
$(\tau\alpha)_{eff}$	Effective Transmission/Absorption Product (optical characteristics of the transparent cover and the absorber surface)	[-]

The zero loss efficiency η_0 is the efficiency of the collector, if the mean fluid temperature or the inlet fluid temperature (depending on the selected collector equation) is equal to the ambient air temperature (ISO 9488, 1999).

For multiple reflections between absorber and transparent cover, the effective transmission absorption product can be summarised to equation (2.14) (Duffie and Beckmann, 2006, Eicker, 2001).

$$(\tau\alpha)_{eff} = \frac{\tau\alpha}{1 - (1 - \alpha)\rho_{glass}} \quad (2.14)$$

with

α	Absorption Coefficient	[-]
τ	Transmission Coefficient	[-]
ρ_{glass}	Reflexion Coefficient of the Glazing	[-]
$(\tau\alpha)_{eff}$	Effective Transmission/Absorption Product	[-]

According to Duffie and Beckmann (2006) and Khartchenko (2004) typical values of $(\tau\alpha)_{eff}$ for single glazed solar collectors are 1–2 % higher than the values of $(\tau\alpha)$. By introducing a correction factor, the heat removal factor F_R (Kalogirou, 2004), the average absorber temperature T_{abs} can be replaced by the collector inlet temperature T_{in} (equation (2.15) and (2.16)).

$$\dot{Q}_{use} = (\tau\alpha)_{eff} A_{abs} G - U_L (T_{in} - T_{amb}) A_{abs} F_R \quad (2.15)$$

$$F_R = \frac{\dot{m}c}{A_{abs} U_L} \left(1 - \exp\left[- \frac{U_L F' A_{abs}}{\dot{m}c} \right] \right) \quad (2.16)$$

with

A_{abs}	Absorber Area	[m²]
c	Heat Capacity Fluid	[J kg^{-1} K^{-1}]
F_R	Heat Removal Factor	[-]
F'	Collector Efficiency Factor (equation (2.23))	[-]
G	Solar Irradiation	[W m^{-2}]
$\dot{m}$	Mass Flow Rate	[kg s^{-1}]
U_L	Overall Collector Heat Losses	[W m^{-2} K^{-1}]
$\dot{Q}_{use}$	Usable Energy	[W]
T_{amb}	Ambient Temperature	[°C]
T_{in}	Collector Inlet Temperature	[°C]
$(\tau\alpha)_{eff}$	Effective Transmission/Absorption Product	[-]

The heat removal factor F_R can be considered as the ratio of heat actually delivered to that if the collector plate were at a uniform temperature equal to the inlet temperature (Kalogirou, 2004).

Finally the collector efficiency can be written as shown in equation (2.17)

$$\eta = F_R(\tau\alpha)_{eff} - F_R U_L \frac{(T_{in} - T_{amb})}{G} \tag{2.17}$$

with

F_R	Heat Removal Factor	[-]
G	Solar Irradiation	[W m^{-2}]
U_L	Overall Collector Heat Losses	[W m^{-2} K^{-1}]
T_{amb}	Ambient Temperature	[°C]
T_{in}	Collector Inlet Temperature	[°C]
$(\tau\alpha)_{eff}$	Effective Transmission/Absorption Product	[-]
η	Collector Efficiency	[-]

Equation (2.17) is known as “Hottel-Whillier-Bliss-Equation” and can be used for designing solar collectors (Goswami et al., 2000, Khartchenko, 2004).

As the absorber temperature under normal operation and in collector tests is not equal to the fluid inlet temperature, the heat removal factor F_R is replaced by the collector efficiency factor F’ (Khartchenko, 2004), cf. equation (2.23). The inlet temperature T_{in} is replaced by the collector mean temperature T_{mean} (equation (2.18)). The formulation for the (linear) instantaneous collector efficiency results finally in equation (2.19).

$$T_{mean} = \frac{T_{in} + T_{out}}{2} \tag{2.18}$$

$$\eta = F'(\tau\alpha)_{eff} - F'U_L \frac{(T_{mean} - T_{amb})}{G} \tag{2.19}$$

with

F'	Collector Efficiency Factor	[-]
G_{col}	Irradiation into the Collector Plane	[W m^{-2}]
T_{in}, T_{out}	Collector In- and Outlet Temperature	[°C]
T_{mean}	Mean Collector Temperature	[°C]
T_{amb}	Ambient Temperature	[°C]
U_L	Overall Collector Heat Loss Coefficient	[W m^{-2} K^{-1}]
$(\tau\alpha)_{eff}$	Effective Transmission/Absorption Product	[-]

Cooper and Dunkle (1981) assume the overall loss coefficient to be linear temperature dependent and therefore replace F'U_L by equation (2.20) resulting in equation (2.21).

$$F'U_L = a + b(T_{mean} - T_{amb}) \tag{2.20}$$

$$\eta = F'(\tau\alpha)_{eff} - a\frac{(T_{mean} - T_{amb})}{G} - b\frac{(T_{mean} - T_{amb})^2}{G} \tag{2.21}$$

with

a	Constant Heat Loss Coefficient	[W m^{-2} K^{-1}]
b	Temperature Dependent Heat Loss Coeff.	[W m^{-2} K^{-2}]
F'	Collector Efficiency Factor	[-]
T_{mean}	Mean Collector Temperature	[°C]
T_{amb}	Ambient Temperature	[°C]
U_L	Overall Collector Heat Loss Coefficient	[W m^{-2} K^{-1}]
η	Collector Efficiency	[-]
$(\tau\alpha)_{eff}$	Effective Transmission/Absorption Product	[-]

The equation (2.21) is also used for the steady state efficiency curve calculation according to DIN EN 12975-2 (2006). According to Duffie and Beckmann (2006) F'($\tau\alpha$) is used as zero loss value η_0, while a and b are replaced by a1 and a2 in standard DIN En 12975-2 (2006). The efficiency curve according to the test standard is always plotted against the reduced temperature Tred (equation (2.22)).

$$T_{red} = \frac{(T_{mean} - T_{amb})}{G} \tag{2.22}$$

with

G	Solar Irradiation	[W m^{-2}]
T_{mean}	Mean Collector Temperature	[°C]
T_{amb}	Ambient Temperature	[°C]
T_{red}	Reduced Temperature	[K m² W^{-1}]

Figure 2.24 visualises the effect of absorption and emission coefficient on the collector efficiency curve measured according to DIN EN 12975-2 (2006). A decrease of the absorption results in a parallel offset of the efficiency curve. An increasing emission leads to a sharp decline of the collector efficiency curve.

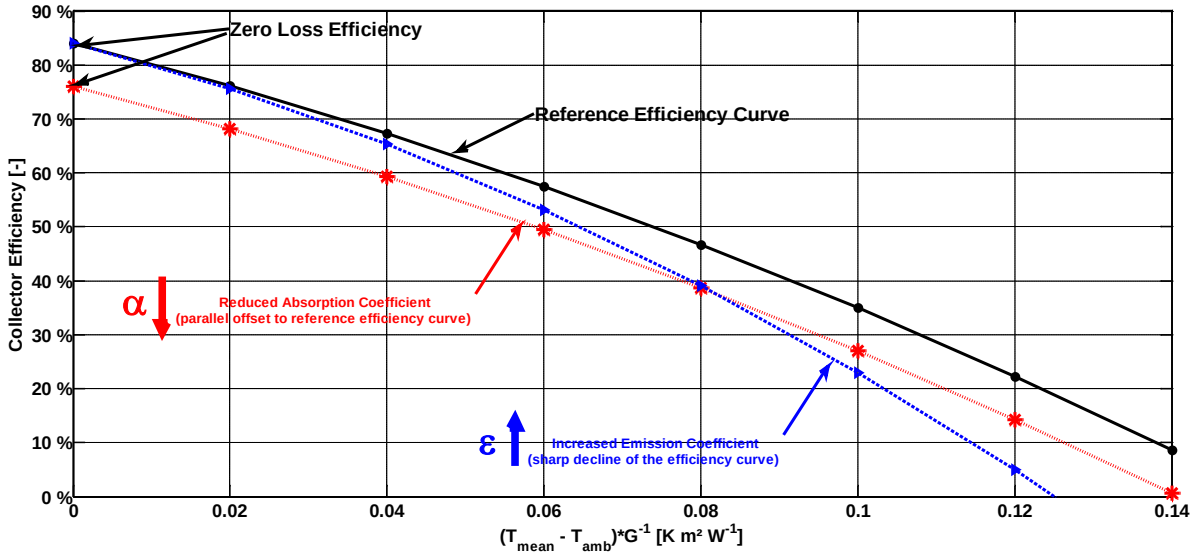

Figure 2.24: Influence of the Selective Coating on the Collector Efficiency

The collector efficiency factor F', already introduced in equations (2.16), (2.19) and (2.21) is an indicator for the performance of the absorber design (Goswami et al., 2000). In Duffie and Beckmann (2006), the collector efficiency F' is summarised to be strongly depended on the heat loss coefficient U_L and the heat transfer coefficient h_{fin}, the dependency of F' on the collector temperature is not that important.

The collector efficiency factor is calculated according to equation (2.23):

$$F' = \frac{\frac{1}{U_L}}{W\left[\frac{1}{U_L[d_{outer} + F(W - d_{outer})]} + \frac{1}{C_b} + \frac{1}{\pi d_{inner} h_{fin}}\right]} \quad (2.23)$$

$$F = \frac{\tanh\left(\frac{m(W - d_{outer})}{2}\right)}{\frac{m(W - d_{outer})}{2}} \quad (2.24)$$

$$m = \sqrt{\frac{U_L}{k_{abs} z_{abs}}} \quad (2.25)$$

with

C_b	Bond Conductance	[W m^{-1} K^{-1}]
d_{inner}	Inner Tube Diameter	[m]
d_{outer}	Outer Tube Diameter	[m]
F	Fin Efficiency	[-]
F'	Collector Efficiency Factor	[-]
h_{fin}	Convective Heat Transfer Coefficient Inside Tubes	[W m^{-2} K^{-1}]
k_{abs}	Heat Conductivity of the Absorber	[W m^{-1} K^{-1}]
U_L	Overall Collector Heat Loss Coefficient	[W m^{-2} K^{-1}]
m	Constant	[m]
W	Distance between Riser Tubes	[m]
z_{abs}	Absorber Thickness	[m]

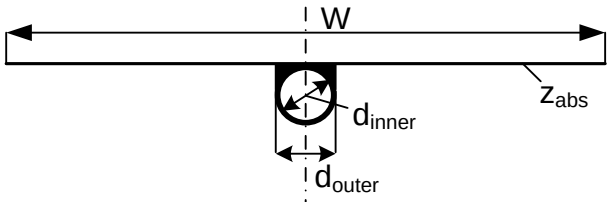

Figure 2.25: Sketch of an Absorber Fin for the Calculation of F

The convective heat transfer coefficient *h* within pipes can be calculated for laminar flow distribution using equations (2.26) and (2.27) (Drück, 2009); it is assumed that the heat transfer *h* over the whole pipe surface equals h_{fin}:

$$h = Nu \frac{\kappa}{d_{inner}} \tag{2.26}$$

$$Nu = \left[Nu_{\infty} + \frac{0.19 \left(\mathrm{Re}\,\mathrm{Pr} \frac{d_{inner}}{l_{pipe}} \right)^{0.8}}{1 + 0.117 \left(\mathrm{Re}\,\mathrm{Pr} \frac{d_{inner}}{l_{pipe}} \right)^{0.467}} \right] \left(\frac{\mu_{mean}}{\mu_{wall}} \right)^{0.14} \quad \text{for } 10^4 > \mathrm{Re}\,\mathrm{Pr} \frac{d_{inner}}{l_{pipe}} > 10^{-1} \tag{2.27}$$

$$\dot{q}_{wall} = const. \rightarrow Nu_{\infty} = 4.36$$
$$T_{wall} = const. \rightarrow Nu_{\infty} = 3.65$$

with

d_{inner}	Inner Tube Diameter	[m]
h	Convective Heat Transfer Coefficient	[W m^{-2} K^{-1}]
l_{pipe}	Tube Length	[m]
Nu, Nu_{∞}	Nusselt Number (Dimensionless Heat Transfer Coefficient)	[-]
Pr	Prandtl Number	[-]
$\dot{q}_{wall}$	Energy Flux along the Pipe	[W]
Re	Reynolds Number	[-]
T_{wall}	Pipe Wall Temperature	[°C]
κ	Heat Conductivity of the Fluid	[W m^{-1} K^{-1}]
$\mu_{mean}; \mu_{wall}$	Dynamic Viscosity of the Fluid inside the Pipe	[kg m^{-1} s^{-1}]

(*mean*) and at the Wall (*wall*)

Duffie and Beckmann (2006) assume the contact breadth of fin and pipe to be equal to the outer fin diameter, while Eisenmann (2003) enhanced the equation by calculating only a reduced contact breadth equal to the welding line. For further calculations the basic equations by Duffie, Beckmann (2006) are considered.

For asymmetrical fins the fin efficiency is calculated by Hermann (2005) by dividing the fin into a left and a right part of breadth W_L and W_R. Asymmetric fins in harp absorbers often can be found at last pipe on the left and or right absorber side. The collector efficiency factor F' results in equation

$$W = W_L + W_R \tag{2.28}$$

$$F_{as} = \frac{\tanh(m(W_R - \frac{d_{outer}}{2})) + \tanh(m(W_L - \frac{d_{outer}}{2})}{m(W_L + W_R - d_{outer})} \tag{2.29}$$

with

C_b	Bond Conductance	[W m^{-1} K^{-1}]
d_{inner}	Inner Tube Diameter	[m]
d_{outer}	Outer Tube Diameter	[m]
F_{as}	Fin Efficiency for the Asymmetric Fin	[-]
m	Constant	[m]
$W_{L,R}$	Left, Right Side Fin Width	[m]
W	Distance between Riser Tubes	[m]

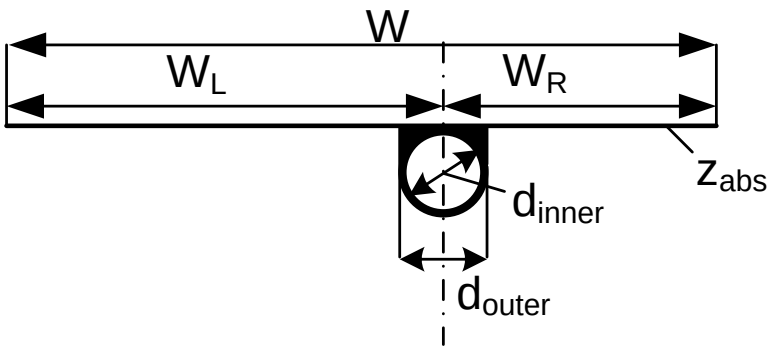

Figure 2.26: Sketch of an Asymmetric Absorber Fin for the Calculation of F

The solution for the collector efficiency factor of an asymmetric absorber fin is represented by equation (2.40).

$$F'_{as} = \frac{\frac{1}{U_L}}{(W_L + W_R)\left[\frac{1}{U_L[d_{outer} + F_{as}(W_L + W_R - d_{outer})]} + \frac{1}{C_b} + \frac{1}{\pi d_{inner} h_{fin}}\right]} \qquad (2.30)$$

with

C_b	Bond Conductance	[W m^{-1} K^{-1}]
d_{inner}	Inner Tube Diameter	[m]
d_{outer}	Outer Tube Diameter	[m]
F_{as}	Fin Efficiency for the Asymmetric Fin	[-]
F'_{as}	Collector Efficiency Factor at the Asymmetric Fin	[-]
h_{fin}	Convective Heat Transfer Coefficient Inside Tubes	[W m^{-2} K^{-1}]
k_{abs}	Heat Conductivity of the Absorber	[W m^{-1} K^{-1}]
U_L	Overall Collector Heat Loss Coefficient	[W m^{-2} K^{-1}]
$W_{L,R}$	Left, Right Side Fin Width	[m]

The influence of asymmetric absorber fins on the overall collector efficiency factor is weighted according to the affected absorber surface (equation (2.41)).

$$F' = \sum_{1}^{n} \frac{A_n}{A_{abs}} F_n' \tag{2.31}$$

with

A_n	Fin Area	[m²]
A_{abs}	Absorber Area	[m²]
F_n'	Collector Efficiency Factor at Fin n	[-]
F'	Overall Collector Efficiency Factor	[-]

The given theory on the solar collector design is brought into a MATLAB (The Mathworks, 2011) script to effectively be used in the collector design phase.

Besides a mathematical calculation of the collector efficiency, there are several measurement approaches. Frey et al. (1998) conducted collector efficiency measurements on 21 different samples of absorber fins. The measurements reflect the dependency of F' on the flow rate, the fin width and the bonding. Table 2.8 shows an excerpt of the test results.

Table 2.8: Excerpt of the Collector Efficiency Measurements Conducted by Frey et al. (1998)

	Sample 4	**Sample 8**	**Sample 15**	**Sample 17**
Drawing	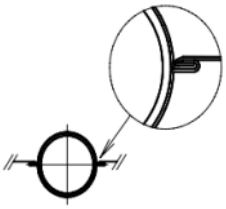	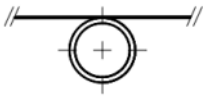	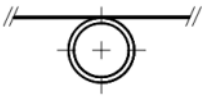	
Fin Dimensions				
Width	145 mm	150 mm	80 mm	120 mm
Thickness	0.22 mm	0.21 mm	0.21 mm	0.21 mm
Material	Copper	Copper	Copper	Copper
Piping	9.6 x 0.5 mm Copper	8.0 x 0.4 mm Copper	8.0 x 0.5 mm Copper	8.0 x 0.5 mm Copper
Coating	Black Chrome	Black Chrome	Black Chrome	Black Chrome
Bonding	Piping Rolled-up	Ultrasonic Welded	Ultrasonic Welded	Piping Clamped
$F'_{20\ l\ h^{-1}}$	0.86	0.81	0.92	0.87
$F'_{40\ l\ h^{-1}}$	0.88	0.84	0.95	0.90
$F'_{60\ l\ h^{-1}}$	0.89	0.86	0.97	0.91

According to a design nomogram developed by Eisenmann et al. (2004), it is possible to achieve material savings of 20–25 % compared to the state-of-the-art at a constant collector efficiency factor of at least 0.9.

Besides the sheet-pipe configuration of solar collectors, there are several different possible designs of the absorber. Bliss (1959) described a method to calculate the collector efficiency factor for a volumetric absorber with only one rectangular duct as seen in equation (2.32):

$$F' = \frac{h_{fin}}{h_{fin} + U_L} \tag{2.32}$$

with

F'	Collector Efficiency Factor	[-]
h_{fin}	Heat Transfer Coefficient Inside the Absorber	[W m^{-2} K^{-1}]
U_L	Heat Loss Coefficient	[W m^{-2} K^{-1}]

A volumetric absorber has the advantage of reduced thermal resistances, e.g. bond resistance. One major disadvantage of this kind of design is the limited permitted system pressure in order to avoid a deformation the absorber plate.

Treikauskas (2005) compared absorbers with corrugated pattern, corrugated sheet absorbers, metal-matrix-absorbers and roll-bond absorbers to state-of-the-art sheet-pipe absorbers with respect to collector efficiency factor and pressure loss. It can be concluded that alternative structural collector shapes outperform the commonly used sheet-pipe absorbers, but have to be reinvestigated whether an uniform flow distribution is achievable (Table 2.9).

Table 2.9: Collector Efficiency and Pressure Losses of Different Absorber Types (Treikauskas, 2005)

	State-of-the-Art Header-Riser and Meander Absorber	***Absorber with Corrugated Pattern***	***Corrugated Sheet Absorber***	***Metal-Matrix-Absorber***	***Roll-Bond-Absorber***
Quantity of Heat Carrier [l]	1.0–1.5	4.8	6.3	4.1	2.1
Heat Capacity [kJ K^{-1}]	8.8	23.7	22.0	23.9	10.7
Thermodynamic Attributes					
Collector Efficiency Factor [-]	0.88–0.95	0.98–0.99	0.98–0.99	0.98–0.99	0.97
Fluid Mechanic Attributes					
Pressure Drop [mbar] at 2 l min^{-1} (~120 kg h^{-1})	10–200	3.5	24.6	—	53.0

Concerning sheet-pipe absorbers, several attempts have been made to describe the pressure losses inside the solar collector analytically. From the hydraulic point of view, a harp absorber is a network consisting of flow resistances. Kikas (1995) described this hydraulic network precisely for laminar flow conditions. For combined laminar and turbulent conditions (which are often found in solar collectors), other approaches have to be taken into consideration. The easiest and also the most imprecise attempt is to understand the risers as a resistance network of parallel flow resistances with each the same resistance (Figure 2.27). The total resistance in the risers is summarised as shown in equation (2.33):

$$\frac{1}{\Delta p_{riser}} = \sum_{1}^{n} \frac{1}{\Delta p_{riser,n}} \tag{2.33}$$

with

n	Number of Risers	[-]
Δp_{riser}	Total Pressure Loss in the Risers	[Pa]

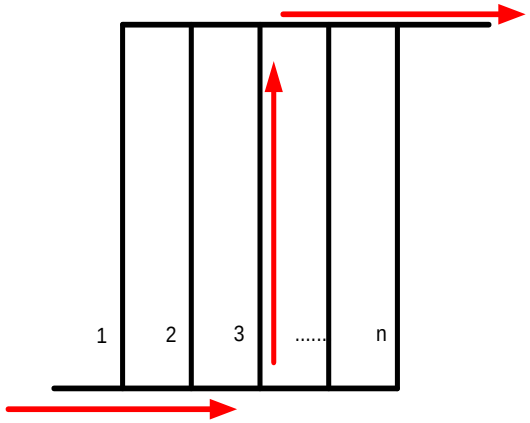

Figure 2.27: Flow Path through a Harp Absorber

For the pressure drop in the headers, only 1 header length is taken into account. This model neglects pressure losses caused by branches and inlet and outlet losses. Assuming a uniform flow distribution, a physically incorrect approach (Weitbrecht et al., 2002), the pressure losses simply consist of header and riser losses, as shown in equation (2.34). However, Weitbrecht did not state any physical explanation for that fact.

$$\Delta p_{col} = \Delta p_{header} + \Delta p_{riser} \tag{2.34}$$

with

Δp_{col}	Total Pressure Drop in the Collector	[Pa]
Δp_{header}	Pressure Drop in the Header	[Pa]
Δp_{riser}	Summarised Pressure Drop of the Risers	[Pa]

For the calculation of the Reynolds Number according to equation (2.35), the mass flow rate and the velocity in the risers has to be divided by the number of risers n (equation (2.36)).

$$\mathrm{Re} = \frac{v_{fluid}\, d_{inner}\, \rho}{\mu_{fluid}} \tag{2.35}$$

with

d_{inner}	Inner Pipe Diameter	[m]
Re	Reynolds Number	[-]
v_{fluid}	Fluid Velocity	[m s^{-1}]
ρ_{fluid}	Fluid Density	[kg m^{-3}]
μ_{fluid}	Dynamic Fluid Viscosity	[kg m^{-1} s^{-2}]

$$\dot{m}_{riser} = \frac{\dot{m}_{col}}{n_{riser}} \tag{2.36}$$

with

$\dot{m}_{col}$	Collector Mass Flow Rate	[kg s^{-1}]
$\dot{m}_{riser}$	Mass Flow Rate through One Riser	[kg s^{-1}]
n_{riser}	Number of Risers	[-]

This simple approach does not meet the needed accuracy for the development of a collector piping for thermosyphon systems. A more precise attempt to describe the pressure losses is illustrated by Späte (1982). Späte converts the riser diameter d_{riser} into an equivalent pipe length with the header diameter d_{header} taking also the number of risers into account (Figure 2.28):

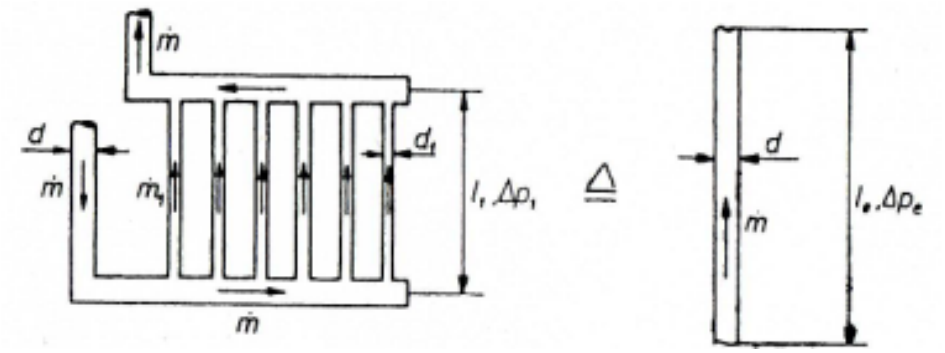

Figure 2.28: Approach of Converting Real Pipe Length into an Equivalent Pipe Length (Späte, 1982)

$$l_{eq} = l_{riser} \frac{d^4_{inner,header}}{n_{riser} d^4_{inner,riser}} \tag{2.37}$$

with

$d_{inner,header}; d_{inner,riser}$	Inner Header; Riser Diameter	[m]
l_{eq}	Equivalent Pipe Length	[m]
l_{riser}	Riser Length	[m]
n_{riser}	Number of Risers	[-]

Additionally, the friction coefficients for the branches and tees are calculated (equation (2.38)):

$$l_{branch} = \sum_{1}^{n_{branch}} \zeta_n \frac{d_{inner,n}}{f_n} \tag{2.38}$$

with

$d_{inner,n}$	Diameter of Branch n	[m]
f_n	Friction Factor (Velocity depended)	[-]
l_{branch}	Equivalent length of Pressure Drop caused by branches	[m]
n_{branch}	Number of Branches	[-]
ζ_n	Friction Coefficient of Branch n	[-]

Adding the header length, the total length of the equivalent pipe is represented by equation (2.39):

$$l_{sum} = l_{eq} + l_{branch} + l_{header} \tag{2.39}$$

with

l_{branch}	Equivalent length of Pressure Drop caused by Branches	[m]
l_{eq}	Equivalent Riser Length	[m]
l_{header}	Header Length	[m]
l_{sum}	Total Equivalent Length of Collector Hydraulics	[m]

As Späte assumes the flow to be laminar within the whole collector, the overall pressure drop is calculated according to equation (2.39) using l_{sum} as pipe length.

Scheller (1985) improved this approach by adding a correction factor investigated by Langhaar (1942). This factor takes turbulence into account caused by bends and tees (equation (2.40)):

$$x_{La} = 1 + \frac{0.038}{\left(\frac{l_{pipe}}{d_{inner}\,\mathrm{Re}}\right)^{0.96}} \tag{2.40}$$

with

d_{inner}	Inner Tube Diameter	[m]
l_{pipe}	Pipe Length	[m]
Re	Reynolds Number	[-]
x_{La}	Langhaar Factor	[-]

For a correct solution of Scheller´s approach, pressure losses in risers and headers have to be calculated separately when laminar and turbulent conditions are coexistent (equation (2.41)):

$$\Delta p_{col} = x_{La,header}\, f_{header}\, \frac{l_{header}}{d_{inner,header}} \frac{\rho}{2} v_{header}^2 + x_{La,riser}\, f_{riser}\, \frac{l_{eq} + l_{branch}}{d_{inner,header}} \frac{\rho}{2} v_{header}^2 \tag{2.41}$$

with

$d_{inner,header}$	Inner Header Diameter	[m]
$f_{header}; f_{riser}$	Friction Factor (Velocity depended)	[-]
l_{branch}	Equivalent length of Pressure Drop caused by branches	[m]
l_{eq}	Equivalent Riser Length	[m]
l_{header}	Header Length	[m]
v_{header}	Velocity in the Header	[m s^{-1}]
$x_{La,header}; x_{La,riser}$	Langhaar Factor for Header and Riser	[-]

Δp_{col}	Collector Pressure Drop	[Pa]
ρ	Fluid Density	[kg m^{-3}]

There are many possibilities to design a lightweight solar collector sufficient for thermosyphon systems by reducing material or by choosing a polymeric cover material. Besides the collector efficiency factor, the coating of the collector has a major influence on the collector efficiency. As the absorber´s pressure drop also is a design driving factor, meander type absorbers are only suitable for thermosyphon systems if a piping diameter above market available piping dimensions of 8–12 mm is chosen. As the diameter directly influences the cost of the absorber the most suitable solution is a harp design.

2.2.3 Storage Tank

There are different types of storage tanks described in the literature. Nowadays, the most common storage type is a well-insulated horizontal double mantle heat exchanger storage tank. Tube heat exchangers inside vertical and horizontal storage tanks were studied in the 1980s. These types of heat exchangers can provide good heat exchange, but are difficult to design taking the thermosyphonic principle into account (Morrison et al., 1999).

Horizontal tanks lead to visually compact systems, but suffer from a reduced stratification when compared to vertical tanks. Khalifa and Mehdi (1999) conducted an experimental and a numerical study on a thermosyphon system with a horizontal 170 l storage tank. They proved that the heat flow inside the storage tank can be considered one-dimensional. Axial and radial temperature gradients were negligible compared to the vertical temperature gradient. Even under cloudy conditions they were able to measure a good stratification inside the storage tank.

Morrison et al. (1998) studied the flow distribution inside a horizontal double mantle heat exchanger storage tank experimentally and numerically. Heat exchanger in- and outlet port were located at the storage tank bottom. The performance of the heat exchanger was found to be dependent on the port location, the inlet temperature in relation to the top temperature of the water and the velocity of the inlet jet. A storage tank simulated with ports as close as possible to the double mantle end (welding line) outperformed a system with ports moved towards the inner of the double mantle (Figure 2.29). In the latter a recirculation zone developed causing energy losses. This recirculation zone caused

a negative heat flux and thus a destruction of the thermal stratification inside the hot water section. At inlet temperatures close to the top temperature of the storage tank water and at high inlet velocity the majority of the heat transfer was found to be close to the bottom. This study was closed with the recommendation to put the inlet port to a higher position in the annulus and to provide the inlet jet rather parallel than perpendicular to the heat exchanger spacing. In a further publication Morrison et al. (1999) investigated the advantages and disadvantages of the heat exchanger entry position of double mantle heat exchanger storages (Figure 2.29). Most of the manufacturers were found to use a bottom entry, as these storages are more suitable for systems equipped with an in-tank backup heater.

At low irradiation conditions, these systems will have a better circulation compared to the top entry systems, as the mantle flow will only rise to the height of the thermal equilibrium. Systems working as solar pre-heaters usually have the inlet at the top of the heat exchanger annulus.

The mentioned danger of reverse thermosyphoning in thermosyphon solar pre-heater systems can be avoided using an adequate collector – heat exchanger inlet design, as described in Chapter 2.2.1.

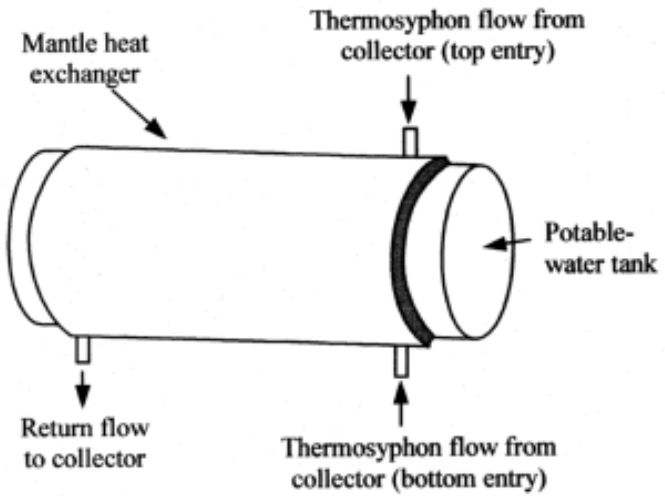

Figure 2.29: Connection Scheme of Double Mantle Heat Exchanger Storages (Morrison et al., 1999)

Several experimental and simulation based investigations on thermally stratified hot water storage tanks can be found in literature. Lavan and Thompson (1977) determined the effect of geometric and dynamic parameters on the thermoclines while tapping hot water experimentally. For the experiments two PMMA storage cylinders of different volume

were used. The results can be summarised in design recommendations for vertical hot water storages. The cold water entry has to be located close to the bottom with a large diameter to slow down the fluid velocity. The storage length to diameter ratio indicates to use long storage tanks with a small diameter. The draw-off efficiency of the storage tank is better the higher the temperature difference between cold and hot water is. These recommendations were summarised in a mathematical correlation to predict the draw-off efficiency of a storage tank. However, the influence of the storage tank materials' heat conductivity was neglected. For two commercial available tanks the authors recommended flow distributors at the top and bottom of the storage as shown in Figure 2.30 to achieve a low fluid velocity at a given inlet diameter.

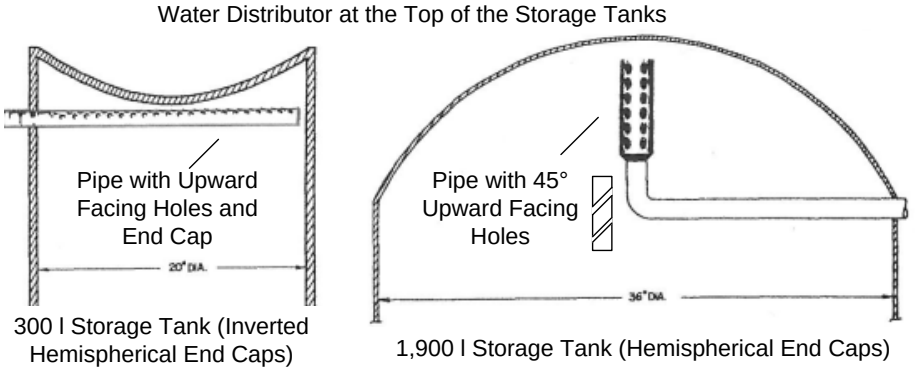

Figure 2.30: Flow Distributors for Pressurised Vertical Storage Tanks Proposed by Zalman and Thompson (1977)

Shah and Furbo (2003) investigated entrance effects in solar storage tanks numerically by 3D CFD and experimentally with a transparent test water tank. The inlet designs studied were a straight pipe inlet, a small hemispherical baffle plate above the inlet pipe and a large flat baffle plate above the inlet pipe. In the CFD model two different draw-off rates 60 l h^{-1} and 600 l h^{-1} were compared. At low flow rates the influence of the flow distributor has minor effects on the mixing inside the storage tank, while at high flow rates, the large baffle plate performed best.

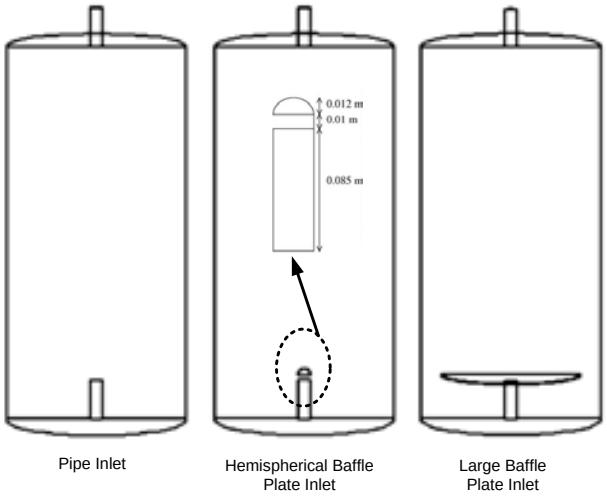

Figure 2.31: Inlet Designs Studied by Shah and Furbo (2003)

The analysis of the experimental results on the inlet design impact showed the necessity for further development of the applied calculation method based on the first and second law of thermodynamics.

Alizadeh (1999) investigated the stratification in horizontal cylindrical storage tanks experimentally and compared the results with two one-dimensional numerical storage tank models. The experiments had a focus on different storage tank states — stratified or fully mixed temperature profile — and two different cold water inlet designs — straight tube inlet and a divergent conical nozzle bent 30 ° to the bottom. The initial stratification was established with a heating rod at the mid-height of a storage tank end. To achieve a mixed temperature profile a pump mixed the water during the heating up period. The conical inlet outperformed the straight tube inlet in terms of maintaining the stratification during drawing off water (Figure 2.32).

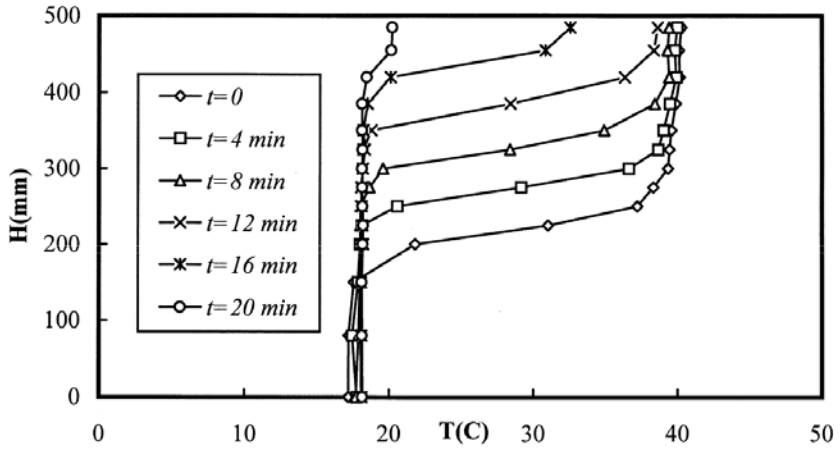

Figure 2.32: Transient Vertical Temperature Distribution Inside the Initially Stratified Storage Tank with Divergent Nozzle at a Flow Rate of 10 l min^{-1} (Alizadeh, 1999)

Especially at the bottom of the storage tank the numerical models developed showed discrepancies to the measurement results as the mixing induced by the inlet jet is not considered.

Cònsul et al. (2004) carried out a CFD simulation concerning the influence of different draw-off flow rates on the thermal stratification of a horizontal storage tank. The storage tank had a straight tube at the inlet. Beginning at a draw-off rate of 180 l h^{-1}, the stratification is destroyed while water is being tapped (Figure 2.33). The flow rate for the storage tank tests according to ISO 9459-2 (1995) is with 600 ± 50 l h^{-1} three times higher

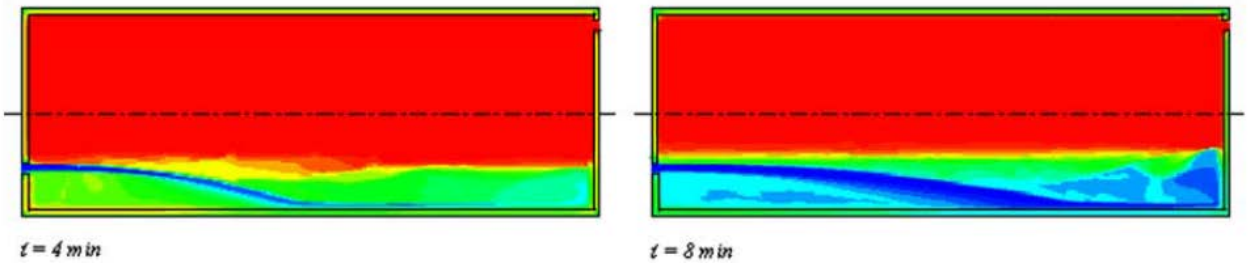

Figure 2.33: Centre Pane of the Storage Tank Investigated by Cònsul et al. (2004) at 180 l h^{-1} Draw-off Rate

Wenfeng et al. (2011) numerically studied the influence of the inlet velocity — 0.25 m s^{-1} (159 l h^{-1}) 0.5 m s^{-1} (318 l h^{-1}) and 1.0 m s^{-1} (636 l h^{-1}) — in a storage tank setup as shown in Figure 2.33 with an in- and outlet diameter of 15 mm. The heat removal efficiency was calculated using the energy contained in the fully mixed storage at 60 °C divided by the energy accumulated during the draw-off till the outlet temperature drop be-

low 32 °C. The efficiency was found to decrease with increasing flow rates from 88.4 % to 77.8 %. However, at a low flow rate the results indicated a difficulty to remove the hot water above the outlet level.

To improve the heat removal efficiency of the prototype system the outlet has to be located as close as possible to the top of the storage tank annulus.

Hegazy and Diab (2002) experimentally investigated an improved design for a 50 l electrical hot water heater by changing the heating element configuration and the inlet design. The change from a vertical straight tube inlet to a horizontal wedged inlet pipe was able to promote thermal stratification and thus a better draw-off efficiency. Based on these findings a further study was carried out by Hegazy (2007) on the inlet design. Three different inlet geometries as shown in Figure 2.34 were tested at a draw-off rate of 300 l h^{-1} and 600 l h^{-1}. The slotted inlet outperformed the other designs in terms of draw-off efficiency and is the simplest solution in terms of manufacturing costs.

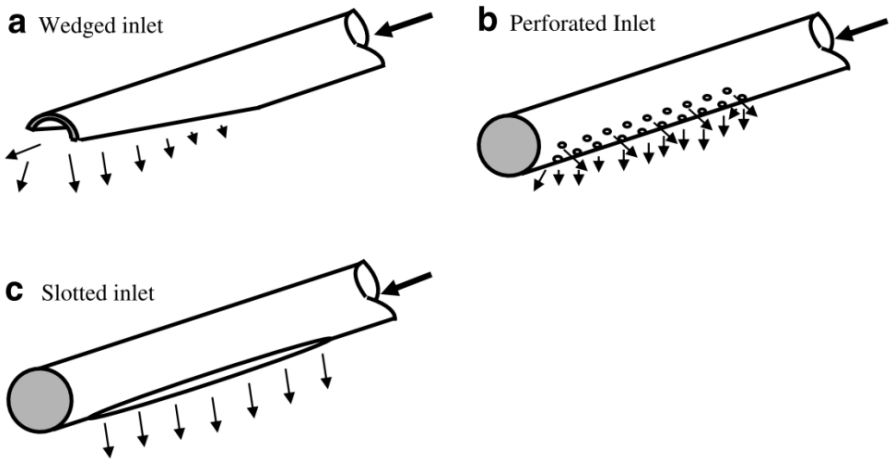

Figure 2.34: Inlet Geometries Tested by Hegazy (2007)

Andrés and López (2002) developed a model of a solar domestic water heater with a mantle heat exchanger for the simulation package TRNSYS (Klein et al., 1997). The fluid inlet of the double mantle is placed at the top of the annular. The heat flux to the surroundings within the TRNSYS model, i.e. the convective heat transmission on the surfaces and the heat conduction through the different layers, like e.g. steel or insulation materials, is modelled as a combined overall heat transfer coefficient. This coefficient has to be estimated and validated by measurement data (cf. Morrison and Braun, 1985). The advantage, thereby, is the reduced amount of variables, e.g. if there are unknown condi-

tions, there is just one parameter to estimate. The heat flux within the storage is obtained by direct coupling between tap water and heat transfer fluid temperature (Figure 2.23). After building up the one-dimensional model, the model was validated using measurement data.

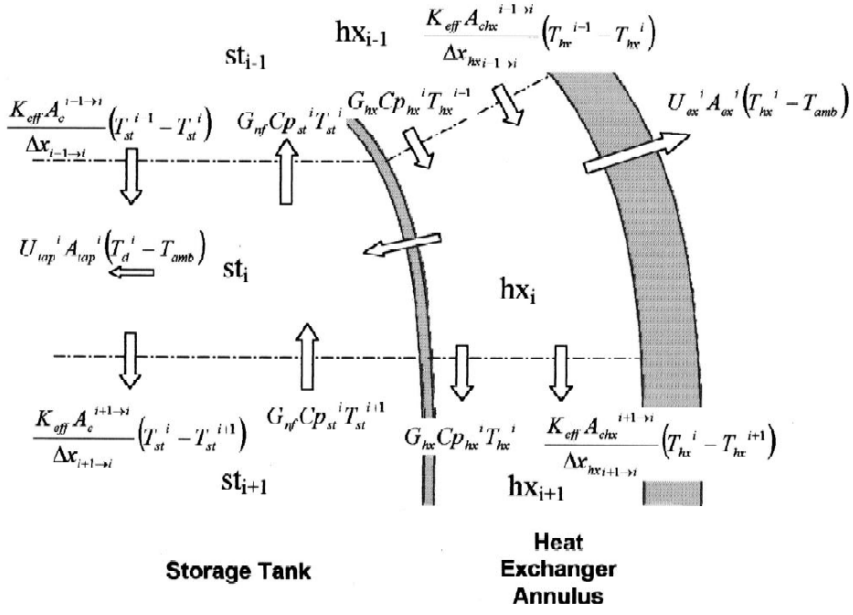

Figure 2.35: Heat and Mass Transfer in Tank and Heat Exchanger Annulus (Andrés and López, 2002)

In contrast to the approach of a fixed overall heat transfer coefficient, Eames and Norton (1998) summarised the effect of the wall conductivity and heat losses on the degradation of the storage tank's thermocline in times with no flow as being either over- or underestimated by the two investigated one-dimensional models. In horizontal storage tanks especially in the lower and upper part of the annulus large differences occur. A better formulation of the effective thermal conductivity is achieved by incorporating the cross section area of fluid and wall (equation (2.42)), as published in Morrison et al. (1999) and shown in Figure 2.36.

$$\kappa_{eff} = \frac{\kappa_{wall} A_{wall} + \kappa_{fluid} A_{fluid}}{A_{fluid}} \tag{2.42}$$

with

A_{wall}	Cross Section Area of the Wall Element	[m²]
A_{fluid}	Cross Section Area of the Fluid Element	[m²]
κ_{eff}	Effective Thermal Conductivity	[W m^{-1} K^{-1}]
κ_{fluid}	Thermal Conductivity of the Fluid	[W m^{-1} K^{-1}]
κ_{wall}	Thermal Conductivity of the Wall	[W m^{-1} K^{-1}]

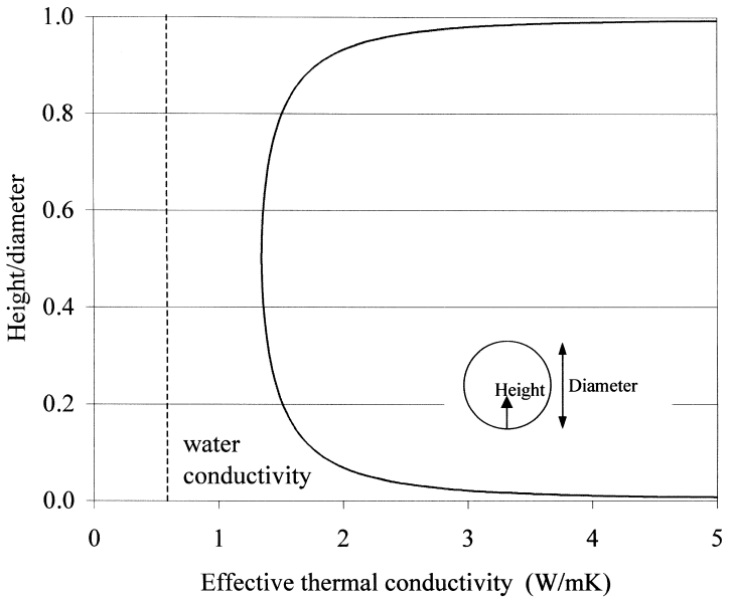

Figure 2.36: Effective Thermal Conductivity of a Horizontal Storage Tank with 450 mm diameter and 3 mm steel walls (Morrison et al., 1999)

From equation (2.42) two design targets can be derived. A reduction of the wall thickness to the required minimum comes along with a reduced effective thermal conductivity and cost savings. The influence of the heat conduction on the stratification was also shown by Shyu et al. (1989) for vertical storage tanks, where a bigger wall thickness was related to a pronounced degradation of the stratification. The use of materials with low heat conductivity such as polymers has to be investigated, whether the heat transfer under normal operation conditions is sufficient and the material can resist the occurring pressure as well as thermal loads.

Hobson and Norton (1988) developed and published a simulation model of direct thermosyphon solar water heaters. The relaxation of the thermocline inside the vertical storage tank was shown to be dominated by the storage walls. The description of the relaxa-

tion was expressed similar to equation (2.42), however, the denominator additionally contained the wall cross section A_{wall}. This calculation scheme was verified experimentally. For a copper storage tank the discrepancy of the diurnal thermal output between measurement and calculation could by decreased from 6 % down to 2.8 % using the effective thermal conductivity correlation. The friction losses in the system were described the most accurate way by applying the non-isothermal flow through pipe sections approach developed by Addlesee (1980). It is valid for $50 \leq Re \leq 2{,}500$ and represented by equation (2.43).

$$f = 600\,\mathrm{Re}^{-1.19} \tag{2.43}$$

with

Re	Reynolds Number	[-]
f	Friction Factor	[-]

Using this approach, the predicted and measured flow rates in the system under steady state conditions differed only by 2 %. The collector model used was a two-dimensional finite difference model, with an accurate transient behaviour. Based on this simulation approach the authors developed a design nomogram for direct thermosyphon solar systems (Hobson and Norton, 1989). The uncertainty in predicting the annual solar fraction was found to be in the range of 8–13 % under climatic conditions of the UK.

An adaption of the simulation model on indirect thermosyphon solar hot water heaters was published by Norton, Edmonds and Kovolos (1992). Thereby the direct flow storage tank model was replaced by a vertical double mantle storage tank model. The friction losses inside the double mantle were neglected by the authors as the incorporation of a friction factor for laminar flow between cylindrical walls lead to an underestimation of the simulated compared to the measured flow rate. This simplification resulted in a simulated flow rate within 10 % accuracy compared to the measured flow rate and a temperature rise in the vertical storage tank differing below 2.5 % to measurement data.

Hafner et al. (1999) developed a simple hot water storage tank model without a heat exchanger for CARNOT. The storage tank provides the basis for the development of a double mantle heat exchanger storage model. It is divided along its height into *n* user setta-

ble nodes. For each node the energy balance is drawn using a finite element calculation method as shown in equations (2.44) and (2.45).

$$\rho_{fluid} c_{fluid} \frac{dT}{dt} = \frac{(UA)_{loss}}{V_n}(T_{amb} - T_n) + \frac{\kappa_{eff}}{dh^2}(T_{n+1} + T_{n-1} - 2T_n) + \frac{\dot{m}_{up} c_{fluid}}{V_n}(T_{n-1} - T_n) + \frac{\dot{m}_{down} c_{fluid}}{V_n}(T_{n+1} - T_n) \quad (2.44)$$

wherein

$$\kappa_{eff} = \frac{4 A_{loss} n \kappa_{wall}}{\pi D_{inner}} + \kappa_{fluid} \quad (2.45)$$

with

A_{loss}	Surface of a Node	[m²]
c_{fluid}	Specific Heat Capacity of the Fluid	[J kg^{-1} K^{-1}]
D_{inner}	Inner Diameter of the Storage Tank	[m]
dT	Temperature Gradient	[K]
dt	Time Step	[s]
$\dot{m}_{down}$	Collector Mass Flow Rate Downwards	[kg s^{-1}]
$\dot{m}_{up}$	Collector Mass Flow Rate Upwards	[kg s^{-1}]
n	Number of Nodes	[-]
T_{amb}	Ambient Temperature	[°C]
T_{n-1}	Temperature of the Previous Node	[°C]
T_n	Temperature of the Considered Node	[°C]
T_{n+1}	Temperature of the Following Node	[°C]
U_{loss}	Heat Loss Coefficient	[W m^{-2} K^{-1}]
V_n	Volume of 1 Node	[m³]
κ_{eff}	Effective Axial Thermal Conductivity	[J kg^{-1} K^{-1}]
κ_{fluid}	Thermal Conductivity of the Fluid	[J kg^{-1} K^{-1}]
κ_{wall}	Thermal Conductivity of the Wall	[J kg^{-1} K^{-1}]

The stratification within the storage tank is assumed to be ideal. The load (cold water) is propagated through every node *n* from the bottom to the top. The energy (temperature) from the heat source is inserted at the first node downwards fulfilling the requirement $T_{source} > T_{node}$. Heat losses are calculated at the storage tank annulus taking insulation properties into account. To achieve realistic behaviour of the storage tank the occurring axial heat conductivity is calculated.

Kleinbach et al. (1993) investigated the multimode and the plug flow approach for modelling direct flow thermal storage tanks and enhanced both approaches by a plume entrainment approach during the cooling down phase to achieve higher accuracy. In an experiment the stratification inside a low flow solar thermal system was measured and shown.

The cooling down phase of the one-dimensional storage tank models cannot be described in a physically correct way. Oliveski et al. (2003) compared the results of two-dimensional calculation models for storage tanks with those of one-dimensional models and experimental data. The one-dimensional calculation schemes use computational artifices to calculate stratification effects during the cooling phase. Franke (1997) interchanges the water layers according to their temperature, while Klein et al. (1997) mix the upper colder layer with the lower hotter layer to a mean temperature. Both mixing methods provide a good approximation of experimental results (Figure 2.37). For that reason the authors recommend one-dimensional (simple) models for long term performance predictions. The calculation method according to Klein et al. (1997) is already in use in the CARNOT models and will also be implemented in the double mantle heat exchanger storage tank model.

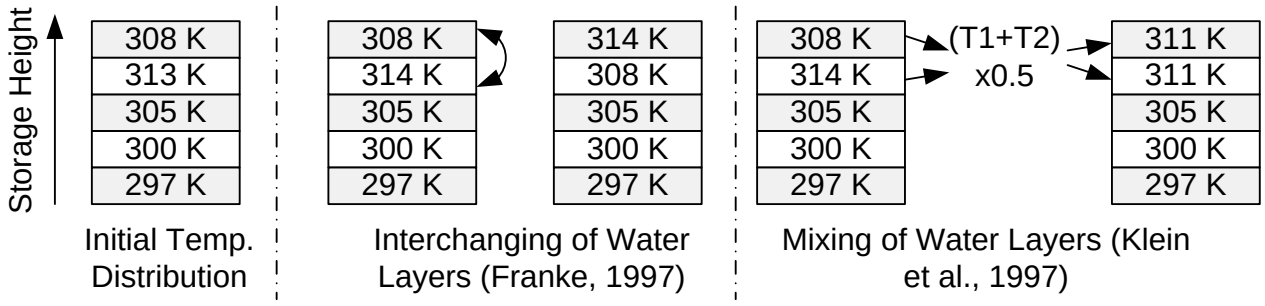

Figure 2.37: Methods for Rearranging Thermal Stratification in One-Dimensional Storage Tank Models

Summary

Literature on thermosyphon system storage tanks shows the necessity of a technically well-designed cold water inlet with a large diameter and a flow diffuser at low manufacturing costs. The closer the hot water outlet is located to the top the easier the hot water can be discharged from the storage tank even at low flow rates.

The effective material conductivity directly influences the degradation of the stratification inside the storage tank.

For solar only systems the heat exchanger inlet shall be located at the top of the storage tank.

Different numerical storage tank models are published from three-dimensional down to one-dimensional tank description. One-dimensional models require the least computational effort but require the implementation of artifices to incorporate the loss of stratification during the cooling down phase. For long term predictions one-dimensional modelling of storage tanks is sufficient.

Finally, the analysis of a TRNSYS double mantle heat exchanger and CARNOT simple storage tank model gives hints regarding the development of a CARNOT double mantle heat exchanger storage model needed for the sensitivity analysis.

The literature review on storage tanks and storage tank simulation is an outline of publications; further readings are added to the bibliography section in Appendix F.

2.2.4 Interconnecting Pipes

Vaxman and Sokolov (1986) discussed the effect of the connecting pipes in thermosyphon systems. They conducted their research using the thermosyphon setup as illustrated in Figure 2.38. In order to suppress reverse thermosyphoning during night the upper

pipe leading from point B to C has to be properly insulated. The insulation of the lower pipe from D to A is not that important.

Reverse thermosyphoning can be completely stopped when the similar stratification along A–B–C and along A–D–C is reached. For systems with draw-off taking part also during night, the authors recommend a height difference between collector outlet and storage tank inlet of 300 mm < ΔH < 800 mm.

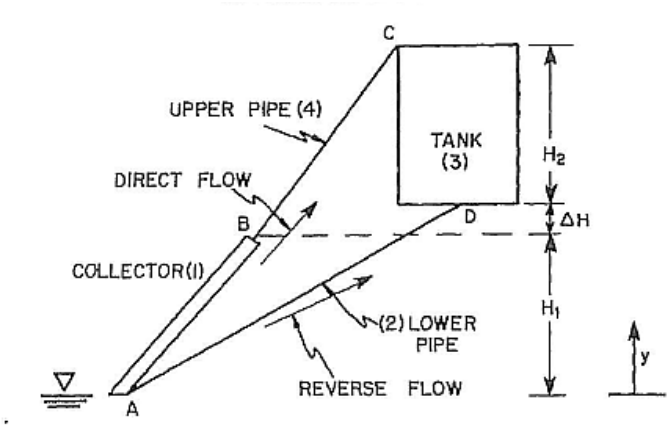

Figure 2.38: Scheme of the Investigated Thermosyphon System (Vaxman and Sokolov, 1986)

Morrison (2001) carried out a variation of the pipe diameter of the interconnecting pipes between collector and storage tank of a closed-coupled thermosyphon system with electrical backup heating. His investigations show an optimum for a daily collector volume flow equal to the daily load volume. The ratio of 1 can be achieved by narrowing the pipe diameter. This optimisation has above all an economic advantage as costs for the piping can be reduced.

It has, however, to be proved whether these results can directly be transferred onto a thermosyphon system running without an electrical backup heater. An electrical backup heater keeps a certain amount of the storage tank at a desired temperature. In order to incorporate solar energy into the storage tank the temperature produced by the collector has to be above the backup heater temperature. To achieve high collector temperatures (at a low mass flow rate) an additional flow resistance using narrow pipes can be implemented. Michaelides and Wilson (1996) simulated the impact of different backup heating configurations on the annual solar fraction. Their results show a thermosyphon system with an external backup heater is able to achieve an annual solar fraction of 86 % under

the conditions of Cyprus. The same system with an internal electrical backup heater in the upper storage tank part performs at f_{sol} = 77 % while the same electrical backup heater at the storage tank bottom lowers the solar fraction to 59 %.

By varying the pipe dimensions, a direct link on the thermosyphonic flow rate is created. A low flow rate is suitable for systems with an internal backup heater, which generally has negative impact on the solar fraction. By insulating the piping between collector outlet and storage tank inlet, reverse thermosyphoning can be prevented.

2.2.5 Heat Transfer Medium

Norton and Edmonds (1991) used a dynamic simulation model in order to analyse the effect of aqueous propylene-glycol concentrations on the system performance of an indirect thermosyphon system and compared it to a drain-down direct system under the conditions of London. For London, a minimum propylene-glycol concentration of 25 % is needed to compensate the lowest temperatures in December as shown in Figure 2.39 to avoid damage to the system.

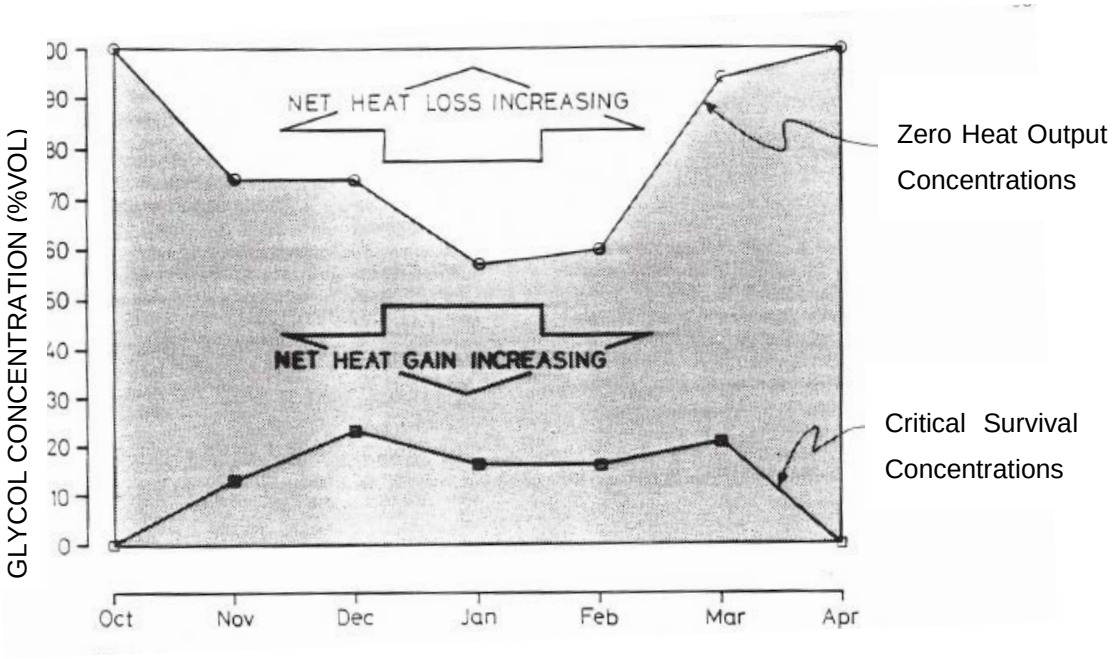

Figure 2.39: Minimum Glycol Concentration Required for Frost Protection Compared to a Concentration Leading to Zero System Output (Norton and Edmonds, 1991)

As maximum propylene-glycol concentration the authors recommend 40 %. A higher concentration leads to a significant reduction of the annual energy output. The indirectly

freeze-protected system is found to outperform by 12 % a drain-down system which does not work during times with frost. This work shows the importance of adopting the freeze-protection to climatic conditions in order to optimise the annual system output.

Antifreeze, in Schellers' (1985) study mono-ethylene-glycol, in the collector circuit up to a concentration of 50 % has only a little influence on the annual solar fraction of thermosyphon systems. Higher concentrations, however, reduce the solar fraction extremely, as the dynamic viscosity of the heat transfer fluid increases. Therefore, a water/antifreeze mixture with an antifreeze rate as small as possible should be chosen.

3 System Simulation

The overall target of the system simulation is to carry out a sensitivity analysis leading to optimised prototype design parameters. As the toolbox used MATLAB/SIMULINK (The Mathworks, 2011) and CARNOT (Hafner et al., 1999) lacks a double mantle heat exchanger storage tank, a model of such device is developed and validated.

3.1 Formulation of Mathematical Descriptions

This chapter deals with the mathematical basics and physical correlations, which are necessary to describe thermosyphon systems. Furthermore, the transfer of this background into simulation is discussed.

3.1.1 Fundamental Requirements

One of the fundamental requirements regarding the modus operandi of thermosyphon systems is the density-temperature correlation of the working fluid (equation (3.1); in most cases either water or a water glycol mixture is used):

$$\rho_{fluid} = \rho(T) \tag{3.1}$$

with

ρ_{fluid}	Fluid Density	[kg m^{-3}]
$\rho(T)$	Density at Temperature *T*	[kg m^{-3}]

Using water as heat transfer fluid, the temperature dependent density varies between 999.85 kg m^{-3} at 0 °C and 958.50 kg m^{-3} at 99.5 °C. This density change is only about 4 % over the whole temperature range. According to the German standard DIN V 4757 (1995), the density between 0–99.5 °C can be described using a fourth-power polynomial (equation (3.2)):

$$\rho(T) = a_0 + a_1 T + a_2 T^2 + a_3 T^3 + a_4 T^4 \quad (3.2)$$

with

a_0	Coefficient 0 (999.85 kg m^{-3})	[kg m^{-3}]
a_1	Coefficient 1 (6.187*10^{-2} kg m^{-3} °C^{-1})	[kg m^{-3} °C^{-1}]
a_2	Coefficient 2 (-7.654*10^{-3} kg m^{-3} °C^{-2})	[kg m^{-3} °C^{-2}]
a_3	Coefficient 3 (3.974*10^{-5} kg m^{-3} °C^{-3})	[kg m^{-3} °C^{-3}]
a_4	Coefficient 4 (-1.110*10^{-7} kg m^{-3} °C^{-4})	[kg m^{-3} °C^{-4}]
T	Fluid Temperature	[°C]
$\rho(T)$	Density at Temperature *T*	[kg m^{-3}]

For water glycol mixtures as heat transfer medium, the density temperature correlations are additionally dependent on the mixing ratio. CARNOT uses fitted data out of Adunka (1991) to describe the correlations. Figure 3.1 shows the density temperature correlations for the heat transfer liquids used in the sensitivity analysis (cf. Chapter 3.5.2).

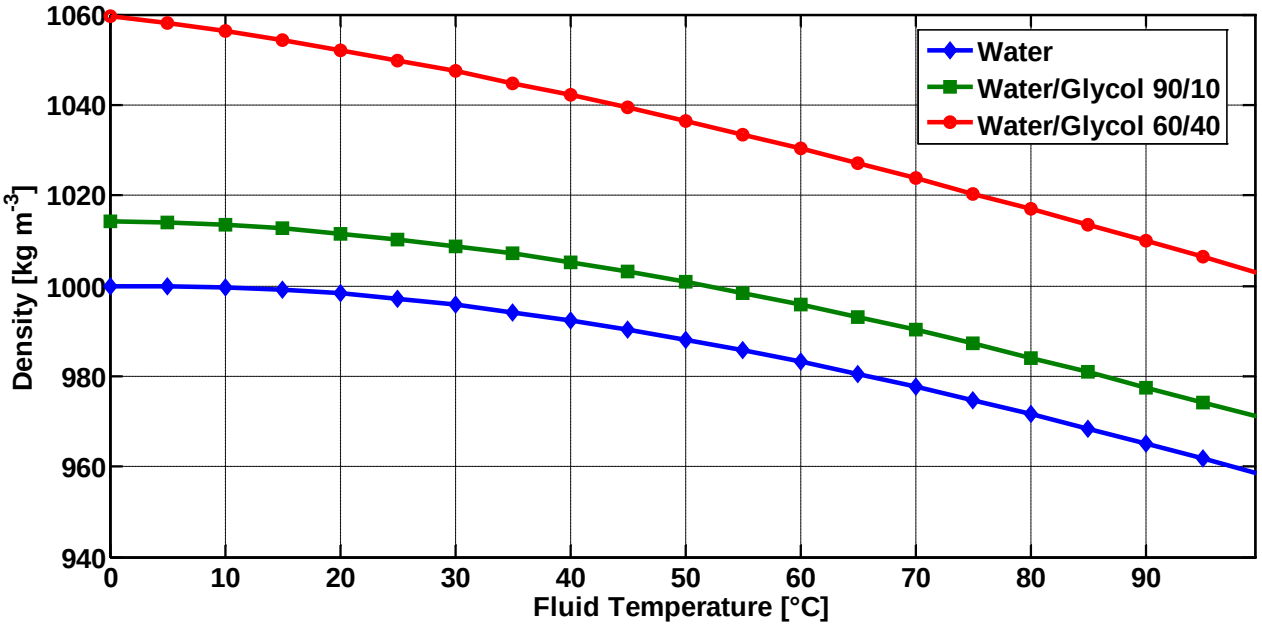

Figure 3.1: Density Temperature Correlations of Water and Water/Glycol Mixtures used in Simulations

3.1.2 Basic Working Principle of a Thermosyphon Solar Water Heater

In general, a thermosyphon system can be compared to a U-tube filled with water as illustrated in Figure 3.2.

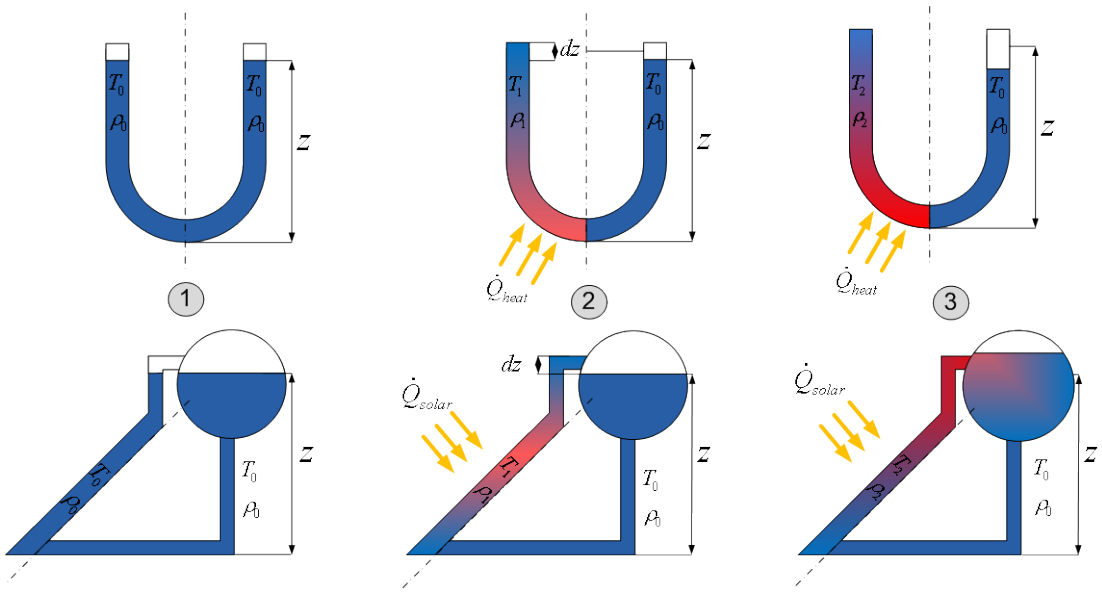

Figure 3.2: Functional Principle of Thermosyphon Systems

At starting time *t = 0*, both the U-tube and the thermosyphon system are filled with fluid (water) of a uniform temperature. Due to the principle of communicating vessels, both branches are filled to the same height *z* (Figure 3.2, case 1). The same conditions are valid for the thermosyphon system. The solar collector and the piping leading to the storage tank correspond to the left side, while storage tank and the returning pipe are part of the right branch.

The water inside the left branch of the U-tube is heated by an external heat source and the thermosyphon system by the sun (Figure 3.2, case 2). The density in the left branch is decreasing according to equation (3.2). The filling height in the left branch increases as described in equation (3.3):

$$dz = \frac{m\Delta\rho}{\rho_0 \rho_1 A_{pipe}} \tag{3.3}$$

with

A_{pipe}	Pipe Cross Section Area	[m²]
dz	Height Increase	[m]
m	Fluid Mass	[kg]
$\rho_{0,1}$	Fluid Density	[kg m^{-3}]
$\Delta\rho$	Density Change	[kg m^{-3}]

The external heat supply is continued until the water in the left branch starts to spill. Hence, the left branch becomes lighter than the right branch. According to the principle of communicating vessels, water flows from right to left until mass balance is reached again. Looking at the thermosyphon system, water flows into the storage tank, where it increases the imbalance additionally (Figure 3.2, case 3) and forces the flow rate.

Theoretically, the increasing imbalance leads to a very high mass flow rate. Due to pressure losses caused by bends, branches and roughness and viscosity inside the hydraulic circuit a balanced system develops, where pressure losses are equal to the pressure gain by buoyancy (equation (3.4)):

$$\Delta p_{buo} = \Delta p_{loss} \tag{3.4}$$

with

Δp_{buo}	Pressure Gain by Buoyancy	[Pa]
Δp_{loss}	Pressure Losses by Fluid Velocity	[Pa]

3.1.3 Flat-Plate Collectors

If the temperature rise between collector inlet and outlet is assumed to be linear, the temperature change can be written as a function of the collector height as illustrated in Figure 3.3 and described by equations (3.5) and (3.6):

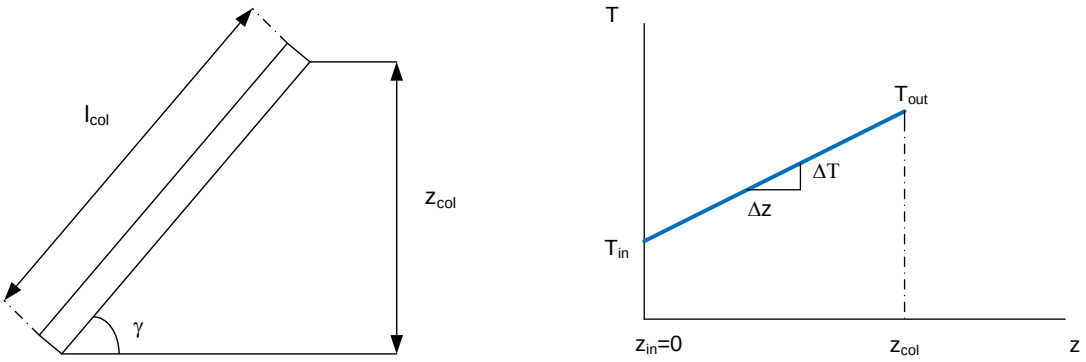

Figure 3.3: Schematic Side View of a Solar Collector and Linear Temperature Height Correlation

$$z_{col} = l_{col} \sin \gamma \tag{3.5}$$

$$T(z) = \frac{\Delta T}{\Delta h} z + T_{in} \tag{3.6}$$

with

h_{col}	Collector Height	[m]
l_{col}	Collector Length	[m]
T_{in}	Collector Inlet Temperature	[°C]
$T(z)$	Temperature at Height *z*	[°C]
ΔT	Temperature Difference between Collector Inlet and Outlet	[K]
z	Specific Collector Height	[m]
Δz	Height Difference between Collector Inlet and Outlet	[m]
γ	Collector Tilt Angle	[°]

A more correct formulation of the temperature rise within the collector is made by using an equation derived from Duffie and Beckmann (2006). A constant overall heat loss coefficient U_L and a constant collector efficiency factor F' (equation (3.7) and (3.8) are taken into account.

$$T(z) = (T_{in} - T_{amb} - \frac{G_{col}}{U_L}) \exp(-\frac{A_{col}(z) U_L F'}{\dot{m} c}) + T_{amb} + \frac{G_{col}}{U_L} \tag{3.7}$$

$$A_{col}(z) = \frac{wz}{\sin \gamma} \tag{3.8}$$

with

$A_{col}(z)$	Collector Area at Height *z*	[m²]
c	Heat Capacity of Collector Fluid	[J kg^{-1} K^{-1}]
F'	Collector Efficiency Factor	[-]
G_{col}	Irradiation in Collector Plane	[W m^{-2}]
$\dot{m}$	Mass Flow Rate	[kg s^{-1}]
$T(z)$	Temperature at Height *h*	[°C]
T_{in}	Inlet Temperature	[°C]
T_{amb}	Ambient Temperature	[°C]
U_L	Overall Heat Loss Coefficient	[W m^{-2}K^{-1}]
w	Collector Width	[m]
z	Collector Height	[m]
γ	Collector Tilt Angle	[°]

Both calculation methods have advantages and disadvantages. For the linear approach, measurement data for inlet and outlet temperature have to be available to calculate the fluid temperature inside the collector. In consequence, this method is not practicable for simulation models, as the goal behind the simulation is to calculate the outlet temperature.

The method propagated by Duffie and Beckmann can be implemented into simulation models. It contains constants, the overall heat loss coefficient and the collector efficiency factor, and calculates the outlet temperature using the available variables irradiation, mass flow and collector inlet temperature. The calculation method by Duffie and Beckmann is compared to data of a collector efficiency test. The collector efficiency factor F' = 0.9 is calculated according to equation (2.23) and the overall heat loss coefficient U_L = 4.58 W m^{-2} K^{-1} is taken from the collector efficiency curve. Data from different temperature steps are taken into consideration in order to identify the temperature dependency of the calculation method (Figure 3.4).

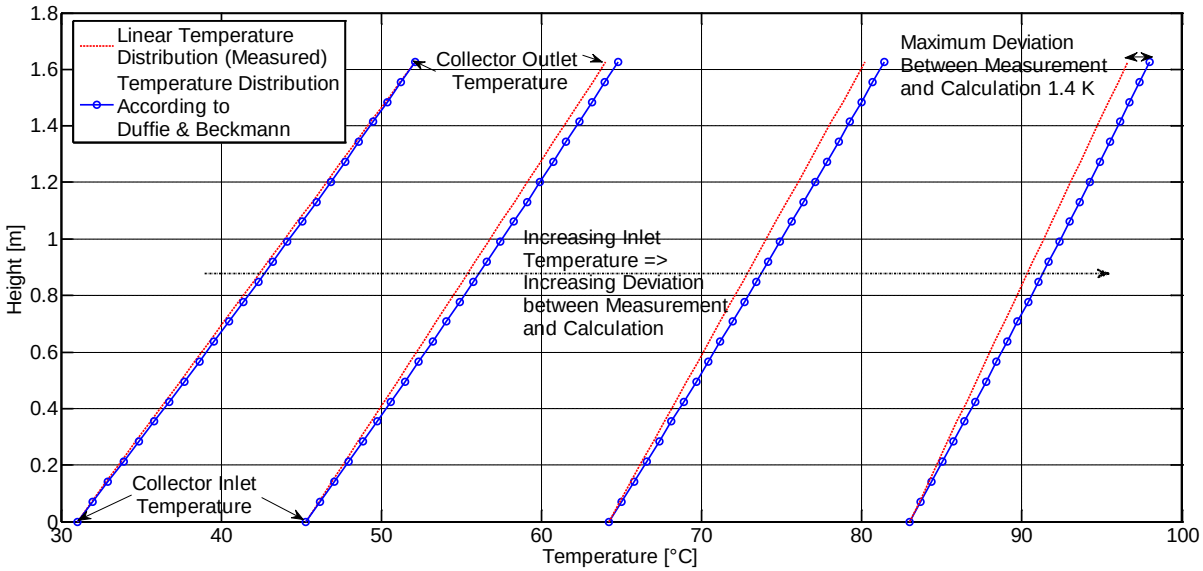

Figure 3.4: Difference Between Calculated and Measured Temperature Distribution Along a Collector

The maximum deviation between calculation and measurement is 1.4 K or 10 % at a collector inlet temperature of 83 °C.

Using equations (3.1) to (3.4), the density change, leading to the thermosyphonic flow inside the solar collector, can be described by equation (3.9)

$$\Delta\rho(z) = \int_0^z \rho_{in}(T_{in}) - \rho(T(z))dz \tag{3.9}$$

with

T_{in}	Collector Inlet Temperature	[°C]
$T(z)$	Temperature at Height *h*	[°C]
z	Collector Height	[m]
$\Delta\rho(z)$	Density Change within the Solar Collector	[kg m^{-3}]

3.2 Possibilities and Challenges using MATLAB / SIMULINK with the Extension CARNOT

The CARNOT (Conventional And Renewable eNergy systems Optimization Toolbox) blockset is an extension for MATLAB / SIMULINK. CARNOT is a tool for the calculation and simulation of heating systems. It provides models for heat sources such as solar col-

lectors, storage tank systems, hydraulics and offers a library for fundamental material calculation. Due to the open source philosophy, CARNOT can be enhanced by every user. The components used for the simulation of thermosyphon systems, except the double mantle heat exchanger storage tank, were validated by Hafner et al. (1999).

In comparison to standard solar-thermal simulation software, CARNOT offers the possibility to analyse the behaviour of a model in detail. Furthermore, the development and testing of new models and control strategies is possible.

3.2.1 Thermo Hydraulic Vector

CARNOT uses data vectors to transport information within the models. The most important vector is the so-called thermo hydraulic vector (THV). The THV bundles all relevant fluid data and fluid states. This includes the fluid identity, e.g. water or water-glycol mixture, fluid pressure, pressure drop coefficients, fluid temperature, velocity and density (Table 3.1). During simulation the THV is passed from block to block. Inside each block the THV is disassembled and the changes to the fluid state are calculated, e.g. the pressure losses and temperature drop in a pipe. Afterwards the THV is reassembled and fed into the subsequent block as entry.

Table 3.1: Structure of the Thermo Hydraulic Vector (Hafner et al., 1999)

No.	Description	Physical Unit	Remarks
1	Flow Identifier (ID)	[-]	ID < 0 no mass flow in the branch ID <= 10,000 no pressure drop calculation ID <= 20,000 only pressure drop calculation ID >= 20,000 calculation of pressure drop and static pressure
2	Fluid Temperature	[°C]	-
3	Mass Flow	[kg s^{-1}]	-
4	Fluid Pressure	[Pa]	-
5	Fluid Type	[-]	1 water 2 air 3 cotton oil 4 silicone oil 5 water-propylene glycol
6	Fluid Mixture	[-]	Percentage of propylene glycol in water-propylene glycol antifreeze mixtures
7	Pipe Diameter	[m]	-
8	Constant Pressure Drop Coefficient	[Pa]	Cf. Chapter 3.2.2.2
9	Linear Pressure Drop Coefficient	[s kg^{-1}]	Cf. Chapter 3.2.2.2
10	Quadratic Pressure Drop Coefficient	[s^2 kg^{-2}]	Cf. Chapter 3.2.2.2
11...20	Not Used	-	-

3.2.2 Mathematical Description of the Simulation Blocks Used

Most of the blocks needed for the thermosyphon system simulation are available in the standard CARNOT library. The double mantle storage tank needed for a realistic system setup is not available so far.

3.2.2.1 Solar Collector

CARNOT's solar-thermal collector model is based on TRNSYS type 101 (Isakson, 1991; Hafner et al., 1999), a matched flow collector model. It is a so-called characteristic curve model. Basis of the calculation is the second order collector efficiency curve derived from normative tests according to DIN EN 12975-2 (2006). The calculation is carried out using a one-dimensional multi node approach. The collector is divided between inlet and outlet

into *n* user settable nodes. Along its width, no division into nodes takes place. Consequently, the flow distribution is considered to be uniform throughout the collector. Each node *n* is taken into consideration in order to calculate the energy balance as shown in equation (3.10). This equation is represented by the block 'unicol_R13' in Figure 3.5.

$$c_{col}\frac{dT}{dt} = \\ = \dot{q}_{sol} + \frac{\dot{m}c_{fluid}}{A_{col}}(T_{n-1} - T_n) + a_1(T_{amb} - T_n) - a_2(T_{amb} - T_n)^2 + u_{wind}v_{wind}(T_{amb} - T_n) + u_{sky}(T_{sky} - T_n) \quad (3.10)$$

with

A_{col}	Aperture Area	[m²]
c_{col}	Thermal Capacity of the Solar Collector per m²	[J m^{-2} K^{-1}]
c_{fluid}	Specific Heat Capacity of the Heat Carrier	[J kg^{-1} K^{-1}]
$\dot{q}_{sol}$	Absorbed Radiation per Collector Area	[W m^{-2}]
dT	Temperature Gradient	[K]
dt	Time Step	[s]
$\dot{m}$	Collector Mass Flow Rate	[kg s^{-1}]
T_{amb}	Ambient Temperature	[°C]
T_{n-1}	Temperature of the Previous Node	[°C]
T_n	Temperature of the Considered Node	[°C]
u_{wind}	Wind Heat Loss Coefficient	[W s m^{-3} K^{-1}]
v_{wind}	Wind Velocity	[m s^{-1}]
u_{sky}	Clear Sky Heat Losses	[W m^{-2} K^{-1}]
T_{sky}	Sky Temperature	[°C]
a_1	Linear Collector Heat Loss Coefficient	[W m^{-2} K^{-1}]
a_2	Quadratic Collector Heat Loss Coefficient	[W m^{-2} K^{-2}]

Equation (3.10) takes wind and sky temperature dependent losses into account, which are already included in the collector efficiency curve. These losses are set to 0 in the simulation runs. The irradiation into the collector plane is composed of direct and diffuse

irradiation portions, the position of the collector against the sun and the optical characteristics of the transparent cover. These correlations are included in the collector model as subsystems (Figure 3.5).

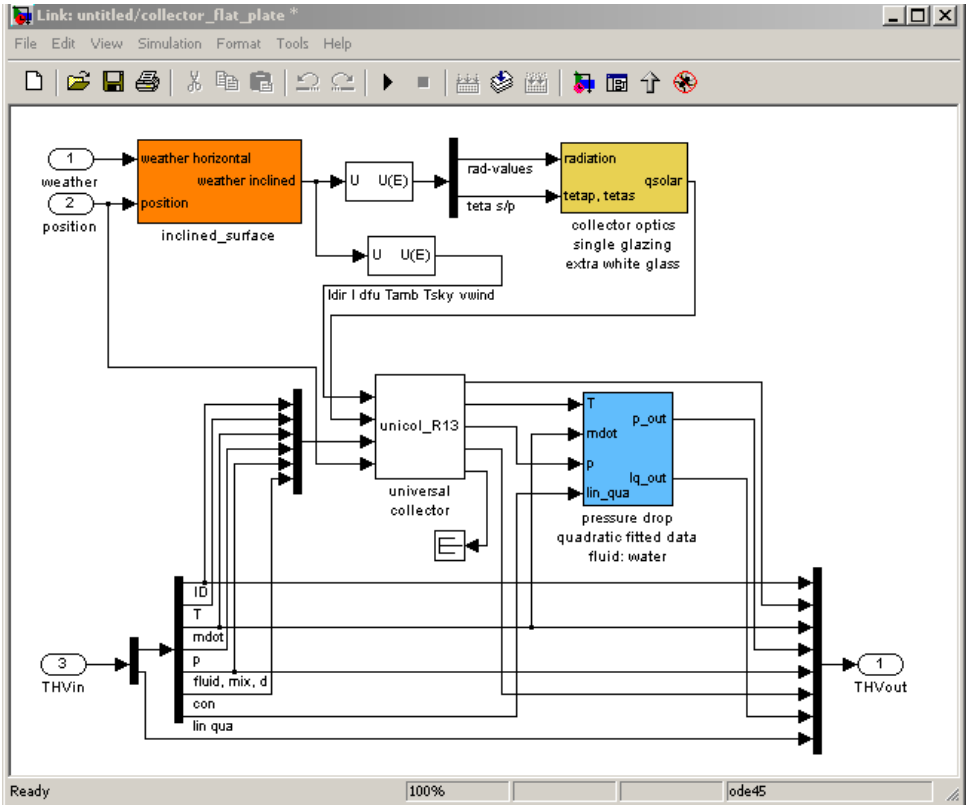

Figure 3.5: CARNOT Collector Subsystem

The subsystem ‘inclined surface’ calculates the irradiation onto the transparent cover. The horizontal direct and diffuse irradiation, sun zenith and azimuth angle, the collector tilt and azimuth angle as well as the isotropic or the Hay-Davis sky model are part of this calculation.

Figure 3.6 exemplarily shows the calculation of the zenith and azimuth angle on a horizontal surface. The calculation for an inclined collector is carried out analogously.

The subsequent block ‘collector optics’ determines the optical characteristics of the transparent collector cover. It includes the glazing properties as well as the incidence angle modifier (IAM) of the direct irradiation. By multiplying the calculated values with the optical efficiency the actual absorbed energy per collector area is computed, which is used in equation (3.10).

Originally, the IAM is interpolated using a value table. In order to improve the usability of the model, the model is enhanced by a calculation method developed by Ambrosetti and Keller (1985). This calculation method is also applied to the collector testing standard DIN EN 12975-2 (DIN, 2006). For the calculation of the IAM of flat-plate collectors only one measurement point is necessary. This value at an irradiance angle of $\theta = 50\ °$ compared to the perpendicular irradiation onto the collector surface (Figure 3.7) can be taken from every collector test report.

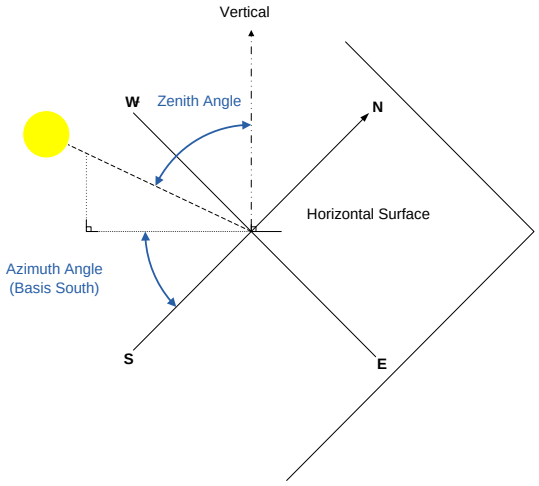

Figure 3.6: Definition of Zenith and Azimuth Angle

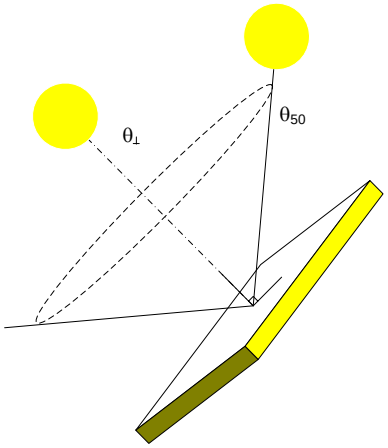

Figure 3.7: Beam Angle $\theta = 50\ °$ for the IAM-Measurement

Equations (3.11) and (3.12) have to be solved for *n*, a collector specific coefficient to describe the IAM for all beam angles.

$$ki(\theta) = 1 - \tan^{n}(\frac{\theta}{2}) \quad (3.11)$$

in which $ki(\theta) = \frac{\eta_\theta}{\eta_\perp}$ (3.12)

with

$ki(\theta)$	Incidence Angle Modifier (IAM)	[-]
θ	Beam Angle	[°]
n	Collector Specific Coefficient	[-]
η_θ	Collector Efficiency at Beam Angle θ	[-]
$\eta_\perp$	Collector Efficiency at Perpendicular Irradiation	[-]

Due to their optical asymmetrical behaviour, evacuated tube collectors and parabolic troughs cannot be described by this formula.

The pressure gain inside the solar collector is calculated according to the density change in every collector node, while friction losses due to fluid velocity are calculated in a sub-system. The calculation of the pressure drop uses an approach given in DIN EN 12975-2 (DIN, 2006). All pressure drop values are measured at 20 °C fluid temperature and evaluated using a quadratic regression (equation (3.13)):

$$\Delta p = p_{loss,qua}\dot{m}^2 + p_{loss,lin}\dot{m} \quad (3.13)$$

with

$\dot{m}$	Mass Flow Rate	[kg s^{-1}]
$p_{loss,lin}$	Linear Velocity Depended Pressure Drop	[Pa s kg^{-1}]
$p_{loss,qua}$	Quadratic Velocity Depended Pressure Drop	[Pa s^2 kg^{-2}]
Δp	Pressure Drop	[Pa]

An adaptation of the friction losses due to the fluid temperature or the fluid viscosity is not calculated, as sheet pipe or volumetric solar collectors are very complex from the hydraulic point of view (cf. Chapter 2.2.2).

3.2.2.2 Thermosyphonic Pump

The circulation of the system is maintained by small pressure differences in the range of 1-30 mm water column (Morrison and Ranatunga, 1980). Beside the pressure gain on the collector side, friction losses result in the equilibrium of gain and losses. The resulting mass flow is described in equation (3.14) as a function of temperature and fluid velocity:

$$\dot{m} = f(T_{fluid}, v_{fluid}) \tag{3.14}$$

with

$\dot{m}$	Mass Flow Rate	[kg s^{-1}]
T_{fluid}	Fluid Temperature	[° C]
v_{fluid}	Fluid Velocity	[m s^{-1}]

The calculation of the pressure differences is one of the most important functions in thermosyphon systems. In CARNOT, a so called thermosyphonic pump is used to calculate the mass flow (Figure 3.8). The thermosyphonic pump is a standard component in CARNOT and is described in brief.

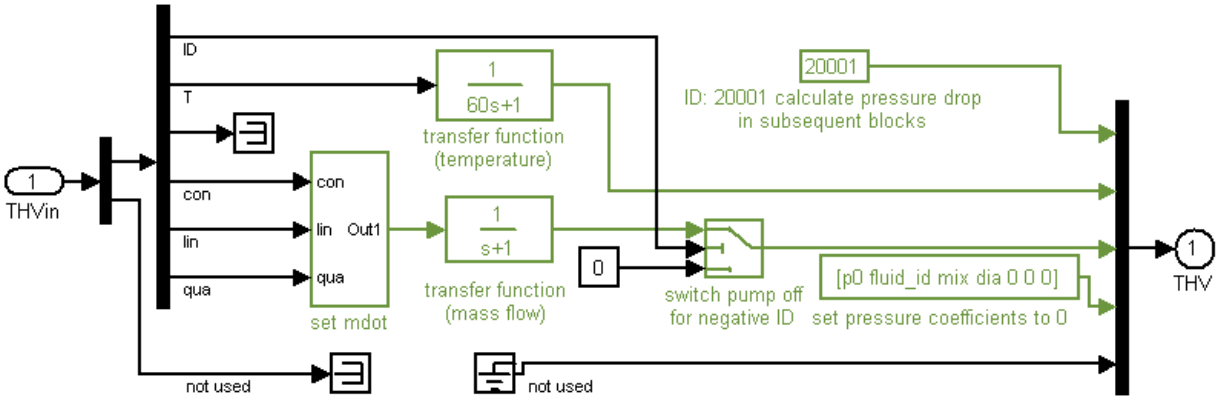

Figure 3.8: Model of the Thermosyphonic Pump in CARNOT

The mass-flow is calculated in the subsystem “set mdot”. It is solved using the standard quadratic equation (3.15). After calculating the mass flow in the thermosyphonic pump, the pressure coefficients are set to zero “[… 0 0 0]” and every subsequent block adds its pressure changes again. For negative fluid IDs (indicating no mass flow in the system), the mass flow is set to 0 kg s^{-1} using the switch function “switch pump off”. To avoid algebraic loops the direct feed through of the fluid temperature and mass flow is suppressed

by using the linear time-invariant (LTI) transfer functions ‘temperature’ and ‘mass flow’ as shown in Figure 3.8.

$$0 = p_{loss,qua} * \dot{m}^2 + p_{loss,lin} * \dot{m} + p_{loss,con} \tag{3.15}$$

with

$\dot{m}$	Mass Flow Rate	[kg s^{-1}]
$p_{loss,con}$	Constant Pressure Drop / Gain and Static Pressure	[Pa]
$p_{loss,lin}$	Linear Velocity Depended Pressure Drop	[Pa s kg^{-1}]
$p_{loss,qua}$	Quadratic Velocity Depended Pressure Drop	[Pa s^2 kg^{-2}]

Equation (3.17) is represented in CARNOT by the scheme shown in Figure 3.9.

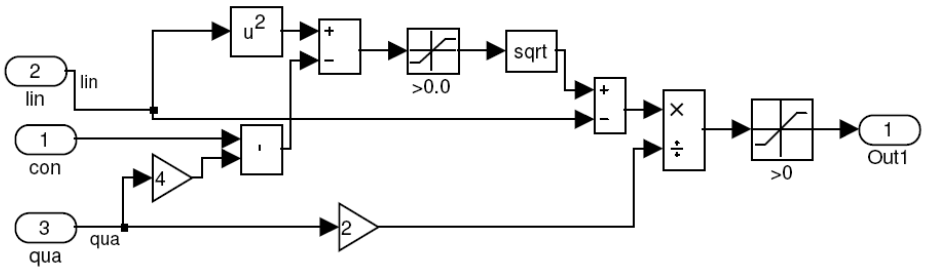

Figure 3.9: Quadratic Approach to Calculate a Mass Flow out of Pressure Terms

The constant coefficient contains the temperature and height dependent static pressure, while the linear and quadratic coefficients include all pressure changes by friction.

All pressure coefficients are fed through every block of the thermosyphon system model and the pressure changes are added. This calculation method requires every block used for the thermosyphon system to have a pressure calculation subsystem.

The accuracy of the thermosyphonic pump in the simulation model is validated using measurement data from system tests (cf. Chapter 3.4).

In order to achieve realistic flow rates through the thermosyphon system, special attention has to be drawn to the system’s height settings. Even slight height and therefore

static pressure differences between the hot and cold leg of the thermosyphon system lead to a faulty system behaviour with e.g. mass-flow during nights.

An m-script[3] originally implemented in CARNOT to check the height differences caused various problems and produced incorrect simulation results. Therefore, the parameterisation was revised in this work using the geometrical correlations within the thermosyphon system as shown in Figure 3.10 and equations (3.16) to (3.20). The related m-script has become part of the updated CARNOT toolbox and can be used by the whole CARNOT user-group.

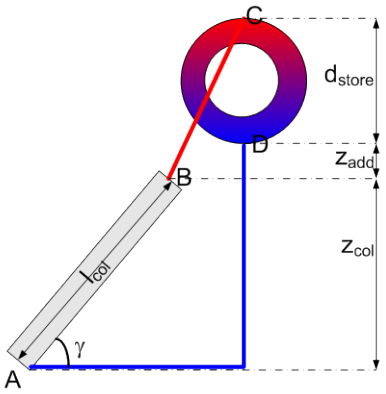

Figure 3.10: Geometrical Correlations for the Calculation of the Heights within the Simulation

$$\overline{AB} + \overline{BC} + \overline{CD} + \overline{DA} = 0 \tag{3.16}$$

Wherein

$$\overline{AB} = l_{col} \sin\gamma \tag{3.17}$$

$$\overline{BC} = z_{add} + d_{store} \tag{3.18}$$

$$\overline{CD} = -d_{store} \tag{3.19}$$

$$\overline{DA} = -z_{add} - l_{col} \sin\gamma \tag{3.20}$$

[3] A m-script is an executable sequence stored in a plain text file

with

$\overline{AB};\overline{BC};\overline{CD};\overline{DA}$	Length of Each Leg	[m]
d_{store}	Storage Tank Diameter	[m]
l_{col}	Collector Length	[m]
z_{add}	Height Difference between Collector and Storage	[m]
γ	Collector Tilt Angle	[°]

3.2.2.3 Piping

The thermal part of the piping is calculated using a finite volume calculation method according to Patankar (1980). The differential equation for an insulated pipe is described by equation (3.21):

$$\frac{c_{wall} * l_{pipe}}{V_{node}} \frac{dT}{dt} = \frac{u_{pipe} * A_{loss}}{V_{node}} (T_{amb} - T_n) + \frac{\kappa_{axial}}{dh^2} (T_{n+1} - T_n) + \frac{\kappa_{axial}}{dh^2} (T_{n-1} - T_n) + \\ + \frac{\dot{m} c_{fluid}}{V_{node}} (T_{n-1} - T_n) \tag{3.21}$$

with

A_{loss}	Inner Surface of the Pipe	[m²]
c_{fluid}	Specific Heat Capacity of the Fluid	[J kg^{-1} K^{-1}]
c_{wall}	Specific Heat Capacity of the Piping Material	[J m^{-1} K^{-1}]
κ_{axial}	Effective Axial Heat Conductivity	[W m^{-1} K^{-1}]
dh	Length of a Node	[m]
l_{pipe}	Pipe Length	[m]
$\dot{m}$	Mass Flow Rate	[kg s^{-1}]
T_{amb}	Ambient Temperature	[°C]
u_{pipe}	Pipe Heat Losses	[W m^{-2} K^{-1}]
V_{node}	Nodal Volume	[m³]
dT	Temperature Gradient	[K]

dt	Time Step	[s]
T_{n-1}	Temperature of the Previous Node	[°C]
T_n	Temperature of the Considered Node	[°C]
T_{n+1}	Temperature of the Following Node	[°C]

The heat loss U_{pipe} is calculated using the approach of a pipe with several concentric layers of different heat conductivity (Figure 3.11 and equation (3.22)).

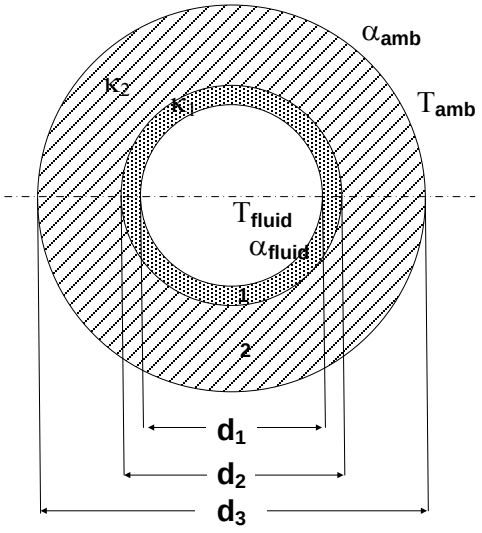

Figure 3.11: Heat Losses at Pipes with Different Concentrically Layers

$$U_{pipe} = \frac{\pi * d_1 * \ln(\frac{d_3}{d_1})}{\frac{1}{\alpha_{amb} * d_3} + \frac{1}{2 * \kappa_{pipe}} * \ln(\frac{d_1}{d_2}) + \frac{1}{2 * \kappa_{iso}} * \ln(\frac{d_2}{d_3}) + \frac{1}{\alpha_{fluid} * d_1}} \quad (3.22)$$

with

d_1, d_2, d_3	Pipe and Insulation Diameters	[m]
$\alpha_{amb}, \alpha_{fluid}$	Convective Heat Transfer Coefficient from the Ambient and the Fluid	[W m^{-2} K^{-1}]
$\kappa_{pipe}, \kappa_{iso}$	Heat Conductivity of Pipe and Insulation Material	[W m^{-1} K^{-1}]
U_{pipe}	Pipe Heat Losses	[W m^{-2} K^{-1}]

To achieve a realistic behaviour of the piping exposed to wind and weather, an additional (constant) convective heat loss is assumed. This heat loss with α_{amb} = 26 W m^{-2} K^{-1} is the mean value of a wind velocity in the range of 1 m s^{-1} < v_{wind} < 3 m s^{-1} for an outer pipe diameter of 50 mm (Elgeti, 2006). The convective heat transfer from the collector fluid to the pipe wall is assumed to be α = 600 W m^{-2} K^{-1}. This value corresponds to natural convection of water which is found to be in the range of 100–600 W m^{-2} K^{-1} (Kneer, 2007).

Besides, radial heat losses axial heat transfer is taken into consideration. For metallic materials the heat carrier fluid used has no influence on the resulting axial heat conductivity. In contrast the axial heat conductivity of materials with low heat conductivity such as polymers is dominated by the heat transfer fluid. The friction losses inside the piping are calculated according to the fluid velocity to be either laminar or turbulent, depending on the Reynolds Number (cf. equation (2.35)).

For a laminar flow regime (Re < 2,320), the calculation of the pressure drop has to be carried out according to equation (3.23):

$$\Delta p = \frac{64}{\mathrm{Re}} \frac{l_{pipe}}{d_{inner}} \frac{\rho}{2} v_{fluid}^2 \qquad (3.23)$$

with

d_{inner}	Inner Tube Diameter	[m]
l_{pipe}	Pipe Length	[m]
Δp	Pressure Drop	[Pa]
v_{fluid}	Velocity of the Fluid	[m s^{-1}]
ρ	Fluid Density	[kg m^{-3}]

For turbulent flow (Re > 2,320) the correlation changes to equation (3.24):

$$\Delta p = f \frac{l_{pipe}}{d_{inner}} \frac{\rho}{2} v_{fluid}^2 \qquad (3.24)$$

with

d_{inner}	Inner Tube Diameter	[m]
f	Friction Factor (Velocity depended)	[-]
l_{pipe}	Pipe Length	[m]
Δp	Pressure Drop	[Pa]
v_{fluid}	Velocity of the Fluid	[m s^{-1}]
ρ	Fluid Density	[kg m^{-3}]

The friction factor *f* in this case is a function of Reynolds number and surface roughness *e* of the pipe (equation (3.25)):

$$f = x(\mathrm{Re}, e) \tag{3.25}$$

with

e	Surface Roughness	[m]
f	Friction Factor (Velocity depended)	[-]
Re	Reynolds Number	[-]
$x(\mathrm{Re}, e)$	Function of Reynolds Number and Roughness	[-]

According to Bohl and Elmendorf (2005), hydraulically smooth pipes are defined as shown in equation (3.26):

$$\mathrm{Re}\frac{e}{d_{inner}} < 65 \tag{3.26}$$

The calculation of *f* is subdivided into three sections according to the Reynolds number (equations (3.27) to (3.29)):

- Blasius formula for the range 2,320 <Re <10^5

$$f = 0.3164\,\mathrm{Re}^{-0.25} \tag{3.27}$$

- Nikuradse formula for the range 10^5 < Re < 5*10^6

$$f = 0.0032 + 0.221\,\mathrm{Re}^{-0.237} \tag{3.28}$$

- Prandtl and Kármán formula for the range Re > 10^6

$$\frac{1}{\sqrt{f}} = 2\lg(\mathrm{Re}\sqrt{f}) - 0.8 \tag{3.29}$$

with

d_{inner}	Inner Tube Diameter	[m]
e	Surface Roughness	[m]
f	Friction Factor	[-]
Re	Reynolds Number	[-]

Pressure losses caused by bends and other obstacles in the piping are added as additional hydraulic pipe length. For laminar flow, correction models for developing flow published in Bohl and Elmendorf (2005) are used.

3.3 Development and Validation of a Double Mantle Heat Exchanger Storage Model

CARNOT lacked a double mantle storage heat exchanger which, however, is indispensable for a realistic system simulation model of modern thermosyphon hot water heaters. Basis to this development besides others are the simple hot water storage tank model already available in CARNOT and a validated TRNSYS double mantle heat exchanger storage tank model (Andrés and López, 2002). Both models are described in Chapter 2.2.3 in brief. The overall requirements to the model development can be summarised:

- Every relevant geometrical parameter has to be tuneable,
- Conduction and convection mechanism have to be considered,
- Stratification effects have to be considered,
- The occurring pressure losses have to be calculated.

The storage tank model is developed using C as programming language. To use the code in MATLAB / SIMULINK it is compiled as a MATLAB executable MEX-file. MEX-files offer two main advantages. MEX-files provide the possibility of speeding up the simulation compared to MATLAB code and allow to call directly standard C-routines without having to rewrite them for MATLAB.

The C-Code of the storage tank can be found in Appendix B. The open source code contributes directly to knowledge as it can be enhanced by every user; the mathematical correlations can be transferred to various simulation environments.

3.3.1 Storage Tank Geometry

Against the background of usability in the product design process, all relevant geometrical storage tank parameters are identified and included into the model as editable parameters.

The storage tank model is one dimensional. It is divided into nodes *n* along its diameter d_{store} while every hot water layer covers the whole storage tank length l_{store} (Figure 3.12). The length of the mantle heat exchanger l_{mantle} can be less or equal to the storage tank length (Figure 3.12). Therefore, a variation in the heat exchanger surface can be simulated and evaluated. The collector fluid inlet is at the top of the heat exchanger annulus, while the outlet is located at the bottom of the heat exchanger. This top to bottom flow direction is a good connection scheme for solar pre-heat thermosyphon systems (cf. Chapter 2.2.3 and 3.5). The cold tap water is fed into the storage tank at the first, respectively bottom node and the hot water is drawn at the last, respectively top node. Due to the calculation scheme used, these heights for collector and hot water circuit are fixed. The head of the storage tank is flat. The possibility of modelling a bumped or dished boiler head is not implemented, as the nodal volume calculation of a three dimensional storage tank head does not bring along additional benefits for the one dimensional calculation scheme.

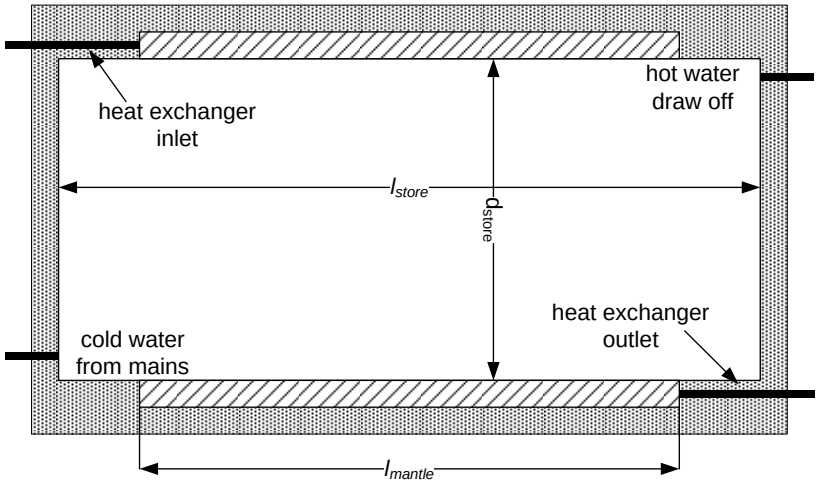

Figure 3.12: Sectional Drawing of the Storage Tank Model

To calculate stratification effects, the storage tank is divided into a user-defined number of layers of either the same height or the same volume. The numeration of the elements is in ascending order from the bottom to the top of the storage tank (Figure 3.13). According to Chapter 2.2.3 (Khalifa and Mehdi, 1999), the heat transfer can be considered to be one dimensional vertical. Thus, symmetry along the vertical axis is taken into consideration.

The following chapter describes the calculation of the geometrical storage tank properties taking a constant node height into consideration. The calculation of the geometrical properties taking a constant volume into account can be seen from the related C-Code in Appendix A. The geometrical properties of the lower part of the storage tank are identical to the upper storage tank properties and have not to be calculated additionally.

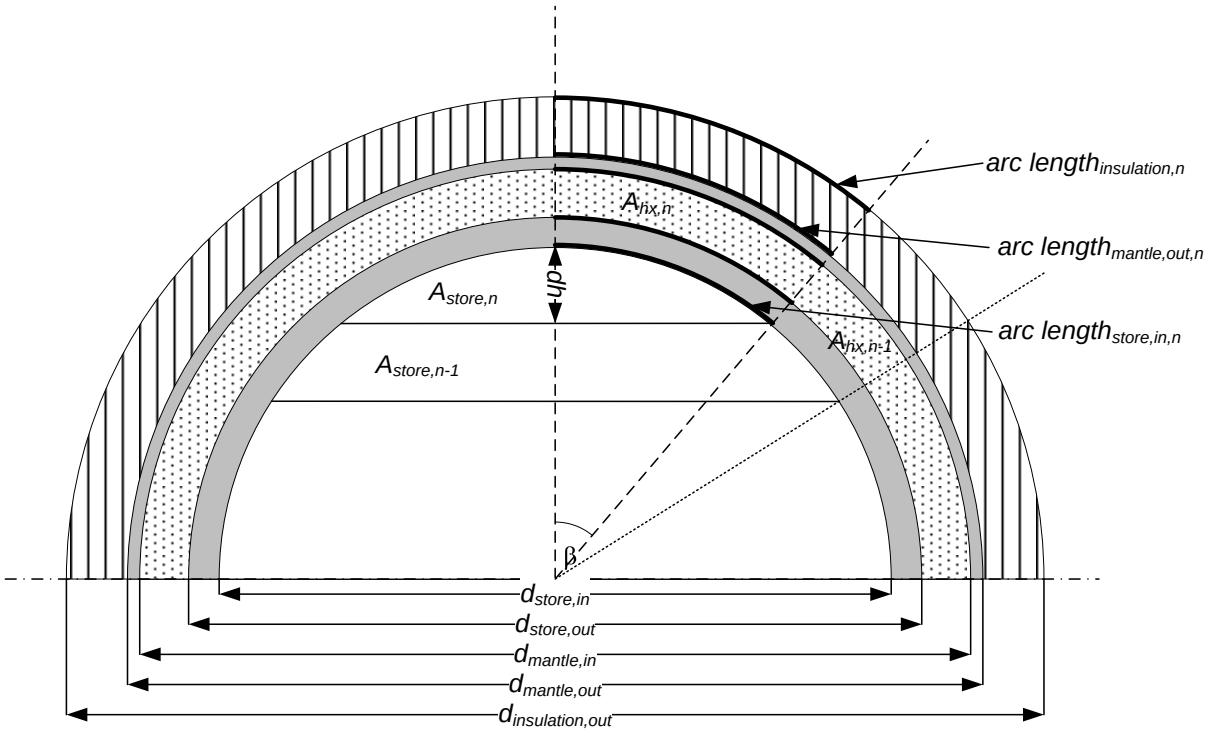

Figure 3.13: Radial Drawing of the Storage Tank Model

The nodal height *dz* is calculated by equation (3.30):

$$dz = \frac{d_{store,in}}{n} \tag{3.30}$$

with

dz	Nodal Height	[m]
$d_{store,in}$	Inner Storage Tank Diameter	[m]
n	Number of Discretised Layers	[-]

After calculating the height of each node, the corresponding angle β_k has to be identified (equation (3.31)):

$$\beta_k = \arccos\left(\frac{\frac{d_{store,in}}{2} - b * dz}{\frac{d_{store,in}}{2}}\right) * \frac{180°}{\pi} \tag{3.31}$$

$$b = (n - k) + 1 \tag{3.32}$$

with

β_k	Chord Angle of Node *k*	[°]
b	Number of Elements in Contradictory Direction to *k*	[-]
k	Index of Current Node	[-]

Using the chord angle β_k, the volume of one layer can be calculated using equations (3.33) to (3.35) by subtracting the area of the triangle below the element and all elements above the considered node from the sector described by β_k (Figure 3.14).

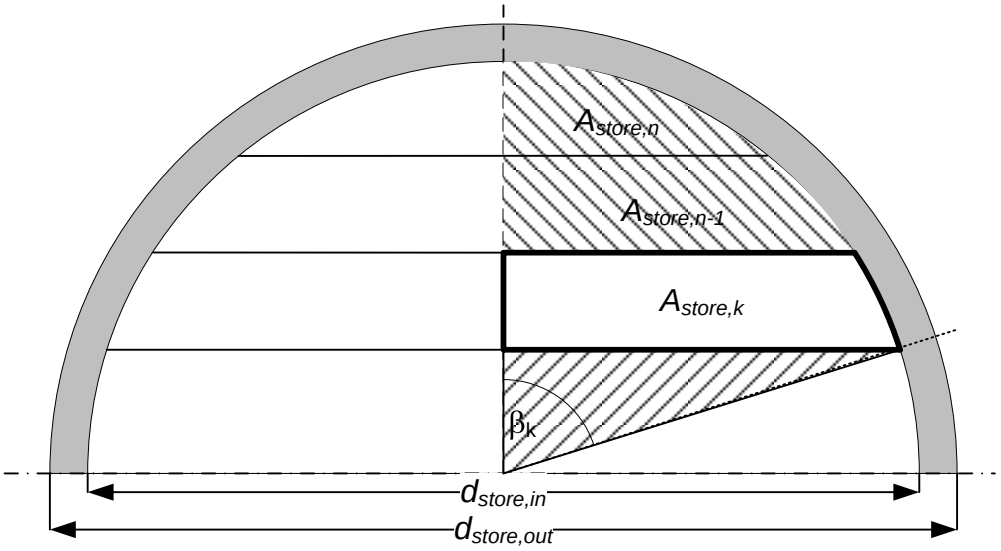

Figure 3.14: Schematic for the Calculation of $A_{store,k}$

$$V_{store,k} = A_{store,k} * l_{store} \tag{3.33}$$

$$A_{store,k} = \underbrace{\frac{\beta_k}{180°}\frac{d_{store,in}^2}{4}\pi}_{Sector} - \underbrace{0.5 * s_k * (0.5 * d_{store,in} - b * dz)}_{Triangle} - \underbrace{\sum_{k+1}^{n} A_{store,i}}_{\substack{Area. \\ Above}} \tag{3.34}$$

$$s_k = \frac{d_{store,in}}{2}\sin\left(\beta_k * \frac{\pi}{180°}\right) \tag{3.35}$$

with

$V_{store,k}$	Volume of Element *k*	[m³]
$A_{store,k}$	Area of Element *k*	[m²]
s_k	Chord Length of Element *k*	[m]

The next step is the calculation of the arc length o_k of each storage tank material according to equation (3.36):

$$o_k = \frac{\beta_k}{180°} \frac{d_{k,layer}}{2} \pi \tag{3.36}$$

with

0_k	Arc Length	[m]
$d_{k,layer}$	Diameter of the Considered Layer at Node k	[m]

To calculate the real volume or the real arc length, every calculated value has to be doubled. As both even and odd numbers of nodes are allowed for the simulation, special attention to the elements around the horizontal symmetry axis has to be drawn in the program code.

For an even element number, the last node of the upper storage tank part is terminated by the symmetry axis, meaning element 1 is equal to element n, element 2 equals element n-1 and so on.

For an odd number of elements, a centrepiece exists, which is halved by the horizontal symmetry axis into an upper and a lower part. The behaviour of this centre node is calculated using *dz/2*. Afterwards, the area, volume and arc length is doubled. The calculation of the other elements is done according to the even case.

3.3.2 Heat Transfer Mechanisms and Stratification

The thermal behaviour of the storage tank is modelled by drawing the energetic balance for every node of collector fluid and hot water. The changes of inner energy per time step have to be equal to the entering and leaving heat flux. The basic equations can be written as shown in equations (3.37) and (3.38):

$$\frac{dQ_{inner}}{dt} = c \cdot \rho_{fluid,k} \cdot V_{node} \cdot \frac{dT}{dt} = \dot{Q}_{in} - \dot{Q}_{out} \tag{3.37}$$

$$\frac{dT}{dt} = \frac{\dot{Q}_{in} - \dot{Q}_{out}}{c \cdot \rho_{fluid,k} \cdot V_{node}} \tag{3.38}$$

with

V_{node}	Nodal Volume	[m³]
Q_{inner}	Inner Energy	[J]
$\dot{Q}_{in,out}$	Heat Flux	[W]
$\rho_{fluid,k}$	Fluid Density at Node k	[kg m^{-3}]

Equations in form of equation (3.38) can be solved within MATLAB using e.g. the built in algorithm ODE45. Figure 3.15 illustrates the considered heat transfer mechanisms for the calculation of the inner energy of the storage tank under normal operating conditions.

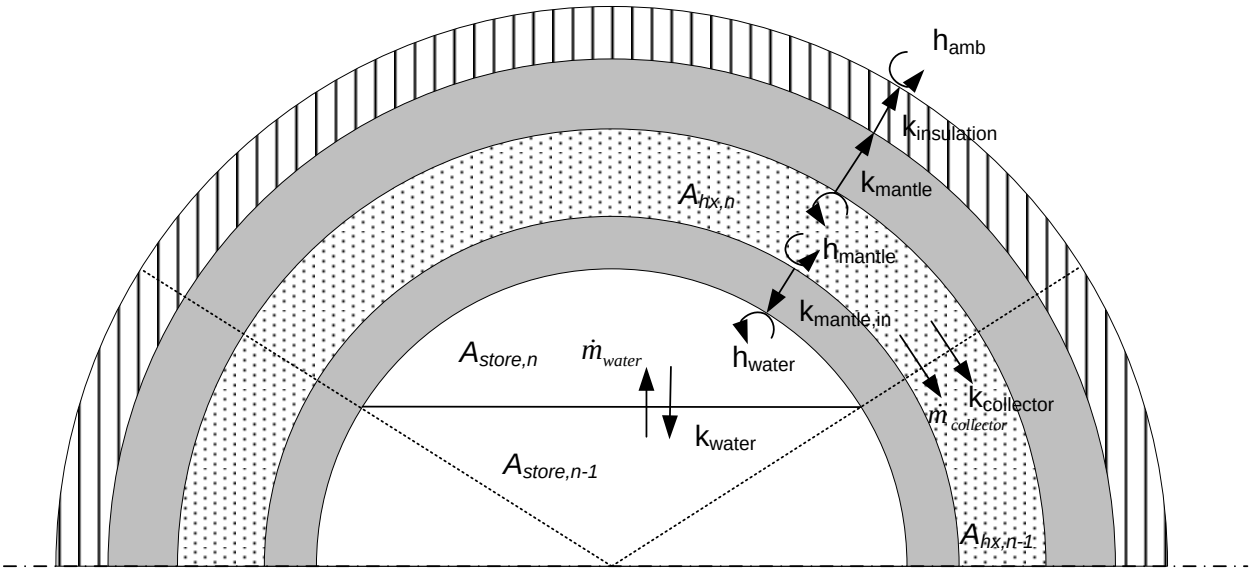

Figure 3.15: Scheme of Considered Heat Transfer Mechanisms

Within the tap water section, heat conduction from the upper, hot nodes towards the lower, cold nodes takes place. While drawing off water, cold water from mains enters the storage tank and is transported depending on the mass flow rate and the draw-off time to the upper nodes.

The collector fluid entering at the top of the storage tank flows towards the storage tank bottom and releases its heat via natural convection at the inner and outer wall of the double mantle. The heat at the inner mantle wall is transported by conduction to the tap water. From there, the heat is transferred to the water by convection. The fluid flow at the storage wall cannot be definitely described (Konrad, 2008). Thus, an imaginary conduction coefficient has to be added to the storage tank material. This coefficient has to be estimated by experimental results.

Heat at the outer mantle wall is transported by conduction through the mantle and insulation material to the ambient. At the ambient, forced convection due to wind takes place. Konrad (2008) calculated a wind dependent convection coefficient $h_{amb} = 13.8\ W\ m^{-2}\ K^{-1}$ for a mean annual wind velocity in the range of $1\ m\ s^{-1} < v_{wind} < 3\ m\ s^{-1}$ based on data published by Elgeti (2006) for a diameter in the range of 0.5–1.0 m.

For areas without heat exchanger connection at the circumference and at the cover plates, heat losses through conduction in the insulation and convection at the ambient are taken into account (Figure 3.16).

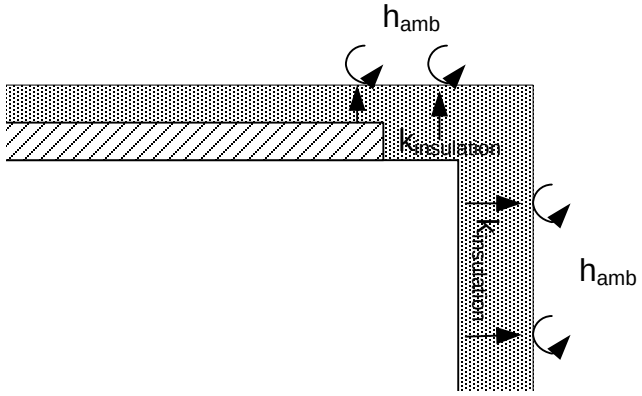

Figure 3.16: Storage Tank Areas without Heat Exchanger

All the heat transfer mechanisms described are combined using the Péclet correlations for flat sheets, which have been proved to be valid for the storage tank. For element *k* of the hot water section, the formulation of the heat transfer is represented by equation (3.39):

$$\frac{dT_{water,k}}{dt} = \frac{1}{\rho_{water,k} \cdot c_{water,k} \cdot V_{water,k}} \cdot (k_{water} \cdot \frac{T_{water,k+1} - T_{water,k}}{dh} \cdot s_{k+1} \cdot l_{store} +$$

$$+ \underbrace{2 \cdot \frac{T_{collector,k} - T_{water,k}}{R_{k_{mantle,circum,in}} + R_{h_{mantle,circum,in}}}}_{\dot{Q}_{in,water}} + c_{water,k} \cdot \dot{m}_{water} \cdot (T_{water,k-1} - T_{water,k}) - k_{water} \cdot \frac{T_{water,k} - T_{water,k-1}}{dh} \cdot s_k \cdot l_{store} -$$

$$- \underbrace{2 \cdot \frac{T_{water,k} - T_{amb}}{R_{k_{mantle,circum,out}} + R_{k_{insulation,store,circum}} + R_{h_{amb,circum}}}}_{\dot{Q}_{out,water}} - 2 \cdot \frac{T_{water,k} - T_{amb}}{R_{k_{mantle,cover}} + R_{k_{insulation,cover}} + R_{h_{amb,cover}}})$$

(3.39)

The correlations for element *k* of the collector fluid are very similar as can be seen in equation (3.40):

$$\frac{dT_{collector,k}}{dt} = \frac{1}{\rho_{collector,k} \cdot c_{collector,k} \cdot V_{collector,k}} \cdot (\underbrace{k_{collector} \cdot \frac{T_{collector,k+1} - T_{collector,k}}{b_{mantle,middle,k}} \cdot d_{mantle,middle} \cdot l_{mantle}}_{\dot{Q}_{in,collector}} +$$

$$+ c_{collector,k} \cdot \dot{m}_{collector} \cdot (T_{collector,k+1} - T_{collector,k}) - \underbrace{k_{collector} \cdot \frac{T_{collector,k} - T_{collector,k-1}}{b_{mantle,middle,k}} \cdot d_{mantle,middle} \cdot l_{mantle}}_{\dot{Q}_{out,collector}} -$$

$$- \frac{T_{collector,k} - T_{water,k}}{R_{k_{mantle,circum,in}} + R_{h_{amb,circum}}} - \frac{T_{collector,k} - T_{amb}}{R_{h_{mantle,circum,out}} + R_{k_{mantle,circum,out}} + R_{k_{insulation,circum,out}} + R_{h_{amb,circum}}})$$

(3.40)

The heat resistances are represented by equations (3.41) to (3.50):

$$R_{k_{mantle,circum,in}} = \frac{(d_{store,out} - d_{store,in})}{k_{mantle}(b_{k,store,out} + b_{k,store,in}) l_{mantle}} \quad (3.41)$$

$$R_{k_{mantle,circum,out}} = \frac{(d_{mantle,out} - d_{mantle,in})}{k_{mantle}(b_{k,mantle,out} + b_{k,mantle,in}) l_{mantle}} \quad (3.42)$$

$$R_{k_{insulation,store,circum}} = \frac{(d_{insulation,out} - d_{store,out})}{k_{insulation}(b_{k,insulation,out} + b_{k,store,in})(l_{store} - l_{mantle})} \quad (3.43)$$

$$R_{k_{mantle,cover}} = \frac{\frac{1}{2}(d_{mantle,out} - d_{mantle,in})}{k_{mantle,in} A_{mantle,k}} \quad (3.44)$$

$$R_{k_{insulation,circum,out}} = \frac{(d_{insulation,out} - d_{mantle,out})}{k_{insulation}(b_{k,insulation,out} + b_{k,mantle,out}) l_{mantle}} \quad (3.45)$$

$$R_{k_{insulation,cover}} = \frac{\frac{1}{2}(d_{insulation,out} - d_{mantle,out})}{k_{insulation,in} A_{insulation,k}} \quad (3.46)$$

$$R_{h_{amb,circum}} = \frac{1}{h_{amb} b_{insulation,out} l_{mantle}} \quad (3.47)$$

$$R_{h_{amb,cover}} = \frac{1}{h_{amb} A_{cover,k}} \quad (3.48)$$

$$R_{h_{mantle,circum,out}} = \frac{1}{h_{mantle} b_{k,mantle,out} l_{mantle}} \quad (3.49)$$

$$R_{h_{mantle,circum,in}} = \frac{1}{h_{mantle} b_{k,store,out} l_{mantle}} \quad (3.50)$$

with

A	Area	[m²]
b	Arc Length	[m]
c	Heat Capacity	[J kg^{-1} K^{-1}]
d	Diameter	[m]
dh	Height Difference	[m]
dt	Time Step	[s]
dT	Temperature Difference	[K]
h	Convective Heat Transfer	[W m^{-2} K^{-1}]
k	Heat Conductivity	[W m^{-1} K^{-1}]
l	Length	[m]
$\dot{m}$	Mass Flow Rate	[kg s^{-1}]
$\dot{Q}$	Heat Flux	[W]
R	Heat Resistance	[K W^{-1}]
s	Chord Length	[m]
T	Temperature	[°C]
V	Volume	[m³]
ρ	Fluid Density	[kg m^{-3}]

Subscripts

amb	Ambient	[-]
circum	Circumference	[-]
collector	Collector	[-]
cover	Cover Plate	[-]
h	Convective	[-]
in	Inner	[-]
insulation	Insulation	[-]
k	Conductive	[-]
mantle	Mantle	[-]
middle	Centre Line	[-]
out	Outer	[-]
store	Storage Tank	[-]
water	Water	[-]

For the energetic calculations, exceptions for the first and last element have to be considered. At the first element, the heat conduction terms $Q_{out,collector}$ and $Q_{out,water}$ are set to zero. The temperature $T_{water,k-1}$ is equal to the water temperature from mains. At the top node, the heat conduction terms $Q_{in,collector}$ and $Q_{in,water}$ are zero. The temperature $T_{collector,k+1}$ is equal to the entering pipe temperature.

3.3.3 Pressure Drop Calculation

In the pressure drop calculation, the static pressure and the dynamic pressure losses of the hydraulic circuits - hot water and collector circuit - are calculated separately. The occurring pressure losses in the hot water circuit are not described in this chapter as these losses only influence the available tap pressure, respectively the maximum draw-off flow rate. The pressure losses of the collector circuit are crucial on the system performance as they are directly influencing the maximum flow rate and so the temperature – flow rate ratio.

In the mantle, a static pressure gain takes place as the inlet is located at the top annulus and the outlet at the bottom of the storage tank (equation (3.51)):

$$\Delta p_{static} = \sum_{k=1}^{n} \rho_{fluid,k} g dh \tag{3.51}$$

with

g	Gravity	[m s^{-2}]
Δp_{static}	Static Pressure Difference	[Pa]
$\rho_{fluid,k}$	Fluid Density at Node k	[kg m^{-3}]

The static pressure difference is added to the constant pressure part in the thermohydraulic vector. The dynamic pressure drop calculation takes diameter changes at the storage tank in- and outlet as well as bends and other obstacles into account (equation (3.52)):

$$\Delta p_{dyn} = \frac{\rho}{2} v_{fluid}^2 \sum \zeta \tag{3.52}$$

with

ζ	Friction Coefficient	[-]
Δp	Pressure Drop	[Pa]
v_{fluid}	Velocity of the Fluid	[m s^{-1}]
ρ	Fluid Density	[kg m^{-3}]

The diameter changes and the corresponding velocity differences were evaluated by Konrad (2008). He concluded that the velocity inside the mantle for a typical double mantle heat exchanger storage tank is nearly zero, so fricition losses in the double mantle can be neglected (Norton et al., 1992). Thus, a dynamic pressure drop only takes place at the inlet. According to Mannhart (2006) $\zeta_{in} = 1$ has to be set.

The friction coefficient ζ_{pipe} of the piping depends on the design of pipe-storage connection. Typical values for ζ_{pipe} can be found in the literature as shown in Figure 3.17 and have to be added to the overall friction coefficient.

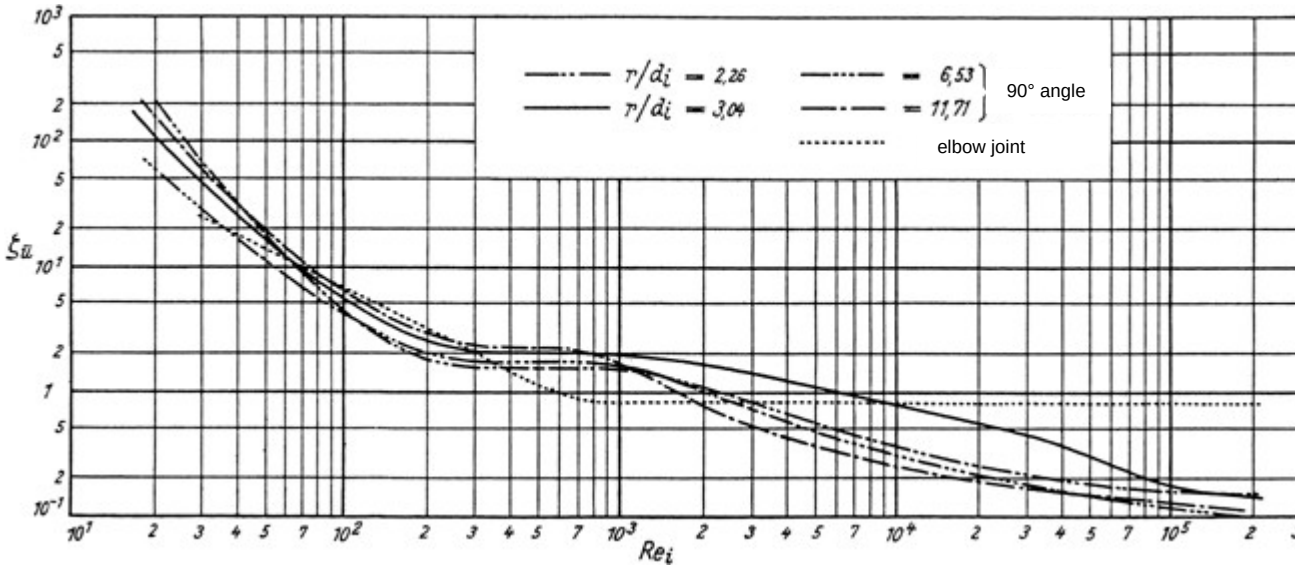

Figure 3.17:Friction Coefficients as a Function of the Reynolds Number for One-Quarter Bends (Kast, 2006)

The values of Δp_{dyn} are added to the overall quadratic system pressure loss as described in equation (3.53):

$$p_{loss,qua} = \frac{\Delta p_{dyn}}{\dot{m}^2} \tag{3.53}$$

with

$p_{loss,qua}$	Quadratic Pressure Loss Value	[Pa s² kg^{-2}]
Δp_{dyn}	Dynamic Pressure Drop	[Pa]
$\dot{m}$	Mass Flow Rate	[kg s^{-1}]

3.3.4 Model Validation

The storage tank model is validated in four steps. During the first step, the behaviour of the storage tank is tested in simulation to calculate realistic results. In a second verification simulation, the double mantle storage tank was directly compared to the validated simple storage tank model. To achieve nearly the same storage tank setup, the double mantle height and its material thickness are set to zero. The insulation characteristics of both systems are assumed to be identical. Both tanks are heated up to 60 °C. Afterwards, the systems are exposed to an ambient temperature of 20 °C and the cooling down phase is logged. The maximum deviation between the temperatures in the centre

node is 0.5 K which can be explained by the convective heat transfer calculation implemented into the double mantle storage tank.

In the third validation step, data of a system measured at the university's test rig are brought into the simulation. The first comparison is made using the heat loss sequence of the 180 l reference storage tank beginning at a uniform temperature of 59.5 °C and taking about 18 h. Figure 3.18 compares both results for the centre (node) of the storage tank directly. The deviation between simulation and test shows a good correlation of below $\Delta T = 1$ K.

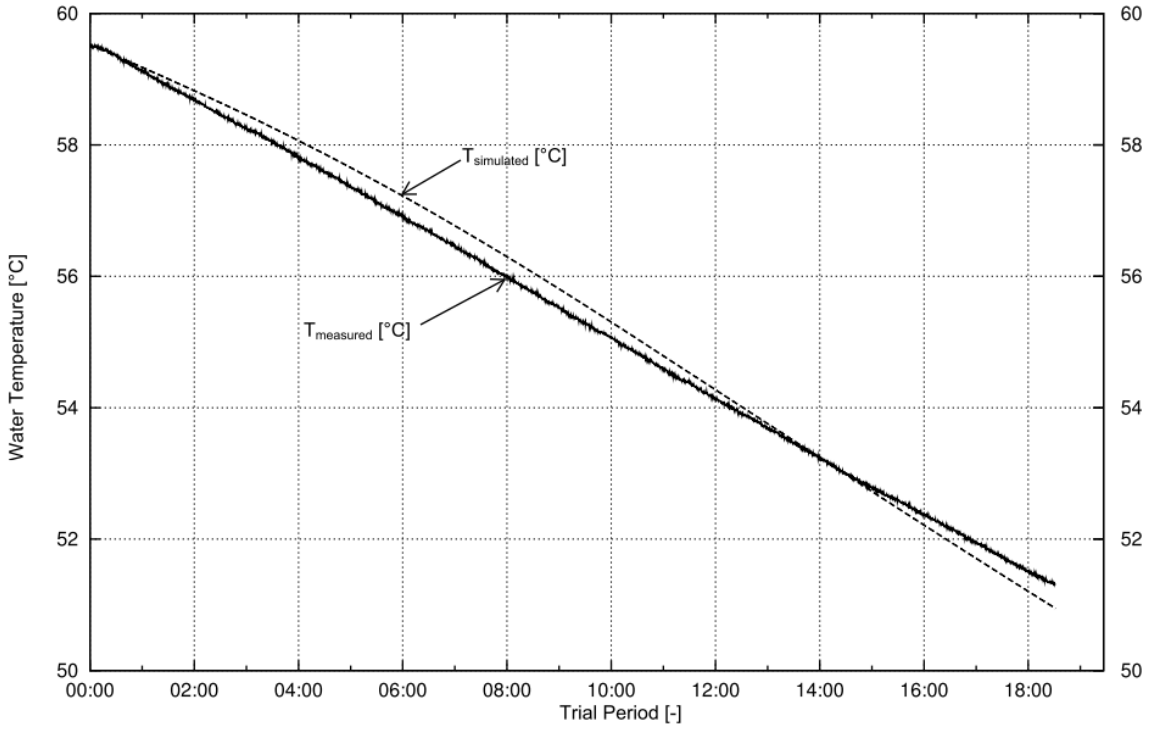

Figure 3.18: Storage Tank Heat Loss Sequence Simulated and Measured

In addition to the cooling down phase, a heating period and an evening draw-off are simulated. Input data for the simulation are the measured volume flow rates and the corresponding temperatures at double mantle and hot water storage. The results are very close to each other. Minor differences can be explained by the assumed storage tank conduction losses to the ambient. The wind dependent convection coefficient h_{amb} is a fixed value in the simulation while in reality the losses caused by wind are variable (Figure 3.19).

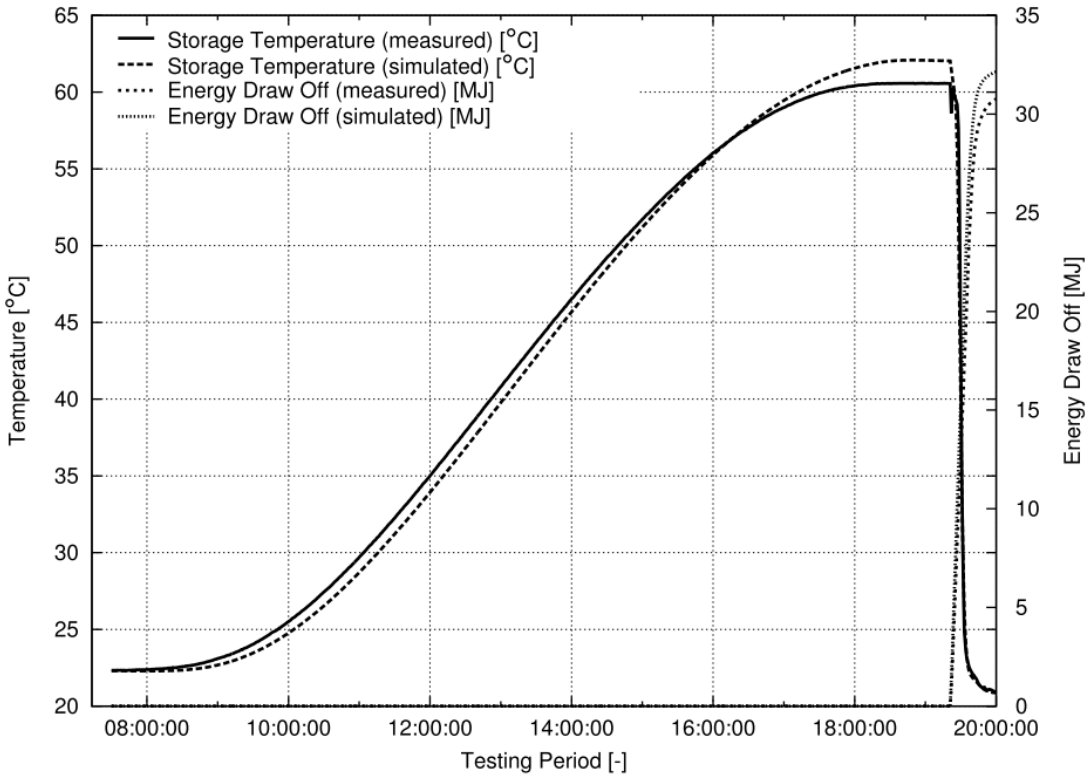

Figure 3.19: Heating-up Period Measured and Simulated

The last test performed in the validation section is the pressure drop calculation within the simulation. The calculation and measurements are carried out up to a flow rate of 400 l h^{-1}, a value exceeding the normal operating conditions by factor 8. Deviations between both pressure drop curves over the whole range are below 20 Pa.

3.4 Modelling and Validation of a System Tested in Ingolstadt

Related to the development is a reference system tested according to ISO 9459-2 (1995) at the university's test rig. The system is especially designed for regions with medium irradiation values, like the northern part of the Mediterranean Basin. The main technical data are listed in Table 3.2.In order to validate the simulation additional measurement equipment was implemented in the reference system – a temperature sensor at the collector inlet and outlet and a magnetic inductive flow meter was included into the pipe from storage tank back to the collector inlet (Figure 3.20). The magnetic inductive flow meter is calibrated for low flow rates but introduces (due to its diameter of only 10 mm) an additional flow resistance to the thermosyphon system. This additional flow resistance is also included into the model validation.

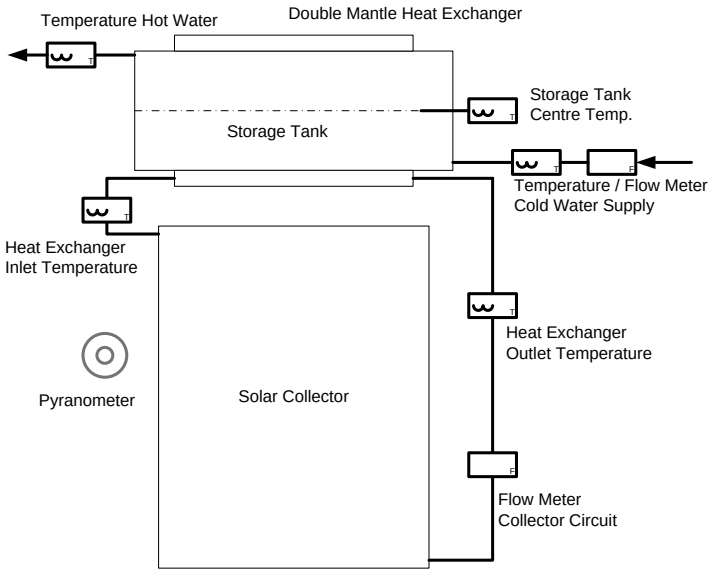

Figure 3.20: Schematic View of Measurement Points used for Simulation Validation

Besides this method other direct flow measurements have been published in literature. Ong (1974, 1976) used a dye tracing method, Morrison (1980) a laser doppler anemometer and Bannerot et al. (1992) introduced a hydrogen bubble flow meter. This bubble flow meter was optimised and verified by Khalifa and Mehdi (1998).

The components described in chapter Table 3.3 are used to build up the reference system in the simulation environment. In order to validate the system simulation, the measurement data recorded during the outdoor tests are used as input values.

Figure 3.21 shows the simulation model composed of a solar collector, the double mantle heat exchanger storage tank, the interconnecting pipes and the thermosyphonic pump. All of these components are linked to each other via the thermo hydraulic vector (THV). Measurement data are fed into the system using the blocks ‘hot water consumption’ and ‘weather data’.

Table 3.2: Technical Data of the Reference System

Collector	
Aperture Area	1.87 m²
Absorber Type	Steel Absorber with 35 Riser Ducts
Coating	Black Chrome (Medium Selective)
Transparent Cover	Heat-Strengthened Low Iron Glass
Insulation	55 mm Glass Wool
Tilt Angle	38 °
Storage Tank	
Type	Double Mantle Heat Exchanger Storage
Nominal Water Volume	180 l
Insulation	Eccentrically Expanded PU-Rigid Foam 12–35 mm
Interconnecting Pipes	
Type	22 x 1 mm Copper Pipes
Insulation	13 mm Elastomeric Foam

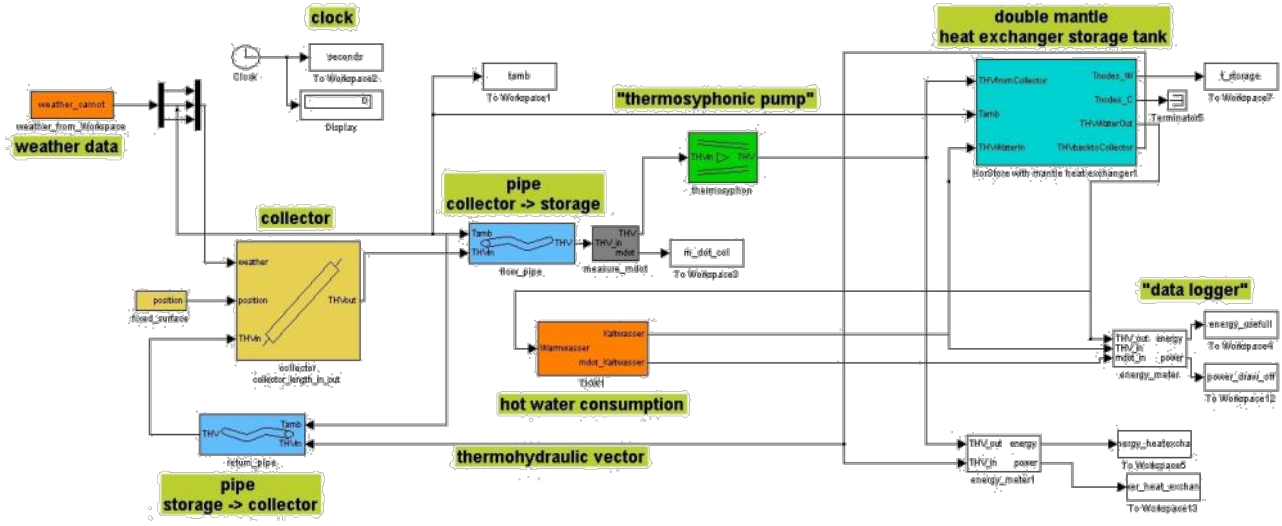

Figure 3.21: CARNOT Model of the Reference System

The simulation results show a good correlation between measured and simulated data, as can be seen in Figure 3.22 showing the flow rate and the accumulated flow through collector and storage over a whole test day.

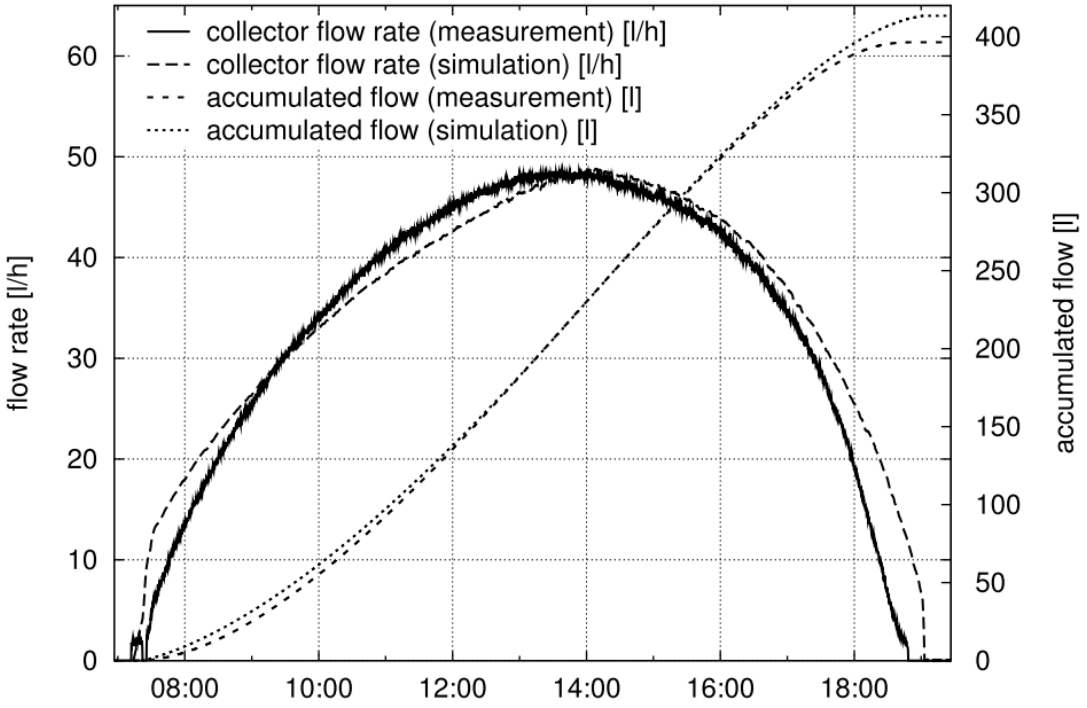

Figure 3.22: Validation of the Flow Rate through the Thermosyphon Model

After validating single measurement days, the annual energy output based on ISO 9459–2 (1995) is compared to the simulation output at the locations Ingolstadt and Rome. Both methods use artificial weather data as described in Chapter 3.5.2. The annual difference of the simulation compared to the normative calculation is in the range of 2-5 %. The simulation output is always below the normative calculation. This can be explained by the more complex variable calculation method of the CARNOT simulation, compared to the simplified assumptions like fixed values for the heat capacity and energetic calculations based on the daily irradiation in the model given in the standard.

3.5 Sensitivity Analysis of Thermosyphon Systems

Basis to the sensitivity analysis is the validated reference thermosyphon system. Typically, to maintain a high hot water comfort level even in times of adverse weather, a heating rod is included in the storage tank. Due to its negative influence on the annual solar fraction it is not modelled. The system simulated is a solar pre-heat system. To fully cover the hot water demand, a continuous-flow water heater is joined to the thermosyphon system. The flow heater only has to cover the temperature gap between storage tank outlet and 45 °C. For sunny periods with storage tank temperatures above 45 °C, a

thermostatic mixing valve is included in order to reduce the tap water temperature to the desired temperature of 45 °C. Such system setup is commercially available and corresponds to the state-of-the-art of modern thermosyphon systems (Figure 3.23). The achievable solar fraction is interpreted according equation (2.2).

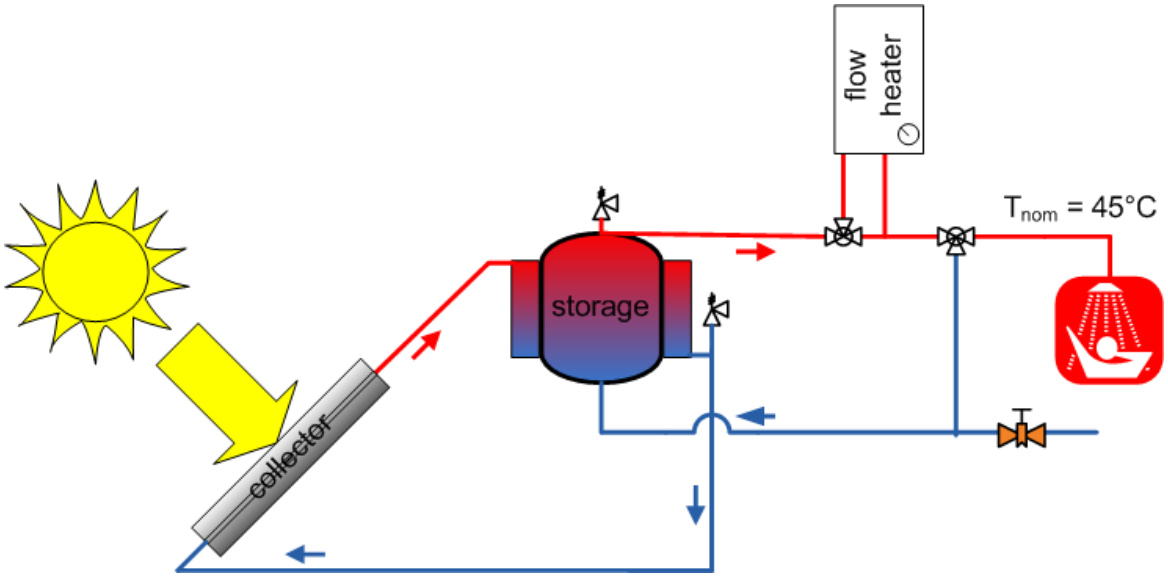

Figure 3.23: Operating Scheme of the Investigated Thermosyphon System with Flow Heater and Thermostatic Mixing Valve

The aim of the sensitivity analysis is to determine the overall performance defined as a function of collector design, storage tank design and system configuration as shown in equation (3.54):

$$\eta_{system} = f(collector_{fictive}, storage_{fictive}, configuration_{fictive}) \tag{3.54}$$

with

η_{system}	Overall System Performance	[-]
$collector_{fictive}$	Varied Collector Parameters	[-]
$storage_{fictive}$	Varied Storage Parameters	[-]
$configuration_{fictive}$	Investigated System Configuration	[-]

Variations in the daily hot water demand directly influence the overall system performance and the results of the sensitivity analysis. To reduce the breadth of the sensitivity analysis, the draw-off pattern is fixed to the values described in Chapter 3.5.1.

Based on the reference system, parameter variations in a fixed bandwidth are defined for each of the parts of the thermosyphon system. The most promising system setup, composed of optimised parts is compared to the reference system to evaluate the optimisation potential.

3.5.1 Hot Water Consumption

Adapted to common simulation tools, the simulated daily hot water demand corresponds to a Central European 3–4 person household at a total amount of 2,540 kWh a^{-1}. During the day, three draw-offs take place, in the morning, during midday and in the evening. Additionally, daily and seasonal variations, taking a reduced hot water demand during summer times into account, are considered. The cold water from mains follows a sinusoidal trend with 8 °C in February and 12 °C in August (Figure 3.24 and Figure 3.25).

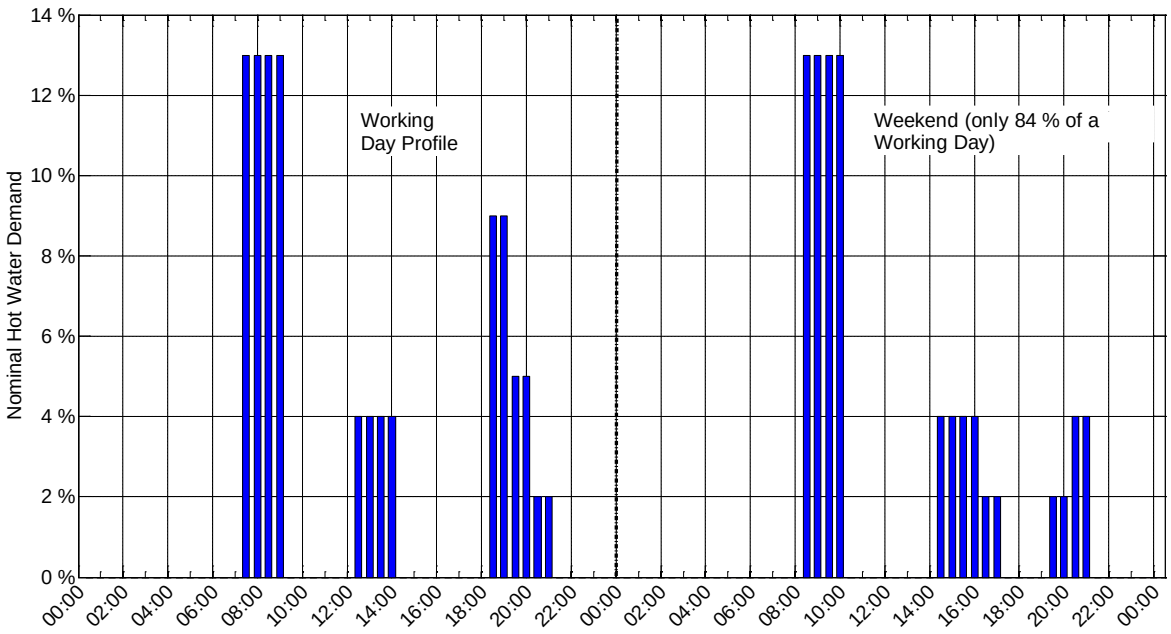

Figure 3.24: Draw-off Patterns at Working Days and Weekend

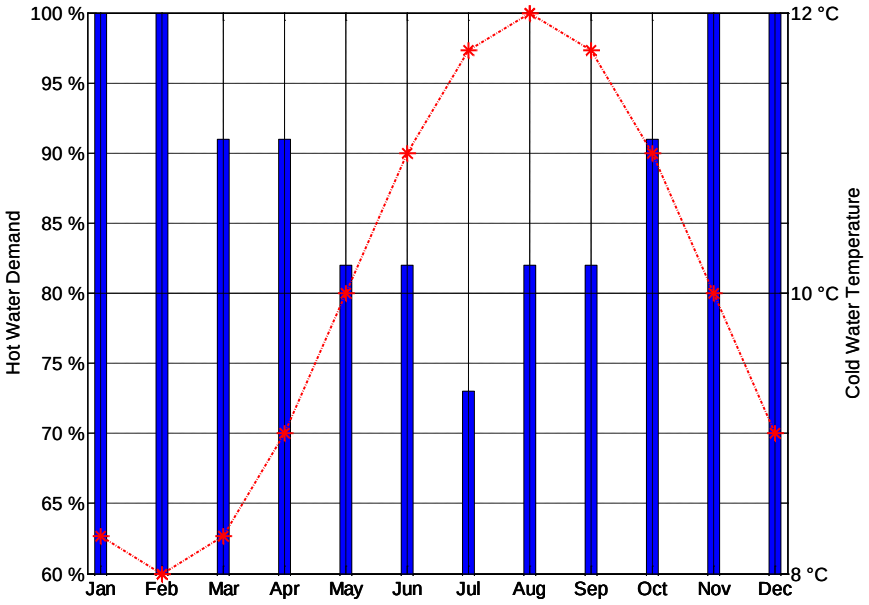

Figure 3.25: Seasonal Variation in Hot Water Demand and Sinusoidal Cold Water Temperature

As no country specific data are available, the Central European hot water profile is used for all geographic locations considered in the simulation.

3.5.2 Influence of Different Climatic Conditions on the System Performance

Thermosyphon systems have to be operated using various water/antifreeze mixing ratios depending on the geographic/climatic conditions. A low antifreeze ratio has a positive influence on the energetic/hydraulic behaviour of the solar-thermal system (cf. Chapter 2.2.5). On this background, the sensitivity analysis is carried out using three climatic different European locations:

- Ingolstadt, Germany, is included as northernmost location with typical central European weather conditions (G_{hor} = 1,118 kWh m^{-2} a^{-1}; T_{amb} = 8.8 °C). The institute´s test rig is located there, which will be used to carry out measurements with the prototype. The working fluid used for this location is a 60/40 water/propylene glycol mixture which allows ambient temperatures of about -15°C in winter (Figure 3.26).

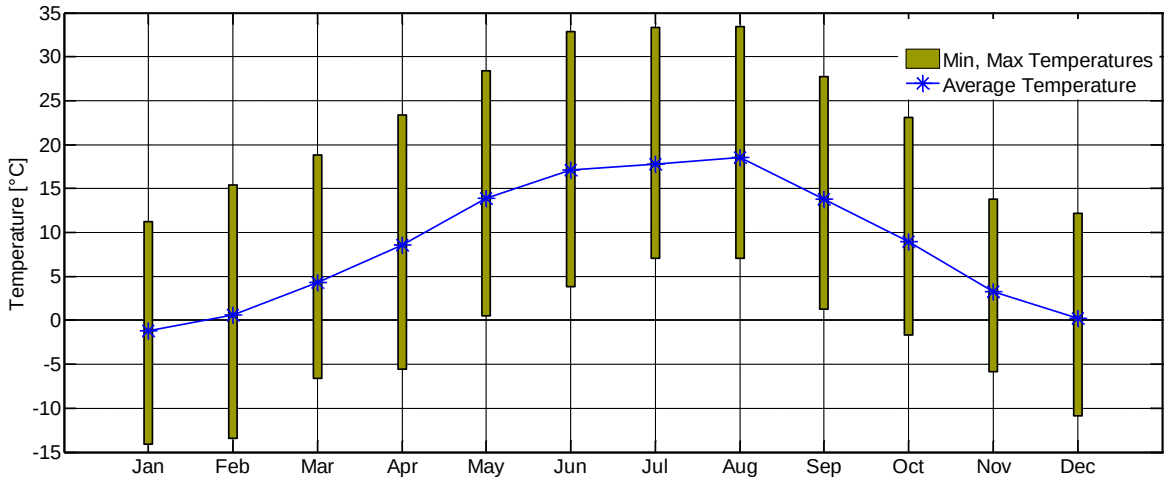

Figure 3.26: Average Temperature and Min/Max Temperatures in Ingolstadt

- Rome, Italy, is a location with a moderate southern European climate (G_{hor} = 1,559 kWh m^{-2} a^{-1}; T_{amb} = 15.6 °C). Even in winter times, there are only very few days with frost (Figure 3.27). A 90/10 water/propylene glycol mixture is sufficient for a safe system operation throughout the year.

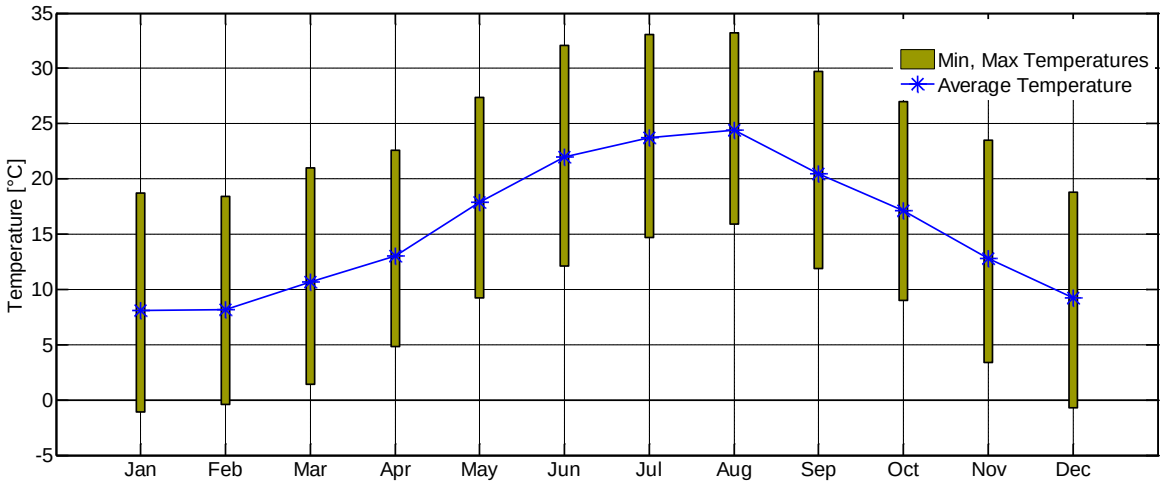

Figure 3.27: Average Temperature and Min/Max Temperatures in Rome

- Malaga, Spain, has a typical southern European climate with a high amount of solar irradiation at high average temperatures and without a real risk of frost (G_{hor} = 1,792 kWh m^{-2} a^{-1}; T_{amb} = 18.2 °C). No antifreeze protection is needed. In order to protect the thermosyphon system, it is recommended to run the system with corrosion protection (Figure 3.28).

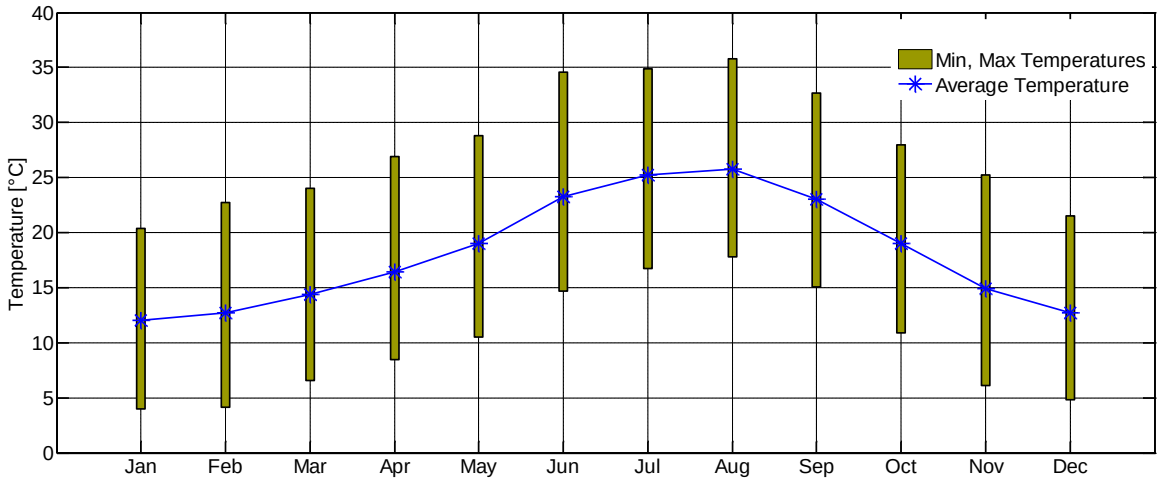

Figure 3.28: Average Temperature and Min/Max Temperatures in Malaga

For the weather data generation, Meteonorm 6.0 (Remund et al., 2006), a meteorological database is used. The data basis for this software is a worldwide network of weather stations. In order to calculate weather data for any location, various mathematical models are included, which are extrapolating the given data. To achieve realistic weather data, the distance from the extrapolated locations to the destination has to be taken into consideration.

The output format of Meteonorm is TRY (Test-Reference-Year). The TRY data are brought into a CARNOT compatible format using an enhanced MATLAB m-script.

3.5.3 Indication of Relevant Collector Parameters

Within the scope of the collector optimisation, the significant absorber design parameters (pressure drop, absorber efficiency and heat capacity), the optical properties (transmission-absorption product, incidence angle modifier), the heat losses as well as geometric dimensions (aperture area and length/width ratio) are varied and simulated. The relevant parameters are listed in Table 3.3 in detail including minima and maxima values, step size, affected design parameter and source.

3.5.4 Storage Tank Parameters

Regarding the storage tank, four relevant parameters are found: the storage tank volume (relative to the collector aperture area), the characteristics of the heat exchanger (heat

exchanger volume and surface area) and the insulation (material and thickness) as described in Table 3.6.

3.5.5 System Configuration

Besides the two major components of a thermosyphon system, the solar collector and the storage tank, the system configuration has a major influence on the energetic performance and the aesthetic appearance. The energy performance is affected by the pipe dimensioning (length and diameter), the piping between storage tank and solar collector, the height ratio between collector and storage tank as well as the system orientation, i.e. collector azimuth and incidence slope (Table 3.5). The collector azimuth is a user dependent factor and not a design factor. Nevertheless, it is varied to document the dependency of the annual energy output on the system orientation.

Table 3.3: Collector Parameters

Parameter	Min / Max Value	Step Size	Model Parameter	Design Parameter	Source
Pressure Drop	969–31,682	5,000	x_1 [Pa s kg^{-1}]	Absorber Design	Market Report Solar Thermal Collectors (Ellinghaus, 2007); (Drück 2011)
	15,068–75,000 (parallel pipes) 5x10^6–20x10^6 (meander type)	15,000 5x10^6	x_2 [Pa s^2 kg^{-2}]		
Collector Size / Tank Size Ratio	2.58–30.95	2.58	$\frac{A_{col}}{V_{store}}$ [m^{-1}]	Collector Size (0.46-5.57 m²)+ Tank Volume at Constant Tank Volume of V_{store} = 180 l	Market Analysis (Brandmayr, 2006)
Collector Shape	1.00–2.50	0.25	l_{col} [m]	Collector Length / Collector Width Ratio at Constant Area A_{col} = 1.87 m²	Market Analysis (Brandmayr, 2006)
	0.74–1.87	1.87x l_{col}^{-1}	w_{col} [m]		
Collector Performance 1	0.612–0.909	0.05	η_0 [-]	Zero Loss Efficiency Influenced by Characteristics Collector Cover (τ) and Coating (absorption α) and the Absorber Design Factor F'	Transparent Cover Materials (Frei, 1998); Solar Glass (Flückinger, 2007), Absorber Coatings (Treikauskas, 2005; COLOR, 2009)
Collector Performance 2	2.4–6.2	0.5	a_1 [Wm^{-2} K^{-1}]	Collector Design (type and amount of insulation, collector design parameters)	Market Report Solar Thermal Collectors (Ellinghaus, 2007)
	0.004–0.1	0.014	a_2 [W m^{-2} K^{-2}]		
Collector Performance 3	0.5–0.97	0.05	ki_{50} [-]	Incidence Angle Modifier (characteristics of collector cover + absorber)	Market Report Solar Thermal Collectors (Ellinghaus, 2007); Range 0.5-0.8 Fictive
Collector Heat Capacity	2,000–26,000 (0.48–6.22 l m^{-1} water equivalent)	4,000	c_{col} [J m^{-2} K^{-1}]	Amount of Fluid Inside Absorber and Thermal Mass of Collector	Market Report Solar Thermal Collectors (Ellinghaus, 2007), Min, Max Values Own Values

Table 3.4: Storage Tank Parameters

Parameter	Min / Max Value	Step Size	Model Parameter	Design Parameter	Source
Tank Size / Collector Size Ratio	5.26–23.69	$\frac{1.87m^2}{V_{store}+0.04m^3}$	$\frac{A_{col}}{V_{store}}$ [m^{-1}]	Tank Volume at Constant Collector Area A_{col} = 1.87 m² and Storage Diameter of d_{store} = 0.392 m	Market Analysis (Brandmayr, 2006)
Inner Storage Diameter	1.35–5.35	1.00	$\frac{l_{store}}{d_{store}}$ [-]	Storage Length and Diameter at Constant Tank Volume of V_{store} = 180 l	Market Analysis (Brandmayr, 2006)
Heat Exchanger Capacity	0.004–0.014 (e.g. water: 23.6–84.5 kJ K^{-1})	0.002	$z_{spacing}$ [m]	Heat Exchanger Capacity Adapted by Variation of Heat Exchanger Spacing	Market Analysis (Brandmayr, 2006)
Heat Exchanger Surface	0.4–1.2	0.2	A_{exch} [m²]	Surface of the Used Double Mantle Heat Exchanger	Market Analysis (Brandmayr, 2006)
Insulation Thickness	0.01–0.10	0.02	z_{ins} [m]	Insulation Thickness at Constant Heat Conductivity of 0.045 W m^{-1} K^{-1}	Market Analysis (Brandmayr, 2006)

Table 3.5: System Configuration Parameters

Parameter	Min / Max Value	Step Size	Model Parameter	Design Parameter	Source
Inner Pipe Diameter	0.006–0.025	0.002	d_{pipe} [m]	Tube Diameter	Commonly Available Tubes
Pipe Insulation	0–0.035	0.005	z_{ins} [m]	Influence of the Tube Insulation on the System Output	Commonly Available Insulation
Collector Storage Height Ratio	-0.40 – 1.00	0.2	z_{add} [m]	Optical system appearance / Collector – Storage Connection	Literature Review (Vaxman, 1986, Scheller, 1985)
Collector Tilt Angle	10–80	10	γ_{tilt} [°]	Optimal System Performance for Each Climatic Condition	Typical Tilt Angles for Pumped Systems
System Azimuth	-60 – +60	15	α [°]	Influence of System Orientation on Annual Energy Output	Typical System Orientation

3.5.6 Simulation Results

Based on the annual energy output of the thermosyphon system, the results of the sensitivity analysis are interpreted based on the annual solar fraction as defined in equation (2.2). A detailed investigation in steps of a few minutes is also possible and in some cases necessary, e.g. for the analysis of the collector pressure drop. A fact that has to be emphasised is that most of the optimum values are independent of the respective geographic location. Table 3.6 shows the weighted classification of the simulation results for Malaga. Column one and two describe the varied parameter; the third column identifies either the directly or indirectly affected component and the fourth column gives an overview of the influence on the annual solar fraction for Malaga. A detailed discussion of the simulation results can be found in Chapter 4.

Table 3.6: Weighted Simulation Results for Malaga

Parameter	Model Parameter	Affected Component	Bandwidth of Solar Fraction for Malaga	Degree of Influence
Collector Size	A_{col}	Collector	28.9 – 91.7 %	**High**
Pipe Insulation	z_{ins}	System	41.9 – 69.9 %	
Zero Loss Efficiency	η_0	Collector	58.3 – 75.2 %	
Collector Tilt Angle	γ_{tilt}	System	54.3 – 69.3 %	
Storage Tank Insulation	z_{ins}	Storage Tank	59.8 – 74.2 %	
Incidence Angle Modifier	ki_{50}	Collector	59.3 – 69.8 %	
Inner Pipe Diameter	d_{pipe}	System	62.7 - 72.1 %	**Medium**
Collector Storage Height Ratio	z_{add}	System	65.7 – 71.9 %	
Linear Heat Loss Coefficient (Collector Performance)	a_1	Collector	64.9 – 70.75 %	
Quadratic Pressure Drop Coefficient	x_2	Collector	62.5 – 67.9 %	
Collector Shape (Length at Given Area)	l_{col}	Collector	64.0 – 69.0 %	**Low**
Storage Volume	V_{store}	Storage Tank	64.3 – 69.2 %	
Storage Tank Diameter (at 180 l)	d_{store}	Storage Tank	65.8 – 70.0 %	
Heat Exchanger Area	A_{exch}	Storage Tank	64.9 – 68.5 %	
Linear Pressure Drop Coefficient	x_1	Collector	65.8 – 68.0 %	
Heat Capacity Collector	c_{col}	Collector	68.0 – 69.1 %	
Quadratic Heat Loss Coefficient (Collector Performance)	a_2	Collector	67.1 – 69.9 %	
Heat Exchanger Spacing	z_{gap}	Storage Tank	68.1 – 68.5 %	

3.6 Building up and Simulation of the Most Promising System Configuration

By combining the results of the sensitivity analysis to a most promising system setup, the annual hot water fraction can be raised by 15 percentage points up to 85 % for the location Malaga as compared to the reference system. This system setup differs from the state-of-the-art as the aperture area is increased to 2.35 m² and the storage tank volume is decreased to 165 l. The height between storage tank and solar collector is set to 0, as the physical approach to avoid reverse thermosyphoning is applied in this new system setup. The relevant technical data are summarised in Table 3.7.

Table 3.7: Technical Data of the Most Promising System Configuration

Parameter	Value	Model Parameter	Design Parameter	Source
Pressure Drop	3,700	x_1 [Pa s kg^{-1}]	Absorber Design (Harp Absorber)	Reference Collector / Sensitivity Analysis
	56,545	x_2 [Pa s² kg^{-2}]		
Collector Size / Collector Shape	2.35 (2.134x1.104)	A_{col} [m^2]	Collector Size	Optimum Ratio of Storage Volume Tank and Collector Area
Collector Performance	0.812	η_0 [-]	Collector Efficiency	Reference Collector / Sensitivity Analysis
	3.52	a_1 [W m^{-2} K^{-1}]		
	0.019	a_2 [W m^{-2} K^{-2}]		
Tank Size	165	V_{store} [m^3]	Tank Dimensions	Sensitivity Analysis
Inner Storage Diameter	500	d_{store} [mm]	Storage Length and Diameter	Sensitivity Analysis and Collector Width
Heat Exchanger Surface	1.0	A_{exch} [m²]	Surface of the Used Double Mantle Heat Exchanger	Sensitivity Analysis
Insulation Thickness	0.04	z_{ins} [m]	Insulation Thickness	Sensitivity Analysis / Technical, Economical Optimum
Inner Pipe Diameter	0.013	d_{pipe} [m]	Tube Diameter	Sensitivity Analysis
Pipe Insulation	0.02	z_{ins} [m]	Influence of the Tube Insulation on the System Output	Sensitivity Analysis / Technical and Economic Optimum
Collector / Storage Height Ratio	0.00	z_{add} [m]	Optical system appearance / Collector – Storage Connection	Reverse Thermosyphoning Prevention
Collector Tilt Angle	35	γ_{tilt} [°]	Optimum System Performance	Sensitivity Analysis

The analysis of the monthly hot water fraction reveals a performance plus of 20 % during spring and autumn compared to the reference system. In summer times, 100 % of the hot water is supplied by the thermosyphon system as shown in Figure 3.29.

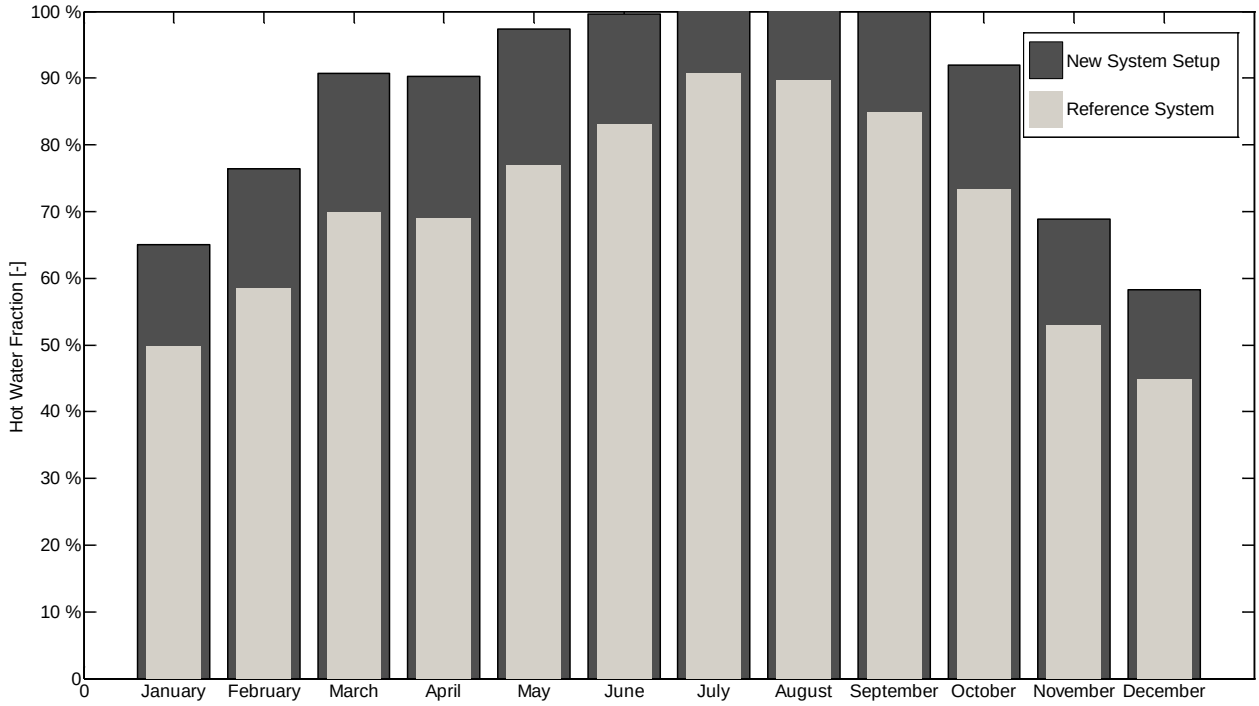

Figure 3.29: Annual Hot Water Fraction of Reference System and the New System Setup

The daily maximum mass flow rate is in the range of 40–45 kg h^{-1}, while the reference system works at values of up to 66 kg h^{-1}. This difference is caused by various effects. The new system setup assumes 0 mm height difference between collector and storage tank and the interconnecting pipes are narrowed from 20 mm to 13 mm. The storage tank is well stratified due to the reduced flow rate. In summer times, the gap between the top temperature and the measurement point at 75 % height is in the range of 15 K. The maximum storage tank temperature is 96 °C.

4 Design and Construction

In the design and construction phase, the outcomes of the market and competition survey as well as the literature review (cf. Chapter 2) and the sensitivity analysis (cf. Chapter 3.5) are brought together. The result of this project stage was a two circuit thermosyphon system prototype, which was tested in the university's laboratories.

The prototype system consists out of a full aluminium collector with 30 mm mineral wool insulation and 2.34 m² aperture area. Collector in- and outlet are piped through the top of the collector casing. The collector tilt angle is set to 35 °. The system is a close-coupled system however 80 mm spacing between collector and storage tank is necessary for installation reasons. The storage tank is a double mantle heat exchanger storage tank with 165 l tap water and an internal expansion vessel. To maintain the stratification during drawing-off water a cold water diffuser is implemented in the storage tank (Figure 4.1).

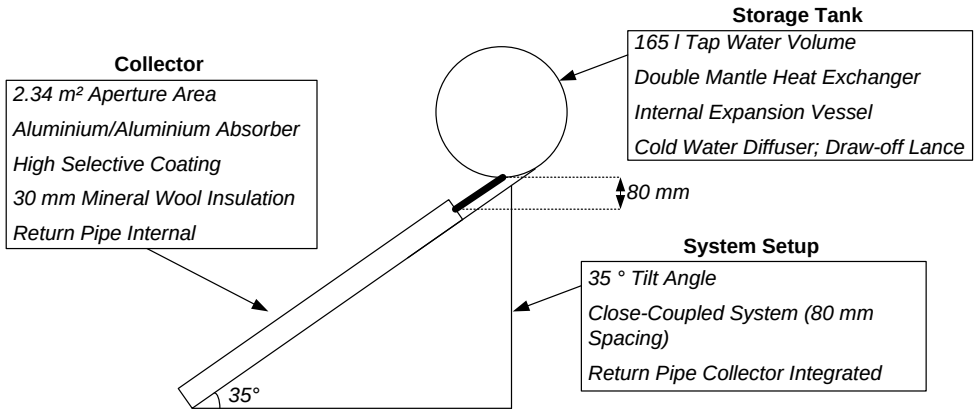

Figure 4.1: Main Technical Specifications of the Prototype System

4.1 Design of Collector and Storage Tank

The design of the collector and storage tank prototype is mainly driven by the outcomes of the sensitivity analysis and reflects the data of the most promising "New System Set-up". Some of the optimum combinations found and simulated in Chapter 3.6 are, however, technically not applicable. An example for such a non-applicable measure is a double mantle gap height of 4 mm. Such a system benefits from a small heat transfer fluid volume resulting in a reduced expansion volume demand and an enhanced operation safety — but cannot be manufactured due to the tolerances of the welding process.

4.1.1 Collector Prototype

The collector size has a major influence on the annual solar fraction. An increased aperture area always comes along with an increased annual solar fraction, but is more likely to cause overheating problems. Furthermore, the production costs of the collector are directly dependent on the collector size. In the simulation, the aperture area is varied from 0.5–5.6 m² at a constant storage tank volume of 180 l.

Against this background, the evaluation of the simulation results is done using two parameters, solar fraction and secure system operation. The system operation is defined to be secure as long as the storage tank temperature at the given draw-off profile does not exceed 90 °C. Under the climatic conditions of Malaga, this security criterion is exceeded at an aperture area of 2.8 m² or a minimum storage tank volume to aperture area ratio of 65 l m^{-2} (Figure 4.2).

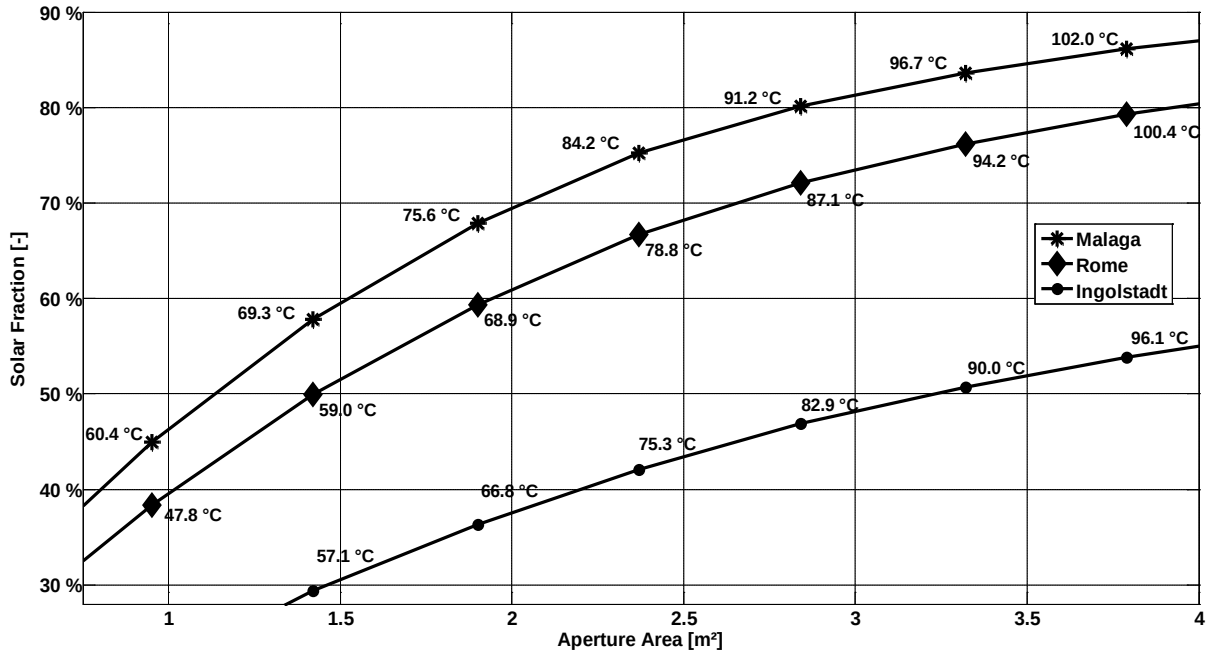

Figure 4.2: Solar Fraction as Function of Aperture Area and Secure System Operation

To determine the optimum shape of the prototype collector, the width to length ratio is varied at the given reference aperture area of 1.87 m². The simulation results at Ingolstadt and Rome show no dependency on the solar fraction of collector length to width. At Malaga, slender but long collectors offer an energetic advantage during winter times

(Figure 4.3). It can be concluded, the standard collector length to width ratio of 2:1 is also suitable for thermosyphon systems.

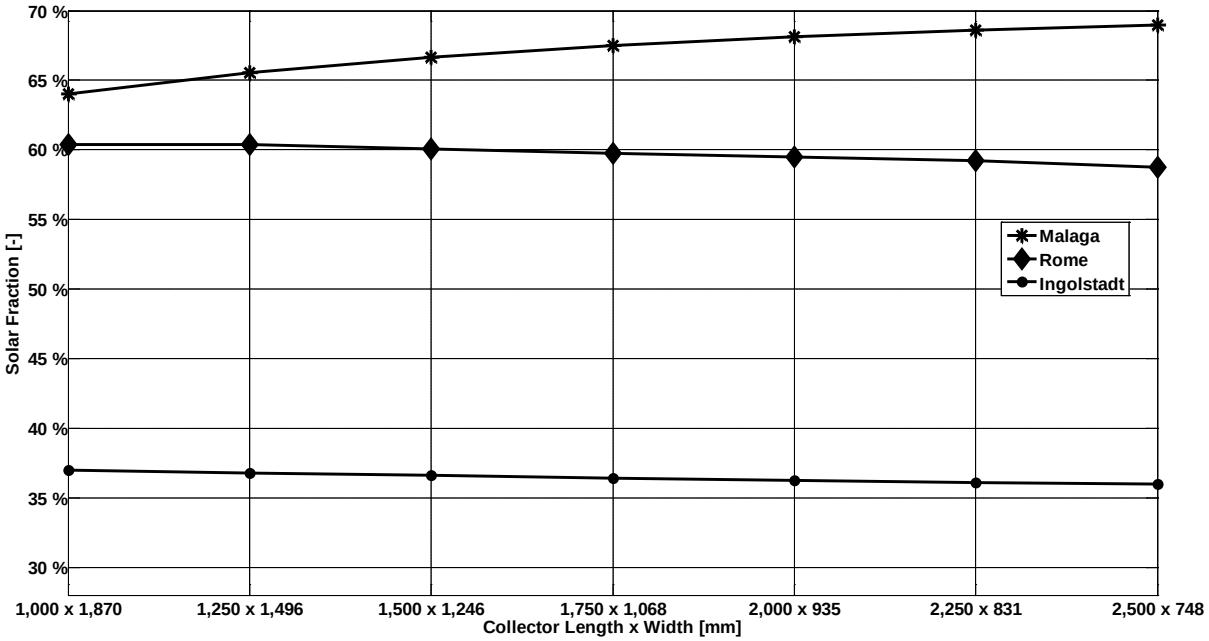

Figure 4.3: Collector Length to Width Ratio

Moving away from the absorber's geometrical dimensions, the analysis clearly shows the necessity of a zero loss efficiency above η_0 = 0.80 as realised in the reference system. The simulation model uses input data out of system tests according EN 12975-2 (2006). The standard uses the mean collector temperature as for the calculation of the collector efficiency. According to equation (2.21) the zero loss efficiency is the product out of the collector efficiency factor F' and the transmission absorption product ($\tau\alpha$). The 0.80 zero loss efficiency can be reached using a transparent cover with a high transmission value $\tau \geq 0.91$ such as low iron glass (cf. Chapter 2.2.2). Long-term stable polymer covers, such as PMMA with a transmission of τ = 0.84 are not recommended. The coating is to have an absorption value of about α = 0.95, just like high selective or black chrome coatings, and the hydraulic design of the collector is to have a collector efficiency factor of more than F' = 0.92 (Figure 4.4).

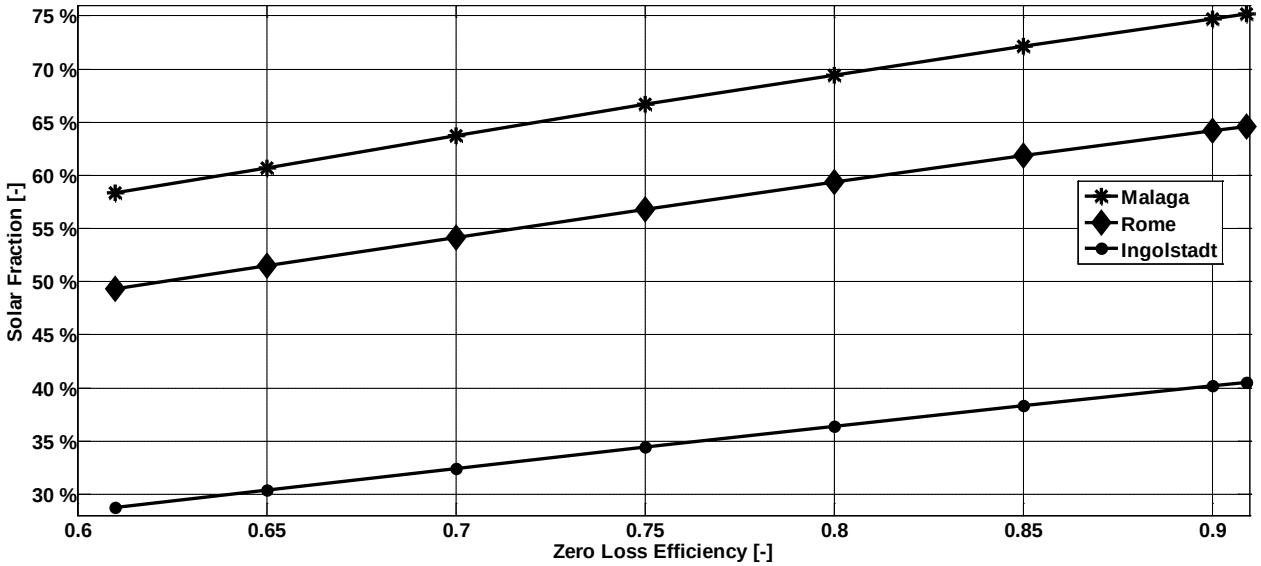

Figure 4.4: Zero Loss Collector Efficiency

An analysis of the collector's operating regime within simulation and on the test rig reveals a peak around the zero loss efficiency of the collector with minor thermal losses (Figure 4.5). This peak is calculated based on the reduced collector temperature[4] (equation (2.22)). From the collector efficiency curve of a typical selective coated flat-plate collector which is included in Figure 4.5, it can be seen that the thermal losses of the collector in thermosyphon systems are not that important. The simulation results of different coatings from highly selective materials down to solar painting lead to the suggestion of using a medium selective coating material like black chrome. Black chrome coatings have a typical emission coefficient of about $\varepsilon = 0.15$.

[4] The reduced collector temperature is usually used in collector certificates according to DIN EN 12975-2 (Deutsches Institut für Normung, 2006) in order to achieve comparability of measurement results for different collectors.

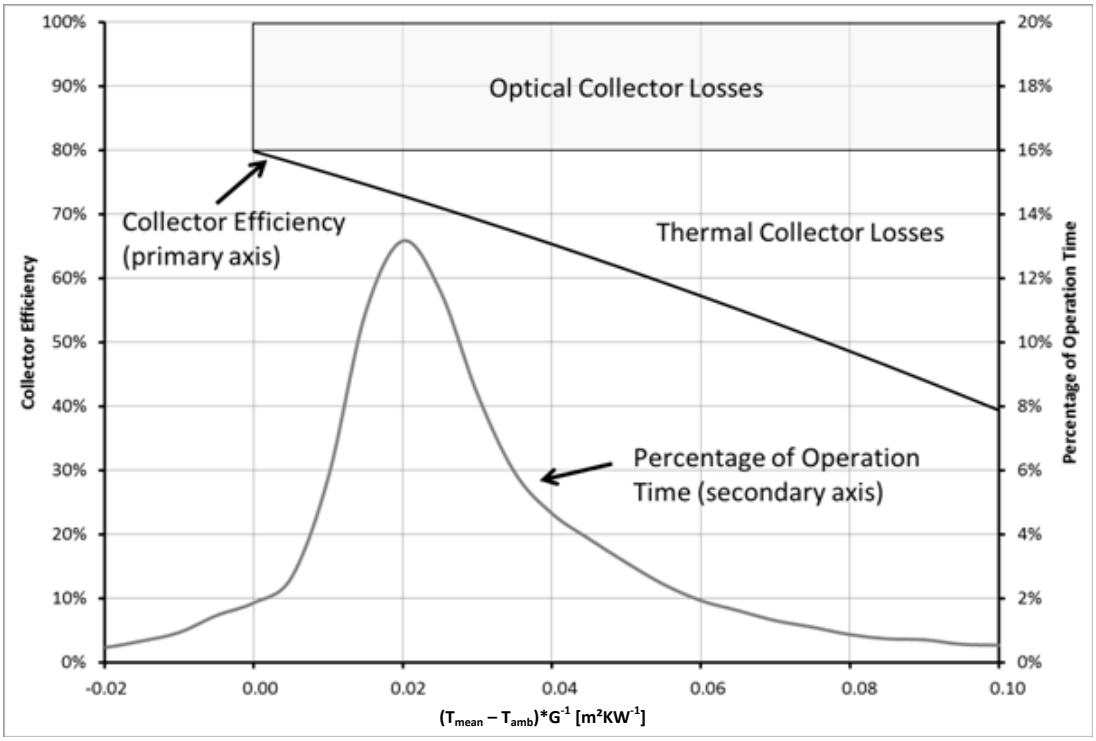

Figure 4.5: Collector Efficiency vs. Percentage of Operation Time

Besides the cover and the coating, the insulation of the collector (ref. Table 3.6) moderately influences the system efficiency. Thus, a reduced insulation thickness of 30 mm, only on the back side of the absorber is fully suitable for the prototype collector. Solar collectors used in central Europe are insulated with 40–50 mm at the backside and 10–20 mm at the casing. The variation of the temperature dependent heat loss coefficient a_2 has nearly no influence on the system efficiency, as the system is normally operated at temperatures below 90 °C. At these temperatures, linear losses influenced by coefficient a_1 dominate.

Regarding the cost reduction potential, the impact of the insulation is rather low, approximately 9 % (Mangold, 1996), but directly affects the necessary height of the collector casing. The height of the collector can be reduced by up to 20 mm. This comes along with a weight advantage of 2–4 kg depending on the frame profile geometry. The related cost advantage depends on the casing material used.

The last parameter varied within the collector optics is the incidence angle modifier. This factor describes the efficiency reduction due to a non-perpendicular irradiation onto the collector (cf. Chapter 3.2.2.1). At an irradiation angle of $\theta = 50$ ° the incidence angle mod-

ifier of flat-plate collectors is in the range of 0.85–0.95. This bandwidth influences the annual energy output by maximum 2.5 % (Figure 4.6).

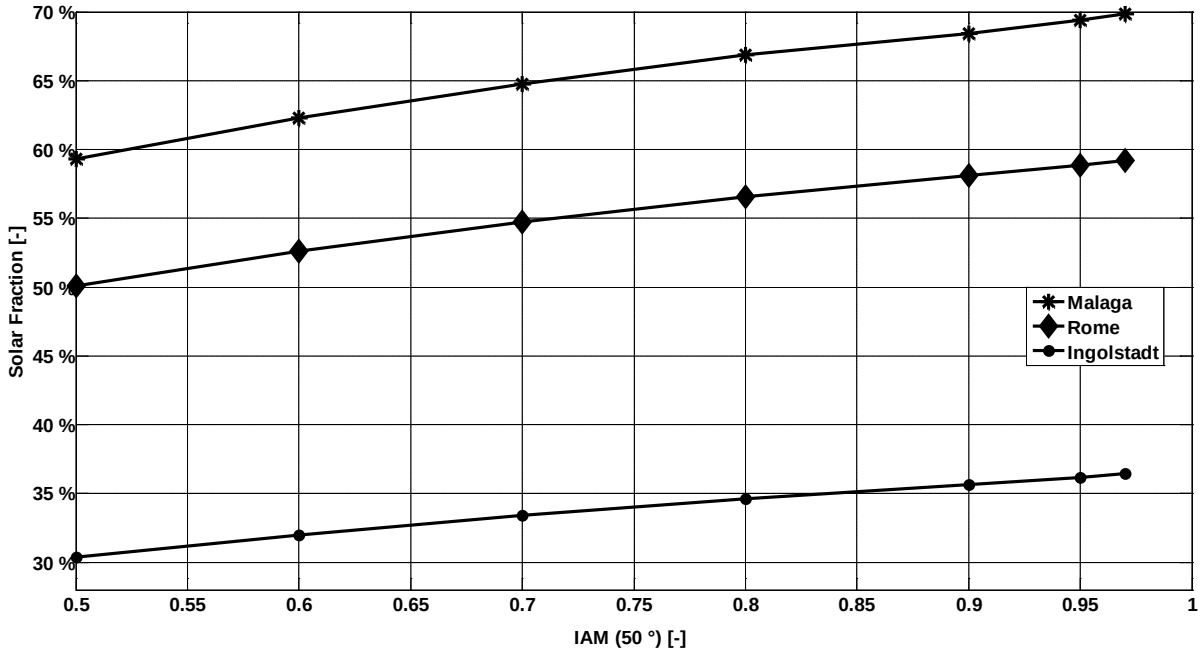

Figure 4.6: Influence of the Incidence Angle Modifier on the Solar Fraction

Values below 0.85 require further material research and are only applicable if solar energy is needed at a certain point of a day or to prevent the solar-thermal system from overheating. For the development of the thermosyphon solar collector, this research is not necessary as overheating can be prevented by a good storage tank volume to aperture area ratio.

The collector capacity affected by the materials used and above all by the fluid inside the absorber, has no influence on the system's annual energy output. On the one hand, a small capacity often comes along with a reduced material usage in the collector and a fast reaction to alternating weather conditions. On the other hand, the material used for the absorber piping can only be reduced to a certain extent as a material reduction is accompanied by reduced pipe diameters. A small pipe diameter leads to higher pressure losses inside the collector and to a reduced mass flow rate in the system. With regard to this material reduction potential and the annual energy output, the pressure drop was simulated with absorbers ranging from header-riser absorbers to meander type absorbers. The results show minor differences in the range of 0–5 % between the minima and maxima values for both collector types (Figure 4.7 and Figure 4.8) and as a result of that

the question arose whether meander type collectors might also be suitable for thermosyphon systems.

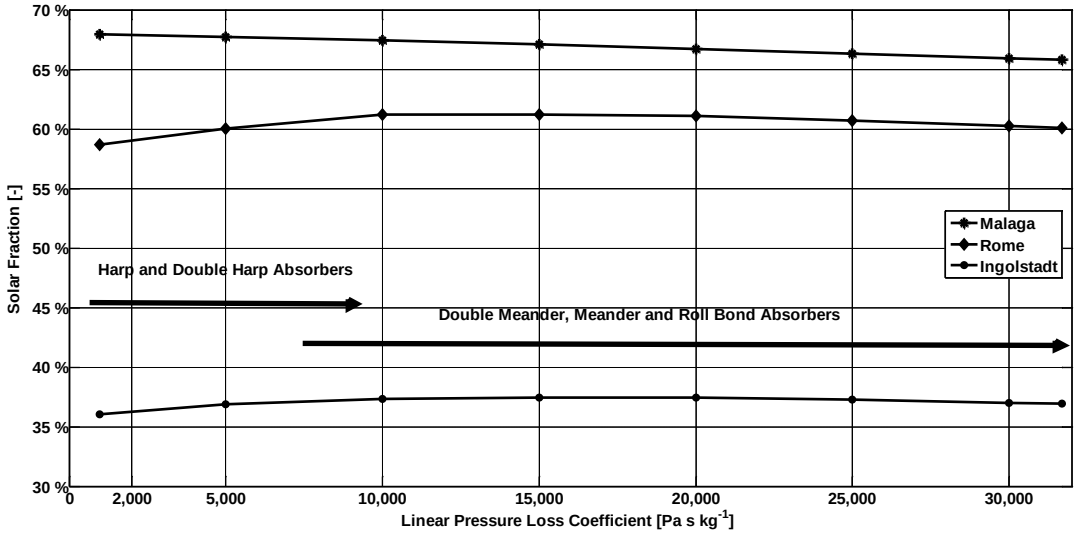

Figure 4.7: Variation of the Linear Pressure Loss Coefficient for Different Absorber Types

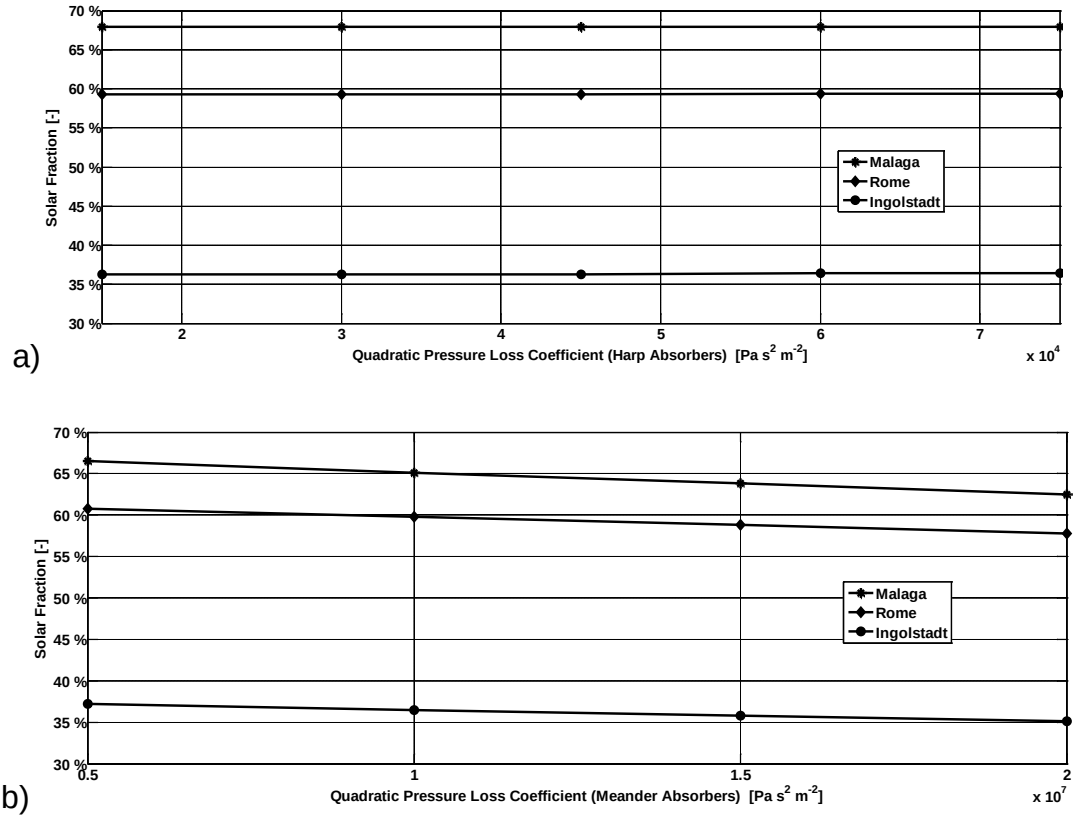

Figure 4.8: Variation of the Quadratic Pressure Loss Coefficient for a) Harp and b) Meander Absorbers

A detailed post processing of the simulation results at cloudy conditions shows very small mass flow rates of only 10–14 kg h^{-1} at a temperature difference of 60–70 K for the me-

ander type absorber. This leads to a highly stratified storage tank and thus, to no energetic penalty compared to the header-riser absorber system. The flow rate of the header-riser absorber at the same conditions is in the range of 35–45 kg h^{-1}, with a typical temperature rise of 20–30 K. In summer times with irradiation values into the collector plane of above 1,000 W m^{-2}, the meander type collector tends to overheat as the simulated collector outlet temperatures reach 100–120 °C. This simulated behaviour of both absorber types is experimentally validated with two nearly identical thermosyphon systems placed under the university's solar simulator. One collector has a meander type and the other one a header-riser absorber with 10 riser tubes. The measured results are in good accordance to the simulation results. Due to the operation characteristics and the overheating problems, the header-riser type absorber is selected for the further development.

To avoid reverse thermosyphoning, the physical approach published by Scheller (1985) as described in Chapter 2.2.1 is applied. The return pipe is located inside the collector casing just below the absorber (without touching it). Additionally, the collector outlet is piped through the top of the collector casing. This leads to 90 ° bends in the upper and lower header resulting in asymmetrical outer absorber fins (Figure 4.9) as a certain offset between bend and riser tube is needed for the manufacturing process.

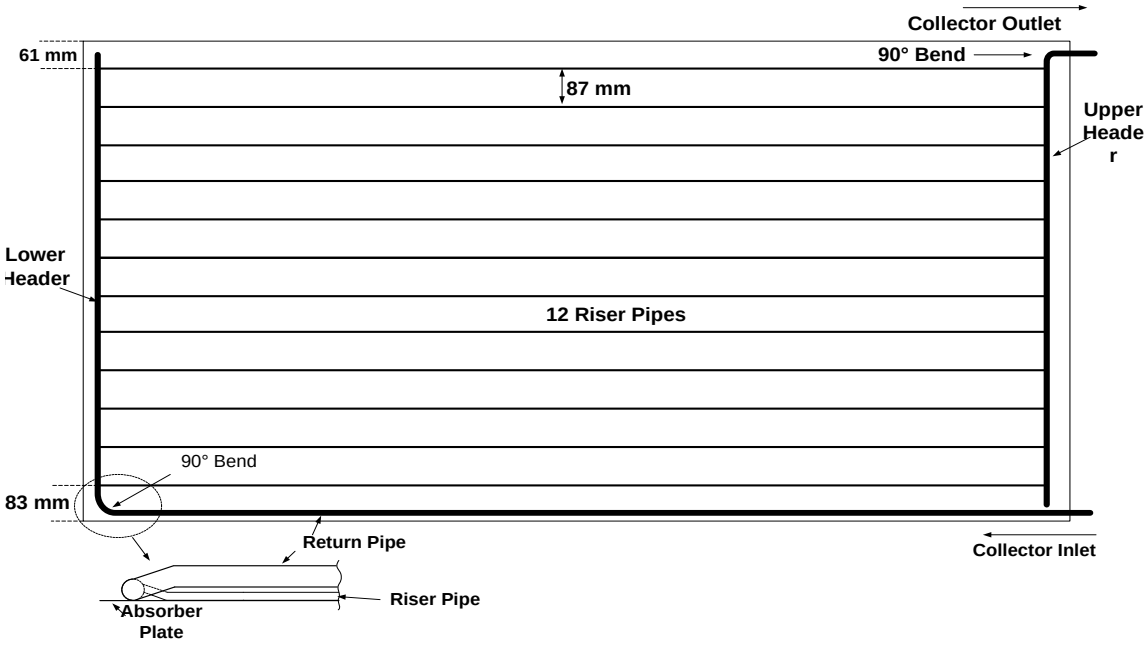

Figure 4.9: Scheme of the Absorber Proposed

The collector efficiency factor F' is calculated analogous to Chapter 2.2.2. A variation of 8-14 riser pipes at a given collector width of 1,101 mm is considered. The results show a theoretical collector efficiency factor in the range of F' = 0.833–0.950. As 12 riser tubes already result in F' = 0.944, 12 riser tubes are taken into account for the further development. The optimum fin width for the inner absorber fins is calculated to w_{fin} = 90 mm (87 mm were technically feasible for the welding process).

Besides a technical optimisation, a closer look at cost reduction potentials is taken. Mangold (1996) conducted a detailed investigation concerning collector production costs. This survey was shown by Treikauskas (2005) to be transferrable on to a modern collector production. The biggest cost reduction potential can be found on the absorber side. By changing the normally used absorber material copper to 100 % aluminium, there is the possibility to reduce the absorber weight in the range of 2.5–3.0 kg (for a 2.5 m² collector). Bigger wall thicknesses for the piping and a 0.5 mm thick absorber-plate for the aluminium type are considered. The use of aluminium pipes is possible as new corrosion resistant aluminium solar alloys have been successfully tested and are available on the market (Holle, 2011). Holle predicts cost savings of 62 % using aluminium for the collector piping. This percentage is realistic as raw material prices for aluminium are only at 30–40 % of those for copper. The technical data of the proposed collector are summarised in Table 4.1.

Table 4.1: Technical Data of the Proposed Collector

Absorber Type	Sheet–Pipe Absorber with 12 Riser Tubes
Absorber Material	100 % Aluminium (Absorber and Piping)
Aperture Area	2.34 m² (1,101 mm x 2,125 mm)
Insulation	30 mm Mineral Wool
Glazing	Heat Strengthened Low Iron Glass
Coating	Selective Coating with Medium Emission Coefficient

4.1.2 Storage Tank Prototype

Direct thermosyphon systems are thermodynamically more efficient but come along with the major disadvantage that storage tank and solar collector operate within one single circuit, as described in the market and competition analysis (cf. Chapter 2.1). Additional-

ly, the decision to incorporate regions with frost (cf. Chapter 3.5.2) in the sensitivity analysis and the proposed full aluminium absorber design (cf. Chapter 2.2.2), results in the necessity that the storage tank prototype is to be a two-circuit double mantle heat exchanger storage. A further advantage of the separation of collector and water circuit is the possibility to operate the solar collector below the tap water pressure. The mantle material used for the prototype is mild steel. Häfner (2009) described a cost driven trend from stainless steel back to enamelled mild steel, representing 70 % of the total produced thermosyphon systems' storage tanks in 2009. The choice of mild steel is based on different reasons. The price for copper is even above stainless steel and based on its heat conductivity, which is eight-times higher than that of mild steel, has a negative influence on the thermocline inside the storage tank (cf. Chapter 2.2.3). Standard polymeric materials, like polyethylene, and polypropylene could have a positive influence on the thermocline, as the heat conductivity is found to be factor 1,000-2,000 below that of copper. By applying the standard boiler formula material thicknesses for polymeric materials in the range of 5.6–11.3 mm are required for a pressurised storage tank operated up to 9 bar. The required wall thickness, however, works like insulation against the heat flux from the double mantle heat exchanger (Table 4.2), hence mild steel is preferred.

Table 4.2: Influence of Material Properties on the Effective Heat Conductivity of the Storage Wall (Flat Plate Assumed)

Storage tank diameter 500 mm, max. operating pressure 9 bar, safety factor 2				
Material	**R_e [N mm^{-2}]**	**z_{min} [mm]**	**k [W m^{-1} K^{-1}]**	**h_{eff} [W m^{-2} K^{-1}]***
Copper	300–400	1.1–1.5	385	2.5–3.5e^{5}
Stainless Steel	185	2.4	14	5.8e^{3}
Mild Steel	185–355	1.3–2.4	~48	2.0–3.6e^{4}
Polymeric Materials (PE, PP, PMMA, PET)	40–80	5.6–11.3	0.15–0.35	13–62.5

*for a straight wall

Detailed studies of market-available storage tanks show promising design aspects regarding the operation safety and an optimised operation of thermosyphon systems.
Vulcano (2008) implements a simple 3 l volume expansion vessel in the storage tank as shown in Figure 4.10.

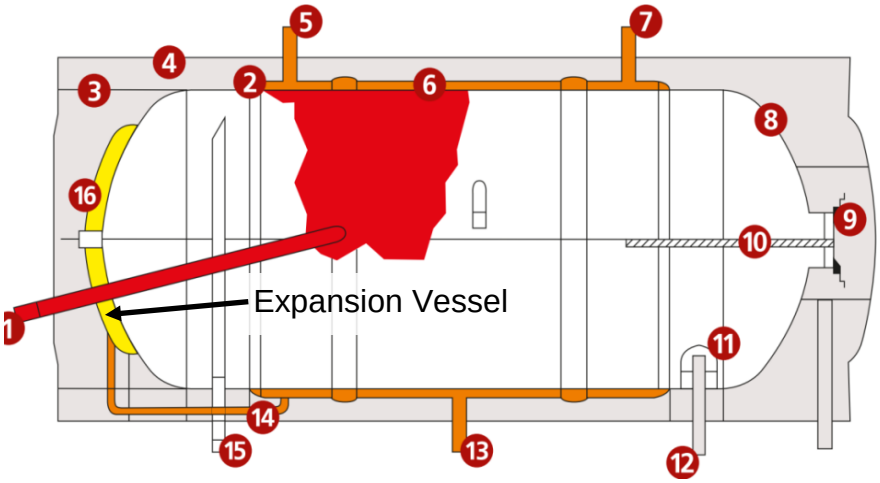

Storage Tank Parts:					
1	Collector Inlet	2	Closing-Off Heat Exchanger	3	PU-Foam Insulation
4	Cover Sheet	5	Filling Neck	6	Double Mantle Heat Exchanger
7	Safety Valve Connection	8	Storage Tank	9	Inspection Port
10	Sacrificial Anode	11	Diffuser Baffle	12	Cold Water Inlet
13	Storage Tank Outlet	14	Connecting Pipe	15	Hot Water Outlet
16	Expansion Vessel				

Figure 4.10: Double Mantle Heat Exchanger Storage with Integrated Expansion Vessel (Vulcano, 2008)

This expansion vessel prevents the system from a pressure rise to the release level of the relief pressure valve during operation and so enhances the operation safety at high fluid temperatures. A modified version of this concept was adapted to the prototype as shown in Figure 4.11. The expansion vessel was located at the inside of the hot water section and made out of a smaller dished boiler end.

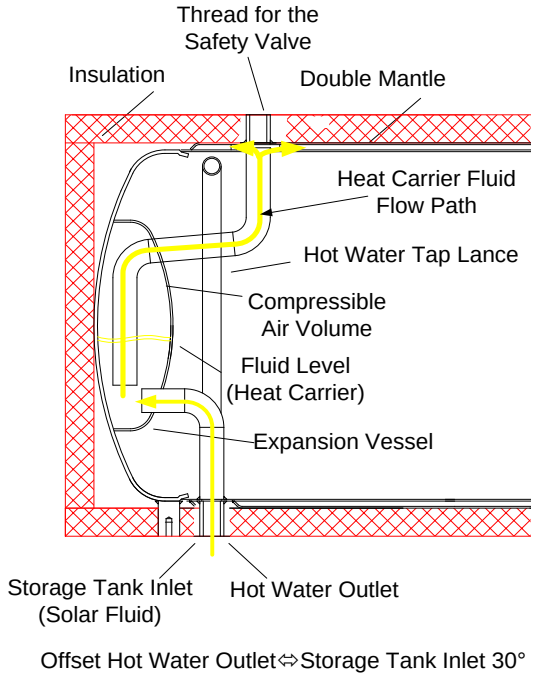

Figure 4.11: Expansion Vessel Included into the Storage Tank (Prototype Generation 1)

A measure to optimise the operation of thermosyphon systems is implemented by Sammler (2008). Sammler positions all connections for collector fluid and water at the storage tank bottom, which offers two advantages. On the one hand an aesthetical system setup can be achieved as the piping can be installed concealed from view. On the other hand, this connection type is suitable to prevent reverse thermosyphoning as no temperature difference between collector inlet and outlet arises (cf. Chapter 2.2.1). The prototype employed the same connection scheme with hydraulic improvements (Figure 4.12).

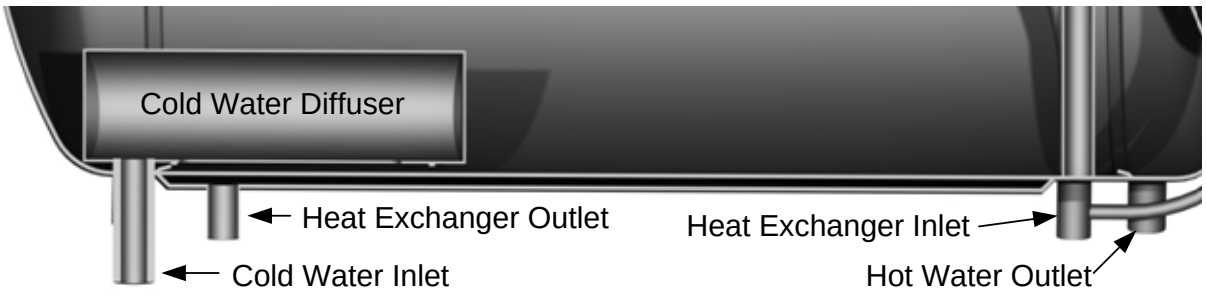

Figure 4.12: Prototype with Bottom Entries

Generally, the stratification inside the hot water section is rapidly destroyed while drawing water. This malfunction, caused by the inlet design of the storage tank, was countered by

using a cold water diffuser. Chapter 5.2 describes the optimisation measures concerning the diffuser in detail.

The sensitivity analysis shows a technical and economic optimum of 50 mm PU foam insulation. An increase of the insulation thickness to 70 mm resulted in an energetic improvement of less than 1.5 %, however, an additional insulation material demand of 45 % (for a storage tank with 520 mm diameter). A reduction of the insulation thickness to 30 mm came along with an energetic penalty of 3 % compared to 50 mm and is not recommended (Figure 4.13). For the prototype, an insulation thickness of 40 mm (areas with double mantle) to 50 mm (areas without double mantle) was chosen.

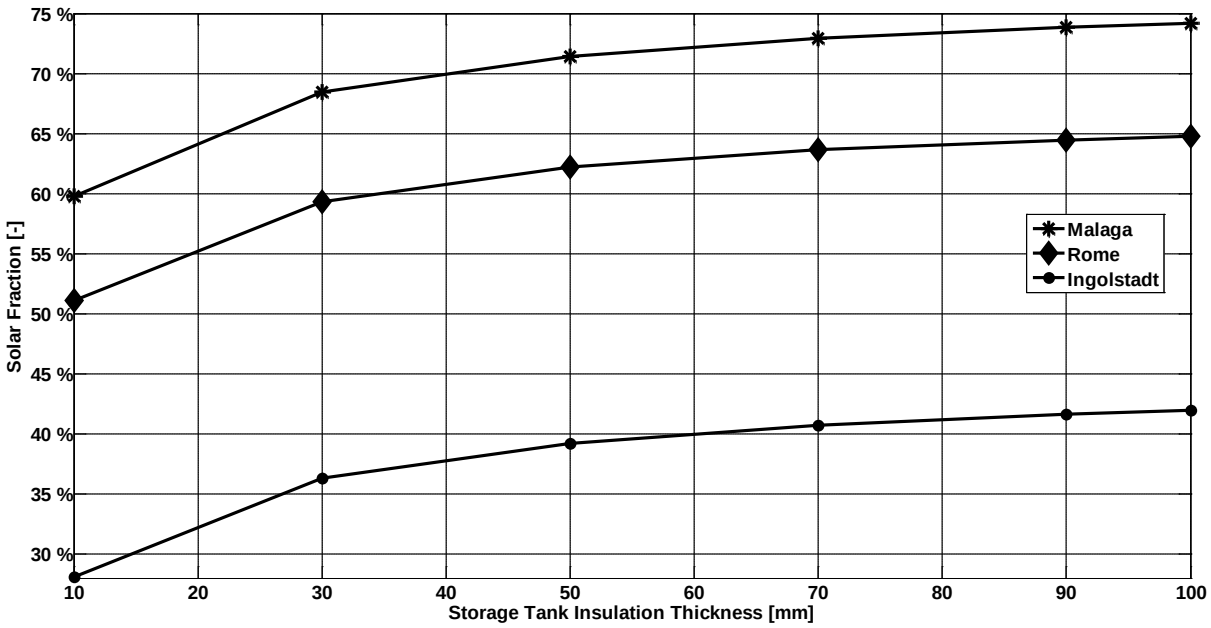

Figure 4.13: Simulation of the Storage Tank Insulation

Figure 4.14 shows the simulation results for a variation of the heat exchanger surface. Independent of the location simulated, a performance increase cannot be seen above 1 m² heat exchanger area.

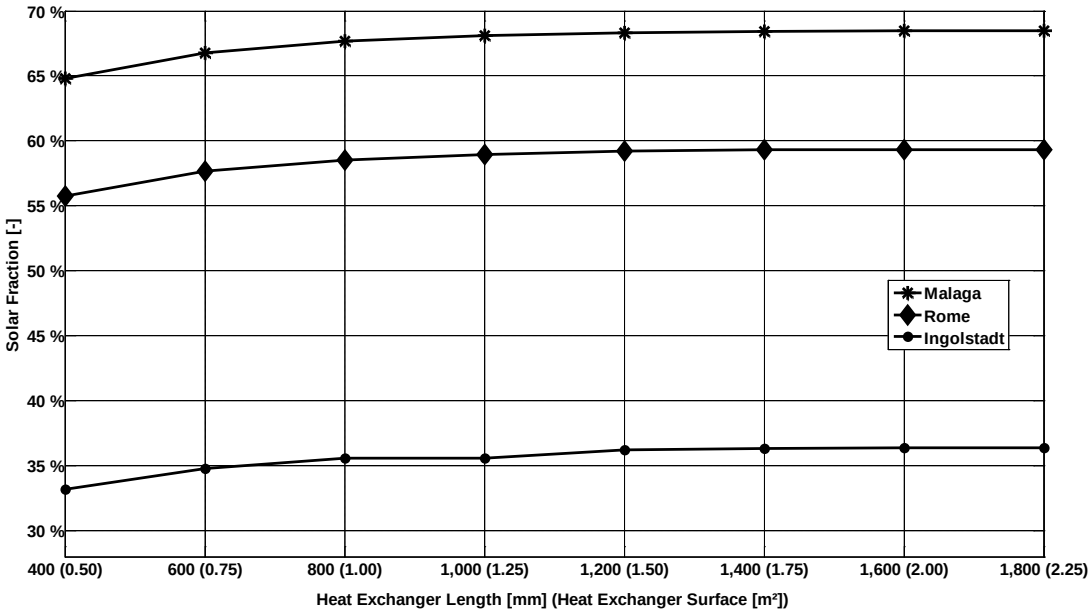

Figure 4.14: Heat Exchanger Surface

The heat exchanger spacing has no influence on the annual system performance. It only has an impact on the heat exchanger volume. In terms of tank production, a spacing of 10 mm is suitable (Figure 4.15).

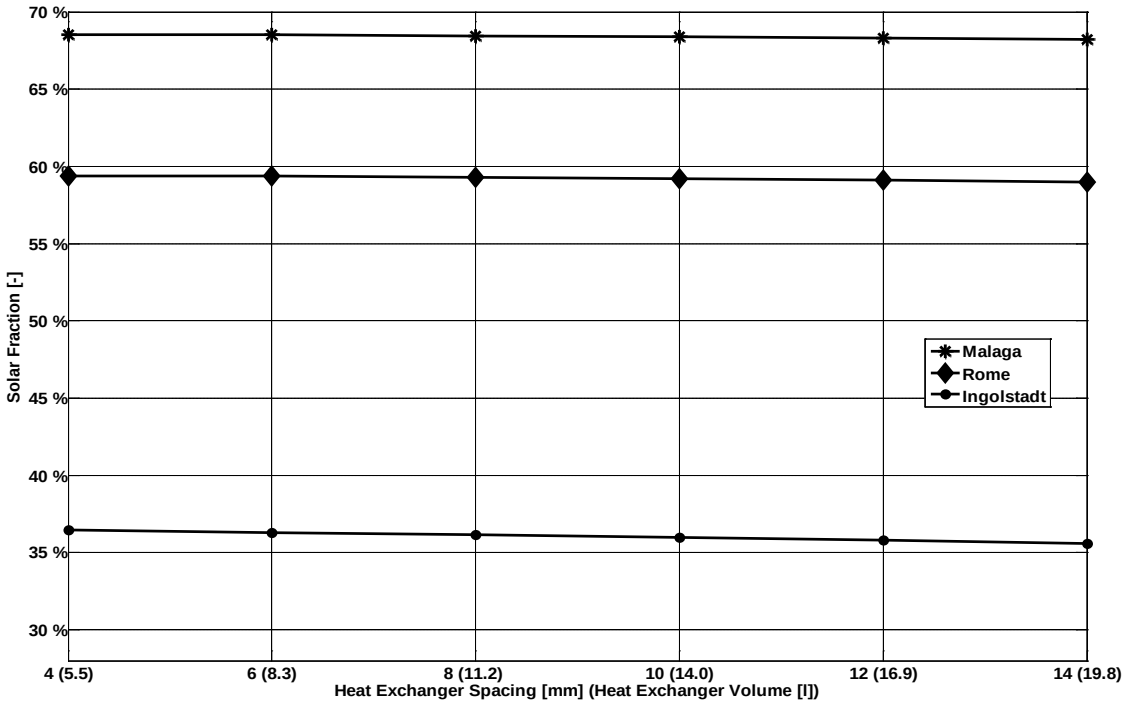

Figure 4.15: Heat Exchanger Volume

The investigations concerning the inner storage tank diameter result in a recommended minimum diameter of 450 mm. A detailed analysis of this result points to the improved stratification due to a bigger diameter. Independent of the location, diameters above 450 mm improve the annual solar fraction by less than 1 % (Figure 4.16).

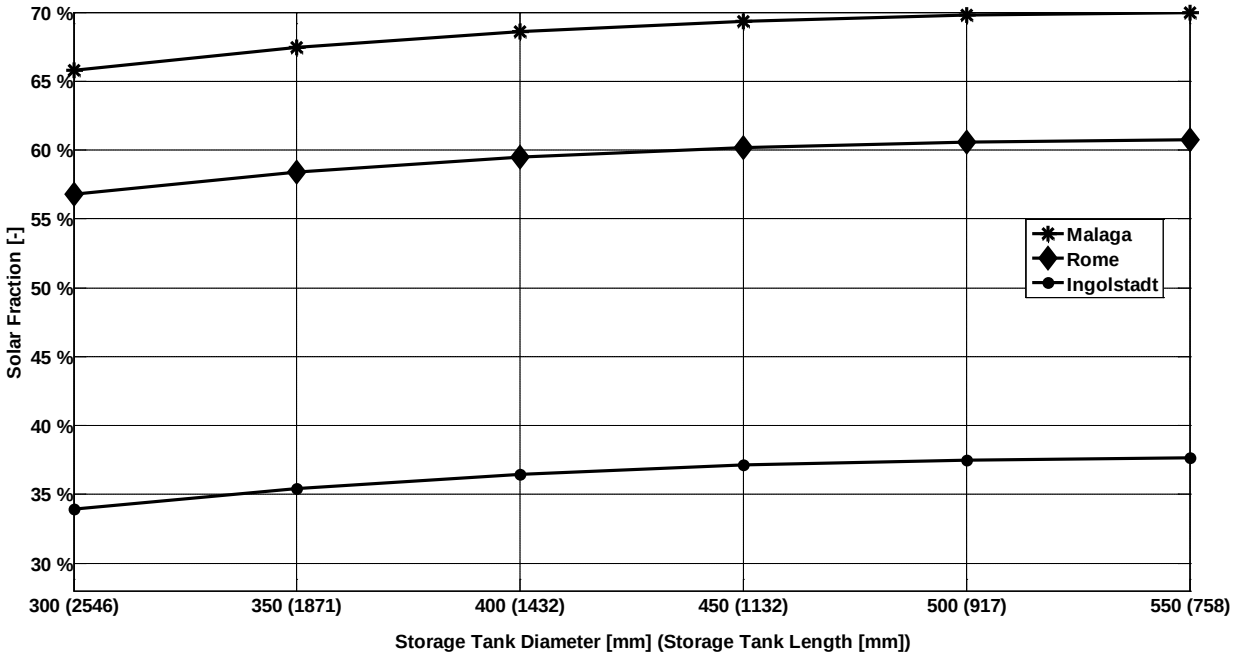

Figure 4.16: Simulated Storage Tank Diameter Variation

Concerning the optimum tap water volume, the sensitivity analysis indicates an optimum storage tank volume to collector aperture area of 65 l·m^{-2}. This value is in absolute conformity to the collector development (Chapter 4.1.1). For the given reference model, a 120 l storage tank performs better than the used 180 l storage tank, as shown in Figure 4.17. For the prototype with 2.34 m² the optimum storage tank volume is 160 l. For aesthetical reasons, the overall storage tank width is aligned to the collector width resulting in an inner storage tank diameter of 500 mm.

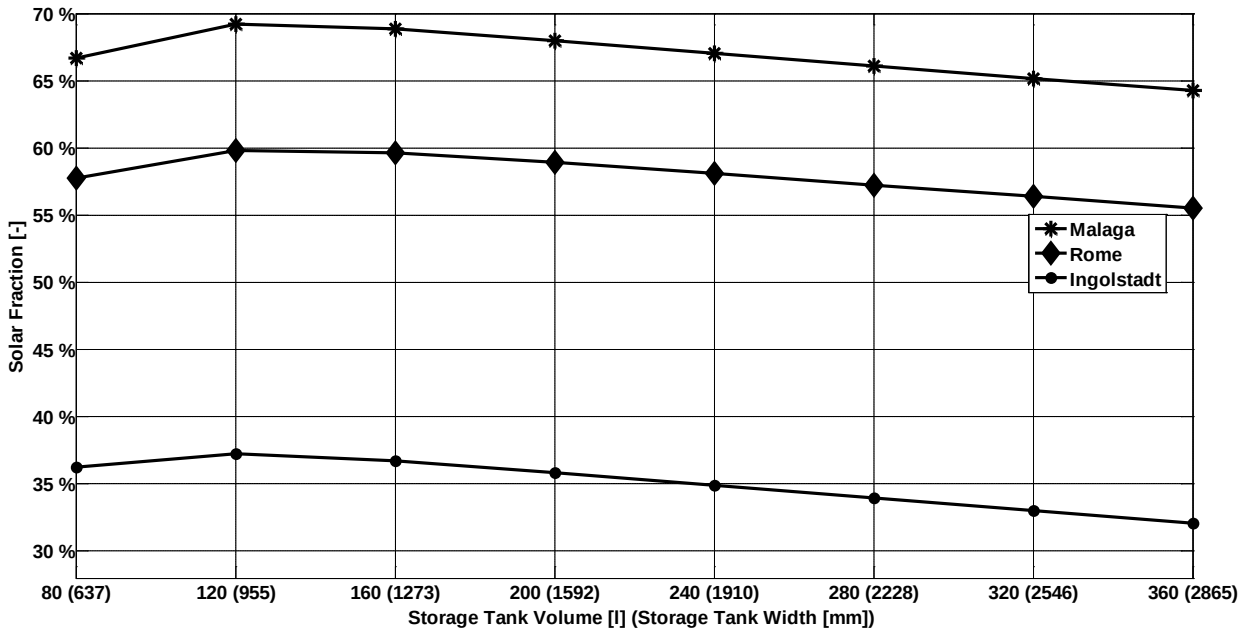

Figure 4.17: Optimum Storage Tank Volume

The simulation outcomes are transferred into a technical drawing of the proposed storage tank, which can be found in Appendix C. The technical data of the storage tank are shown in Table 4.3.

Table 4.3: Technical Data of the Proposed Storage Tank

Nominal Volume	165 l
Heat Exchanger Type	Double Mantle Heat Exchanger
Heat Exchanger Area	1 m²
Insulation	40–50 mm PU–Foam
Circuit Points	Collector and Water Connectors at the Bottom
Material	Enamelled Steel
Width / Diameter (incl. Insulation)	1,150 mm / 600 mm
Hydraulics	Cold Water Diffuser and Draw–off Lance

4.2 Detailed Design of the System–Prototype

The system design is initiated with the analysis of the collector to storage tank height ratio. The bandwidth of the height variation is 1,400 mm, beginning with a collector outlet at the same height as the storage tank inlet (Figure 4.18; BD = -400 mm).

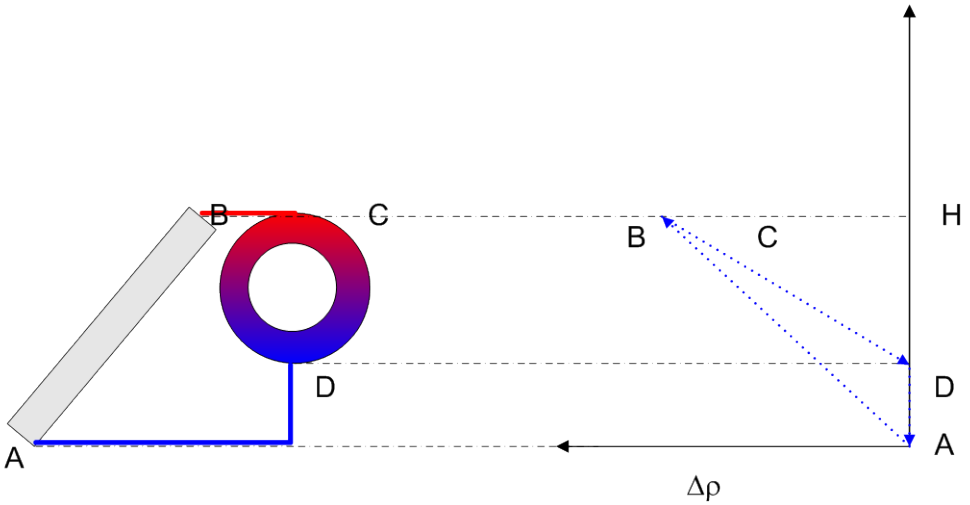

Figure 4.18: Minimum Storage Tank Height

The maximum height difference BD is +1,000 mm as shown in Figure 4.19.

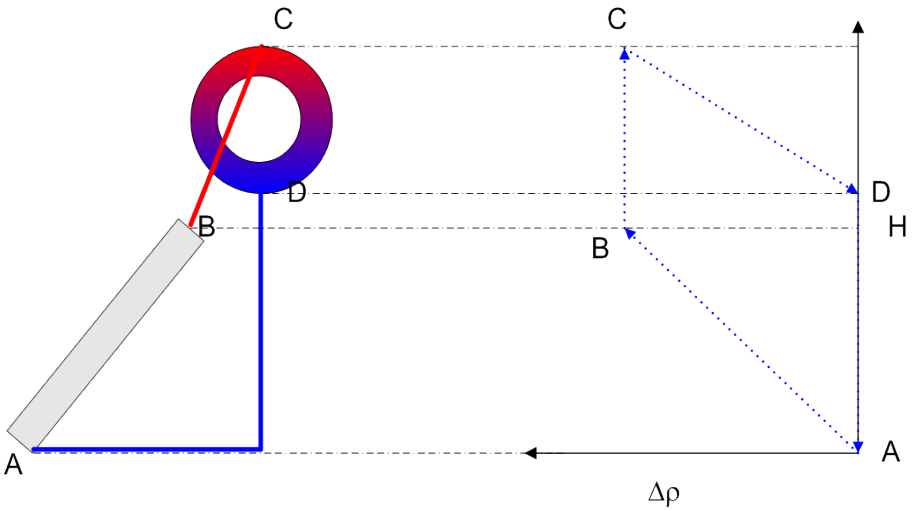

Figure 4.19: Typical Storage Tank to Collector Ratio

Beforehand to the simulation, Figure 4.18 and 4.16 can be used to describe the expected thermosyphonic flow rates analytically at a stationary working point. Starting at collector inlet (A), the fluid is heated due to solar irradiation. The density decreases as shown in the diagram on the right side (A to B). The piping from collector outlet to storage tank inlet is lossless, so no density changes occur from B to C. Within the storage tank the heat carrier fluid cools down to the temperature at the collector inlet, so the density increases from C to D. The piping from storage tank outlet to collector inlet is assumed to be lossless (path D to A). The vectors form a closed area which is an indicator of the system

buoyancy. The bigger the height difference BD, the bigger the flow rate at a reduced temperature difference between collector in- and outlet.

The simulation results reflect this theoretical approach. Systems with a low storage tank position work at a high temperature difference at a low flow rate, whereas systems with a high storage tank position work at relatively low temperatures compared with a high mass flow rate. Concerning the annual solar fraction, a low system setup outperforms the systems with storage tank above the collector outlet. Regarding the reverse thermosyphoning prevention, a storage tank located above the collector outlet offers the possibility to use a physical approach, while a low system setup needs an additional non return valve. Due to its lower complexity, a close-coupled system setup is followed. As space for the piping installation between collector and storage tank is needed, the prototype shows a height difference of 80 mm (Figure 4.20).

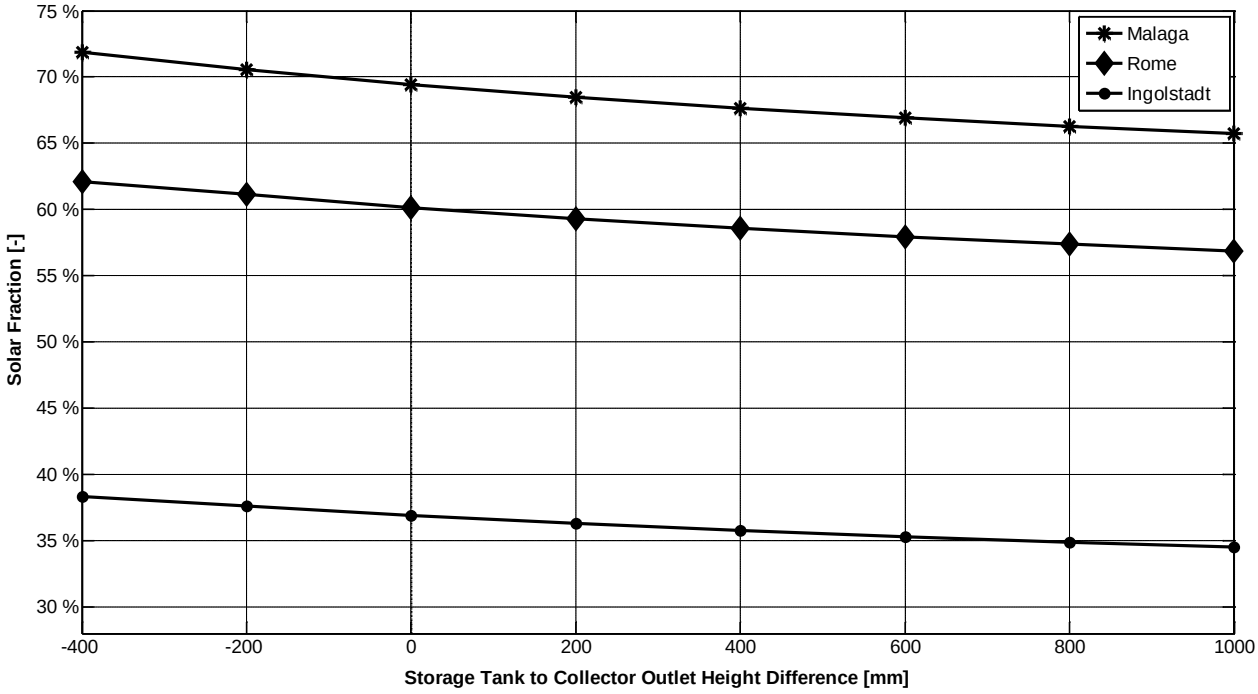

Figure 4.20: Storage Tank to Collector Height Ratio

The system support design is based on the energetic optimal collector tilt angle. This angle also influences the geometrical and aesthetical appearance of the prototype. Figure 4.21 shows the simulation results. In the range of 20–40 ° there are nearly no differences in the annual solar fraction. For the system support a tilt angle of 35 ° is chosen.

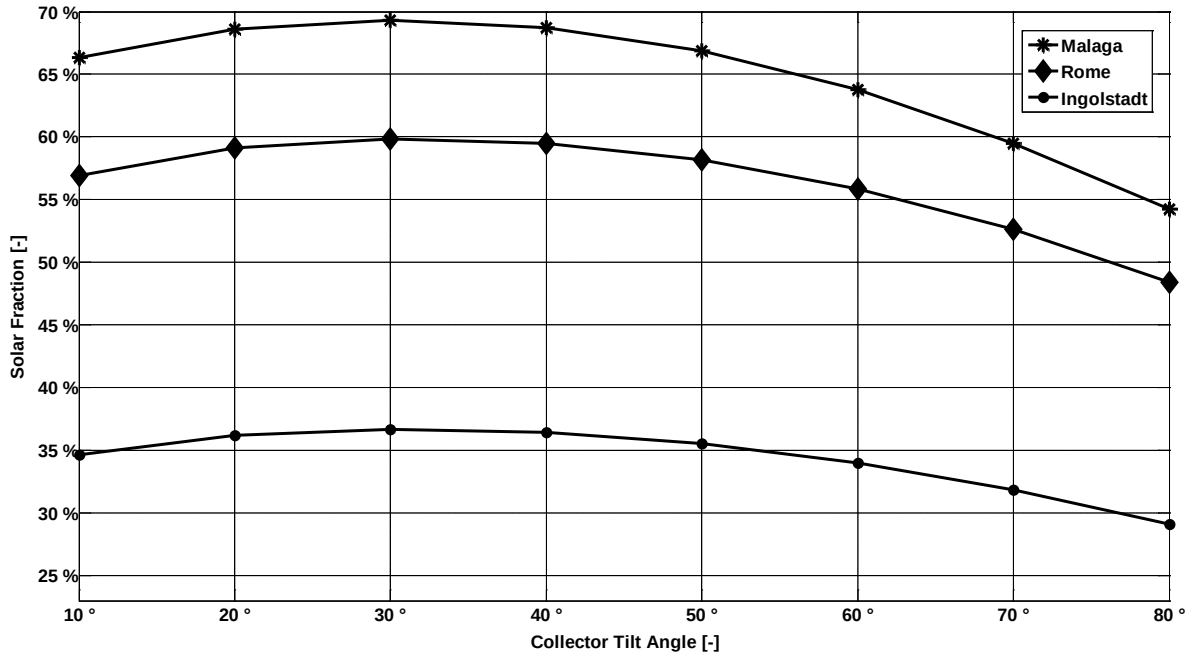

Figure 4.21: Collector Tilt Angle

The variation of the inner pipe diameter for the interconnecting pipes leads to an optimum pipe diameter of 13 mm. Larger diameters on the one hand lower the flow resistance, but on the other hand they come along with a higher heat loss on the surface and a higher heat capacity (Figure 4.22) that makes the system slow in reaction.

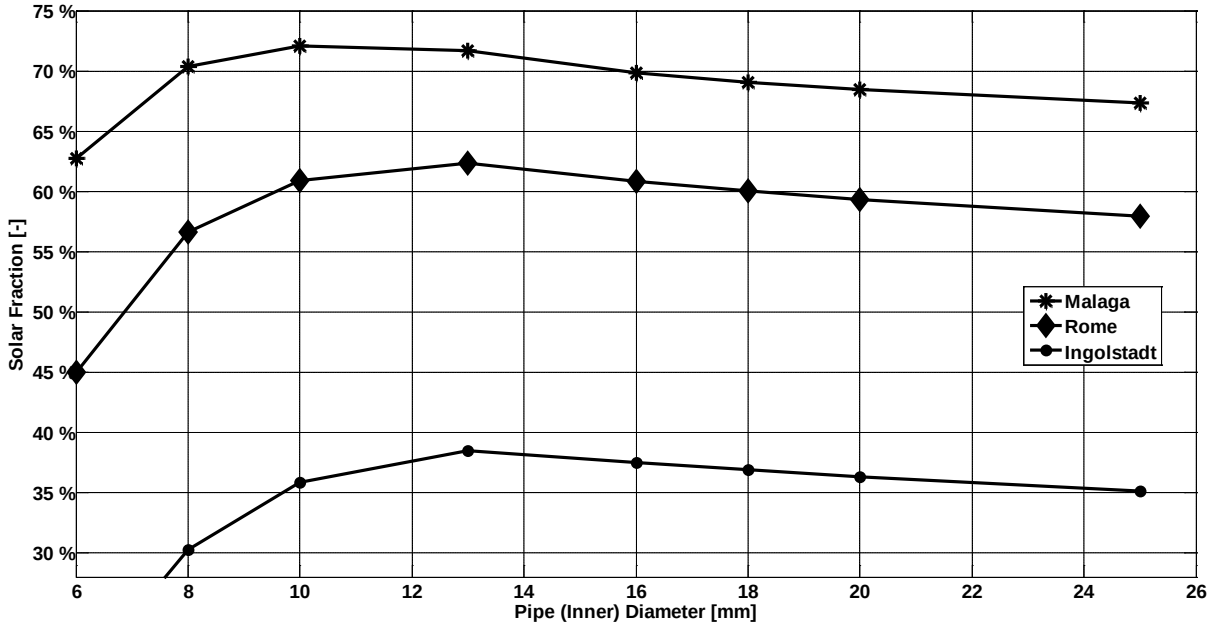

Figure 4.22: Variation of the Pipe Diameter

Due to the manufacturing process, the prototype collector deflects from these measures. The return pipe and the lower header are one bended pipe with an inner diameter of 16.4 mm, which is included directly into the collector casing.

From the economic point of view a recommendation for 15–20 mm insulation thickness (Figure 4.23) can be derived from the simulation results. If 25 mm insulation thickness was chosen the amount of insulating material needed, already doubles compared to 15 mm.

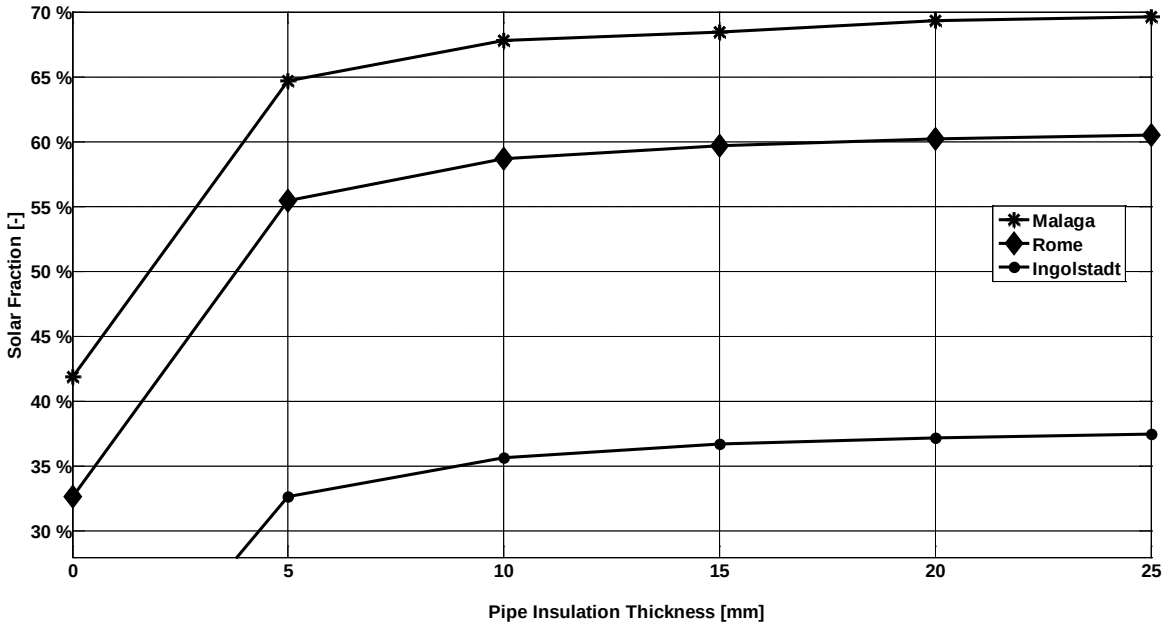

Figure 4.23: Influence of the Pipe Insulation Thickness

4.3 Construction of the System-Prototype

To reduce material usage (costs) and to allow a quick and secure installation of the thermosyphon system a preassembled system support layout was developed and proposed to the project partner. The system support uses only prefabricated parts and incorporates the collector frame as structural system part. A new pivot design fixes the collector tilt angle securely to 35 °. To fix the support on site only 2 screws are necessary. A detailed description of the system support can be found in Appendix E.

The construction of the prototype was done in two steps. The first step was the construction of a collector and a storage tank at the project partners' company according to the described design parameters. Both components were then tested intensively in the university laboratories as described in Chapter 5.1 to 5.3. The goal behind these tests was to determine further optimisation potential beforehand to the adaption of the system to mass production. The solar collector prototype for example has a removable transparent cover making it possible to equip the collector with various temperature sensors (Figure 4.24).

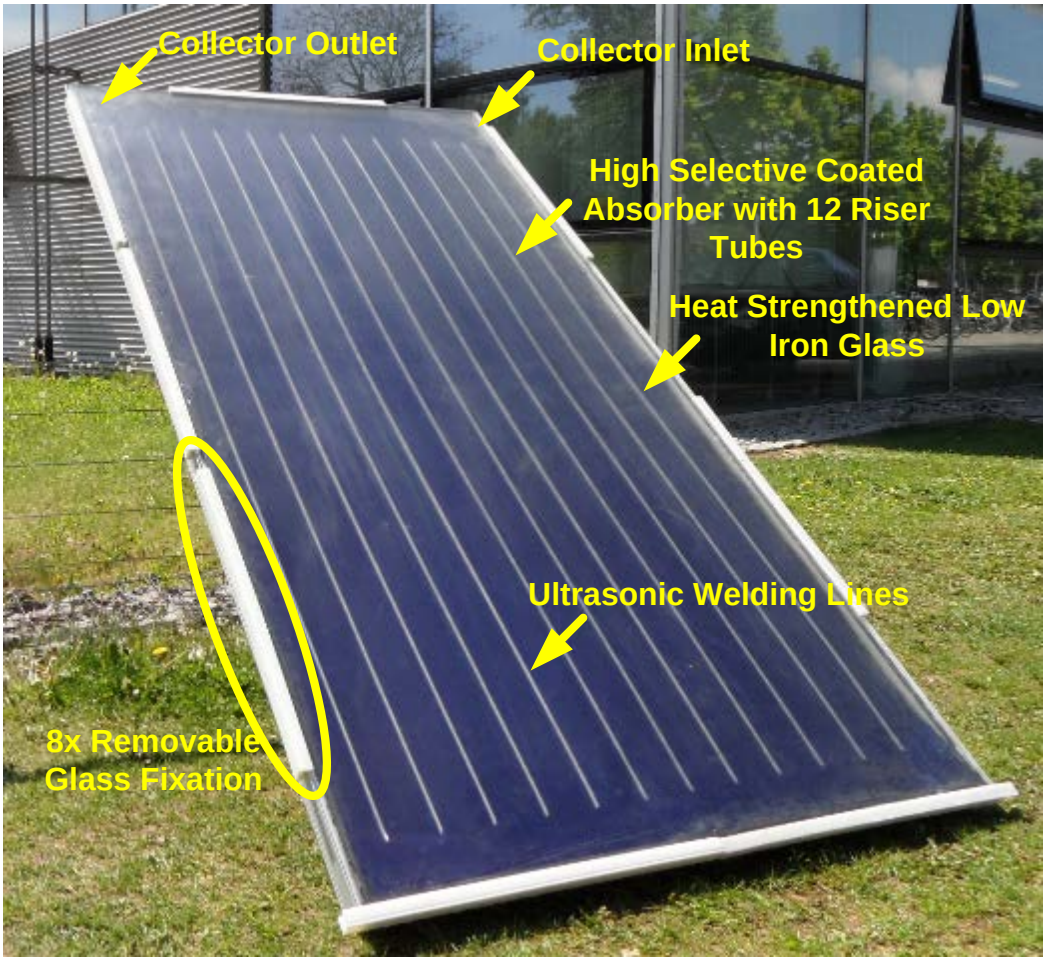

Figure 4.24: Prototype Collector with Removable Transparent Cover

The storage tank was manufactured manually to the dimensions of the storage tank design. It is equipped with 16 threads for temperature sensors at its cover. The storage tank was not enamelled nor was a sacrificial anode included. To optimise the draw-off quality of the storage tank, a removable cold water diffuser is clipped in. The insulation is a low

expansion polyurethane foam. The insulation quality is not comparable to high density polyurethane foam, usually used as storage tank insulation material. The outer coating is a riveted sheet metal which will be replaced by an aluminium sheet in mass production (Figure 4.25).

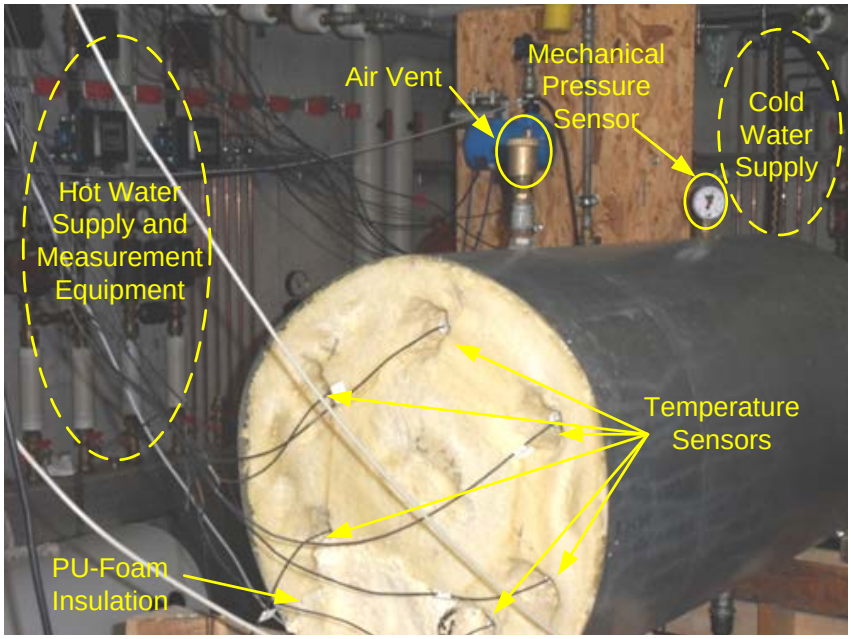

Figure 4.25: Storage Tank Prototype Tested in the Laboratory

The interconnecting pipes and the system support are not part of this first prototype.

The second prototype was closer to mass production. It included a sealed improved solar thermal collector (Chapter 5.1) manufactured semi-automatically, the safety equipment, a system support as described in Chapter 4.2 and an enamelled storage tank with a fixed diffuser. The storage tank, a purchased part, included some compromises between technical optimisation potentials (Chapter 5.2) and costs.

5 Proof of Concept

The collector and storage tank of the prototype are tested in detail separately before performing a characterisation of the whole system in an outdoor test.

5.1 Collector Tests

To visualize the flow distribution inside the absorber, an infrared thermography testing rig is constructed according to Figure 5.1. The hydraulic setup is allowing an immediate switch from the cold fluid temperature close to the ambient temperature to the test temperature. The advantage of this setup is that there occurs no temperature mix inside the absorber. For the tests the absorber is taken out of the collector casing to avoid optical reflections at the glazing. To enhance the emissivity of the absorber, the absorber surface investigated is painted black. The test is carried out with the absorber in vertical position as the tilt angle in such a pumped pressurised system setup has no influence on the flow distribution. The flow distribution is only dependent on the fluid velocity and the hydraulic design of the absorber.

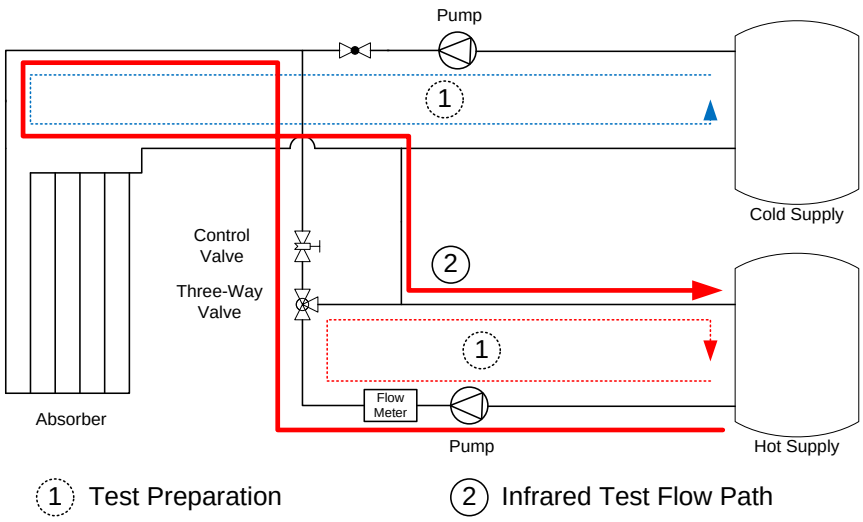

Figure 5.1: Absorber Infrared Test Setup

Each test sequence starts by setting the test volume flow rate using the control valve (Figure 5.1). The transient absorber behaviour is recorded using the infrared camera. The tests are performed at flow rates typical of thermosyphon systems — 20 l h^{-1}, 40 l h^{-1} and 60 l h^{-1} — see also Figure 3.22. Additional tests are carried out at high flow rates of

120 l h^{-1} and 240 l h^{-1}.The flow inside the absorber was expected to be well distributed even at low or laminar flow rates due to the header design according to Wagner (2008) where an optimum ratio of the converging to the diverting header cross sectional area of 0.5–0.7 is recommended. The upper, converging header realised in the absorber has a diameter of 22x0.8 mm, while the lower, diverging header consists of a 18x0.8 mm pipe. This results in a ratio of 0.65 and lies within the recommended design range. During the tests, this homogenous flow distribution could not be observed as shown in the infrared sequence for 60 l h^{-1}.

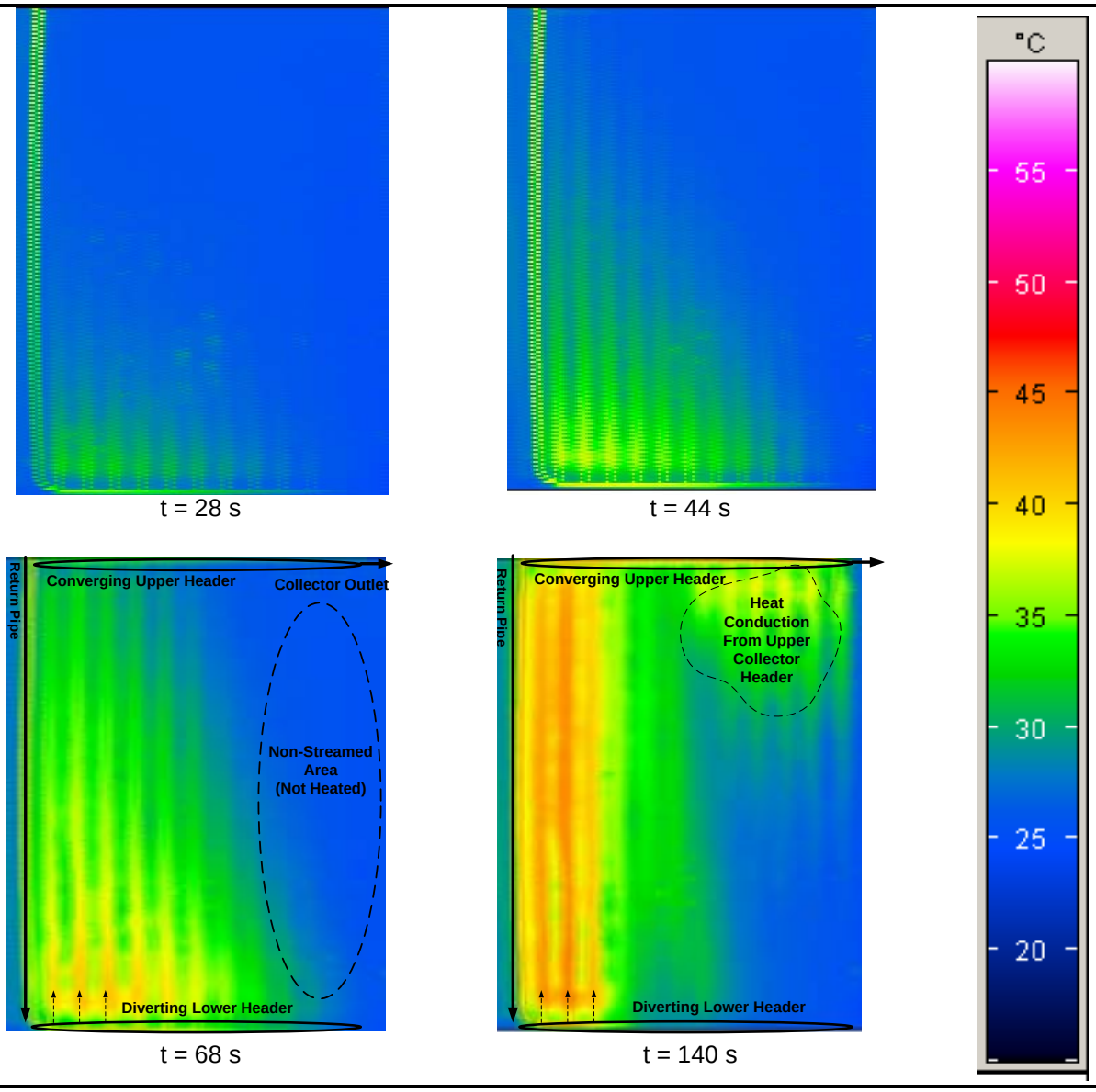

Figure 5.2: Infrared Test Sequence at 60 l h^{-1}

The inhomogeneous flow distribution of the prototype absorber measured at the university's testing rig could be verified by a CFD simulation done by the industrial partner to back up the infrared tests. At higher flow rates, the flow distribution measured became more and more homogenous. One of the optimisation possibilities is to add further riser tubes to lower the flow rate through each riser and homogenise the flow distribution even at low flow rates. Another approach is to use different riser diameters to control the flow distribution by the occurring pressure drop. But these approaches are limited by manufacturing restrictions, e.g. automatized welding of different pipe diameters on to one absorber sheet, on the one hand and the production costs on the other hand, e.g. by adding further riser pipes.

The pressure drop of the solar collector (field) influences thermosyphon systems and pumped systems in different ways. In thermosyphon systems the pressure drop affects the flow rate through the system. Therefore a high pressure drop in the solar collector comes along with a low flow rate and high temperature rise of the fluid while passing from collector in- to outlet, while a low pressure drop comes along with a lower temperature rise but a higher flow rate.
In forced circulated systems, the pressure drop affects two design variables. On the one hand a high pressure drop in the collector (field) comes along with a higher (parasitic) energy demand for the pump. On the other hand the experimental and analytical data published by Dunkle and Davey (1970) of a large parallel collector field composed out of 12 harp absorbers shows up a maldistribution of the flow rate (Figure 5.3 (A)), especially in the centre of the collector field. At a high overall flow rate, the authors measured a temperature difference of 22 K from the centre to the collector field outlet. A high temperature rise indicates a low flow rate inside the considered absorber. The authors worked out the recommendation for the connection of large collector fields, to connect the collectors either in a series-parallel (Figure 5.3 (B)) or a parallel-serial setup (Figure 5.3 (C)). Forced or natural circulated systems with up to 24 risers in parallel offer a satisfactory flow distribution.

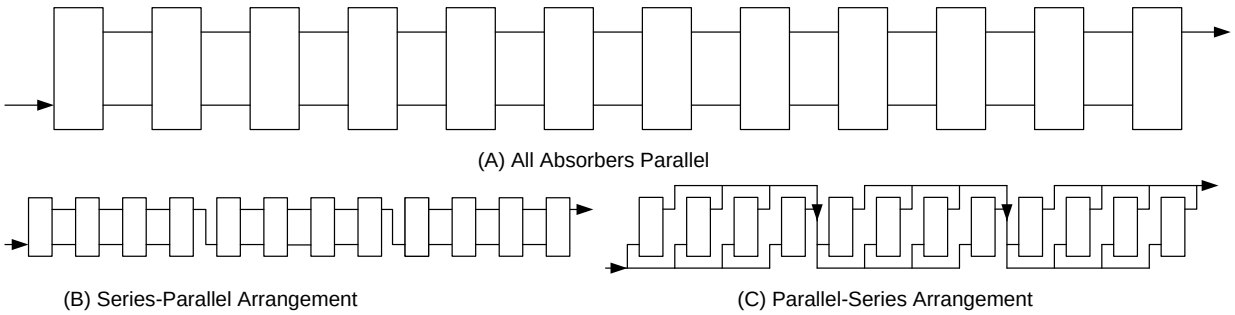

Figure 5.3: Absorber Bank Connection Schemes Investigated by Dunkle and Davey (1970)

This finding on natural circulation systems is in accordance to experimental investigations of a harp absorber in a thermosyphon system by Chuawittayawuth and Kumar (2002). The results show under partly cloudy, cloudy and clear sky with high radiation fluctuation the temperature distribution and thus the flow rate through the collector to be fairly uniform. Under clear sky conditions the first 2 risers (closest to the collector inlet) show significantly lower flow rates compared to the other 7 risers. An explanation for this behaviour is not given.

Besides a homogenous flow distribution, a high zero loss efficiency is needed for a good system performance. Furthermore, the collector efficiency curve is needed for the simulation validation. It was measured according to DIN EN 12975–2 (2006). The chosen measurement method is an indoor steady state procedure. The university's indoor solar simulator offers the advantage of defined and reproducible test conditions as compared to outdoor tests. The experimental setup of the solar simulator used is illustrated in Figure 5.4.

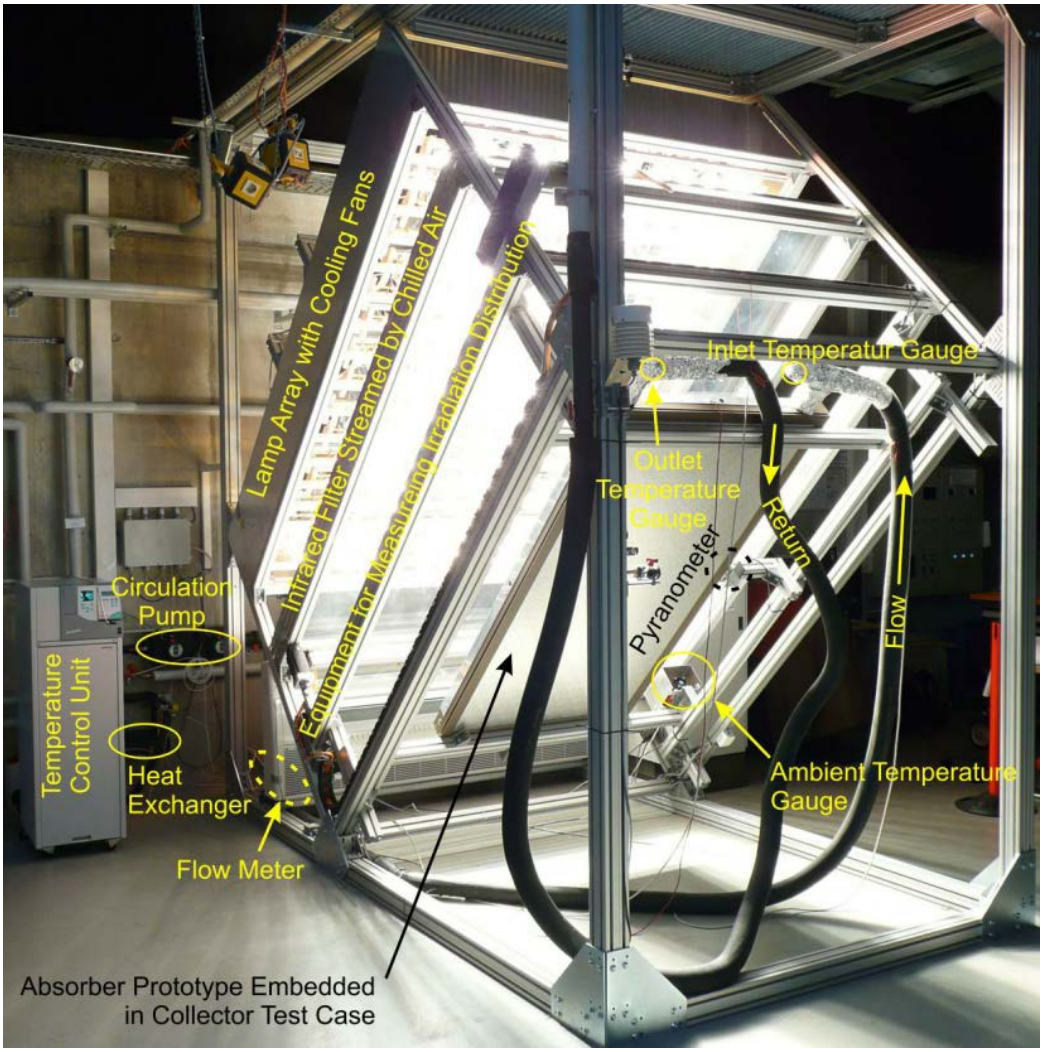

Figure 5.4: Experimental Setup of Ingolstadt University's Solar Simulator (Treikauskas, 2009)

The prototype collector was tested using 3 different volume flow rates. The first flow rate of 60 l h^{-1} was close to the maximum flow rate achievable during normal system operation. The second flow regime tested at 170 l h^{-1} corresponds to the given flow rate in the test standard of 72 l h^{-1} m^{-2} aperture area. The third flow rate was set to 280 l h^{-1}. Resulting from the infrared tests, an improved flow distribution with a slightly better performance was expected. The measured efficiency curves were close to market available flat-plate collectors. However, the zero loss efficiency does not meet the design point of more than 0.80 (Table 5.1 and Figure 5.5). The parameters η_0, a_1 and a_2 of the efficiency curve were estimated from test results using the least square fitting method given in the test standard. The curves in Figure 5.5 are plotted against $(T_{mean} - T_{amb})G^{-1}$ using equation (2.21).

Table 5.1: Coefficients for the Efficiency Curve Calculation Derived from Collector Testing

		Prototype Collector			Standard Flat-Plate Collector	Reference Collector
$\dot{V}$	[l h^{-1}]	60	170	280	140	135
η_0	[-]	0.787	0.773	0.773	0.776	0.811
a_1	[W m^{-2} K^{-1}]	-3.744	-3.716	-3.235	-3.716	-3.521
a_2	[W m^{-2} K^{-2}]	-0.013	-0.015	-0.016	-0.014	-0.019

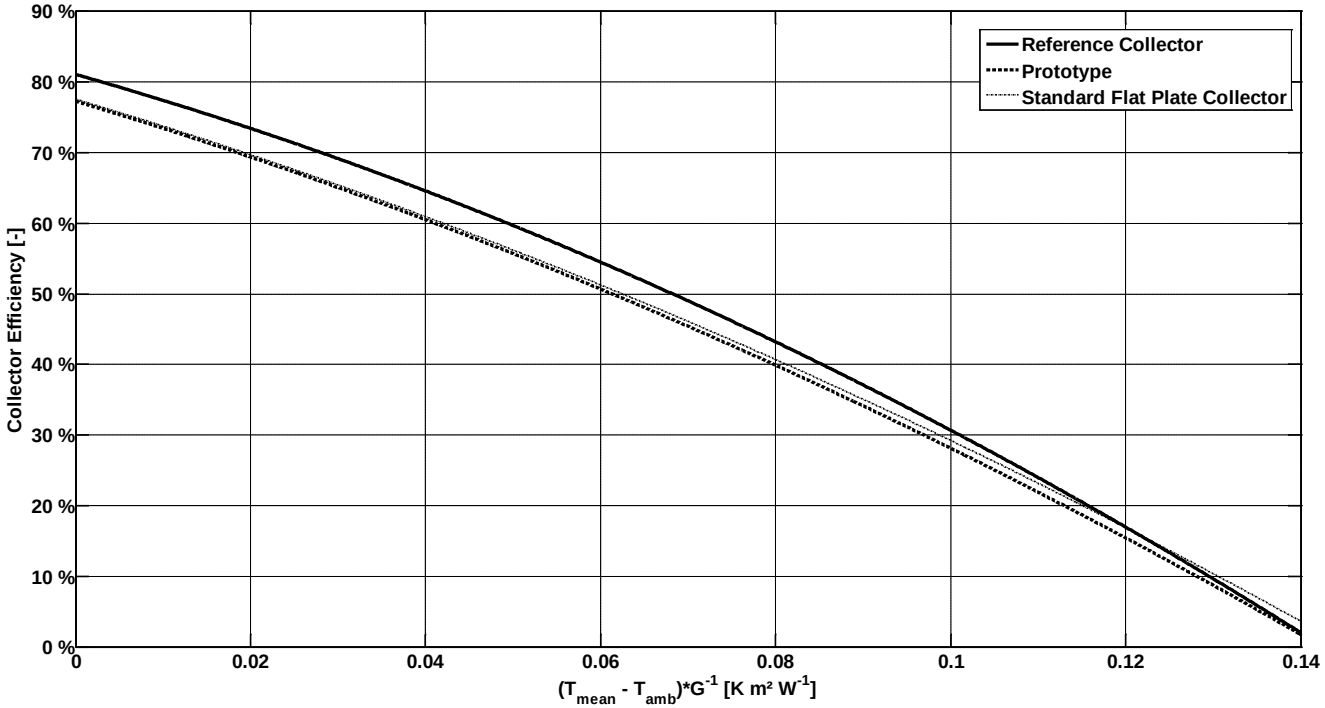

Figure 5.5: Measured Collector Efficiency Curves

To improve the zero loss efficiency it is necessary to homogenise the flow distribution inside the absorber, as theoretical calculations with a uniform flow distribution reveal an efficiency of 0.80. Besides that the welding quality at the beginning and the end of each welding line has to be improved. Removing the absorber from the casing leads to a shear off between absorber plate and piping as illustrated in Figure 5.6.

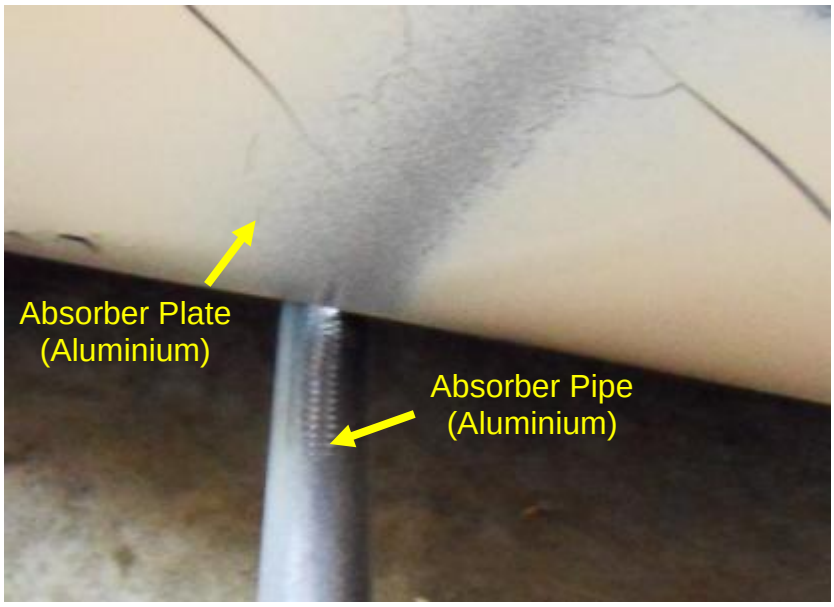

Figure 5.6: Shear Off between Absorber and Piping Weld

Apart from the efficiency curve, the thermal behaviour of the solar collector was investigated in detail. For these measurements, the collector was equipped with 9 temperature sensors inside as shown in Figure 5.7. The tests were carried out at a flow rate of 60 l h^{-1} and with the collector in stagnation. Stagnation in this case meant, the collector fluid was removed and the empty solar collector was irradiated by the solar simulator.

The stagnation temperature of the collector was extrapolated according to measurement data to 202°C at 1,000 W m^{-2} and T_{amb} = 30 °C applying the method given in the test standard. Stagnation temperatures in the range of 200–220 °C are typical of selectively coated flat-plate collectors.

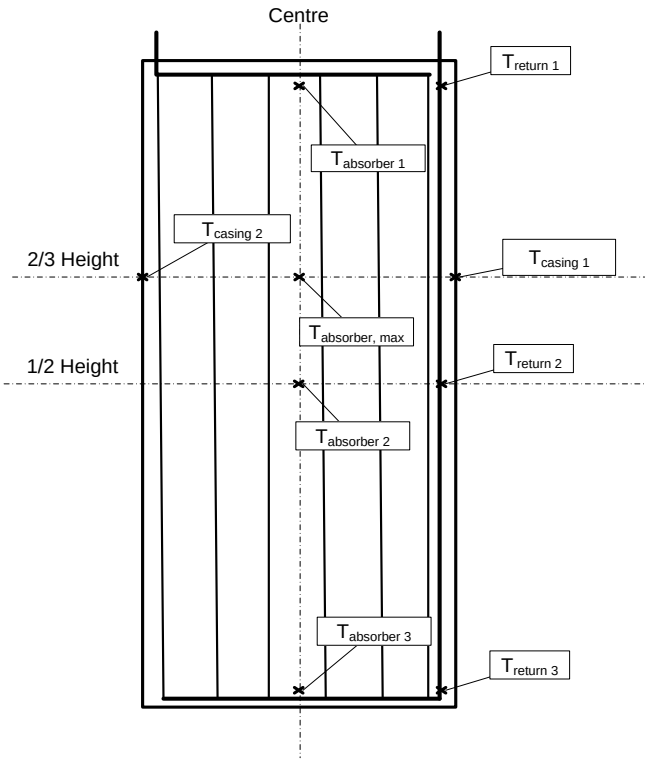

Figure 5.7: Metering Points for the Collector Characterisation

Even more relevant to the efficiency of the thermosyphon system and the developing flow rate is the thermal separation of absorber and return pipe (cf. Appendix A), which is piped inside the collector casing just below the absorber sheet at a mean distance of 6 mm. This separation was proved by evaluating the temperature difference between absorber and return pipe at the collector bottom, in the centre and near the outlet. The tests were carried out at collector inlet temperatures ranging from 18–75 °C. As expected, the absorber temperature was always clearly above the pipe temperature. The chosen bandwidth of inlet temperatures corresponds to normal system operation temperatures. The difference in temperature was found to depend on sensor position and inlet temperature. The return pipe was not insulated — therefore a slight temperature rise from sensor $T_{return\ 1}$ to $T_{return\ 3}$ was noticed. The temperature difference from $T_{return\ 1}$ to $T_{return\ 2}$, was in the range of 0.5–1.5 K, depending on the inlet temperature. The significance of the measurement data was limited by two facts. The temperature sensors used for the calculation of the pipe temperatures are clamp on sensors. Hence, the exact fluid temperature was not measured. More important was that these sensors were also affected by the air temperature inside the casing, which was always above the entering fluid temperature. It was concluded that the temperature rise inside the return pipe in this case was overesti-

mated. A more precise measurement of the thermal behaviour could be done by inserting T-branches into the return pipe which would allow putting the temperature sensors directly into the flow. This idea could not be realised as the return pipe had to be cut and reassembled for this purpose and the collector was needed for the system tests.

The last test sequence carried out with the collector prototype was the measurement of the casing temperatures, an indicator for the collector edge losses U_e. According to Chapter 2.2.2 the edge losses for a well-designed system are considered to be rather small.

The aim of the test was to determine in which magnitude the unconventional absorber design — return pipe inside the casing and the asymmetric outer fin geometry — influenced the casing temperature during operation (Figure 5.8). Two temperature sensors were placed at the inside of the casing at 2/3 collector height. Convection and radiation from pipes and absorber plate were considered to be relevant for the occurring heat transfer towards the casing.

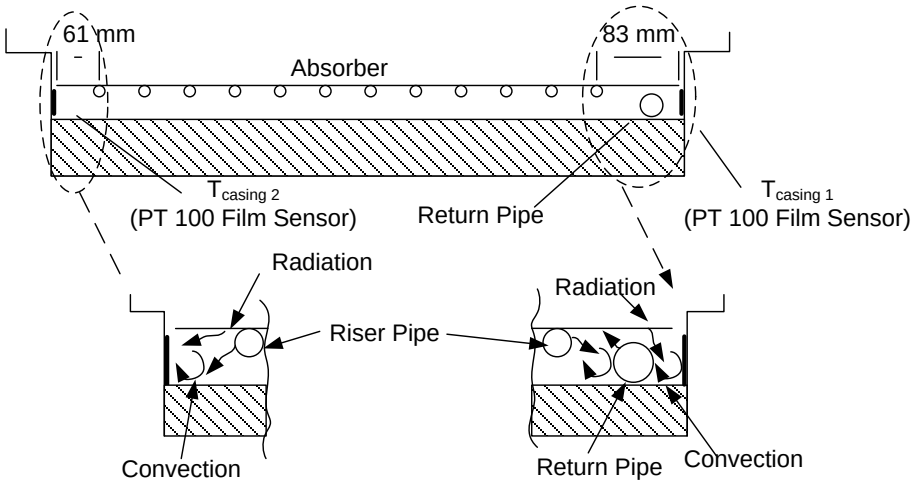

Figure 5.8: Schematic View of the Measurement Points at the Collector Casing

At normal operation conditions up to T_{inlet} = 64 °C inlet temperature (T_{outlet} = 81 °C), the differences at both casing sides were less than 5 K.

At T_{inlet} = 81 °C (T_{outlet} = 98 °C), the temperature on the right side $T_{casing\ 1}$ of the absorber was 10 K above the left side as shown in Figure 5.9. This indicates a higher heat flux towards the casing at fluid temperatures close to 100 °C and thus increasing edge losses.

The temperature dependent losses result in a reduction of the overall collector efficiency at high temperatures, not relevant for thermosyphon systems because such high temperatures may cause overheating problems.

There were identified two possible reasons for the measurement results. On the one hand there was the return pipe carrying hot fluid close to the casing and sensor $T_{casing\ 1}$. On the other hand the width of the right fin is 83 mm while the left fin width is only 61 mm. This caused higher temperatures and thus losses at the right fin edge ($T_{casing\ 1}$).

Due to the rather low temperature difference during normal operating temperatures no additional measures like insulating this pipe were considered to reduce the thermal losses and so the collector edge losses U_e.

A further fact that requires little temperature difference on both casing sides is the implemented physical approach to avoid reverse thermosyphoning, where the in- and outlet of the collector have to cool down equally to avoid thermal imbalances and so reverse flow.

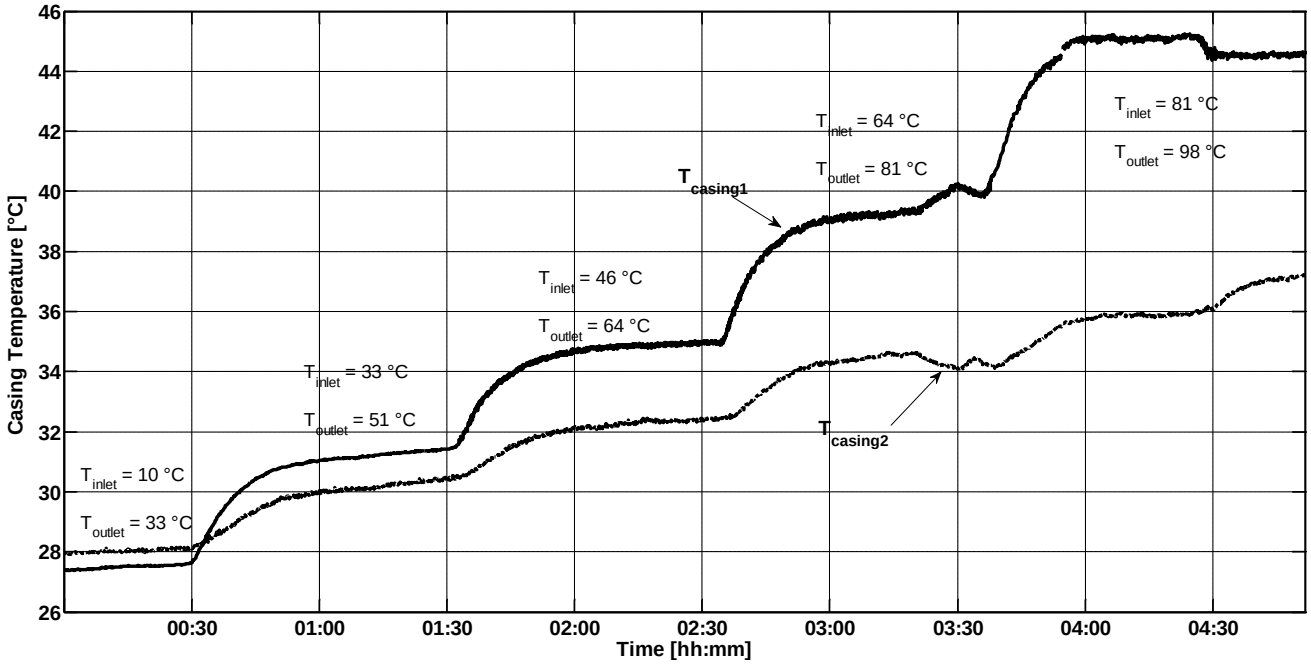

Figure 5.9: Measured Casing Temperatures at Mass Flow Rate 60 kg h^{-1}

5.2 Storage Tank Tests

The storage tank is evaluated in two steps. The first tests are carried out to study the behaviour of the solar circuit with its special expansion vessel design. This vessel can cope

with a volume expansion of up to 3.5 l and is supposed to keep the system pressure below the safety valve opening pressure of 2.5 bar_{abs}. The calculation of the volume expansion through temperature rise inside the thermosyphon system is done taking an uniform system temperature into account. This overestimates the real volume expansion as a temperature gradient of 20–40 K between collector outlet (storage tank inlet) and storage tank outlet (collector inlet) is a normal value during operation. The solar fluid volume of the system including storage tank, interconnecting pipes and solar collector is about 14 l.

The basis of the calculation is the Boyle-Mariotte formula and the density temperature correlation of the solar fluid used (equation (5.1)):

$$p_{air,2}(T) = \frac{p_{air,0} V_{air,0}}{V_{air,0} - V_{fluid,0}\left(\frac{\rho_{fluid,0}}{\rho_{fluid}(T)} - 1\right)} \tag{5.1}$$

with

p_{air}	Pressure Inside the Vessel	[Pa]
T	Considered Fluid Temperature	[°C]
V_{air}	Air Volume Inside the Vessel	[m³]
ρ_{fluid}	Solar Fluid Density	[kg m^{-3}]

The calculation and the functionality are proved in a laboratory test by pumping additional fluid into the expansion vessel. This additional fluid corresponds to the temperature dependend volume expansion of the heat transfer fluid. The measured volume pressure data is in good correlation with the extrapolated calculation data for values above 100 °C. During normal operation (temperatures below 100 °C) a pressure rise below 0.25 bar as illustrated in Figure 5.10 will occur. An optimisation measure derived from the test is the possibility to use a smaller expansion vessel in the system and allow a higher pressure rise during operation, as commonly available safety valves open at either 2.5 bar (3.5 bar_{abs}) or 5.5 bar (6.5 bar_{abs}).

The second test carried out within the heat exchanger circuit is a pressure drop measurement with special regard to the expansion vessel. This vessel is in the main fluid stream and causes an additional dynamic pressure drop, as the inflowing fluid enters a region with no velocity (cf. Chapter 3.3.3). Compared to the reference storage, the proto-

type shows a higher pressure drop in the relevant volume flow range of 0–65 l h^{-1} (Figure 5.11).

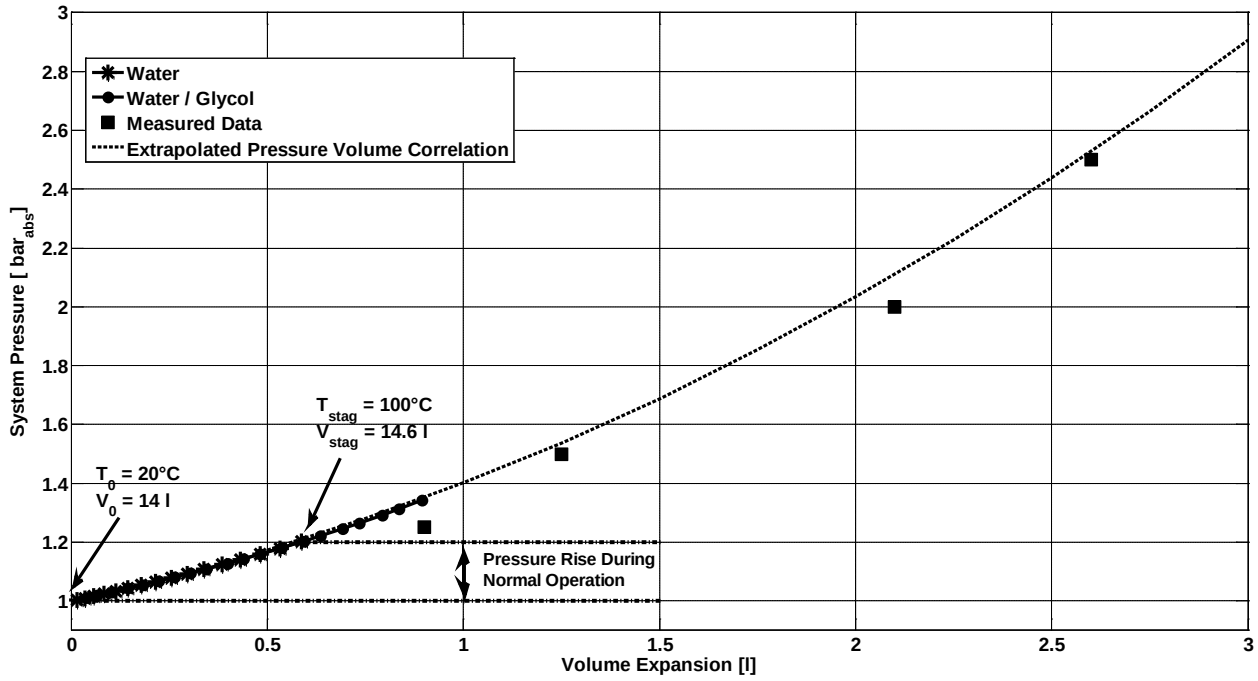

Figure 5.10: Pressure Volume Expansion Characteristics of the Storage Tank

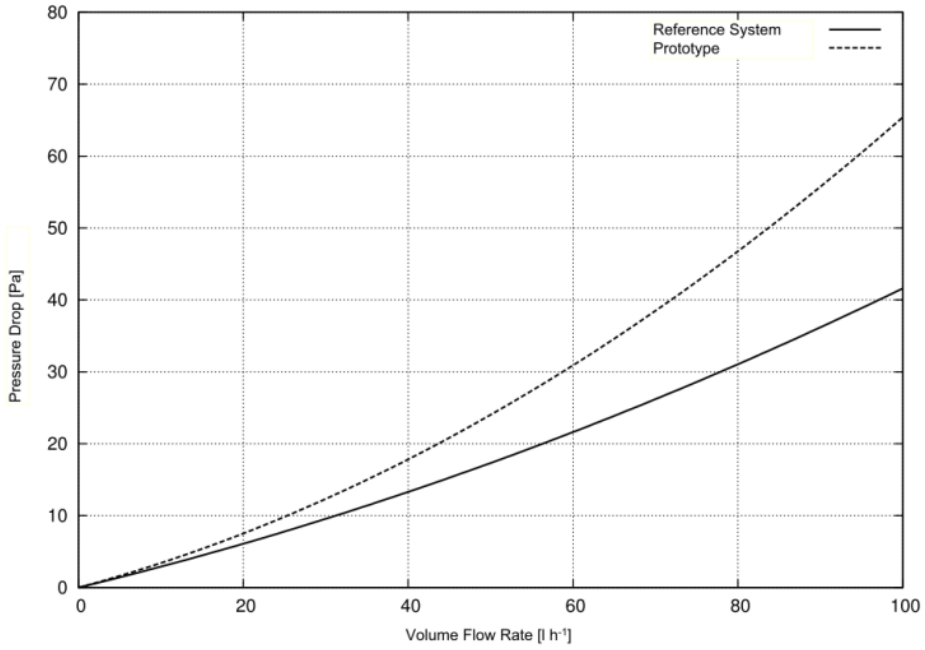

Figure 5.11: Pressure Drop of Prototype and Reference Storage Tank

From this background a detailed analysis of the expansion vessel design shows related optimisation possibilities resulting in a lower overall pressure drop. In prototype genera-

tion 2 the fluid will not be piped through the expansion vessel, but is only hydraulically connected through a tee branch as can be seen in Figure 5.12.

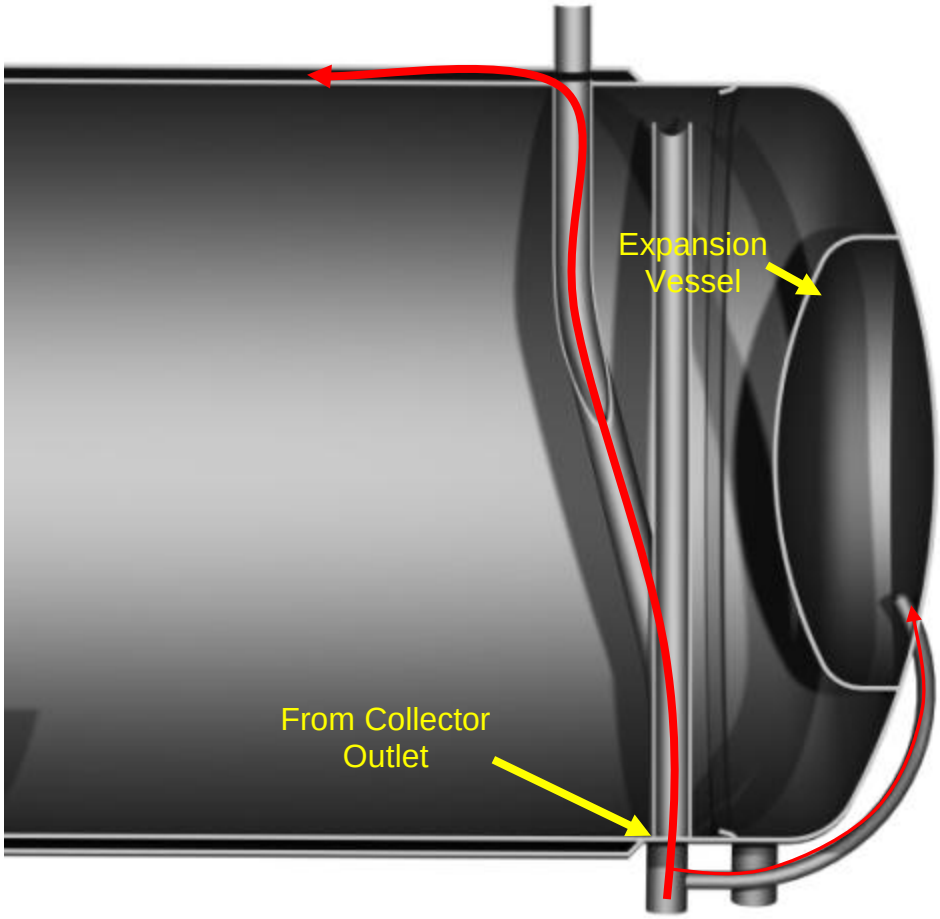

Figure 5.12: Expansion Vessel Integrated within the Storage Tank (Prototype Generation 2)

The second measurement cycle within the storage tank tests is carried out to improve the hot water draw-off quality in terms of available unmixed hot water. The test procedure is analogous to the mixing tests described in ISO 9459–2 (1995). By using the double mantle heat exchanger, the water inside the storage tank is heated up to a uniform temperature of 65–67 °C. During the heating up period the hot water volume is mixed using a pump. At the desired temperature, the heat supply is stopped and the draw-off is started. The parameters for the draw-off are a constant cold water temperature ranging from 17–20 °C and a flow rate of 600±50 l h^{-1}. The (hot) heat exchanger remains filled during the draw-off.

An ideal storage tank is able to deliver all its volume of hot water at a constant temperature before directly switching from hot water to cold water temperature. In a real storage tank mixing effects take place lowering the delivered amount of usable hot water. These mixing effects and therefore the hot water quality are strongly dependent on the water inlet design. A well-designed inlet stratifies the entering cold water at the storage tank bottom and additionally prevents the entering cold water from mixing with the hot water. During the tests, the storage tank is considered to be unmixed as long as the hot water temperature does not drop by more than 2 K. For the comparability of different storage tanks with different volumes, the draw-off is normalised in times the water volume as to be seen in Figure 5.13.

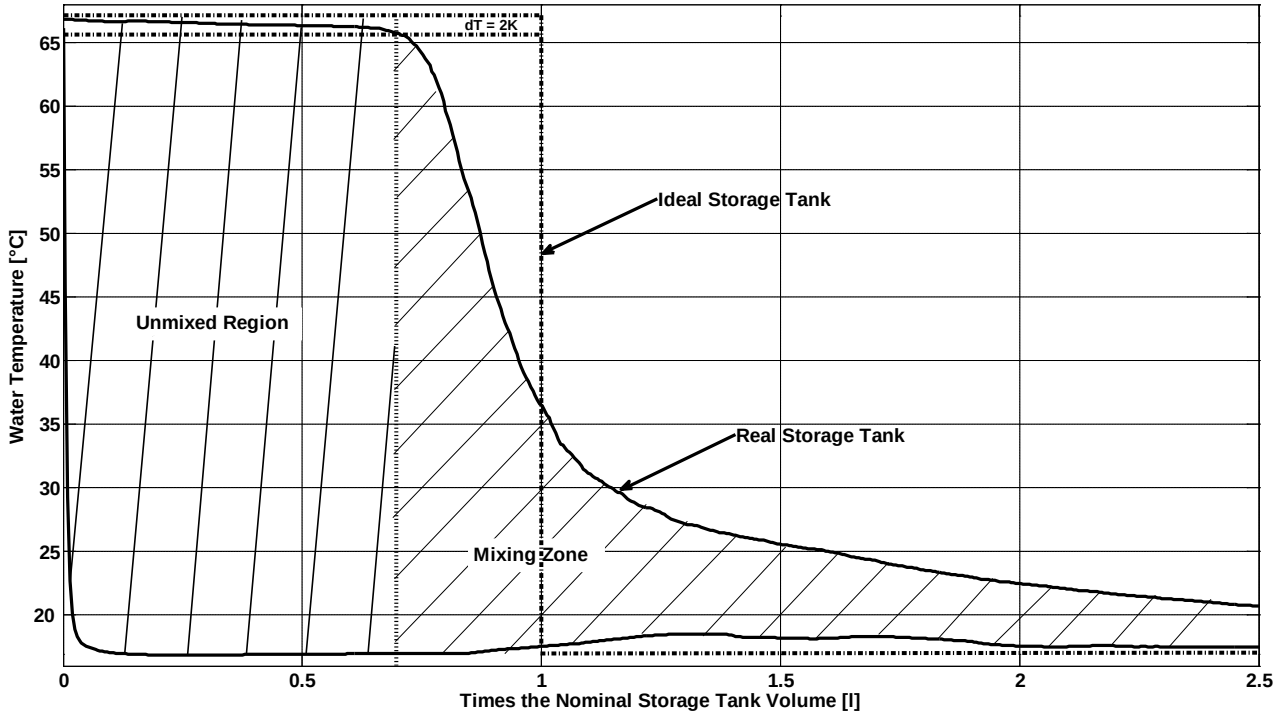

Figure 5.13: Differentiation of an Ideal and a Real Storage Tank

A benchmark of thermosyphon system storage tanks with a nominal volume in the range of 150–180 l tested at Ingolstadt University showed that especially low cost systems were only able to deliver 0.4–0.6 times their storage tank volume before the mixing zone starts. Well engineered systems were able to deliver more than 0.7 times the storage tank volume. The reference storage tank uses a die casted inlet diffuser which enhances the draw-off volume to 0.95.

A detailed investigation of the reasons for the reduced draw-off efficiency of some storage tank designs was carried out and will briefly be discussed.

In one of the storage tanks tested the cold water was distributed by a ½" inlet pipe without flow distributor. The small pipe diameter caused a high fluid velocity (and Reynolds number) at the draw-off rate of 600 l h^{-1} and thus mixing of the cold inlet jet with the hot water inside the storage tank occurred (Table 5.1).

Table 5.1: Reynolds Number and Fluid Velocity of Water at 600 l h^{-1} and 20 °C Water Temperature

D_{inner}	Re [-]	v [m s^{-1}]
1"	8,330	0.33
3/4"	11,110	0.59
1/2"	16,660	1.32

The rest of the storage tanks employed small and simple baffle plates which were not able to compete with the reference storage tank at the given flow rate of 600 l h^{-1} (Figure 5.14). This measured performance is in good accordance to findings by Shah and Furbo (2003) where three different inlet designs — no baffle plate, a small hemispherical baffle plate and a big baffle plate — were compared.

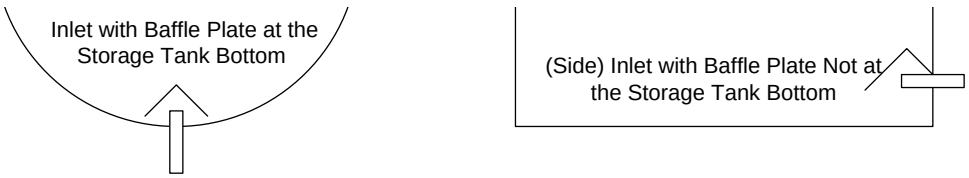

Figure 5.14: Baffle Plates Used in the Storage Tanks

Some storage tanks have a high length to diameter ratio of more than L/D = 3.0, so the vertical thermocline is more likely to be destroyed during drawing hot water off compared to the lower L/D = 1.7 ratio applied in the prototype (Figure 5.15).

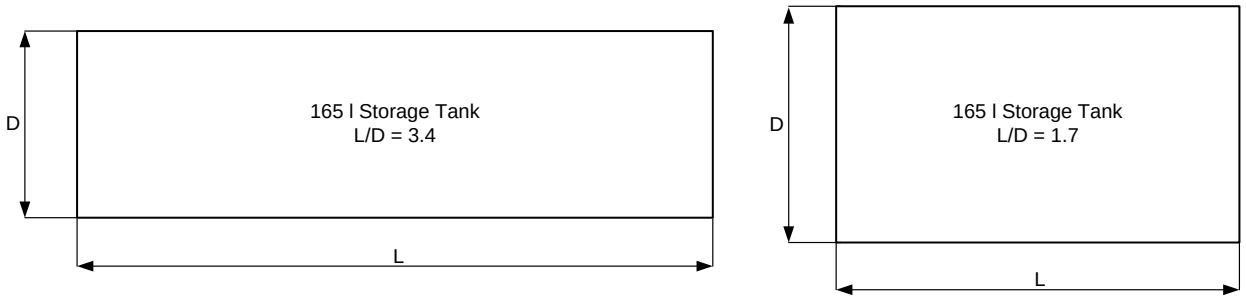

Figure 5.15: Storage Tank Length to Diameter Ratio

The distance between cold water inlet and hot water outlet in some cases is very close. This causes regions in the storage tank separated from the main flow (Figure 5.16).

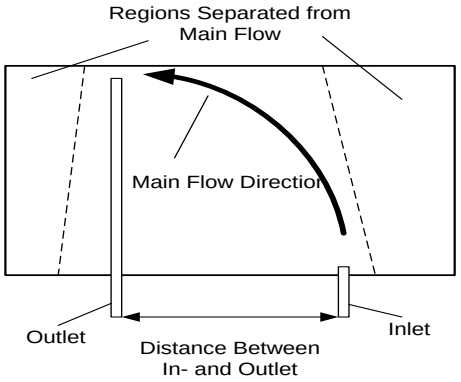

Figure 5.16: Distance Between In- and Outlet

A further reason for a low normalized draw-off volume is the height of the hot water draw-off pipe or distributor. The higher it is located, the higher the usable hot water volume is.

The findings of the benchmark tests were applied to the prototype design in order to achieve a normalised draw-off volume of more than 0.9 by using a simple, low-cost diffuser shape consisting of market available prefabricated parts.

Four tests were carried out. The first test was done completely without a diffuser. Mixing inside the storage tank took place after 0.74 times the storage tank volume. This basically good performance can be explained by the outcomes of previous tests. The prototype storage tank has in- and outlet diameters of 1” located as close as possible to the storage tank head. The hot water draw-off lance implemented and piped through the storage tank ensures that the hot water was taken at the top of the annulus.

For the second test a diffuser with equally distributed boreholes at its side was used (Table 5.2). This diffuser improved the usable hot water amount to 0.91 times the storage tank volume. However the boreholes at the side distributed the cold water at 60 mm (12 %) height from the storage tank bottom.

In test three and four a slotted and a wedged diffuser with the opening at the bottom designed on the basis of Hegazy (2007, cf. Chapter 2.2.3) were used. Both diffuser types improved the hot water availability to 0.96 (cf. Table 5.2). The cold water was distributed at 10 mm (2 %) height.

Figure 5.17 presents the measurement data of the slotted diffuser. The area between cold water and hot water curve represents the energy draw-off during the test. This area was bigger than that of an ideal storage tank as the test was carried out with the double mantle filled with hot water. This water was an additional heat source for the tap water inside the storage tank, theoretically allowing the storage tank to perform better than an ideal storage.

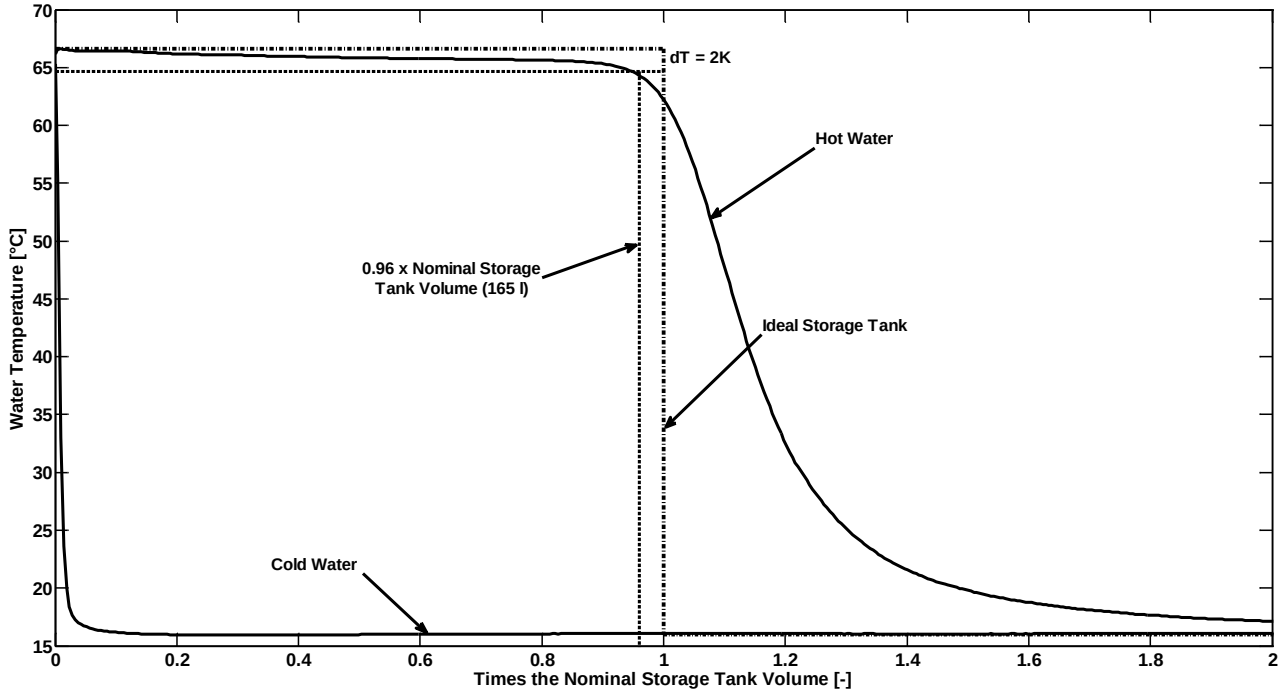

Figure 5.17: Draw-off Curve Using the Slotted Diffuser

In terms of production the slotted diffuser offers one main advantage compared to the wedged and “borehole” diffuser, as the opening is produced in only one work step with a

single tool, and will be implemented in prototype generation 2. Table 5.2 summarises the diffuser tests.

Table 5.2: Tested Diffuser Shapes

Diffuser Type	**No Diffuser**	**Diffuser with Bore-holes**	**Slotted Diffuser**	**Wedged Diffuser**
Picture		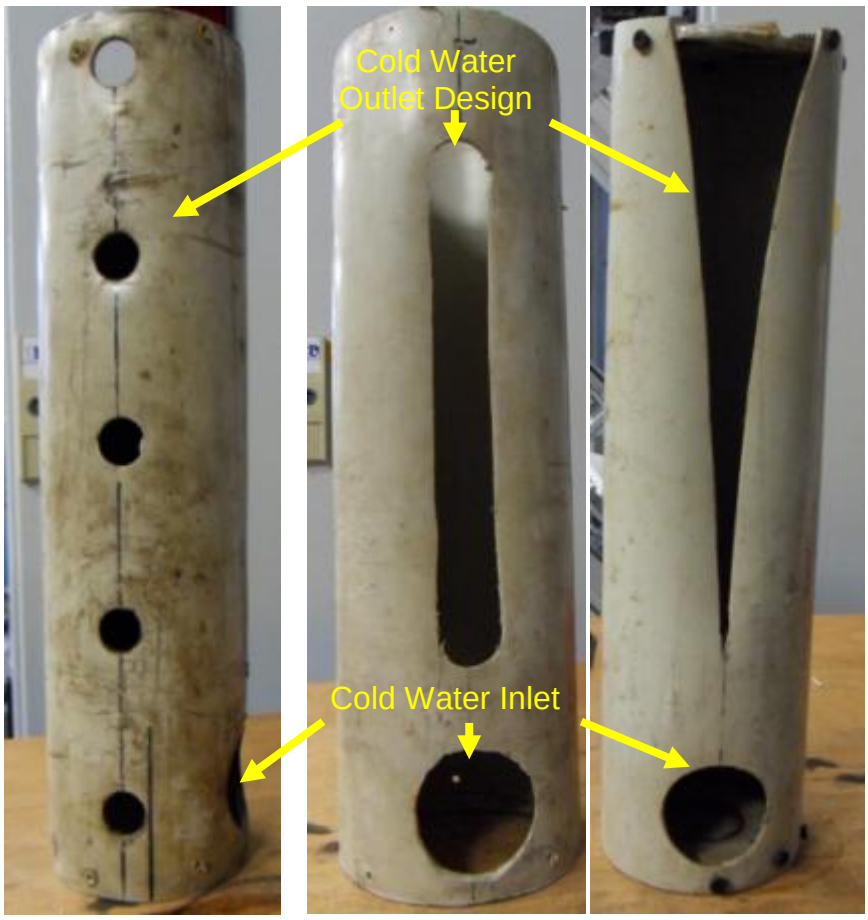		
Outlet Position	Vertical into the Tank	Outlet along the Side	Bottom Outlet	Bottom Outlet
Hot Water Ratio	0.74	0.91	0.96	0.96

The storage tank prototype was insulated with low expansion polyurethane foam. This foam did not offer the required insulation quality to determine realistic overnight losses of the storage tank and de-stratification effects as discussed in Chapter 2.2.3. Those tests have to be carried out with the prototype generation 2 which will be better insulated using high expansion polyurethane foam. The application of an enamel coating with low conductivity will also lower the effective vertical heat conductivity of the storage tank.

5.3 Experimental Optimisation of the Prototype

Within the thesis, the testing rig was enhanced with a process measuring and control technology device allowing fully automated test sequences. A simplified hydraulic scheme of the improved configuration can be seen in Figure 5.18.

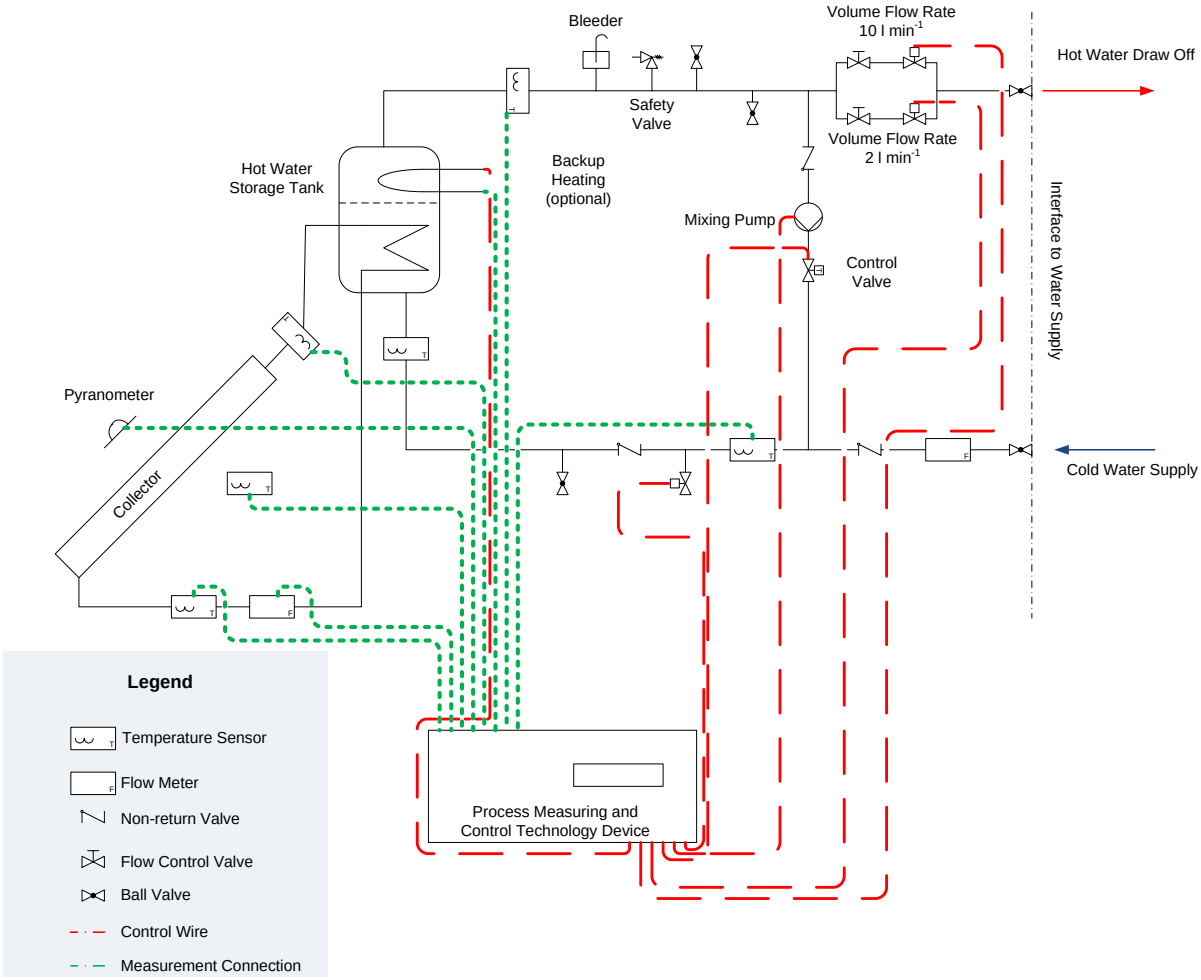

Figure 5.18: Hydraulic Scheme of the Testing Rig

The prototype thermosyphon system consisting of the collector and storage tank of prototype generation 1 was installed under a tilt angle of 35 ° in the testing rig to prove the interaction of the components (Figure 5.19).

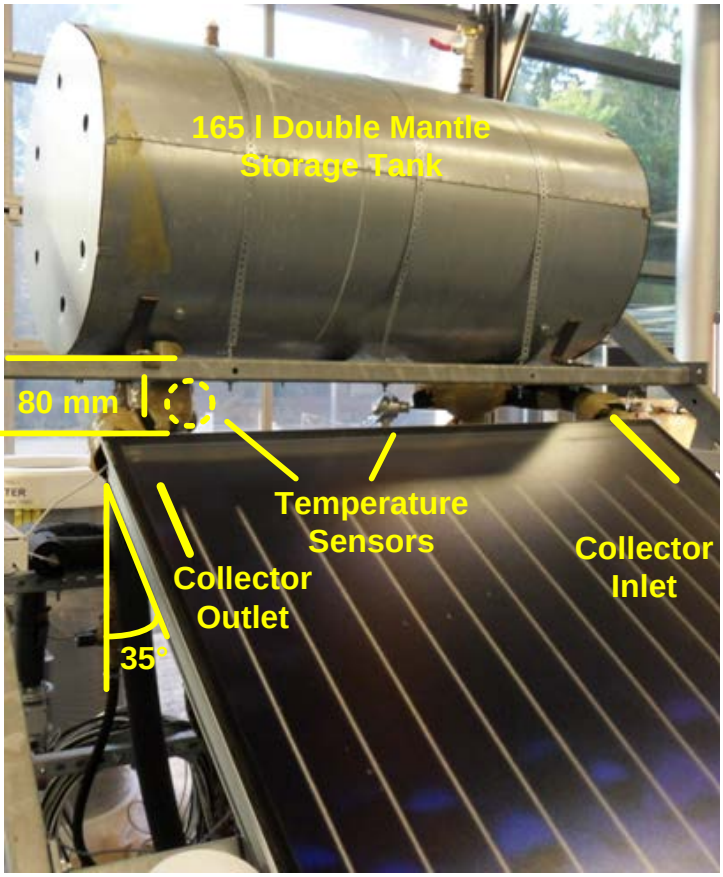

Figure 5.19: Thermosyphon Prototype (Generation 1) on the Testing Rig

The interconnecting pipes were temperature resistant hoses, but in the mass production system aluminium or stainless steel will be employed.

Two test days in conformity to ISO 9459–2 (1995) were collected and evaluated. A test sequence covers about 14.5 hours, including system preconditioning, heating up period, draw-off and data evaluation as illustrated in Figure 5.20. For a valid test day, the irradiation must not exceed a given range of 8–25 MJ m^{-2}.

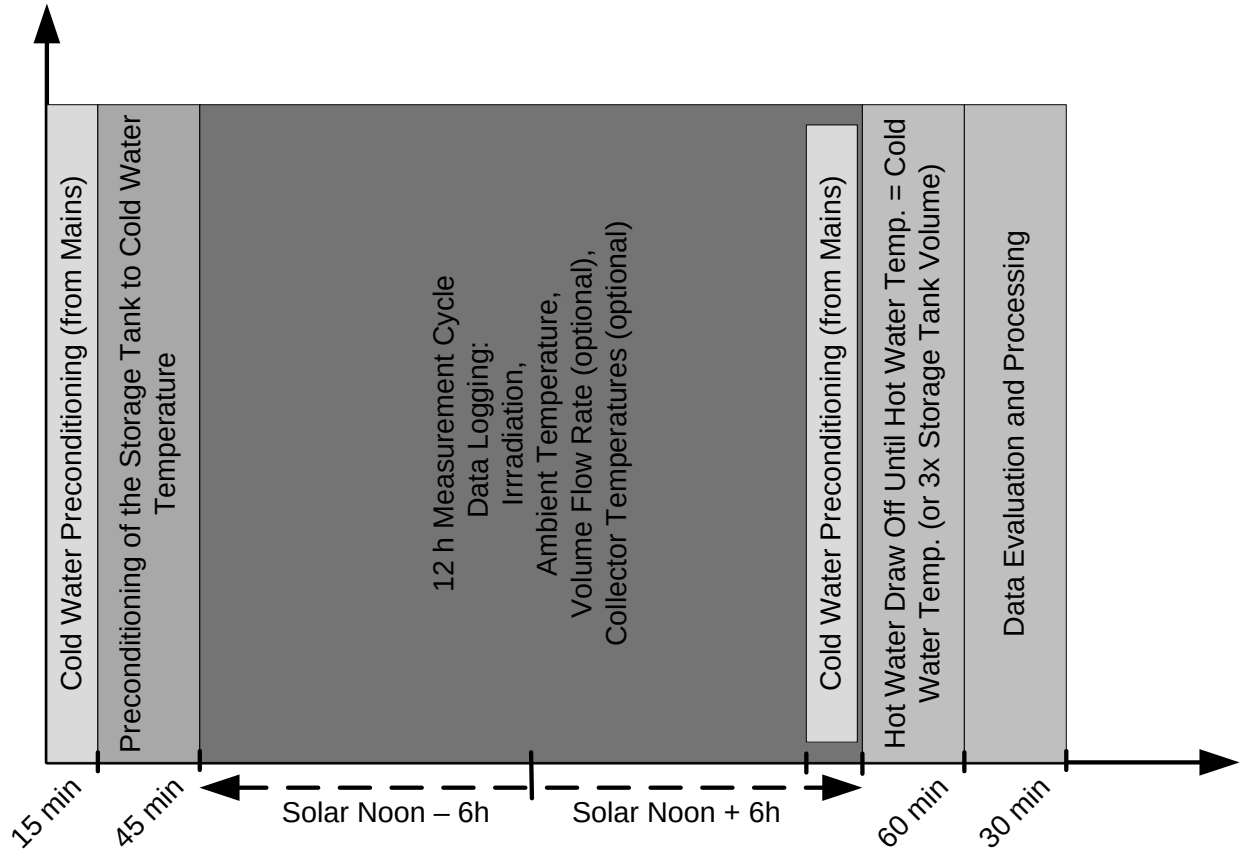

Figure 5.20: Course of Events of a Testing Day

Both test days were compared to similar test days recorded with the reference system. As a quality label, the ratio energy drawn-off Q compared to irradiance on the aperture area H* was chosen. Both, reference system and prototype system worked in the same bandwidth of Q/H* = 50–60 % as shown in Table 5.3. Other systems tested in Ingolstadt range from 35–45 %. This ratio was dependent on the ambient and the cold water temperature. In a full system test cycle consisting of at least 4 test days, this dependency is erased by a regression analysis. The results from the regression analysis are independent of the climatic conditions under which the system was tested, so the results are transferrable to any location worldwide. The system performance is represented by equation (2.3) introduced in Chapter 2.2.1.

Table 5.3: Useful Energy Gained by Reference and Prototype System

H [MJ m^{-2}]	H* [MJ]	Q [MJ]	Q/H* [-]	$T_{ambient, av}$ [°C]	$T_{cold\ water, av}$ [°C]
Reference System (Aperture Area 1.87 m²)					
23.0	43.0	22.1	**51.4 %**	17.1	18.0
24.9	46.6	28.4	**60.9 %**	21.5	20.2
Prototype System (Aperture Area 2.34 m²)					
22.7	53.1	30.7	**57.8 %**	22.3	21.9
24.3	56.9	32.5	**57.1 %**	18.9	20.2

In terms of hot water the prototype was able to deliver 150 l or 0.90 times of its volume hot water before the draw-off curve drops steeply (Figure 5.21). This value was in good accordance to the laboratory tests with a fully mixed storage tank resulting in 0.96 times the storage tank volume. However, the 2 K criterion applied in the laboratory tests was not applicable for the system tests as the storage tank had no uniform temperature due to stratification effects during the solar driven heating up period and the lack of mixing of the hot water beforehand to the draw-off.

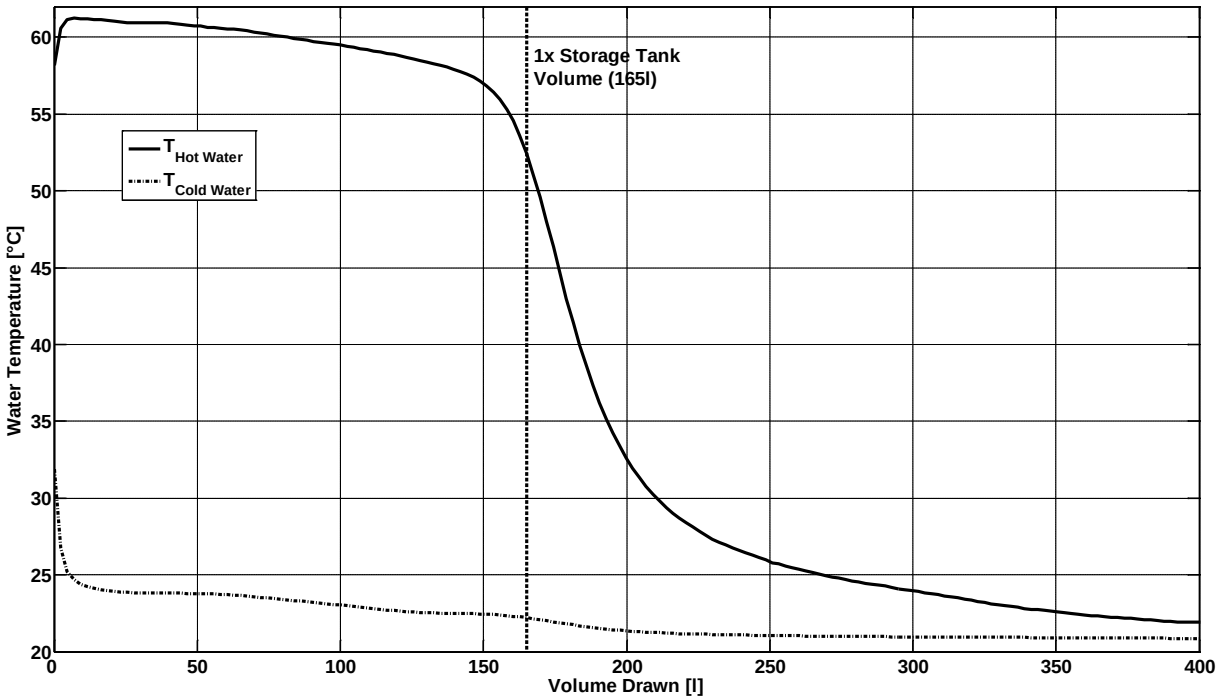

Figure 5.21: Draw-off Curve of the Prototype System

6 Conclusions and Outlook

The objective of the work described in this thesis was to develop an optimised thermosyphon solar hot water heater based on a detailed evaluation of the shortcomings of commercially-available thermosyphon systems. A realistic simulation model was developed, validated and used in a sensitivity analysis of the influences of major design variables. Input data of the simulation model focused on geometrical data and the material properties of the system and system parts. This allowed a direct link between the system design and the material selection on the system's annual efficiency. A further goal behind the sensitivity analysis was to show the dependency of the system layout on the geographic location investigated. The outcomes of the simulation and a literature review were transferred into a thermosyphon system prototype design. The prototype was constructed and subjected to laboratory testing. The outcomes of the research are discussed in more detail below.

6.1 System Layout

Various different system layouts — direct flow evacuated tube thermosyphon systems, evacuated tube heat pipe thermosyphon systems, direct flow flat-plate collector systems and two circuit flat-plate collector systems — were reviewed and discussed in this thesis. In terms of durability, freeze resistance and payback time, systems using flat-plate collectors, double mantle heat exchanger storage tanks and a liquid heat carrier fluid were found to offer the most promising basis for the research.

To ensure a high hot water availability in times of adverse weather a solar preheat system setup with an external continuous flow heater was pursued. A heating element inside the storage tank was found to lower the annual solar fraction.

The night-time performance of thermosyphon systems was found to be dominated by heat losses to the surroundings, by reverse thermosyphoning and by a loss of the thermocline inside the storage tank caused by the conductivity of the tank's wall material. To avoid reverse thermosyphoning two different approaches were considered. The first approach, which was not followed up, was to include non-return valves into the collector circuit. The reason for this decision is based on the unknown long-term stability of this

measure. The other way was to adjust the tank and the collector inlet/outlet co-locations, which avoids a thermal imbalance inside the thermosyphon system during the cooling down phase. Thus, the system is prevented from reverse flow and the related additional heat losses.

The available amount of hot water was found to be dominated by mixing of the hot water with the incoming cold supply from mains. Several different approaches to avoid mixing and to position cold water inlet and hot water outlet were found in literature. The idea of a cold water diffuser and a water draw-off lance were examined as this solution offered a good performance combined with simplicity in design.

Different collector absorber designs — harp, meander and volumetric absorbers — for thermosyphon systems were discussed in brief. Compared to copper, aluminium alloys can effect a noticeable cost reduction potential in the range of 60 %. Aluminium was used for collector hydraulics of pumped systems in the past, but disappeared from the market as corrosion problems — inside the fluid channels and at the selective coating — arose. Aluminium alloys however have been investigated further and long term stable selective coatings have been developed by research institutes and industry. Nowadays, aluminium alloys out of the [3xxx] family are available for solar thermal piping. The use of a mix-installation of copper, zinc and aluminium was found to be critical for the expected durability. However, thermosyphon systems are normally sold as full packages; this allowed a matching material selection to be proposed in this thesis — aluminium in combination with mild steel and stainless steel and the use of a solar fluid containing aluminium corrosion inhibitors.

6.2 System Simulation

Based on a reference system tested in Ingolstadt, a simulation model was built up and validated in this thesis. The simulation environment chosen was MATLAB /SIMULINK and the extension CARNOT. CARNOT is a block-based simulation open source library focused on building energy systems. Within the model development, CARNOT was extended by a new one-dimensional double mantle heat exchanger storage tank model. One-dimensional models were found to offer sufficient simulation results for long term performance predictions. The double mantle model is a further development of the

TRNSYS double mantle heat exchanger storage tank model developed by Andrés and Lopéz (2002) and the simple hot water storage tank model included in CARNOT (Hafner et al., 1999). Such models use computational constructs to describe the loss of stratification inside the storage tank. For this model, the de-stratification was calculated by a mixing of the layers according to Klein et al. (1999). The model developed also allows varying the heat exchanger surface by setting the heat exchanger length as an exogenous input.

The model input data for the storage tank are geometrical data and material properties directly linking the system performance with the storage tank design. The storage tank model was validated using measurement data from the reference system tested at the university's testing rigs.

The storage tank model was intended to describe a solar pre-heat system with the heat exchanger inlet at the top of the heat exchanger and the heat exchanger outlet at the bottom of the storage tank, as found in the literature review. Therefore, a variation of the inlet height was not considered.

The collector model used in the simulation was a one-dimensional model based on a measured efficiency curve according to DIN EN 12975-2 (2006). Two-dimensional models were found to offer additional benefits for the design of solar collectors, as material properties and design parameters can be directly incorporated and evaluated. However, two-dimensional models require more knowledge about the physical processes inside the collector and additional computational power. For annual predictions, the accuracy of one-dimensional models was considered to be sufficient.

The wind speed and wind-dependent heat loss rates were chosen to be constant throughout day and year to allow a good comparability between the different locations simulated. Thus, additional convective heat losses lowering the annual solar fraction caused by windy and stormy weather were not modelled. Additionally, the wind-dependent heat losses differ at each location investigated and are also influenced by the installation site of the thermosyphon system, such as the front of a house or on a roof top.

The linear and quadratic collector pressure drop coefficients were treated as physically independent from one another. These parameters are normally obtained from laboratory tests by polynomial fitting of measurement data. Thus, the coefficients are related to the specific hydraulic design of the collector. The model, however, is able to accommodate any pressure drop curves.

Boiling of the heat transfer medium was not considered, as the system was simulated to work at a constant collector circuit pressure of 2 bar. This allowed temperatures of up to 120 °C in the collector circuit filled with water without boiling. The system pressure in a closed thermosyphon system differs throughout the day related to the temperature dependent fluid density but this effect was not accounted for in the simulation.

The system simulation was used to carry out a sensitivity analysis to find out the most significant design-driving factors, using a standard draw-off profile. This draw-off profile did not take holidays or days without hot water demand into account. For such days, technical measures like overheating protection valves, which keep the hot water temperature below 95 °C, have to be incorporated into the storage tank prototype.

Eighteen geometrical and physical parameters were investigated in a defined bandwidth under the climatic conditions of three different European locations — Ingolstadt, Rome and Malaga. Effective system design, however, was found to be nearly independent from the location. The dimensions of the system proposed differ from the state-of-the-art which has a 180 l storage tank and a 2 m² solar collector. The prototype collector area was enlarged to nearly 2.5 m², while the storage tank volume was scaled down to 165 l of hot water. The system was close-coupled with a collector tilt angle of 35 °. The thermosyphon system faced directly south. In combination with a thermostatic mixing valve, this combination increased the solar fraction from 70 % to 85 % for Malaga. This increased solar fraction lowers the auxiliary energy to cover 100 % of the annual hot water demand by about 400 kWh a^{-1} and therefore offers a useful contribution to the reduction of greenhouse gases.

The continuous flow heater was assumed to have an efficiency of η = 100 % — its transient behaviour was not taken into account. Inclusion of the dynamic working characteristics of real continuous flow-heaters will increase the auxiliary energy demand — depend-

ing on the type of heater used — for the hot water preparation and thus lower the achievable annual solar fraction. According to Recknagel et al. (2007), an electrical continuous flow heater has an efficiency of nearly 99 %, however requires a high power input. Simple gas-fired continuous flow heaters have a low efficiency of 16–49 %, although gas fired continuous flow heaters with electronic ignition have an efficiency of 84 %.

6.3 Thermosyphon System Prototype

Based on the outcomes of the literature review and the system simulation, a thermosyphon system prototype was designed and constructed. The absorber was entirely made out of aluminium, as aluminium offered essential advantages compared to copper or copper/aluminium to be used in a two-circuit thermosyphon system. In the past, the use of full aluminium absorbers was not possible as the systems were mainly single circuit systems. This thesis reopens the path towards 100 % aluminium absorbers in two-circuit thermosyphon systems.

Operating temperatures up to 80 °C are sufficient for thermosyphon systems, so the panel back insulation could be reduced to 30 mm. The resulting reduction of collector size and the material selection of aluminium produced a weight advantage of 25 % compared to a typical copper solar collector, hence easier collector handling during installation will be possible.

The collector return pipe was integrated into the collector casing at an average distance of 6 mm from the absorber sheet. This separation was necessary to avoid re-heating of the collector fluid before entering the diverting lower collector header. The thermal separation of pipe and absorber was validated in a collector test using the university's solar simulator. At typical operation temperatures, the heat losses from the return pipe to the collector casing were found to be small, hence no additional measures like insulating the return pipe were taken into consideration. For practical reasons, the inner diameter of the return pipe was at 16.4 mm, while 13 mm was indicated by the simulation.

In simulation and from experimental measurements, the absorber coating was found to require high absorption values of more than α = 95 % combined with a medium emission coefficient, such as black chrome, to achieve a high annual solar fraction in combination

with a reduced danger of overheating problems. For technical reasons, the prototype collector was produced with a highly selective coating.

The measured efficiency of the prototype collector was found to be comparable to that of modern flat-plate collectors. There was still potential towards a higher zero loss efficiency, as the welding quality of absorber and collector hydraulics at the welding line ends was poor. The collector efficiency curve derived from the collector tests was used as an input for the one-dimensional solar collector simulation model.

In an infrared test sequence, the flow distribution of the fluid when being pumped through the absorber was found to be inhomogeneous. During operation in a thermosyphon system, the flow is developed by buoyancy forces and thus an even flow distribution is more likely to develop (Chuawittayawuth and Kumar, 2002).

The overall performance of the prototype collector with its 12 riser pipes, however, showed a good potential for the use in a thermosyphon system.

The storage tank developed was of a double mantle configuration. Following on from the results of simulation, a collector to storage tank ratio of 65 l per square metre collector area was used. The storage tank was designed as a solar pre-heat thermosyphon system. The entrance of the collector fluid into the double mantle was located at the top of the annulus whereas the outlet was located at the storage tank bottom. An internal expansion vessel was included into the storage tank, to ensure a limited pressure rise during operation in the collector circuit. The use of an external expansion vessel was not followed up, as this solution implies additional installation effort and might be a source of errors occurring during installation by typically unskilled labour.

The working principle of the expansion vessel integrated within the hot water region of the storage tank was experimentally proved to keep the system pressure below the opening pressure of the safety valve required for the thermosyphon system in the university´s laboratory.

An analysis of the storage tank pressure drop revealed a higher pressure drop in the first prototype compared to that in the reference component. A closer look at the hydraulic design of the first prototype showed an improvement due to the hydraulic connection of

the expansion vessel, which have been taken into account for the design of the second prototype.

The main focus in the area of available hot water was to maintain thermal stratification during draw-off. For this reason, several cold water diffuser shapes were tested in combination with a hot water draw-off lance. A simple slotted diffuser made out of prefabricated parts was able to increase the unmixed volume to 0.96 of the tank volume, compared to a value of 0.74 without a diffuser. The performance of the prototype compared favourably to that of the reference storage tank. The reference system, however, used an expensive die casted diffuser shape. The work on the diffuser shape showed good potential for simple but effective geometries based on prefabricated parts, like standard pipes, which can easily be implemented into the storage tank.

From the tests performed with the prototype and further storage tank testing within this programme of research and the literature review, the following design guideline can be stated. The distance between the inlet and outlet should be maximised, while the length to diameter ratio should be kept below 2. The connecting pipes should have a diameter of 25 mm, combined with a hot water draw-off lance and a cold water diffuser having its opening as close as possible to the storage tank bottom.

The prototype storage tank was manually insulated using low density polyurethane foam which did not match the insulation quality of rigid high density polyurethane foam. Therefore tests on the nocturnal heat losses were not performed with the first storage tank prototype.

The inner mantle and the heat exchanger mantle were made out of mild steel for several reasons. Compared to copper or stainless steel, this material offers a sufficient strength at lower material costs. Regarding the degradation of the thermocline by heat conduction in the mantle material, mild steel outperforms copper by factor 8. Standard polymers with a low heat conductivity would perform better, but require large wall thicknesses up to 11 mm to work in a pressurised storage tank. Such a wall thickness, however, would work as an insulation against the heat flux from the double mantle heat exchanger, hence lower the overall system efficiency.

For aesthetic reasons and to achieve a low length to diameter ratio, the overall width of the storage tank was limited to the collector width and all connections were placed concealed from view at the storage tank bottom.

In autumn 2011, the interaction of storage tank and solar collector was successfully tested by carrying out single measurement days according to ISO 9459–2 (1995). The performance found exceeded that of many standard systems available on the market and compared favourably with that of the reference system. A full test cycle according to the given test standard would, however, be necessary to be able to eliminate the influence of cold water and ambient temperature on the system performance.

By applying further component improvements as described above, a practical system will be able to significantly outperform the reference system. However, before these improvements could be put into production some further tasks have to be done.

The storage tank and collector would have to be tested and evaluated according to the first test pre-series (first prototype) to show if the improvement measures which have been found during the laboratory tests can practically achieve the expected additional efficiency. Optional components like a combination of continuous flow heater and thermostatic mixing valve would have to be selected beforehand to the certification of the system at an accredited institute.

A system simulation model providing solar fraction forecasts at user-defined locations would need to be prepared. The simulation model would have to be reduced to a minimum of required input parameters, which will allow using the model for simple performance estimations by the manufacturers.

6.4 Recommendations for Further Investigations

The closed development cycle described in this thesis — analysis of thermosyphon systems in theory, transferring the mathematical model into simulation, validation of the simulation, design and construction of a prototype based on simulation results and the testing and improvement of the prototype —was demonstrated.

The developed and validated double mantle heat exchanger storage tank model as well as the thermosyphon system model provides researchers in the field of solar-thermal ap-

plications as well as manufacturers with the opportunity to easily adapt their thermosyphon systems to differing climatic conditions and customers´ demands.

In order to optimise the accuracy and the significance of the system simulation, the following tasks are proposed to be investigated.

The introduction of a physical two-dimensional collector model would allow the simulation of solar collectors in thermosyphon systems to be based more on physical correlations, rather than measured efficiency curves. A comparison of the one- and two-dimensional collector models in terms of transient behaviour, annual system performance and computational effort would be a worthwhile task.

The collector pressure drop calculation, based on the hydraulic design and not measured pressure drop coefficients, should be implemented within the collector model. This allows a direct link between collector hydraulics and achievable solar fraction without the necessity of performing pressure drop tests beforehand to the simulation.

The influence of different cold water entrance models, like the plume entrainment approach (Kleinbach et al., 1993) into the one-dimensional storage tank model and their influence on the annual solar fraction could be investigated. Additionally the behaviour of the enhanced one-dimensional models could be compared to the result of a CFD simulation based on the same storage tank geometry to be able to balance additional accuracy with computational effort.

The storage tank model should be enhanced by a heat exchanger inlet height set by the user, in order to be able to determine the dependency of the system efficiency on the heat exchanger configuration.

Different water draw-off profiles and their influence on the annual solar fraction should also be analysed. The danger of overheating in times of zero hot water demand should be simulated to provide the basis for the selection of safety equipment for the thermosyphon system.

In order to provide more information on the prototype system performance, the following tasks are proposed.

The prototype collector suffered from a shear off between absorber plate and piping at the welding line ends, the collector efficiency curve should be re-tested on the solar simulator after optimising the welding quality, to ascertain the welding's influence on heat transfer and to gain data for more detailed simulation studies.

To quantify the measured thermal resistance between absorber plate and return pipe, the collector test should be carried out a second time with temperature sensors inside the flow and in the space between absorber plate and return pipe.

The flow distribution inside the absorber should be measured when the flow is driven by buoyancy. To illustrate the flow pattern, temperature sensors should be applied to the collector riser pipes and the system flow rate logged. The use of an infrared camera is not directly applicable, as the collector is glass-covered. The data collected should be compared to a CFD simulation on the collector's buoyancy driven flow distribution.

The heat losses of storage tank prototype generation 2 should be measured and evaluated. For this test, additional temperature sensors should be placed inside the storage tank to estimate the de-stratification effects caused by the storage tank wall conductivity. The prototype tests should be completed by a full system test according to ISO 9459–2 (1995).

As a basis for the development of overheating protection measures, such as temperature-driven valves inside the collector circuit, stagnation tests would have to be performed with the prototype system. The aim of such stagnation tests is to quantify the incidence of storage tank temperatures of more than 95 °C.

The long-term performance analysis of the developed thermosyphon system at different locations under real operating conditions is a further task that should be carried out. Data collected during these tests should be used as a basis for further simulation studies. The long-term performance tests should include an analysis of the corrosion resistance of the aluminium piping, which could be done by chemical analysis of the heat transfer fluid at regular intervals.

References

ADDLESEE, A.J. (1980) Frictional Resistance of Low Reynolds Number Flows Destabilized by Heat Transfer, *Letters in Heat and Mass Transfer*, 7, pp. 249-255.

ADUNKA, F. (1991) Handbuch der Wärmeverbrauchsmessung, 2nd ed., Vulkan Verlag, Essen.

ALIZADEH, S. (1999) An experimental and numerical study of thermal stratification in a korizontal cylindrical solar storage tank, *Solar Energy*, 76 (6), pp. 409-421.ö

AMBROSETTI, P. and KELLER, J. (1985) Das neue Bruttowärmeertragsmodell für verglaste Sonnenkollektoren, 2nd ed., Eidgenössisches Institut für Reaktorforschung, Würlingen (CH).

ANDOH A., et al. (2010) Thermal performance study of a solar collector using a natural vegetable fiber, coconut coir, as heat insulation, *Energy for Sustainable Development*, 14, pp. 297-301.

ANDRÉS, A. and LÓPEZ, J. (2002) TRNSYS model of a thermosiphon solar domestic water heater, Solar Energy, 72 (2), pp. 89–98.

ASKELAND, D.R. (1996) Materialwissenschaften: Grundlagen, Übungen, Lösungen (The science and engineering of materials), 1st ed., Spektrum Akademischer Verlag GmbH, Heidelberg, Berlin, Oxford.

BACCOUCHE, A (2011) Tunisia Solar Thermal Program Residential, Industrial and hotels sectors In: *World Sustainable Energy Days 2011, Proceedings, Wels Austria, March 2011.*

BANNEROT, R.B. Bannerot, et al. (1992) A Simple Device for Monitoring Flow Rates in Thermosyphon Water Heaters, *ASME Journal of Solar Energy Engineering*, 114, pp. 47-52.

BEITZ, W. and GROTE, K.-H. (1997) DUBBEL Taschenbuch für den Maschinenbau, 19th ed., Springer Verlag, Berlin.

BELESSIOTIS, V. and MATHIOULAKIS, E. (2002) Analytical Approach of Thermosyphon Solar Domestic Hot Water System Performance, *Solar Energy*, 72(4), pp. 307-315.

BELGIUM. EUROPEAN COMMISSION (1997) *Energy for the future: renewable sources of energy – White paper for a community strategy and action plan.*
Brussels: COM(97) 599.

BLISS, R. W. JR (1959) The derivations of several “Plate-efficiency factors” useful in the design of flat-plate solar heat collectors, *Solar Energy*, 3(4), pp. 55-64.

BOHL W. and ELMENDORF W. (2005) *Technische Strömungslehre*. 13th ed. Würzburg: Vogel Industrie Medien GmbH & Co. KG.

BRANDMAYR, S. (2006) Forschungsvorhaben Optimierte Thermosiphon-Solaranlage: Vorstudie und Projektplanung. Diploma Thesis, Ingolstadt University of Applied Sciences.

BRANDMAYR, S. and ZÖRNER, W. (2007) Thermosiphon Systems: Market, State-of-the-Art and Trends In: *3rd European Solar Thermal Energy Conference - estec2007 Proceedings, Freiburg, June 2007*. Freiburg: European Solar Thermal Industry Federation ESTIF, pp. 182-188.

BRANDMAYR, S. et al. (2008) Simulation of Thermosiphon Solar Hot Water Systems Using Matlab/Simulink and Carnot In: *Eurosun 2008 – 1st International Conference on Solar Heating, Cooling and Buildings, Proceedings*, *Lisbon, October 2008*. Lisbon: SPES – Sociedade Portuguesa de Energia Solar.

BURDIHARDJO, I., MORRISON, G.L. and BEHNIA M. (2002) Performance of a Water-in-Glass Evacuated Tube Solar Water Heater In: *ANZSES Annual Conference 2002*,Newcastle, November 2002. [ONLINE] Available at: http://www.solar1.mech.unsw.edu.au/glm/papers/Budihardjo3.pdf [Accessed 06. May 2008].

BURDIHARDJO, I., MORRISON, G.L. and BEHNIA M. (2003) Development of TRNSYS Models for Predicting the Performance of Water-in-Glass Evacuated Tube Solar Water Heaters in Australia In: *Destination Renewables – ANZSES 2003*, Melbourne, November 2003. [ONLINE] Available at: http://www.solar1.mech.unsw.edu.au/glm/papers/BUDIHARDJO6.pdf [Accessed 06. May 2008].

BURDIHARDJO, I., MORRISON, G.L. and BEHNIA M. (2007) Natural circulation flow through water-in-glass evacuated tube solar collectors, *Solar Energy*, 81 (12), pp. 1460-1472.

BURDIHARDJO, I. and MORRISON, G.L. (2009) Performance of water-in-glass evacuated tube solar water heaters, *Solar Energy*, 83 (1), pp. 49-56.

BUHRMANN (1983) Physics of selective surfaces, *Advances in Solar Energy – An annual review of research and development*, 3, pp. 207-280.

CADERNAS DE, M. (2012) New brazing technologies for aluminium direct flow absorbers and collectors. In: *SMEThermal 2012 Proceedings, Berlin, February 2012.*

CHEN, B.-R.; CHANG, Y.-W.; LEE, W.-S.; CHEN, S.-L. (2009) Long-term thermal performance of a two-phase thermosyphon solar water heater, *Solar Energy*, 83, pp. 1048-1055.

CHIEN, C.C et al.(2011) Theoretical and experimental investigations of a two-phase thermosyphon solar water heater, *Energy*, 36, pp. 415-423.

CHOW, T.-T. et al. (2011) Performance evaluation of evacuated tube solar domestic hot water systems in Hong Kong, *Energy and Buildings*, 43 (12), pp. 3467-3474.

CHUAWITTAYAWUTH, K. and KUMAR, S. (2002) Experimental investigation of temperature and flow distribution in a thermosyphon solar water heating system, Renewable Energy, 26 (3), pp. 431-448.

COLOR (N.N. 2009): Technische Informationen – SUNCOLOR TS S BLACK [Brochure], Firm Color, d.d., Ljubljana.

CÒNSUL, R. et al. (2004) Virtual prototyping of storage tanks by means of three-dimensional CFD and heat transfer numerical simulations, *Solar Energy*, 77, pp.179-191.

COOPER, P.I. and DUNKLE, R. V. (1981) A non-linear flat-plate collector model, *Solar Energy*, 26 (2), pp. 133-140.

DEUTSCHES INSTITUT FÜR NORMUNG (1995).*DIN V 4757-4:1995 Solarthermische Anlagen – Teil 4: Sonnenkollektoren; Bestimmung von Wirkungsgrad, Wärmekapazität und Druckabfall.* Beuth Verlag GmbH.

DEUTSCHES INSTITUT FÜR NORMUNG (2005). DIN 1055-4:2005 Einwirkungen auf Tragwerke – Teil 4: Windlasten. Beuth Verlag GmbH.

DEUTSCHES INSTITUT FÜR NORMUNG (2006). DIN EN 12975-2:2006 *Thermische Solaranlagen und ihre Bauteile – Kollektoren – Teil 2: Prüfverfahren.* Beuth Verlag GmbH.

DEUTSCHES INSTITUT FÜR NORMUNG (2006). DIN EN 12976-2:2006 *Thermische Solaranlagen und ihre Bauteile – Vorgefertigte Anlagen – Teil 1: Prüfverfahren.* Beuth Verlag GmbH.

DRÜCK, H. (2011) *Prüfbericht Wärmeleistung und Dauerhaftigkeit eines Sonnenkollektors 09COL873S/1* [Online]
Available at: http://www.itw.uni-stuttgart.de/abteilungen/tzs/tests/archiv/Tests2010s.pdf [Accessed 01. December 2011].

DRÜCK H. (2011) Solartechnik (Teil 1) – Manuskript zur Vorlesung, University of Stuttgart [Online] Available at: http://www.itw.uni-stuttgart.de/lehre/lehrveranstaltungen/Dokumente/solar1/solvo_teil1.pdf [Accessed: 16. May 2011].

DUFFIE, J.A. and BECKMAN, W.A. (2006) *Solar engineering of thermal processes.* 3rd ed. New York: John Wiley & Sons.

DUNKLE, R.V. and DAVEY, E.T. (1970) Flow distribution in solar absorber banks In: *International Solar Energy Society Conference*, Melbourne, March 1970.

EAMES, P.C. and NORTON, B. (1998) The effect of tank geometry on thermally stratified sensible heat storage subject to low Reynolds number flows, *International Journal of Heat Mass Transfer*, 41(14),pp. 2131-2142.

EICKER, U. (2001) Solare Technologien für Gebäude, 1st ed., Teubner GmbH, Stuttgart/Leipzig/Wiesbaden.

EISENMANN, W. (2003) Untersuchungen zu Leistungsfähigkeit und Materialaufwand von Sonnenkollektoren mit serpentinen- und harfenartiger Rohrverlegung. Düsseldorf: VDI Verlag.

EISENMANN W., VAJEN K., ACKERMANN, H. (2004) On the correlations between collector efficiency factor and material content of parallel flow flat-plate solar collectors, Solar Energy, 76(4), pp. 381-387.

ELLINGHAUS, T. (2007) Die Förderampel steht auf grün, Erneuerbare Energien, 17 (5), S. 66-76.

ELGETI, K. (2006) Wärmeverlust von Wänden und Rohrleitungen – 4 Bestimmung des Wärmeverlustes bei Wind In: 10th ed. Verein Deutscher Ingenieure, VDI-Gesellschaft Verfahrenstechnik und Chemieingenieurwesen (GVC) *VDI-Wärmeatlas*, Berlin & Heidelberg: Springer Verlag.

EPP, B. (2012) Panel Discussion Collector Production. In: *SMEThermal 2012 Proceedings, Berlin, February 2012.*

ESEN, M.; ESEN, H. (2005): Experimental investigation of a two-phase closed thermosyphon solar water heater, Solar *Energy*, 79, pp. 459-468.

EUROPEAN SOLAR THERMAL INDUSTRY FEDERATION (2005) *Solar thermal markets in Europe (trends and market statistics 2004),* Brussels: European Solar Thermal Industry Federation.

EUROPEAN SOLAR THERMAL INDUSTRY FEDERATION (2006) *Solar thermal markets in Europe (trends and market statistics 2005),* Brussels: European Solar Thermal Industry Federation.

EUROPEAN SOLAR THERMAL INDUSTRY FEDERATION (2007a) *Solar thermal markets in Europe (trends and market statistics 2006),* Brussels: European Solar Thermal Industry Federation.

EUROPEAN SOLAR THERMAL INDUSTRY FEDERATION (2007b) Key Issues for Renewable Heat in Europe (K4RES-H) – Setting verifiable targets for Solar Thermal – WP3, Task 3.1*,* [pdf] Brussels: European Solar Thermal Industry Federation.
Available at:
www.erec.org/fileadmin/erec_docs/Projcet_Documents/K4_RES-H/D3_EGEC.pdf
[Accessed 1 May 2009].

EUROPEAN SOLAR THERMAL INDUSTRY FEDERATION (2008) *Solar thermal markets in Europe (trends and market statistics 2007),* Brussels: European Solar Thermal Industry Federation.

EUROPEAN SOLAR THERMAL INDUSTRY FEDERATION (2009) *Solar thermal markets in Europe (trends and market statistics 2008),* Brussels: European Solar Thermal Industry Federation.

EUROPEAN SOLAR THERMAL INDUSTRY FEDERATION (2010) *Solar thermal markets in Europe (trends and market statistics 2009),* Brussels: European Solar Thermal Industry Federation.

EUROPEAN SOLAR THERMAL INDUSTRY FEDERATION (2011) *Solar thermal markets in Europe (trends and market statistics 2010),* Brussels: European Solar Thermal Industry Federation.

FAWER, M. and MAGYAR, B. (2009) *Solar industry – The first green shoots of recovery, Basel: Sarasin Bank*. [Online] Available at: http://www.sarasin.ch/internet/iech/index_iech/private_clients_iech/private_clients_sustainability_iech/en/solarstudie_2009.pdf [Accessed: 27 April 2012].

FLÜCKINGER, F. (2007) Qualitäts-Zertifikat Solarglas NANJ0711100SGZ [Online] Available at: http://www.solarenergy.ch/publ/komponenten/NANJ0711100SGZ.pdf [Accessed: 14. May 2009].

FRANKE, R. (1997) Object-oriented modelling of solar heating systems, Solar Energy, 60, pp. 171-180.

FREI, U. (1998) Kollektoren in Solarthermischen Systemen, In: 1998 TRISOLAR. Bregenz, Austria 5-7 February 1998
Available at: http://www.solarenergy.ch/publ/kollektoren/trisolar.pdf
[Accessed: 5 January 2009].

FREI, U. (2012) Antireflective Coated Glass for Thermal Collectors pros, cons and risks. 3rd *SMEThermal Solar Thermal Materials, Equipment and Technology Conference , Berlin , 2012*.

FREY, R., FREI, U., BRUNOLD, S. (1998) *Bestimmung des Kollektorwirkungsgradfaktors F‘ an flüssigkeitsführenden Solarabsorbern* [Online]
Available at: http://www.solarenergy.ch/publ/kollektoren/fstrich.pdf
[Accessed: 4 October 2008].

FURBO, S. and SHAH, J. L. (2003) Thermal advantages for solar heating systems with a glass cover with antireflection surfaces, *Solar Energy*, 74, pp. 513-524.

GERMAN – TUNISIAN CHAMBER OF COMMERCE AND INDUSTRY (2005) *Solarenergie in Tunesien – Exportinitiative Erneuerbare Energien*, Tunis.

GIECK, K. and GIECK, R. (1995) *Technische Formelsammlung.* 30th ed. Germering: Gieck Verlag.

GMÜR, M (2002) *Thermosiphon-Kollektorsystem für den Spanischen Markt*, Diploma thesis, Rapperswil: Hochschule für Technik
Abstract available at: http://www.hsr.ch/uploads/tx_icscrm/m_da_2002_gmuer_markus.pdf
[Accessed: 12 September 2008].

GOMBERT, A. et al. (1997) Glazing with very high solar transmittance, *Solar Energy*, 62 (3), pp. 177-188.

GOSWAMI, D.Y.; KREITH, F. and KREIDER J.F. (2000) *Principles of Solar Engineering.* 2nd ed., Taylor & Francis, Philadelphia.

GUPTA C.L. and GARG H.P. (1968) System design in solar water heaters with natural circulation, *Solar Energy*, 12, pp. 163-182.

HAFNER, B., PLETTNER, J., WEMHÖNER, C. (1999) CARNOT Blockset: Conventional And Renewable eNergy systems OpTimization Blockset – User's Guide, Solar-Institut Jülich, University of Applied Sciences Aachen.

HAHNE, E. (1998) *Prüfbericht Kollektortest 98COL133* [Online] Available at: http://www.itw.uni-stuttgart.de/abteilungen/tzs/PDF-Pruefberichte/98col133.pdf [Accessed 01. September 2009].

HAHNE, E. (2000) The ITW solar heating system: An oldtimer fully in action, *Solar Energy*, 69 (6), pp. 469-493.

HEGAZY, A. and DIAB, M. (2002) Performance of an improved design for storage-type domestic electrical water-heaters, *Applied Energy*, 71, pp. 287-306.

HEGAZY, A. (2007) Effect of inlet design on the performance of storage-type domestic electrical water heater, *Applied Energy*, 84, pp. 1338-1355.

HERMANN, M. (2005) *Bionische Ansätze zur Entwicklung energieeffizienter Fluidsysteme für den Wärmetransport. .* Ph. D. Universität Karlsruhe.

HOBSON, P.A. and NORTON, B. (1988) Verified Accurate Performance Simulation Model of Direct Thermosyphon Solar Energy Water Heaters, *ASME Journal Solar Energy Engineering*, 110, pp. 282-292.

HOBSON, P.A. and NORTON, B. (1989) A design nomogram for direct thermosyphon solar-energy water heaters, *Solar Energy*, 43 (2), pp.85-95.

HOLCK, O. et al. (2003) Solar collector design with respect to moisture problems, *Solar Energy*, 75, pp. 269-276.

HOLLE, A. (2011) Are aluminium absorbers market-ready? In: *SMEThermal 2011 Proceedings, Berlin, February 2011.*

HUANG J. et al. (2010) Experimental investigation on thermal performance of thermosyphon flat-plate solar water heater with a mantle heat exchanger, *Energy,* 35, pp. 3563-3568.

HUSSEIN, H.M.S (2003) Optimization of a natural circulation two phase closed thermosyphon flat plate solar water heater, *Energy Conversion and Management*, 44, pp. 2341-2352.

HYDRO (N.N. 2010) HyLife™ Solar high temperature corrosion tests report. [Online] Available at: http://www.hydro.com/pagefiles/8185071/HyLife%C2%AESolar%20Cyclic%20high%20temperature%20corrosion%20tests%20short%20report-v4.pdf [Accessed: 4 October 2011].

HYDRO (N.N. 2012) We make solar shine with aluminium! [Brochure], Hydro Aluminium Precision Tubing Tonder, d.d., Tonder (DK).

IWATA, H., MORIE, A., MASUDA, T. (1980) Development of a thermosyphon solar water-heater, *Technical Report of the Matushita Electric Works Ltd.,* 20, pp. 43-49.

ISAKSON, P. (1991) Matched Flow Solar Collector Model for TRNSYS. In: TRNSYS Users and Programmer's Manual, Solar Energy Laboratory, University of Wisconsin-Madison.

ISO (1995). In *Standard 9459–2. Test Methods for Solar Collectors – Part 2: Outdoor Test Methods for System Performance Characterization and Yearly Performance Prediction of Solar-only Systems*, ISO, Switzerland.

ISO (1994) In *Standard 9806–1 Test methods for solar collectors – Part 1: Thermal performance of glazed liquid heating collectors including pressure drop*, ISO, Switzerland.

ISO (1999) In *Standard 9488 Sonnenenergie - Vokabular*, ISO, Switzerland.

JORGENSEN G. et al. (2005) Durability of Polymeric Glazing and Absorber Materials. In: *2005 DOE Solar Energy Technologies*. Denver (Colorado), United States of America 7-10 November 2005
Available at: http://www.osti.gov/bridge/product.biblio.jsp?query_id=1&page=0&osti_id=882609 [Accessed: 18 December 2008].

KALOGIROU, A (2004) Solar thermal collectors and applications, *Progress in Energy and Combustion Science*, 30, pp. 231-295.

KAMMER, C. (2009) *Aluminium Taschenbücher Band 1-3*, 16th ed., Aluminium-Verlag Marketing & Kommunikation GmbH, Düsseldorf.

KARAGHOULI, A.A. and ALNASER, W.E. (2001) Experimental study on thermosyphon solar water heater in Bahrain, *Renewable Energy*, 24, pp. 389-396.

KAST, W. (2006) Druckverlust in Leitungen mit Querschnittsänderungen- 5.1 Rohrbögen In: 10th ed. Verein Deutscher Ingenieure, VDI-Gesellschaft Verfahrenstechnik und Chemieingenieurwesen (GVC) *VDI-Wärmeatlas*, Berlin & Heidelberg: Springer Verlag.

KIKAS N.P. (1995) Laminar Flow Distribution In Solar Systems, *Solar Energy*, 554 (4), pp.209-217.

KHARTCHENKO, N. (2004) Thermische Solaranlagen. 2nd ed. VWF, Berlin.

KHALIFA, A.-J. N.; MEHDI, M.M. (1998) On the verification of a hydrogen bubble flow meter used for monitoring flow rates in thermosyphon solar water heaters, *Energy Conversion & Management*, 39 (12), pp. 1295-1302.

KHALIFA, A.-J. N.; MEHDI, M.M. (1999) On the verification of one dimensional heat flow in a horizontal thermosyphon storage tank, *Energy Conversion & Management*, 40, pp. 961-974.

KLEIN, S. A. et al. (1997) *TRNSYS, a Transient System Simulation Program. User' s Manual (version 14.2)*, Solar Energy Laboratory, University of Wisconsin–Madison.

KLEINBACH, E.M.; BECKMANN, W.A. and KLEIN, S.A. (1993) Performance study of one-dimensional models for stratified thermal storage tanks, *Solar Energy*, 50, pp. 155-166.

KNEER, R. (2007) Vorlesung Wärme- und Stoffübertragung*, Lecture Notes University of Aachen* [Online]. Available at: http://www.wsa.rwth-aachen.de/uploads/tx_lnetfiles/Skript_WSUE_Kapitel1_Einleitung_2009-01-20.pdf [Accessed: 12. May 2009].

KONRAD, M. (2008) *Weiterentwicklung der Simulationsumgebung Matlab/Simulink - Carnot: Modellieren, Programmieren und Validieren eines Doppelmantel-Warmwasserspeichers für Thermosiphon-Solaranlagen*. Bachelor Thesis, Ingolstadt University of Applied Sciences (unpublished).

KÖHL, M. et al. (1989) Accelerated ageing test procedures for selective absorber coatings including lifetime estimation and comparison with outdoor test results, *Solar Energy Materials*, 19, pp. 257-313,

KÖHL, M.; KÜBLER, V. and HECK, M. (2007) Optimisation of the micro-climate in solar collectors, *Solar Energy Materials & Solar Cells*, 91, pp. 721-726.

LANGHAAR, H.L. (1942) Steady Flow in the Transition Length of a Straight Tube, *Journal of Applied Mechanics*, pp.55-58.

LAVAN, Z. and THOMPSON, J. (1977) Experimental study of thermally stratified hot water storage tanks, *Solar Energy*, 19, pp. 519-524.

MANGOLD, D. (1996) Kostenanalyse der Herstellung von Solarkollektoren und mögliche Kostenreduktionen durch Massenfertigung, In: Proceedings *6. Symposium Thermische Solarenergie, Bad Staffelstein (Germany)*, May 1996, p. 330 – 334.

MANNHART, M. (2006) Hydromechanik – Skriptum zur Vorlesung im Wintersemester 2006/2007, Technical University of Munich (Lecture Notes).

MAUTHNER, F. and WEISS, W. (2011) *IEA SHC Report: Solar Heat Worldwide 2009, Edition 2011* [Online]. Available at: http://www.aee-intec.at/0uploads/dateien757.pdf [Accessed: 12 December 2011]

MEYER, J:-P. (2011) Kleben statt Clinchen, *Sonne Wind & Wärme*, (04), pp. 76-90.

MEYER, J.-P. (2010) Optimism predominates. *Sun &Wind Energy*, (06), pp. 42-61.

MEYER, J:-P. (2009) Blau, geschlossen, sicher, *Sonne Wind & Wärme*, (04), pp. 94-101.

MICHAELIDIS, I and WILSON, D. (1996) Simulation studies of the position of the auxiliary heater in thermosyphon solar water heating systems, *Renewable Energy*, 10 (1), pp. 35-42.

MORRISON, G.L. and RANATUNGA, D.B.J. (1980) Transient response of thermosyphon solar collectors, *Solar Energy*, 24, pp. 55-61.

MORRISON, G.L. and RANATUNGA, D. (1980) Thermosyphon circulation in solar collectors, *Solar Energy*, 24, pp. 191–198.

MORRISON, G.L. and BRAUN, J.E. (1985) System Modelling and Operation Characteristics of Thermosyphon Solar Water Heaters, *Solar Energy*, 34 (4), pp. 389-405.

MORRISON G.L. et al. (1998) Analysis of horizontal mantle heat exchangers in solar water heating systems, *Solar Energy*,*64 (1-3)*,pp. *19-31.*

MORRISON, G.L., ROSENGARTEN G. And BEHNIA M. (1999) Mantle Heat Exchangers for Horizontal Tank Thermosyphon Solar Water Heaters, *Solar Energy*, 67 (1), pp. 53-64.

MORRISON, G. L. (2001) Solar water heating In: GORDON, J. (ed.): *Solar Energy. The State of the Art*, ISES Position Papers, London: James&James Ltd.

MORRISON, G. L., BUDIHARDJO, I. and BEHNIA, M. (2004) Water-in-glass evacuated tube solar water heaters, *Solar Energy*, 76, pp. 135–140.

MORRISON, G. L., BUDIHARDJO, I. and BEHNIA, M. (2005) Measurement and simulation of flow rate in a water-in-glass evacuated tube solar water heaters, *Solar Energy*, 78, pp. 257–267.

NADA, S.A; EL-GHETANY, H.H; HUSSEIN, H.M.S (2004) Performance of a two-phase closed thermosyphon solar collector with a shell and tube heat exchanger, *Applied Thermal Engineering*, 24, pp. 1959-1968.

NIKLASSON, G. and GRANQVIST, C. (1983) Surfaces for selective absorption of solar energy: an annotated bibliography 1955-1982. *Journal of materials science*, 18 (12), pp. 3475-3534.

NORTON, B. ; EDMONDS, J.E.J. and KOVOLOS, E. (1992) Dynamic simulation of indirect thermosyphon solar energy water heaters, *Renewable Energy*, 2 (3), pp. 283-297.

NORTON, B. and EDMONDS, J (1991) Aqueous propylene glycol concentrations for the freeze protection of thermosyphon solar energy water heaters, *Solar Energy*, 47 (5), pp. 375-382.

NORTON, B. and PROBERT, S.D. (1983) Recent Advances in Natural-Circulation, Solar-Energy Water Heater Designs, *Applied Energy*, 15 (1), pp. 15-42.

OLIVESKI, R.D.C.; KRENZINGER, A. and VIELMO, H.A. (2003) Comparisson between models for the simulation of hot water storage tanks, *Solar Energy*, 75 (2), pp. 121-134.

ONG, K.S. (1974) A finite-difference method to evaluate the thermal performance of a solar water heater, *Solar Energy*, 16 (3/4), pp. 137-147.

ONG, K.S. (1976) An improved computer program for the thermal performance of a solar water heater, *Solar Energy*, 18 (3), pp. 181-191.

ORDAZ-FLORES, A.; GARCIA-VALLADARES, O.; GOMEZ, V.H (2011) Experimental characterisation and technical feasibility of a closed two-phase vs a conventional solar water heating thermosyphon, *Applied Thermal Engineering*, 31 (6-7), pp. 1313-1322.

OSTERMANN, F. (1998) *Anwendungstechnologie Aluminium*, 1st ed., Springer, Berlin.

PEUSER, F.; REMMERS, K.-H. and SCHNAUSS, M (2001) *Langzeiterfahrung Solarthermie*. 1st ed. Berlin, Solarpraxis Supernova AG.

PILGARD, O. (2005) *Heizen und Kühlen mit erneuerbaren Energien: Auf dem Weg zu einer europäischen Richtlinie* [Online]
Available at: http://www.solarserver.de/solarmagazin/artikelfebruar2005.html
[Accessed: 12 April 2008].

QUASCHNING, V. (2009) *Regenerative Energiesysteme*. 6th ed. Munich, Carl Hanser Verlag.

RECKNAGEL, H.; SPRENGER, E. and SCHRAMEK, E.-R. (2007) *Taschenbuch für Heizung und Klimatechnik*, 73rd ed. Oldenbourg Industrieverlag, Munich.

REDPATH, D.A.G.; EAMES, P.C.; LO, S.N.G. and GRIFFITH, P.W. (2009) Experimental investigation of natural convection heat exchange within a physical model of the manifold chamber of a thermosyphon heat-pipe evacuated tube solar water heater, *Solar Energy*, 83 (7), pp. 988-997.

REDPATH, D.A.G., LO, S.N.G. and EAMES, P.C. (2010) Experimental investigation and optimisation study of a direct thermosyphon heat-pipe evacuated tube solar water heater subjected to a northern maritime climate, *International Journal of Ambient Energy*, 31 (2), pp. 91-101.

REDPATH, D.A.G. (2012) Thermosyphon heat-pipe evacuated tube solar water heaters for northern maritime climate, *Solar Energy*, 86 (2), pp. 705-715.

REMUND, J.; KUNZ, S. and SCHILTER, C. (2006) METETONORM Version 6.0 Handbook part I, Bern.

REYER, E., SCHMID, K., VÖLKNER, S. (2002) *Kompendium der Dämmstoffe*. 3rd ed. Stuttgart, Fraunhofer IRB Verlag.

ROESCH, C. (1999) Monitoring “Nachwachsende Rohstoffe im Wohnungsbau”, Vierter Sachstandsbericht [Online]

Available at: http://www.tab-beim-bundestag.de/de/pdf/publikationen/berichte/TAB-Arbeitsbericht-ab061.pdf [Accessed: 12 April 2011]

RUESCH, F. and BRUNOLD, S. (2009) 20 Jahre Freibewitterung von Kollektorabdeckungsmaterialien. In: *19. Symposium Thermische Solarenergie,* Bad Staffelstein, Germany 6-8 May 2009, pp. 303-308.

SAMMLER (N.N. 2008) Homepage Sammler (Technical Datasheets) [Online] Available at: http://www.sammler.gr/top/tank/s150Model.pdf [Accessed: 14. November 2008].

SANDNER, H.; NEUBRONNER, M. and BODMER, TH. (2006) Stoffwerte von reinen Metallen und Metalllegierungen. In: 10th ed. Verein Deutscher Ingenieure, VDI-Gesellschaft Verfahrenstechnik und Chemieingenieurwesen (GVC) VDI-Wärmeatlas, Berlin & Heidelberg: Springer Verlag.

SCHELLER, W. (1985) *Solaranlagen zur Warmwasserbereitung – Analytische Untersuchungen von Thermosiphon- und Pumpenanlagen unter mitteleuropäischen Klimabedingungen.* Ph. D. Rheinisch-Westfälische Hochschule Aachen.

SHAH L. J. and FURBO S. (2003) Entrance effects in solar storage tanks, *Solar Energy*, 75, pp. 337-348.

SHARIAH, A. et al. (1994) Computer simulation and optimization of design parameters for thermosyphon solar water heater, *Proceedings of the Joint Solar Engineering Conference*, *ASME 1994*, pp. 393-399.

SHARIA, A. et al. (1999) Effect of thermal conductivity of absorber plate on the performance of a solar water heater, *Applied Thermal Engineering*, 19, pp. 733-741.

SHYU, R.; LIN, J. and FANG, L. (1989) Thermal analysis of stratified storage tanks, *ASME Journal Solar Energy Engineering*, 111, pp. 54-61.

SPÄTE, F. (1982) *Bestimmung des thermischen Verhaltens von zwei Thermosiphonanlagen*. Diploma Thesis Kernforschungsanlage Jülich.

THE MATHWORKS (N.N. 2011) SIMULINK 7 – User's Guide [Online] Available at: http://www.mathworks.com/access/helpdesk/help/pdf_doc/simulink/sl_using.pdf [Accessed 28. May 2011].

STANDARD METALLWERKE (N.N. 2012): S-LIFE ® Solar [Brochure], Standard Metallwerke Werl, d.d., Werl (D) [ONLINE] Available at: http://www.standard-metall.de/files/sww_s-life_solar.pdf [Accessed 10. January 2012].

TREIKAUSKAS, F.-D. (2005) *A Novel Design of an Absorber for Solar-Thermal Systems with Provision for New Materials and Production Processes.* Transfer Report Leicester: De Montfort University.

TREIKAUSKAS, F.-D. (2009) *Development of a volumetric solar thermal absorber.* Ph. D. De Montfort University Leicester.

UNITED STATES OF AMERICA. CENTRAL INTELLIGENCE AGENCY (2009) *The world factbook*. [Online]
Available at: https://www.cia.gov/library/publications/the-world-factbook/geos/TS.html and https://www.cia.gov/library/publications/the-world-factbook/geos/GM.html.
[Accessed 27 May 2009].

VAXMAN, M. and SOKOLOV, M. (1986) Effects of Connecting Pipes in Thermosyphonic Solar Systems, *Solar Energy*, 37(5), pp. 323-330.

VERBAND DEUTSCHER MASCHINEN- UND ANLAGENBAU (2010) *Strommix in der EU 27*, Frankfurt am Main: Verband Deutscher Maschinen- und Anlagenbau e.V. [Online]
Available at: http://www.etz.de/files/vdma+ps_strommix_ausblick_final.pdf [Accessed 12. November 2011].

VESTLUND, J.; RÖNNELID, M. and DALENBÄCK, J.-O. (2009) Thermal performance of gas-filled flat plate solar collectors, *Solar Energy*, 83, p. 896-904.

VIESSMANN-WERKE (N.N. 2008) Planungshandbuch Solarthermie. 1st ed., Viessman Werke, Allendorf.

VULCANO (N.N. 2008) Homepage Vulcano (Portugal) [Online]
Available at: http://www.vulcano.pt/index.php?article=785&visual=1&id=89
[Accessed 14. November 2008].

WAGNER, W. (2008) Strömung und Druckverlust, 6th ed., Vogel Buchverlag, Würzburg.

WALCHER, W. (1989) Praktikum der Physik, 6th ed., B.G. Teubner, Stuttgart.

WEITBRECHT, V.; LEHMANN, D. and RICHTER, A., 2002. Flow distribution in solar collectors with laminar flow conditions. *Solar Energy*, 73 (6), p. 433-441.

WENFENG, G. et al. (2011) Numerical Study on Mixing Characteristics of hot Water inside the Storage Tank of a Solar System with Different Inlet Velocities of the Supply Cold Water, *Proccedia Environmental Sciences*, 11, pp. 1153-1163.

WENXIAN, L. and ENRONG, L. (1995) The impact of the auxiliary electric heater in the storage tank on the performance of a thermosyphon solar water system with an auxiliary electric heater (TSAEH). *Energy*, 20 (12), pp. 1265-1270.

WILHELMS, C. and SCHABBACH, T. (2006) *Theoretical evaluation of promising system: Drainback solar water heating system* [Online], Kassel University
Available at: http://www.swt-technologie.de/NEGST_WP1.E3a_SDHW_drainback_vs_db_2006_03_26.pdf
[Accessed 5 June 2008].

YILMAZ, T. (1991) Computer simulation of two-phase flow thermosyphon solar water heating system, *Energy Conversion and Management*, 32 (2), pp. 133–144.

Appendix A:

Influence of the Return Pipe on the Flow Rate

The influence of a return pipe directly welded to the absorber fins of a flat-plate collector on the mass flow rate is evaluated and compared to a collector without connection of down comer pipe and absorber. For the quantification of the influence some assumptions are taken into account:

1. Collector size 1x2 m² with 10 absorber fins
2. Heat carrier fluid: water
3. Heat converted:
    a. Case 1: Absorber fins and return pipe separated (return pipe internal or external)
    b. Case 2: Absorber fin and return pipe welded
4. Heat capacity constant (at inlet temperature)
5. Pressure drop of the system according to measurement data from a double mantle storage tank and a solar collector at 20 °C
6. Collector and storage tank close-coupled – interconnecting pipes neglected
7. Case 2: welded down comer pipe with absorber fin = 1/10*collector area
8. Collector tilt angle γ = 45 °

The system works at equilibrium of pressure gain and pressure losses at a particular mass flow rate (equation (3.4)), which is to be calculated. The mass flow dependent pressure drop is calculated according to equation (3.15), the constant pressure drop coefficient is set to $p_{loss,con} = 0$.

Pressure drop coefficients are taken from measurements of a flat-plate collector and a storage tank (Table A.1).

Table A.1: Pressure Drop Parameters Measured

	$p_{loss,qua}$ [Pa s² kg^{-2}]	$p_{loss,lin}$ [Pa s kg^{-1}]
Collector	45,360	2,778
Storage Tank	19,440	941
Total	64,800	3719

Another possibility was to calculate the pressure drop of collector and storage tank according to Chapter 2.2.2 and 3.3.3.

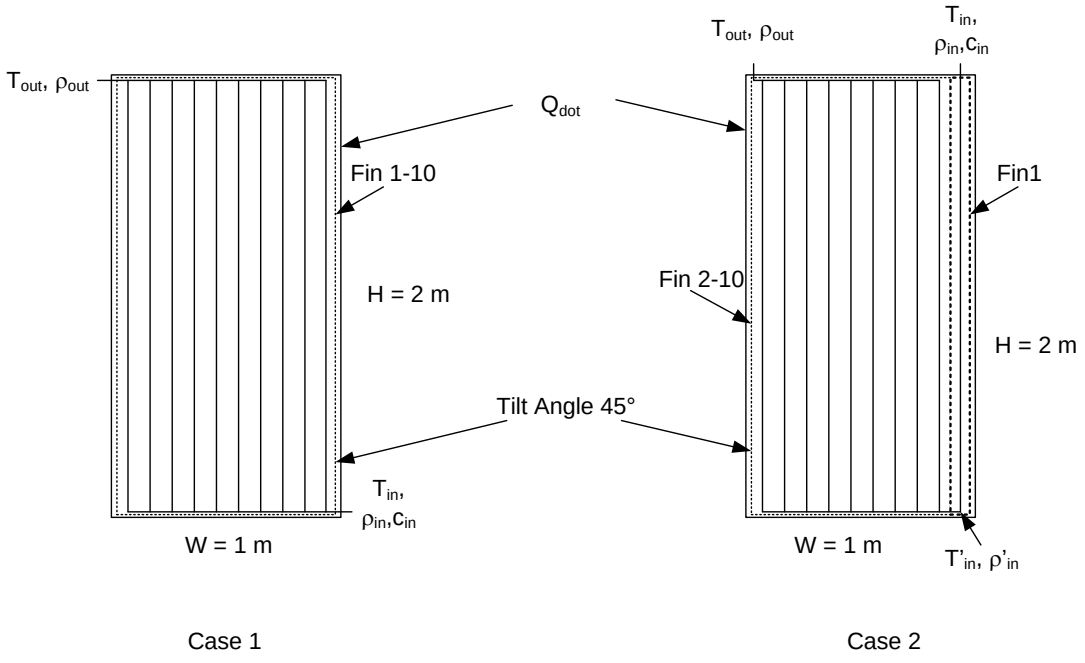

Figure A.1: Collector Layouts Considered

The converted energy Q_{dot} and the collector inlet temperature T_{in} is varied to show the dependency of the mass flow rate.

Case 1:

$$\Delta p_{buo} = \left(\rho(T_{in}) - \rho(T_{out})\right) gH \sin(\gamma) \tag{A.1}$$

$$\dot{Q} = \dot{m} c (T_{out} - T_{in}) \tag{A.2}$$

$$\rho(T_{out}) = f\left(\frac{\dot{Q}}{\dot{m} c} + T_{in}\right) \tag{A.3}$$

$$\Delta p_{loss} = \dot{m}^2 p_{loss,qua} + \dot{m} p_{loss,lin} \tag{A.4}$$

The density function of water is calculated according to the fourth power polynomial given in Chapter 3.1.1, equation (3.2).

$$\Delta p_{buo} = \Delta p_{loss} \tag{A.5}$$

By combining equations (A.1) – (A.5) the dependencies can be written as shown in equation (A.6).

$$\left[\rho(T_{in}) - \left(a_0 + a_1\left(\frac{\dot{Q}}{\dot{m}c} + T_{in}\right) + a_2\left(\frac{\dot{Q}}{\dot{m}c} + T_{in}\right)^2 + a_3\left(\frac{\dot{Q}}{\dot{m}c} + T_{in}\right)^3 + a_4\left(\frac{\dot{Q}}{\dot{m}c} + T_{in}\right)^4\right)\right] gH\sin(\gamma)$$
$$= \dot{m}^2 p_{loss,qua} + \dot{m} p_{loss,lin} \qquad \text{(A.6)}$$

Equation (A.6) is solved using a MATLAB script. For the mass flow four solutions are existent: 2 real solutions —1 positive and 1 negative— and 2 complex solution. The real positive solution represents the mass flow (Table A.2).

Table A.2: Mass Flow Rates Calculated for Case 1

	m_{dot} [kg h^{-1}] at T_{in} [°C]				
Q_{dot} [W]	20	30	40	50	60
800	45.8	51.6	56.2	59.7	62.7
1,000	51.4	57.6	62.4	66.3	69.4
1,200	56.4	62.9	68.0	72.1	75.5
1,400	61.0	67.8	73.2	77.4	80.9

Case 2:

In case 2 the down comer pipe is welded with the absorber. The fluid coming down from the storage tank is already reheated by passing the return pipe. This causes buoyant forces in contradictory direction to the main flow. Therefore a buoyant term (equation (A.7) has to be added to equation (A.4) resulting in equation (A.8).

$$\Delta p_{buo,-} = \left(\rho(T_{in}) - \rho(T'_{in})\right) gH\sin(\gamma) \qquad \text{(A.7)}$$

$$\Delta p_{loss} = \dot{m}^2 p_{loss,qua} + \dot{m} p_{loss,lin} + \Delta p_{buo,-} \qquad \text{(A.8)}$$

The outlet temperature of fin 1 T'_{in} is the inlet temperature of absorber fins 2–10. It is calculated using the correlations (A.9) and (A.10).

$$\dot{Q}_{fin1} = \dot{m}c(T'_{in} - T_{in}) \qquad \text{(A.9)}$$

$$\dot{Q}_{fin1} = \frac{\dot{Q}}{n_{fin}} \tag{A.10}$$

The density at T'$_{in}$ is represented by equation (A.11)

$$\rho(T'_{in}) = \left(a_0 + a_1\left(\frac{\dot{Q}_{fin1}}{\dot{m}c} + T_{in}\right) + a_2\left(\frac{\dot{Q}_{fin1}}{\dot{m}c} + T_{in}\right)^2 + a_3\left(\frac{\dot{Q}_{fin1}}{\dot{m}c} + T_{in}\right)^3 + a_4\left(\frac{\dot{Q}_{fin1}}{\dot{m}c} + T_{in}\right)^4 \right) \tag{A.11}$$

The system is driven by the buoyant forces occurring from fins 2–10 (equation (A.12)).

$$\Delta p_{buo,+} = \left(\rho(T'_{in}) - \rho(T_{out})\right) gH\sin(\gamma) \tag{A.12}$$

The energy available at these riser tubes is shown by equation (A.13) and (A.14).

$$\dot{Q}_{fin2-10} = \frac{\dot{Q}(n_{fin} - 1)}{n_{fin}} \tag{A.13}$$

$$\dot{Q}_{fin2-10} = \dot{m}c(T_{out} - T'_{in}) \tag{A.14}$$

The density of the outlet temperature can be written as function of the available energy Q_{dot} and the inlet temperature T_{in} (equation (A.15)).

$$\rho(T_{out}) = \left(a_0 + a_1\left(\frac{\dot{Q}_{fin1} + \dot{Q}_{fin2-10}}{\dot{m}c} + T_{in}\right) + a_2\left(\frac{\dot{Q}_{fin1} + \dot{Q}_{fin2-10}}{\dot{m}c} + T_{in}\right)^2 + a_3\left(\frac{\dot{Q}_{fin1} + \dot{Q}_{fin2-10}}{\dot{m}c} + T_{in}\right)^3 + a_4\left(\frac{\dot{Q}_{fin1} + \dot{Q}_{fin2-10}}{\dot{m}c} + T_{in}\right)^4 \right) \tag{A.15}$$

$$\dot{Q}_{fin2-10} = \dot{m}c(T_{out} - T'_{in}) \tag{A.16}$$

The whole thermosyphon system finally is described by equation (A.17)

$$0 = \left(\rho(T_{in}) + \rho(T_{out}) - 2\rho(T'_{in})\right) gH\sin(\gamma) + \dot{m}^2 p_{loss,qua} + \dot{m}p_{loss,lin} \tag{A.17}$$

$$\rho(T'_{in}) = \left(a_0 + a_1\left(\frac{\dot{Q}_{fin1}}{\dot{m}c} + T_{in}\right) + a_2\left(\frac{\dot{Q}_{fin1}}{\dot{m}c} + T_{in}\right)^2 + a_3\left(\frac{\dot{Q}_{fin1}}{\dot{m}c} + T_{in}\right)^3 + a_4\left(\frac{\dot{Q}_{fin1}}{\dot{m}c} + T_{in}\right)^4 \right) \tag{A.18}$$

Equation (A.17) is solved by a MATLAB script. The results are shown in Table A.3.

Table A.3: Mass Flow Rates Calculated for Case 2

	m_{dot} [kg h^{-1}] at T_{in} [°C]				
Q_{dot} [W]	20	30	40	50	60
800	42.9	47.7	51.5	54.6	57.1
1,000	48.2	53.3	57.4	60.7	63.4
1,200	53.0	58.4	62.7	66.1	69.0
1,400	57.5	63.1	67.5	71.1	74.1

The mass flow of case 2 is always below case 1 and varies in the range of 5.8–8.8 per cent (Table A.4). The higher the inlet temperature is, the higher the difference between both flow rates becomes.

Table A.4: Difference in the Mass Flow Rate of Case 1 and Case 2

	Mass Flow Difference of Case 1 and 2 [%] at T_{in} [°C]				
Q_{dot} [W]	20	30	40	50	60
800	6.4	7.6	8.2	8.6	8.8
1,000	6.1	7.4	8.0	8.4	8.6
1,200	5.9	7.2	7.9	8.3	8.5
1,400	5.8	7.1	7.8	8.2	8.4

Appendix B:

Storage Tank C-Code

```
/*
* multiport stratified thermal storage with double jacket heat exchanger
*
*--------------------------------------------------------------------
*Version                         Changes                 Date
* 0.1.0                          created                 feb2008
*--------------------------------------------------------------------
* Model description:
*       The storage is modelled as a lying cylinder. The inner cylinder,
*       is surrounded by another cylinder, the mantle. Between mantle and
*       storage wall collector-fluid is flowing. The whole system is surrounded by an
*       isolating material.
*       Water inlet is at bottom and outlet at top. Collector fluid inlet is at top and outlet at bottom.
*
* Implementation:
*       As a base for this code the Simulink templates for s-functions and the c-files
*       "store.c" and "store_hx_r13.c" of the carnot library are applied.
*       Result is a level 2 - function with 3 Input-ports and 2 output-ports.
*
*       Input:
*               port 1:     ambient temperature
*               port 2:     10 needed values of the THV Input vector of the collector-fluid
*               port 3:     10 needed values of the THV Input vector of the water
*       Output:
*               port 1: node temperatures of collector-fluid from bottom to top and pressure
*               port 2: node temperatures of water from bottom to top  and pressure
*
* Calculations:
*       pressure drop:      calculation  dp = dp0 + dp1*mdot + dp2*mdot^2
*               1) hydrostatic pressure between inlet and outlet:
*                       dp0 = rho * Grav * (n*dh)
*               2) pressure drop at the inflow:
*                       dp2 = zeta * 0.5 * rho * v^2
*                       pressure drop at outlet is 0, because v in the storage is approximately 0
*
*       differential equations for every nodes' energy balance:
*               Generally there are influences of heat conduction, heat loss, and changes conditional on mass flow
*                       rho * Vnode * c * dT/dt = Alpha * Aloss * (Tambient - Tnode)(heat loss term)
*                                               + lambda*A/d*(TnodeAbove - Tnode) (heat conduction from top to bottom)
*                                               + mdot*c*(TnodeAbove - Tnode)       (mass flow term)
*                       --> this equation is adapted to water and fluid terms
*
*       with:
*       rho     =       density
*       Vnode   =       volume of the actual node
*       c       =       heat capacity
*       T       =       temperature
*       t       =       time
*       Alpha   =       heat loss coefficient
*       Aloss   =       surface where heat loss happens
*       lambda  =       heat conductivity
*       lambdaS =       heat conductivity which considers thermal resistance of convection in the tank (use lower value)
*       A       =       area of heat conductivity
*       d       =       length, where heat conduction happens
*       mdot    =       mass flow
*       zeta    =       coefficient for resistance
*
*-------------------------------------------------------------------------------------------
* INPUT-VECTOR: See at #define section
*
* STATES-VECTOR:
*       includes all node temperatures of water and collector fluid, so its dimension is 2*node:
*
*               Tbottom
*               T1
*               T2
*               x =  .
*                    .
*               Ttop
*
```

```
* OUTPUT_VECTOR:
*       includes number of measurement points temperatures of water and collector fluid, both pressures at outlet and
*       2 * 3 coefficients of pressure drop term:
*
*               TbottomWater
*               T1Water
*               .
*               .
*               TtopWater
*               pressure water at outlet
*               constant  |
*               linear          |> coefficients
*               quadratic |
*       y=      TbottomColl
*               T1Coll
*               .
*               .
*               TtopColl
*               pressure collector fluid at outlet
*               constant  |
*               linear          |> coefficients
*               quadratic |
*
*-----------------------------------------------------------------------------------------------------------
*
*CREATED FOR "CENTRE OF EXCELLENCE FOR RENEWABLE ENERGY RESEARCH AT INGOLSTADT UNIVERSITY OF AP-
PLIED SCIENCES"
*
*-----------------------------------------------------------------------------------------------------------
*
*       Date                    Author                  Change
*       21.04.2008              Martin Konrad           Negative mass flow (signed by THV[11] = 1), are considered.
*                                                       If it is negative, collector fluid will flow into bottom node and
*                                                       leave the storage at the top node
*       07.06.2008              Martin Konrad           new way of calculating geometries of inner tank; selectable by a
*                                                       checkbox at input mask -->
*                                                       on: nodes have same volume; off: nodes have same height
*                                                       Numerical calculation of some geometrical values by bisection
*                                                       of interval (no analytical solution)
*
*/
#define S_FUNCTION_NAME HorStore
#define S_FUNCTION_LEVEL 2

#include "tmwtypes.h"
#include "simstruc.h"
#include "carlib.h"
#include <math.h>

//define constants
#define PI      3.14159265358979
#define GRAV    9.81
#define NUSSELT_MANTLE  7.5
#define ALPHA_START 45.0
#define MAX_DIFF    0.000001

#define SAMEVOLUMES                             *mxGetPr(ssGetSFcnParam(S,0)) //True for geometrie calculations with
equal volumes
#define MANTLE_D_OUT                    *mxGetPr(ssGetSFcnParam(S,1)) /* outer diameter of the mantle [m] */
#define MANTLE_D_IN                             *mxGetPr(ssGetSFcnParam(S,2)) /* inner diameter of the mantle [m] */
#define MANTLE_FEED_PIPE_D              *mxGetPr(ssGetSFcnParam(S,3)) /* diameter of the mantle-feed-pipe [m] */
#define ZETA_ADDITIONAL_MANTLE  *mxGetPr(ssGetSFcnParam(S,4)) /* additional value for zeta (mantle inflow)[-] */
#define STORE_D_OUT                             *mxGetPr(ssGetSFcnParam(S,5)) /* outer diameter of the store [m] */
#define STORE_D_IN                              *mxGetPr(ssGetSFcnParam(S,6)) /* inner diameter of the store [m] */
#define STORE_FEED_PIPE_D               *mxGetPr(ssGetSFcnParam(S,7)) /* diameter of the store-feed-pipe [m] */
#define ZETA_ADDITIONAL_STORE   *mxGetPr(ssGetSFcnParam(S,8)) /* additional value for zeta (store inflow)[-] */
#define ISOLATION_D                             *mxGetPr(ssGetSFcnParam(S,9)) /* diameter of the isolation [m] */
#define ALPHA_AMB                               *mxGetPr(ssGetSFcnParam(S,10)) /* heat loss coefficient mantle - air
[W/(m^2*K)] */
#define LAMBDA_MANTLE                   *mxGetPr(ssGetSFcnParam(S,11)) /* heat conductivity in the mantle [W/(m*K)] */
#define LAMBDA_STORE                    *mxGetPr(ssGetSFcnParam(S,12)) /* heat conductivity in the store [W/(m*K)] */
#define LAMBDA_ISOLATION                *mxGetPr(ssGetSFcnParam(S,13)) /* heat conductivity isolation [W/(m*K)] */
#define TINI                                    *mxGetPr(ssGetSFcnParam(S,14)) /* initial storage temperature °C */
```

```
#define NODES                                   *mxGetPr(ssGetSFcnParam(S,15)) /* number of nodes */
#define M_PTS                                   *mxGetPr(ssGetSFcnParam(S,16)) /* number of measurement points */
#define LENGTH_STORE                    *mxGetPr(ssGetSFcnParam(S,17)) /* length of store [m]*/
#define LENGTH_MANTLE                   *mxGetPr(ssGetSFcnParam(S,18)) /* length of mantle [m]*/
#define N_PARAMETER     19

//InputVector:

#define T_AMB       *u[0]  /* ambient temperature */
#define FLOW_ID_C           *u[1]  /* flowd ID collector */
#define T_IN_C          *u[2]  /* inlet temperature */
#define MDOT_IN_C    *u[3]  /* massflow */
#define PRESS_IN_C   *u[4]  /* pressure */
#define FLUID_ID_C          *u[5]  /* fluid ID (defined in CARNOT.h) */
#define PERCENT_C           *u[6]  /* mixture  (defined in CARNOT.h) */
#define D_IN_C          *u[7]  /* diameter at inlet in m */
#define CON_C               *u[8]  /* constant term in pressure drop */
#define LIN_C       *u[9]  /* linear term in pressure drop */
#define QUA_C               *u[10]  /* quadratic term in pressure drop */
#define NEG_MASSFLOW  *u[11]  /* flag for negative massflow */
#define FLOW_ID_W           *u[12] /* flowd ID water */
#define T_IN_W      *u[13] /* inlet temperature */
#define MDOT_IN_W    *u[14] /* massflow */
#define PRESS_IN_W   *u[15] /* pressure */
#define FLUID_ID_W   *u[16] /* fluid ID (defined in CARNOT.h) */
#define PERCENT_W           *u[17] /* mixture  (defined in CARNOT.h) */
#define D_IN_W              *u[18] /* diameter at inlet in m */
#define CON_W               *u[19] /* constant term in pressure drop */
#define LIN_W       *u[20] /* linear term in pressure drop */
#define QUA_W       *u[21] /* quadratic term in pressure drop */
#define N_INPUT     22

//StateVector:

//Water
#define TNW_BELOW       x[i-1]
#define TNW_ABOVE       x[i+1]
#define TNW                         x[i]            // actual node temperature water
#define TOP_W    (nodes-1)
#define BOTTOM_W   0

//Collector-fluid
#define TNC_BELOW       x[i+nodes-1]
#define TNC_ABOVE       x[i+nodes+1]
#define TNC             x[i+nodes]      //temperature in the part of the collector fluid which 'belongs' to node i of water
#define TOP_C           (2*nodes-1)
#define BOTTOM_C        nodes

static int geometry_init = 0;

//needed for geometrical computations in MDL_DERIVATIVES
//defined global to be able to free memory in MDL_TERMINATE
static double *volW;
static double *volC;
static double *bMa;
static double *bMi;
static double *bSa;
static double *bSi;
static double *bIso;
static double *s;
static double *delta_h;

#define MDL_CHECK_PARAMETERS
#if defined(MDL_CHECK_PARAMETERS) && defined(MATLAB_MEX_FILE)
/*
function mdlCheckParameters:
        validates parameters and returns error-messages if necessary
*/
static void mdlCheckParameters(SimStruct *S)
{
        if (M_PTS > NODES)
        {
                ssSetErrorStatus(S,"Error: number of measurement points must be smaller or equal number of nodes");
```

```
                return;
    }
        if ( LAMBDA_STORE < 0 || LAMBDA_MANTLE < 0 || LAMBDA_ISOLATION < 0)
        {
                ssSetErrorStatus(S,"Error: All heat conductivities must be positive");
                return;
    }
        if (ALPHA_AMB<0)
        {
                ssSetErrorStatus(S,"Error: heat loss coefficient must be positive");
                return;
    }
        if (LENGTH_MANTLE > LENGTH_STORE)
        {
                ssSetErrorStatus(S,"Error: mantel must have a shorter or equal length as store");
                return;
    }
    if (TINI<-273.15)
        {
                ssSetErrorStatus(S,"Error: Initial temperature can't be less than 0 K");
                return;
    }
        if(ISOLATION_D < MANTLE_D_OUT || MANTLE_D_OUT < MANTLE_D_IN || MANTLE_D_IN < STORE_D_OUT ||
STORE_D_OUT < STORE_D_IN)
        {
                ssSetErrorStatus(S,"Error: correct sequence of diameters must be:\nd isolation > d_mantle_out > d_mantle_in >
d_store_out > d_store_in");
                return;
    }
        /*if (MANTLE_FEED_PIPE_D > (0.5*(MANTLE_D_IN-STORE_D_OUT)))
        {
                ssSetErrorStatus(S,"Error: Mantle feed pipe too tall. Won't fit...");
                return;
    }  */
}
#endif



/*
function mdlInitializeSizes:
        specifies the numbers of parameters, number ports, ports' width and more initialisation
*/
static void mdlInitializeSizes(SimStruct *S)
{

        int_T nInputPorts  = 3;  // number of input ports
    int_T nOutputPorts = 2;  // number of output ports
    int_T needsInput   = 1;  // direct feed through

    int_T inputPortIdx  = 0; // counter variables for initialisation-loop
    int_T outputPortIdx = 0;


    ssSetNumSFcnParams(S, N_PARAMETER);  // Number of expected parameters
    if (ssGetNumSFcnParams(S) != ssGetSFcnParamsCount(S))
        {
       return;
    }

    // Register the number and type of states the S-Function uses

    ssSetNumContStates(    S, (2*NODES));   // number of continuous states
    ssSetNumDiscStates(    S,                          0);   // number of discrete states


    // Configure the input ports. First set the number of input ports.

    if (!ssSetNumInputPorts(S, nInputPorts)) return;            //number of input ports
    ssSetInputPortWidth(S,0,1);                                 //number of elements the ports transmit
        ssSetInputPortWidth(S,1,11);
        ssSetInputPortWidth(S,2,10);
```

```
        // initialize the ports concerning direct feed through
    for(inputPortIdx;inputPortIdx<nInputPorts;inputPortIdx++)
        {
            ssSetInputPortDirectFeedThrough(S, inputPortIdx, needsInput);
        }
    // configure the output ports. First set the number of output ports.

    if (!ssSetNumOutputPorts(S, nOutputPorts)) return;      //number of output ports
        ssSetOutputPortWidth(S,0,M_PTS+4);          //number of elements the ports transmit
        ssSetOutputPortWidth(S,1,M_PTS+4);

    ssSetNumSampleTimes(S,1);   // number of sample times

    // Set size of the work vectors
    ssSetNumRWork(      S, 0);   /* number of real work vector elements   */
    ssSetNumIWork(      S, 0);   /* number of integer work vector elements*/
    ssSetNumPWork(      S, 0);   /* number of pointer work vector elements*/
    ssSetNumModes(      S, 0);   /* number of mode work vector elements   */
    ssSetNumNonsampledZCs( S, 0);   /* number of nonsampled zero crossings   */

        // validate parameters at the beginning of the simulation
        if(ssGetNumSFcnParams(S) == ssGetSFcnParamsCount(S))
        {
            mdlCheckParameters(S);
        }
}

/*
function mdlInitializeSampleTimes:
        Specifiy that we inherit our sample time from the driving block.
*/

static void mdlInitializeSampleTimes(SimStruct *S)
{
    ssSetSampleTime(S, 0, 0.0);
    ssSetOffsetTime(S, 0, 0.0);
}

#define MDL_INITIALIZE_CONDITIONS

/*
function mdlInitializeConditions:
        Initializes the states vector
*/
static void mdlInitializeConditions(SimStruct *S)
{
    real_T *x0   = ssGetContStates(S);          //get pointer to the states vector at beginning
        double t0 = TINI;
    int    nodes = (int)NODES;
    int i;

    for (i = BOTTOM_W; i <= TOP_C; i++)
        {
            x0[i] = t0;                         //initialized with TINI
        }
}

/*
function mdlOutputs:
        Calculates pressure drops and fills output vector with values
*/
static void mdlOutputs(SimStruct *S, int_T tid)
{
        //get pointer to output-, states- and input-vector
    real_T          *y = ssGetOutputPortRealSignal(S,0);
    real_T          *x = ssGetContStates(S);
    InputRealPtrsType   u  = ssGetInputPortSignalPtrs(S,0);

        //get work data from user input
        int nodes           =       (int)NODES;
        int mpts            =       (int)M_PTS;
        double dstoreIn     =       STORE_D_IN;
        double dmantleIn=  MANTLE_D_IN;
```

```
        //deltas of pressure drop coefficients
double conW  = 0.0;
double quaW  = 0.0;
double conC = 0.0;
double quaC = 0.0;

double interval_size, pW, pC, rho, v, re, zeta, dp, dh, pdyn, zeta_additional_store, zeta_additional_mantle;
int i, location, inverse;

//eliminate inversed thermocline
        //you can comment out following lines for simulating just cool down
        //if you don't you may have one value which is very different to the other
        //this effect causes on geometry (some nodes may have a larger surface to cool down)
/*do
        {
   inverse = 0;
   for(i = TOP_W; i > BOTTOM_W; i--)
                {
      if (TNW < TNW_BELOW)
                        {
         TNW = 0.5*(TNW+TNW_BELOW); // mix the two nodes
         TNW_BELOW = TNW;
      }
                        if(TNC < TNC_BELOW)                     // collector fluid has the same number of nodes as water
                        {
                                TNC = 0.5*(TNC+TNC_BELOW);
                                TNC_BELOW = TNC;
                        }
   }
} while (inverse);*/


        //Calculations for the store:

        zeta_additional_store = ZETA_ADDITIONAL_STORE;
// friction: calculate only if there is massflow
pW = 0.0;
        rho = density(FLUID_ID_W, PERCENT_W, T_IN_W, PRESS_IN_W);
if (fabs(MDOT_IN_W) > 0.0 && FLOW_ID_W > 10000.0)
        {
   v   = 4.0 * MDOT_IN_W / (rho * STORE_FEED_PIPE_D * STORE_FEED_PIPE_D * PI);
   re  = v * STORE_FEED_PIPE_D / viscosity(FLUID_ID_W, PERCENT_W, T_IN_W, PRESS_IN_W);
   zeta = 1.0 + zeta_additional_store;                          // sharp edged entry + possible bends
   pdyn = rho*v*v*0.5;
   pW = -zeta*pdyn;
   quaW = zeta*pdyn/(MDOT_IN_W*MDOT_IN_W);
}

// hydrostatic pressure
if (FLOW_ID_W > 20000.0)
        {
   dh = dstoreIn/nodes;
   dp = 0.0;
   for (i = BOTTOM_W; i <= TOP_W; i++)
                {
      dp += rho*GRAV*dh;
                }

   pW  -= dp;
   conW += dp;
}

        // set temperature of every measurement-point from bottom (0) to top (mpts-1)
interval_size =  nodes/mpts;
for(i = 0; i < mpts; i++)
        {
        location = (int)i*interval_size;
        y[i] = x[location];
}
y[mpts-1] = x[TOP_W];     //temperature of the top node
// pressure
y[mpts]   = PRESS_IN_W + pW;
```

```
            // pressure drop terms
    y[mpts+1] = CON_W + conW;
    y[mpts+2] = LIN_W;
    y[mpts+3] = QUA_W + quaW;

            //Calculations for the collector fluid
            zeta_additional_mantle = ZETA_ADDITIONAL_MANTLE;
            // friction: calculate only if there is mass flow
    pC = 0.0;
            rho = density(FLUID_ID_C, PERCENT_C, T_IN_C, PRESS_IN_C);
    if (fabs(MDOT_IN_C) > 0.0 && FLOW_ID_C > 10000.0)  {
       v   = 4.0 * MDOT_IN_C / (rho * MANTLE_FEED_PIPE_D * MANTLE_FEED_PIPE_D * PI);
       re  = v * MANTLE_FEED_PIPE_D / viscosity(FLUID_ID_C, PERCENT_C, T_IN_C, PRESS_IN_C);
       zeta = 1.0 + zeta_additional_mantle;                    // sharp edged entry + possible bends
       pdyn = rho*v*v*0.5;
       pC = -zeta*pdyn;
       quaC = zeta*pdyn/(MDOT_IN_C*MDOT_IN_C);
    }
    //hydrostatic pressure
    if (FLOW_ID_C > 20000.0)
            {
       dh = dmantleIn/nodes;
       dp = 0.0;
       for (i = BOTTOM_C; i <= TOP_C; i++)
                   {
          dp += rho*GRAV*dh;
                   }

       pC  += dp;
       conC -= dp;

    }
            // set temperature of every measurement-point from bottom to top
    interval_size =  nodes/mpts;
    for(i = mpts+4; i < 2*mpts+4; i++)
            {
            location = (i-4)*interval_size;
            y[i] = x[location];
    }
            y[mpts+4]  =          x[BOTTOM_C];      // avoid failure in case of rounding
    y[2*mpts-1+4] = x[TOP_C];      // temperature of the top node
    // pressure
    y[2*mpts+4] = PRESS_IN_C + pC;
    // pressure drop terms
    y[2*mpts+5] = CON_C + conC;
    y[2*mpts+6] = LIN_C;
    y[2*mpts+7] = QUA_C + quaC;
}

#define MDL_DERIVATIVES
/*
function mdlDerivatives:
            Calculates the derivatives of the temperatures for each node by means of the differential equations noted at the beginning
*/
static void mdlDerivatives(SimStruct *S)
{
            //get pointers to derivatives-, states- and input-vector
    real_T          *dx = ssGetdX(S);
    real_T          *x  = ssGetContStates(S);
    InputRealPtrsType  u  = ssGetInputPortRealSignalPtrs(S,0);

            //allocate memory for geometrical values of each node dynamicaly
    int       nodes=NODES;
            /*
            static double *volW;
            static double *volC;
            static double *bMa;
            static double *bMi;
            static double *bSa;
            static double *bSi;
            static double *bIso;
            static double *s;
```

```
static double *delta_h;*/
//work data from user input
double    dstoreIn  =          STORE_D_IN;
double    dstoreOut=           STORE_D_OUT;
double    dmantleIn=           MANTLE_D_IN;
double    dmantleOut           =          MANTLE_D_OUT;
double  disolation  =          ISOLATION_D;
double    dh                              =          dstoreIn / nodes;
double    lengthStore          =          LENGTH_STORE;
double  lengthMantle=          LENGTH_MANTLE;
double    lambdaS              =          LAMBDA_STORE;
double    lambdaM              =          LAMBDA_MANTLE;
double    lambdaIso            =          LAMBDA_ISOLATION;
double    Tamb                 =          T_AMB;
double    QalphaAmb            =          ALPHA_AMB;
double    dhyd      =          MANTLE_D_IN - STORE_D_OUT; //hydraulic diameter of the mantle
bool      samevolumes =        SAMEVOLUMES;
double    cC, cW, rhoW, rhoC;
double    alpha, volWBelow, volCBelow, bMaBelow, bMiBelow, bSaBelow, bSiBelow, bIsobelow, Vist,Vsoll, border_up,
border_down;
double QalphaMantle, lambdaC, lambdaW, negflow;
int i = 0;
int l = 0;
int neg = 0;
int count = 0;
//geometry
        int k = 1;
        int stop= 0;
        if(geometry_init == 0)
        {
        volW      = (double*) malloc(nodes * sizeof(double));
        volC      = (double*) malloc(nodes * sizeof(double));
        bMa               = (double*) malloc(nodes * sizeof(double));
        bMi               = (double*) malloc(nodes * sizeof(double));
        bSa               = (double*) malloc(nodes * sizeof(double));
        bSi               = (double*) malloc(nodes * sizeof(double));
        bIso      = (double*) malloc(nodes * sizeof(double));
        s                 = (double*) malloc(nodes * sizeof(double));
        delta_h = (double*) malloc(nodes * sizeof(double));

        if(TOP_W%2 == 0)                                //odd number of nodes
        {
                stop = (TOP_W / 2) + 1;
        }
        else                                                                    //even number of nodes
        {
                stop = (TOP_W + 1) / 2;
        }
        for(i = TOP_W; i>=stop; i--)
        {
                if(i == TOP_W)      //initialisation with 0, because there's no "below"-value at the beginning
                {
                        volWBelow         =         0;
                        volCBelow         =         0;
                        bMaBelow          =         0;
                        bMiBelow          =         0;
                        bSaBelow          =         0;
                        bSiBelow          =         0;
                        bIsobelow         =         0;
                }
                else
                {
                        volWBelow         +=        volW[i+1];
                        volCBelow         +=        volC[i+1];
                        bMaBelow          +=        bMa[i+1];
                        bMiBelow          +=        bMi[i+1];
                        bSaBelow          +=        bSa[i+1];
                        bSiBelow          +=        bSi[i+1];
                        bIsobelow         +=        bIso[i+1];
                }
                //*************************************************************************************************************
                //same volumes
                if(samevolumes == true)
```

```
		{
		Vsoll	=	(dstoreIn*dstoreIn/4)*PI/nodes *lengthStore;
		border_up	= 91;//avoid problems caused by imprecision at Vist-calculation
		border_down = -1;
		alpha	=	ALPHA_START;
		do
		{
			s[i]	=	2 * sin(alpha*PI/180) * 0.5 * dstoreIn;
			Vist	=	(((alpha/180)*0.25*dstoreIn*dstoreIn*PI) –
			(0.5*s[i]*(cos(alpha*PI/180)*0.5*dstoreIn)))*lengthStore - volWBelow;
			if((Vist-Vsoll) < 0.0)
			{	border_down = alpha;
				alpha = (border_up+alpha)/2;
			}
			else
			{
				border_up = alpha;
				alpha = (border_down+alpha)/2;
			}
		}while(fabs(Vist-Vsoll) > MAX_DIFF);
		}
		//*****************************************************************************************************************
		//same height
		//*****************************************************************************************************************
		else
		{
		alpha			=	acos((0.5*dstoreIn-k*dh)/ (0.5*dstoreIn)) * 180 / PI;
		s[i]			=	2 * sin(alpha*PI/180) * 0.5 * dstoreIn;
		Vist	=	(((alpha/180)*0.25*dstoreIn*dstoreIn*PI) –
		 (0.5*s[i]*(cos(alpha*PI/180)*0.5*dstoreIn)))*lengthStore - volWBelow;
		}
		//*****************************************************************************************************************
		s[TOP_W-i+1]	=	s[i];
		volW[i]		Vist;//(((alpha/180)*0.25*dstoreIn*dstoreIn*PI) - (0.5*s[i]*(0.5*dstoreIn-
		k*dh)))*lengthStore - volWBelow;
		volW[TOP_W-i]	=	volW[i];	//reflect to the other side
		volC[i]			=	(alpha/360)*PI*0.25*(dmantleIn*dmantleIn-
		dstoreOut*dstoreOut)*lengthMantle - volCBelow;
		volC[TOP_W-i]	=	volC[i];	//reflect to the other side
		bMa[i]			=	(alpha/360)*dmantleOut*PI - bMaBelow;
		bMa[TOP_W-i]	=	bMa[i];		//reflect to the other side
		bMi[i]			=	(alpha/360)*dmantleIn*PI - bMiBelow;
		bMi[TOP_W-i]	=	bMi[i];		//reflect to the other side
		bSa[i]			=	(alpha/360)*dstoreOut*PI - bSaBelow;
		bSa[TOP_W-i]	=	bSa[i];		//reflect to the other side
		bSi[i]			=	(alpha/360)*dstoreIn*PI - bSiBelow;
		bSi[TOP_W-i]	=	bSi[i];		//reflect to the other side
		bIso[i]			=	(alpha/360)*disolation*PI - bIsobelow;
		bIso[TOP_W-i]	=	bIso[i];	//reflect to the other side
		k++;
}
		//center node (if it exists)
		if(TOP_W%2 == 0)
		{
			volWBelow		+=	volW[stop];
			volCBelow		+=	volC[stop];
			bMaBelow		+=	bMa[stop];
			bMiBelow		+=	bMi[stop];
			bSaBelow		+=	bSa[stop];
			bSiBelow		+=	bSi[stop];
			bIsobelow		+=	bIso[stop];
			if(samevolumes==true)
			{
				volW[stop-1]	=	Vsoll;
			}
			else
			{
				volW[stop-1]	=(0.25*dstoreIn*dstoreIn*PI)*lengthStore - 2*volWBelow;
			}
			volC[stop-1]	=	(0.25*0.5*PI*(dmantleIn*dmantleIn-
			dstoreOut*dstoreOut))*lengthMantle - 2*volCBelow;
			bMa[stop-1]		=	0.5*dmantleOut*PI - 2*bMaBelow;
			bMi[stop-1]		=	0.5*dmantleIn*PI - 2*bMiBelow;
```

```
                        bSa[stop-1]             =       0.5*dstoreOut*PI - 2*bSaBelow;
                        bSi[stop-1]             =       0.5*dstoreIn*PI - 2*bSiBelow;
                        bIso[stop-1]    =       0.5*disolation*PI - 2*bIsobelow;
                }
                geometry_init = 1;
        }
//equations
i = 0;
for(i = TOP_W; i >= BOTTOM_W; i--)
{
        negflow = NEG_MASSFLOW;
        if(negflow == 1)
        {
                neg = TOP_W-i;
                count = -1;
        }
        else
        {
                neg = i;
                count = 1;
        }
        //heat capacity and density
        cW                      =       heat_capacity(FLUID_ID_W, PERCENT_W, TNW, PRESS_IN_W);
        cC                      =       heat_capacity(FLUID_ID_C, PERCENT_C, TNC, PRESS_IN_C);
        rhoW            =       density(FLUID_ID_W, PERCENT_W, TNW, PRESS_IN_W);
        rhoC            =       density(FLUID_ID_C, PERCENT_C, TNC, PRESS_IN_C);
        lambdaC         =       thermal_conductivity(FLUID_ID_C, PERCENT_C, TNC, PRESS_IN_C);
        lambdaW         =       thermal_conductivity(FLUID_ID_W, PERCENT_W, TNW, PRESS_IN_W);
        QalphaMantle =  NUSSELT_MANTLE * lambdaC / dhyd;
        //water
        dx[i]           =       0;
        //heat conduction in the medium
        if(i<TOP_W)
        {
                dx[i]   =       lambdaW * s[i+1] *lengthStore / dh * (TNW_ABOVE - TNW); //downwards to node
        }
        if(i>BOTTOM_W)
        {
                dx[i]   -=      lambdaW * s[i] *lengthStore / dh * (TNW - TNW_BELOW);   //downwards from node
        }
        //massflow
        if(i>BOTTOM_W)
        {
                dx[i]   -=      MDOT_IN_W * cW * (TNW - TNW_BELOW);     //heat loss by mass flow
        }
        else
        {
                dx[i]   -=      MDOT_IN_W * cW * (TNW - T_IN_W);                //position at the inlet
        }
        //heat conduction --> heat exchange
        dx[i]           +=      2*(TNC - TNW) / ((1/(QalphaMantle*bSa[i]*lengthMantle)) + (0.5*(dstoreOut-
dstoreIn)/(lambdaS*lengthMantle*(0.5*(bSa[i]+bSi[i])))));
        //heat loss at the outer positions (there may be no mantle)
        if(lengthStore != lengthMantle)
        {
        /*heat conduction through store*/
        /*heat conduction through isolation*/
        /*convection at the surface*/
        dx[i]   -=      2*(TNW - Tamb) / ( (0.5*(dstoreOut-dstoreIn)/(lambdaS*(lengthStore-
lengthMantle)*(0.5*(bSa[i]+bSi[i])))) + (0.5*(disolation-dstoreOut)/(lambdaIso*(lengthStore-
lengthMantle)*(0.5*(bSa[i]+bIso[i])))) + (1/(QalphaAmb*bIso[i]*(lengthStore-lengthMantle))));
        }
        //heat loss at front and back surface
        dx[i]           -=      2*(TNW - Tamb) / ( (0.5*(dstoreOut-dstoreIn)/(lambdaS*(volW[i]/lengthStore))) +
(0.5*(disolation-dmantleOut)/(lambdaIso*(volW[i]/lengthStore))) + ( 1 / (QalphaAmb * (volW[i]/lengthStore))));

        //normalize
        dx[i]           =       dx[i] / (rhoW*volW[i]*cW);
        //collector fluid
        if(i==TOP_W)            //Initialisation of all derivatives before calculating
        {
                for(l=0;l<=TOP_W;l++)
                {
```

```
                                        dx[l+nodes] = 0;
                                }
                        }
                        //heat conduction in the medium
                        if(i < TOP_W)
                        {
                                dx[i+nodes]             +=      lambdaC * 0.5*(dmantleIn - dstoreOut) *lengthMantle /(0.5*(bMi[i]+bSa[i]))
                                                                * (TNC_ABOVE - TNC);                    //downwards to node
                        }
                        if(i>BOTTOM_W)
                        {
                                dx[i+nodes]             -=      lambdaC * 0.5*(dmantleIn - dstoreOut) *lengthMantle /(0.5*(bMi[i]+bSa[i]))
                                                                * (TNC - TNC_BELOW);    //downwards from node
                        }
                        //Massenstr÷me
                        if(((neg<TOP_W) && (count == 1))  || ((neg > BOTTOM_W) && (count == (-1))))
                        {
                                dx[neg+nodes]           +=      0.5 * MDOT_IN_C * cC * (x[neg+nodes+count] - x[neg+nodes]);
        //heat loss by mass flow
                        }
                        else
                        {
                                dx[neg+nodes]           +=      0.5 * MDOT_IN_C * cC * (T_IN_C - x[neg+nodes]);
        //position at the inlet
                        }
                        //heat conduction --> heat exchange
                        dx[i+nodes]             -=      (TNC - TNW) / ((1/(QalphaMantle*bSa[i]*lengthMantle)) + (0.5*(dstoreOut-dstoreIn)
                                                        /(lambdaS*lengthMantle*(0.5*(bSa[i]+bSi[i]))));
                        //heat loss at ambient
                        dx[i+nodes]             -=      (TNC - Tamb) / ((1/(QalphaMantle*bMi[i]*lengthMantle))+(0.5*(dmantleOut-
                                                        dmantleIn)/(lambdaM*lengthMantle*(0.5*(bMa[i]+bMi[i])))) + (0.5*(disolation-
                                                        dmantleOut)/(lambdaIso*lengthMantle*(0.5*(bIso[i]+bMa[i])))) +
                                                        (1/(QalphaAmb*bMa[i]*lengthMantle)));  //Peclet-Glch ; therm. widerstõnde
        }
        //NORMALIZE (can't be done until all calculations on the derivatives are done because of different ways of passing the loop
                        in case of neg. mass flow)
        for(i = TOP_W; i >= BOTTOM_W; i--)
        {
                dx[i+nodes]                     =       dx[i+nodes] / (rhoC*volC[i]*cC);}

        //free allocated memory
        /*free(volW);
        free(volC);
        free(bMa);
        free(bMi);
        free(bSa);
        free(bSi);
   free(bIso);
        free(s);
        free(delta_h);*/
}
/*
function mdlTerminate:
needed routine to terminate simulation
*/
static void mdlTerminate(SimStruct *S)
{
        geometry_init = 0;
        free(volW);
        free(volC);
        free(bMa);
        free(bMi);
        free(bSa);
        free(bSi);
   free(bIso);
        free(s);
        free(delta_h);
}
#ifdef  MATLAB_MEX_FILE    // Is this file being compiled as a MEX-file?
#include "simulink.c"      // MEX-file interface mechanism
#else
#include "cg_sfun.h"       // Code generation registration function
#endif
```

Appendix C:

Technical Details and Drawings – Prototype Absorber

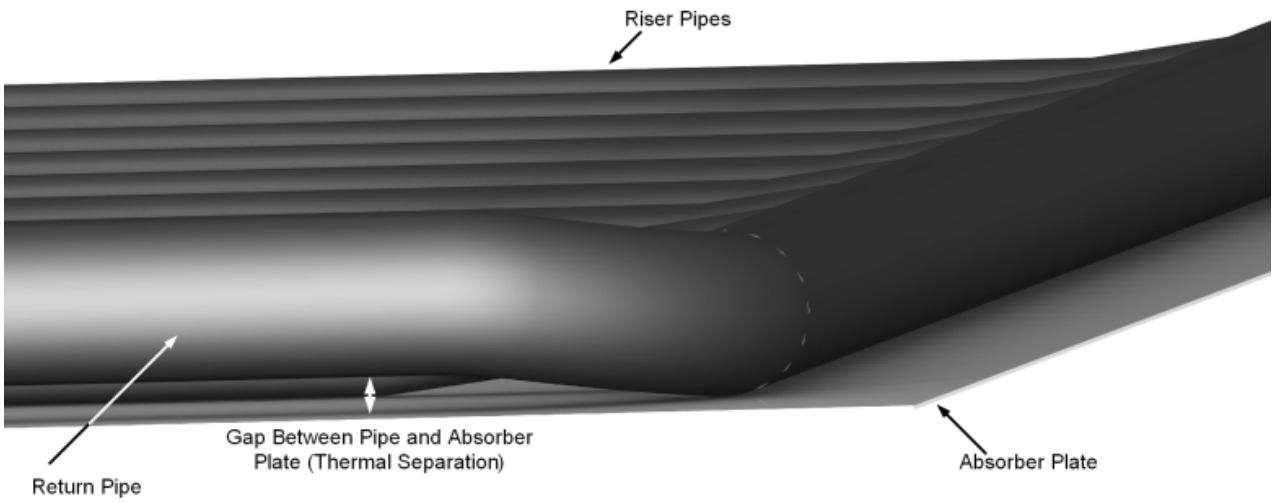

3D Absorber Model

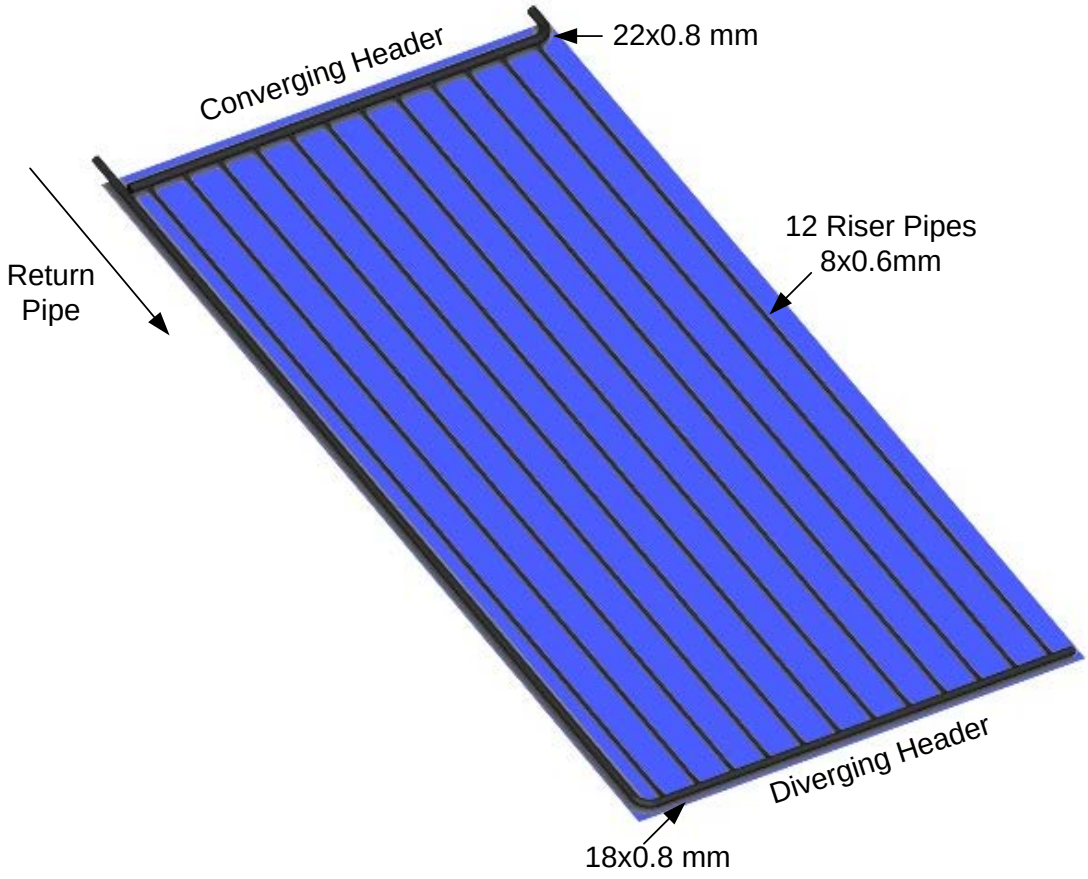

Isometric View of the Absorber

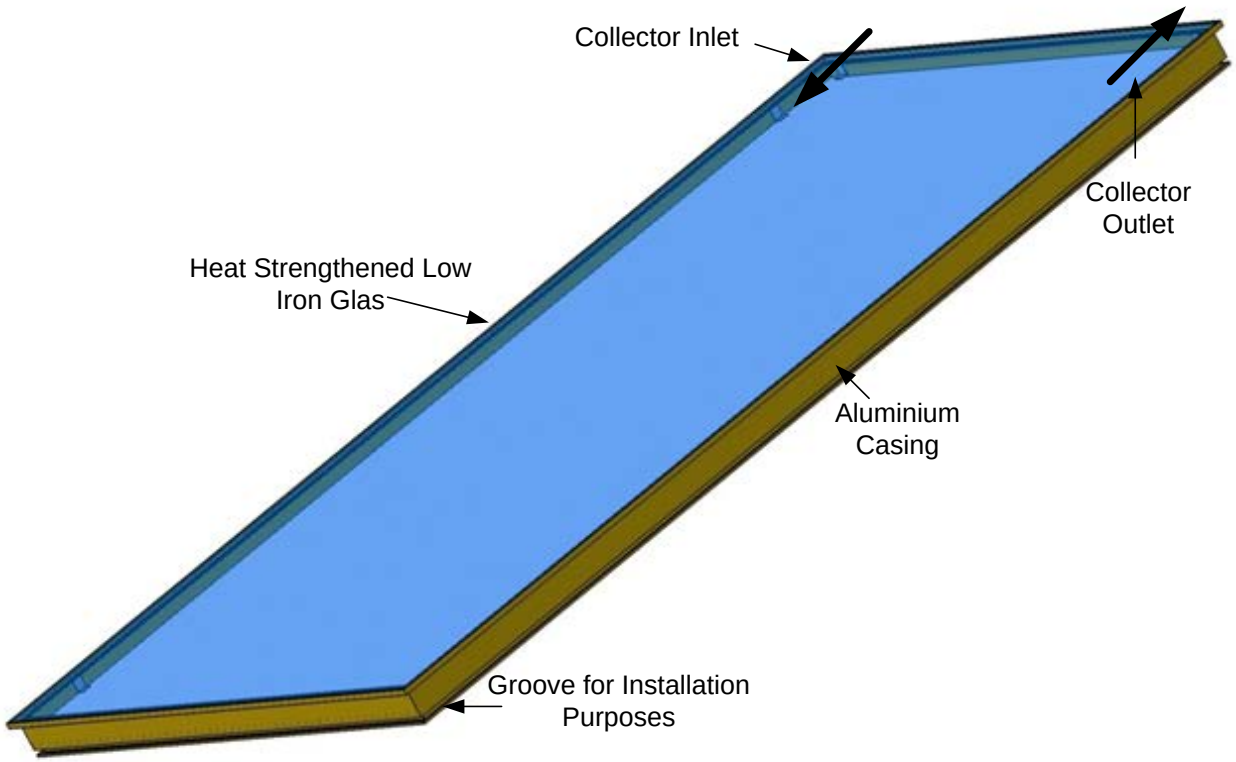

3D Collector Model

Appendix D:

Technical Drawing – Storage Tank

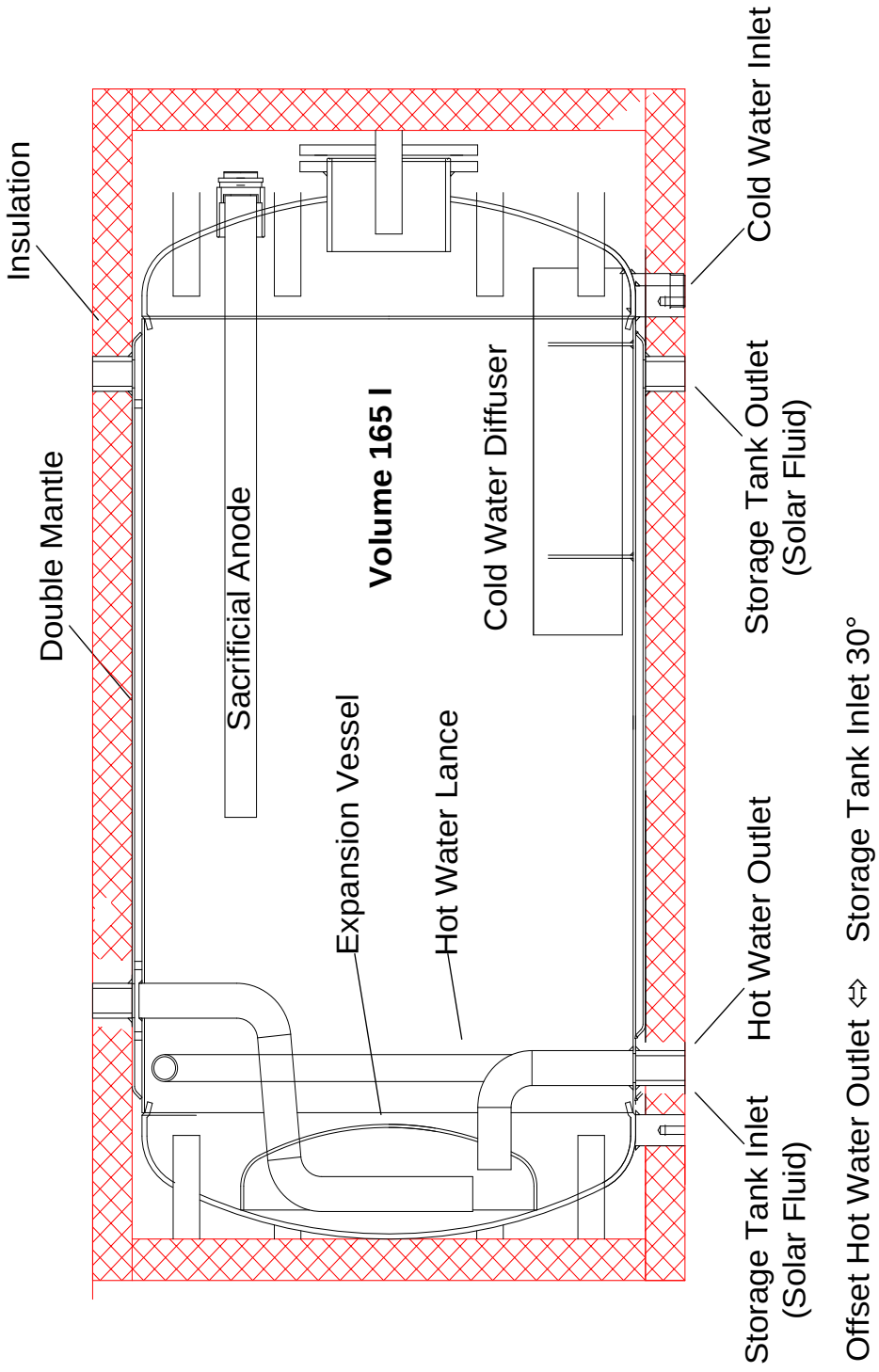
Insulation
Double Mantle
Sacrificial Anode
Volume 165 l
Cold Water Diffuser
Expansion Vessel
Hot Water Lance
Cold Water Inlet
Storage Tank Outlet
(Solar Fluid)
Hot Water Outlet
Storage Tank Inlet
(Solar Fluid)
Offset Hot Water Outlet ⇔ Storage Tank Inlet 30°

Appendix E:

Technical Design – System Support

Concerning the system design, several system supports are analysed. A majority of the systems on the market include a large number of single components, which have a negative influence on installation time and quality (Figure E.1). Another problem showing up is the necessity to use many different tools during system construction.

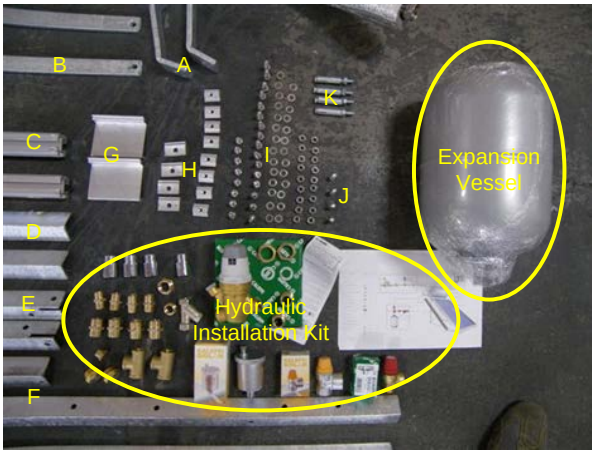

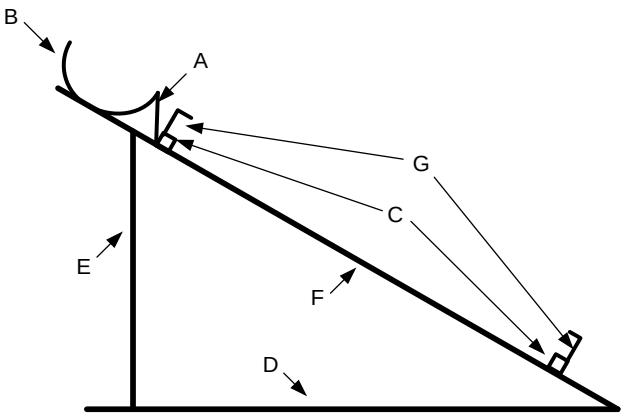

List of Parts:

A+B	2x Storage Tank Support	H	12 x Mounting Rail Nut (M8 & M10)
C	2 x Collector Mounting Rail	I	24 x Screws M8 18 x Screw Nut M8 24 x Washer
D+E+F	à 2 x L-Section	J	4 x Screws M10
G	4 x Collector Fixation	K	4 x Anchor Bolt

Figure E.1: Typical Amount of Single Components for a Thermosyphon System

The aim of the development is to provide a support consisting of few parts only which can be put together using a minimum amount of different tools. To reduce installation time a preassembled system is proposed. The system stand is mounted to the collector at the manufacturer. At the installation site it is simply opened and fixed with one screw at each lower corner (Figure E.2). To reduce material usage, the collector is used as a supporting system part, consequently, the collector mounting is found just in the upper collector part (Figure E.3). To reduce production cost only semi-finished products like L sections are proposed.

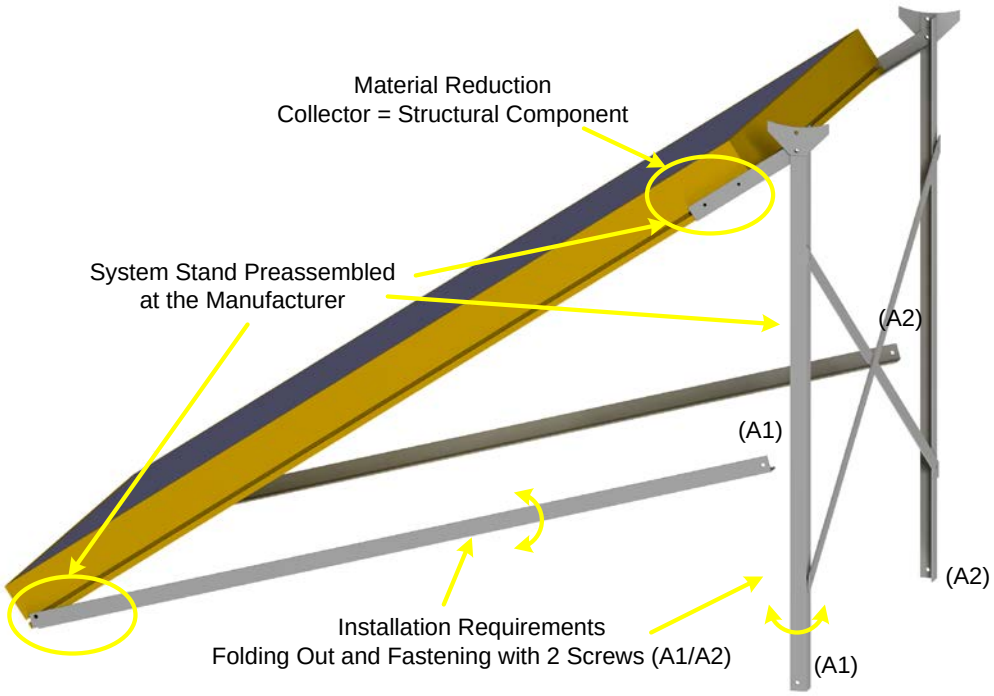

Figure E.2: Erecting the Thermosyphon System

For the upper pivot a special design allowing the preassembly at the manufacturer and adjusting the system tilt angle at 35 ° as shown in Figure has been developed in the research project. This fact implements a high intrinsic safety to the system installation as the angle of the vertical support is limited to angles of 0–90 °.

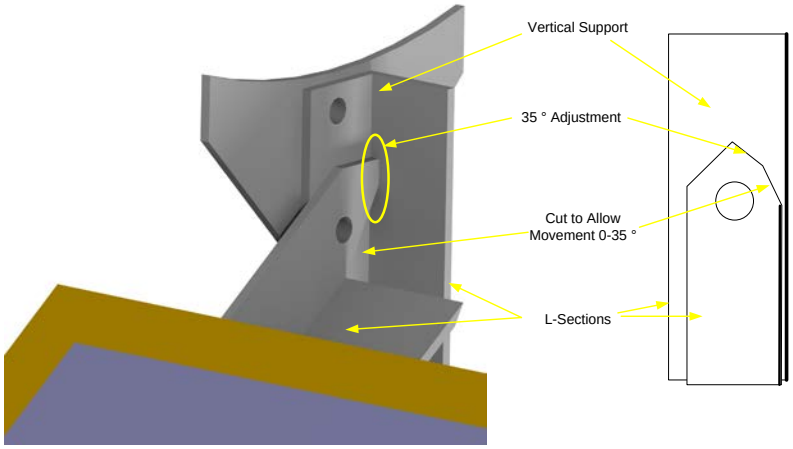

Figure E.3: Upper Pivot With 35 ° Adjustment

A further step that has to be undertaken for the improved close to production thermosyphon system is the verification of the system stability considering standard DIN 1055–4 (DIN, 2005).

Appendix F:

Bibiliography

SOLAR COLLECTORS

AGBO, S.N. and OKOROIGWE, E.C. (2007) Analysis of Thermal Losses in the Flat-Plate Collector of a Thermosyphon Solar Water Heater, *Research Journal of Physics*, 1 (1), pp.35-41.

BADESCU, V. (2006) Optimum fin geometry in flat plate solar collector systems, *Energy Conversion and Management*, 47, pp. 2397-2413.

DAYAN, M. (1997) *High performance in low-flow solar domestic hot water systems*. M.Sc. University of Wisconsin-Madison.

FAN, J.; SHAH, L. and FURBO, S. (2007) Flow distribution in a solar collector panel with horizontally inclined absorber strips, *Solar Energy*, 81, pp. 1501-1511.

HELLSTROM, B. et al. (2003) The impact of optical and thermal properties on the performance of flat plate solar collectors, *Renewable Energy*, 28 (3), pp. 331-344.

HOBBI, A. and SIDDIQUI, K. (2009) Experimental study on the effect of heat transfer enhancement devices in flat-plate collectors, *International Journal of Heat and Mass Transfer*, 52, pp. 4650-4658.

MARSHALL, R. (1999) A generalised steady state collector model including pipe losses, heat exchangers, and pump powers, *Solar Energy*,66 (6), pp. 469-477.

RESCH, K.; WALLNER, G. and HAUSNER, R. (2009) Phase separated thermotropic layers based on UV cured acrylate resins – Effect of material formulation on overheating protection properties and application in a solar collector, *Solar Energy*, 83, pp. 1689-1697.

RESCH, K. and WALLNER, G. (2009): Thermotropic layers for flat-plate collectors—A review of various concepts for overheating protection with polymeric materials, Solar Energy Materials & Solar Cells, 93, pp. 119-128.

ROBERTS, D.E and FORBES, A. (2012): An analytical expression for the instantaneous efficiency of a flat plate solar water heater and the influence of absorber plate absorptance and emittance, Solar Energy, 86, pp. 1416-1427.

ROMMEL, M and MOOCK, W. (1997) Collector efficiency factor F' for absorbers with rectangular fluid ducts contacting the entire surface, *Solar Energy*, 60 (3/4), pp.199-207.

ROSA DA, A.V. (2009) *Fundamentals of Renewable Energy Processes*. 1st ed. London: Elsevier.

SAKHRIEH, A.; AL-GHANDOOR, A. (2012): Experimental investigation of the performance of five types of solar collectors, Energy Conversion and Management, In Press, Corrected Proof.

SLAMAN, M. and GRIESSEN, R. (2009) Solar collector overheating protection, Solar Energy, 83, pp. 982-987.

VESTLUND, J.; DALENBÄCK, J.-O. and RÖNNELID, M. (2011) Thermal and mechanical performance of sealed, gas-filled, flat plate solar collectors, Solar Energy, 86, pp. 13-25.

WALLNER, G.; RESCH, K. and HAUSNER, R. (2008) Property and performance requirements for thermotropic layers to prevent overheating in an all polymeric flat-plate collector, *Solar Energy Materials & Solar Cells*, 92, pp. 614-620.

STORAGE TANKS

ALTUNTOP, N. et al. (2005) Effect of obstacles on thermal stratification in hot water storage tanks, *Applied Thermal Engineering*, 25, pp. 2285-2298.

CHAURASIA, P.B.L. (2000) Use of alternate insulating materials for storage of solar water heaters, In: *Proceedings of Terrastock 2000, 8th International Conference on Thermal Energy Storage, Stuttgart, September 2000*, Stuttgart: Institut für Thermodynamik und Wärmetechnik, pp. 579-582.

HAN, Y.M; WANG, R.Z and DAI, Y.J (2009) Thermal stratification within the water tank, *Renewable and Sustainable Energy Reviews,* 13, pp. 1014-1026.

HELWA, N.H.; MOBARAK, A.M.; EL-SALLAK, M.S. and EL-GHETANY, H.H. (1995) Effect of Hot Water Consumption on Temperature Distribution in a Horizontal Solar Water Storage Tank, *Applied Energy*, 52, pp. 185-197.

HUANG, M. J. et al. (2011) Microencapsulated phase change slurries for thermal energy storage in a residential solar energy system, *Renewable Energy*, 36 (11), pp. 2932–2939.

JINBAO, H.; SHAOXUAN, P.; WENFENG, G. and YI, Q. (2010) Experimental investigation on thermal performance of thermosyphon solar water heater with a mantle heat exchanger, *Energy*, 35, pp. 3563-3568.

KENJO, L.; INARD, C. and CACCAVELLI, D. (2007) Experimental and numerical study of thermal stratification in a mantle tank of a solar domestic hot water system, *Applied Thermal Engineering*, 27, pp. 1986-1995.

KNUDSEN, S. and FURBO, S. (2004) Thermal stratification in vertical mantle heat-exchangers with application to solar domestic hot-water systems, *Applied Energy*, 78, pp. 257-272.

KNUDSEN, S.; MORRISON, G.L.; BEHNIA, M. and FURBO, S. (2005) Analysis of the flow structure and heat transfer in a vertical mantle heat exchanger, *Solar Energy*, 78, pp. 281-289.

SHAH, L.J.; MORRISON, G.L. and BEHNIA, M. (2000) Characteristics of vertical mantle heat exchangers for solar water heaters, *Solar Energy*, 67 (1-3), pp. 79-91.

SMYTH, M.; EAMES, P. C.; NORTON, B. (2001) Annual performance of heat retaining integrated collector/storage solar water heaters in a northern maritime climate, Solar Energy, 70 (5), pp. 391–401.

SMYTH, M.; EAMES, P. C.; NORTON, B. (2003) Heat retaining integrated collector/storage solar water heaters, Solar Energy 75 (1), pp. 27–34.

SOO TOO, Y.C.; MORRISON, G.L. and BEHNIA, M. (2009) Performance of solar water heaters with narrow mantle heat exchangers, *Solar Energy*, 83, pp. 350-362.

(THERMOSYPHON) SOLAR DOMESTIC HOT WATER SYSTEMS

AGBO, S.N. and UNACHUKWU, G.O. (2007) Design and Performance of a Domestic Thermosyphon Solar Water Heater for an Average-Sized Family in Nsukka Urban, *Trends in Applied Sciences Research*, 2 (3), pp. 224-230.

ALSHAMAILEH, E. (2010) Testing of a new solar coating for solar water heating applications, *Solar Energy*, 84, pp. 1637-1643.

AXAOPOULOS, P.; PANAGAKIS, P. and KYRITSIS (1998) Experimental comparison of solar-assisted heat pump vs. a conventional thermosyphon solar system, *International Journal of Energy Research*, 22, pp. 1107-1120.

BRADLEY, D.E. (1997) *Promising Freeze Protection Alternatives in Solar Domestic Hot Water Systems*. M.Sc. University of Wisconsin-Madison.

CARVALHO, M.J. and NARON, D.J. (2001) Comparison of test methods for evaluation of thermal performance of preheat and solar-only factory made systems, *Solar Energy*, 69 (6), pp. 145-156.

CHANG, J.M.; SHEN, M.C. and HUANG, B.J. (2004) A proposed modified efficiency for thermosyphon solar heating systems, *Solar Energy*, 76 (6), pp. 693-701.

GAA, F.O.; BEHNIA, M and MORRISON, G. L. (1996) Experimental study of flow rates through inclined open thermosyphons,*Solar Energy*,57 (5), pp. 401-408.

GHONEIM, Z. A. and NASSR, I.S. (1995) Performance analysis of a thermosyphon solar water heating system part II: night time performance, *Proceedings of the Joint Solar Engineering Conference, ASME 1995*, pp. 1093-1098.

HOBSON, P.A. and NORTON, B. (1989) A design nomogram for direct thermosyphon solar-energy water heaters, *Solar Energy*, 43 (2), pp. 89-95.

JOSHI, S.V.; BOKIL, R.S. and NAYAK, J.K. (2005) Test standards for thermosyphon-type solar domestic hot water systems: review and experimental evaluation, *Solar Energy*, 78 (6), pp. 781-798.

KANBOUR, S.I. and KADHUM, S.A. (1990) Modelling of thermosiphon solar water heating systems, In: *ENERGY and the ENVIRONMENT, Proceedings of the 1st World Re-*

newable Energy Congress, Volume 2, Reading (UK), September 1990. Oxford: Pergamon Press, pp. 744-748.

KISHOR, N. et al. (2010): Fuzzy model representation of thermosyphon solar water heating system, *Solar Energy*, 84, pp. 948-955.

KUT, D. and HARE, G. (1983) *Applied Solar Energy*, 2nd ed., Butterworths, London.

MALKIN, M.P. (1985) *Design of thermosyphon solar domestic hot water systems*. M.Sc. University of Wisconsin-Madison.

MICHAELIDES, I.M. et al. (1992) An investigation into the performance and cost effectiveness of thermosyphon solar water heaters, *Renewable Energy*, 2 (3), pp. 219-225.

MINNERLY, B.V. (1989) *A long-term performance prediction method for solar domestic hot water systems*. M.Sc. University of Wisconsin-Madison.

MISHRA, R.S. (1992) Theoretical and experimental studies of pressurized and non-pressurized solar water heating systems of thermosyphonic type, *Renewable Energy*, 2 (4/5), pp.371-384.

MORRISON, G.L. (1986) Reverse circulation in thermosyphon solar water heaters, *Solar Energy*, 36 (4), pp. 377-379.

NORTON, B. and PROBERT, S.D. (1983) Achieving thermal rectification in natural-circulation solar-energy water heaters, *Applied Energy*, 14 (3), pp. 211-225.

NORTON, B.; EAMES, P. C. and LO, S. N. G. (2001) Alternative approaches to thermosyphon solar-energy water heater performance analysis and characterization, *Renewable and Sustainable Energy Reviews*, 5 (1), pp. 79–96.

ORDAZ_FLORES, A. (2007) Evaluation of the thermal performance of a solar water heating thermosyphon using different working fluids, In Proceedings: *ISES World Congress — Solar Energy and Settlement*, Beijing (CN), September 2007.

PRAPAS, D.E. and SOTIROPOULOS, B.A. (1991) The elimination of the reverse circulation in thermosiphon solar water heaters, *Solar Energy*, 46 (4), pp. 237-239.

SHARIAH, A.M. and LÖF, G.O.G. (1996) The optimization of tank-volume-to-collector-area ratio for a thermosyphon solar water heater, *Renewable Energy*, 7 (3), pp. 289-300.

SHARIAH, A.M. and LÖF, G.O.G. (1997) Effects of auxiliary heater on annual performance of thermosyphon solar water heater simulated under variable operating conditions, *Solar Energy*, 60 (2), pp. 119-126.

SHARIAH, A.; DAJEH, D. and MALHI, N. (1999) Best connection scheme of collector modules of thermosyphon solar water heater operated at high temperatures, *Renewable Energy*, 17, pp. 573-586.

SOPIAN, K. et al. (1994) Performance monitoring of a thermosyphon solar hot water heater with a parallel thermoplastic natural rubber tube absorber*, Renewable Energy*, 4 (5), pp. 561-577.

TANG, R. et al. (2010) Experimental and modelling studies on thermosiphon domestic solar water heaters with flat-plate collectors at clear nights, *Energy Conversion and Management*, 51, pp. 2548-2556.

ZERROUKI, A. et al. (2002) Input/output results and long-term performance prediction of a domestic thermosiphon solar water heater in Algiers, Algeria, Renewable Energy , 25 (1), pp. 153-161.

Appendix G:

Publications

BRANDMAYR, S. und ZÖRNER, W. (2007) Thermosiphonsysteme: Markt, Technik und Entwicklungstrends. In*: 17. Symposium Thermische Solarenergie*, Bad Staffelstein, May 2007, pp. 121-123.

BRANDMAYR, S. and ZÖRNER, W. (2007) Thermosiphon Systems: Market, State-of-the-Art and Trends In: *3nd European Solar Thermal Energy Conference - estec2007 Proceedings, Freiburg, June 2007*. Freiburg: European Solar Thermal Industry Federation ESTIF, pp. 182-188.

BRANDMAYR, S.; HANBY, V.; KONRAD, M. and ZÖRNER, W. (2008) Simulation of Thermosiphon Solar Hot Water Systems Using Matlab/Simulink and CARNOT. In: *Eurosun 2008 – 1st International Conference on Solar Heating, Cooling and Buildings*, Lisbon, October 2008, pp. 546-547.

BRANDMAYR, S.; TRINKL, C. und ZÖRNER, W. (2009) *Effizienter Einsatz von Simulationstools in der Solartechnik.* In*: 1st Solarthermie-Technologiekonferenz*, Berlin, February 2009.

BRANDMAYR, S.; HANBY, V. and ZÖRNER, W. (2009) Simulation von Thermosiphon-Solaranlagen unter Matlab/Simulink und CARNOT. In*: 19. Symposium Thermische Solarenergie*, Bad Staffelstein, May 2009, pp. 444-449.

BRANDMAYR, S.; HANBY, V. and ZÖRNER, W. (2009) Sensibilitätsanalyse von Thermosiphon-Solaranlagen unter Matlab/Simulink und CARNOT. In: *20. Symposium Thermische Solarenergie*, Bad Staffelstein, May 2010, pp. 428 - 433.

BADER, T.; BRANDMAYR, S.; HANBY, V. and ZÖRNER, W. (2010) Simulation of thermosyphon systems for solar domestic hot water production. In: *3rd IASTED African Conference on Power and Energy Systems*, Gaborone (Botswana), September 2010.

BRANDMAYR, S.; HANBY, V.; TRINKL, C. and ZÖRNER, W. (2010) Thermosyphon Systems: Sensitivity Analysis Regarding Optimum Energetic Performance and Cost Effectiveness. In: Eurosun 2010 – 2nd International Conference on Solar Heating, Cooling and Buildings, Graz, September 2010, p. 141